ULTIMATE LOAD BEHAVIOUR OF STEEL BOX GIRDERS AND THEIR COMPONENTS

A Thesis submitted for the degree of Doctor of Philosophy in the Faculty of Engineering of the University of London

by Paul Alexander Frieze,
BSc, BE, MSc, DIC

Imperial College of Science and Technology, London

October 1975

To my Wife

and my Parents

ABSTRACT

The object of the work presented in this thesis is to investigate the relationship between component collapse and overall collapse of steel box girders. To this end, both experimental and theoretical data are presented and compared.

Tests on five quarter-scale box girder models are described. Normal welding techniques were used in their fabrication so that realistic imperfections were introduced into the models. In each of the models collapse was initiated by plate buckling in either the webs or the compression flange. In the case of flange failure, significant interaction between the plate and the stiffener occurred prior to collapse of the entire cross-section.

A theoretical method for analysing the large deflection elasto-plastic response of rectangular plates typical of those found in box girders, is described. Dynamic relaxation is used to numerically solve the plate equations and a single-layer yield function with an associated flow rule are used for behaviour in the plastic regime. Comparisons with more expensive finite element and other finite difference methods confirm the soundness of the technique.

For compression flanges subjected to pure bending and bending and shear, use of the theoretical plate average stress-strain curves in conjunction with rigorous inelastic column theory gives good correlation with the experimental results. Similar correlation is also achieved using a simple elastically based strut approach. Only in cases where the longitudinal

stiffening is extremely stocky is the plate strength information alone sufficient to predict flange collapse. Redistribution of direct stresses between panels of a flange occurs before collapse in the case of a wide stiffened girder subjected to point load conditions and failing with the plate in compression.

For webs subjected to bending and shear, reasonable theoretical bounds to their shear strengths are obtained by loading the plates in pure shear and in shear plus bending.

A parametric study of practical compression plates is presented. A range of realistic levels of initial deformation and residual stress is covered. Initial bow is found to influence behaviour throughout the complete loading history, whereas residual stress only affects that part of the average stress-strain curve between first yield and yield of the edges at approximately twice yield strain. Design curves are presented for constrained and unrestrained plates for levels of initial imperfections suitable for design. The results of the study now form the basis of a new design method included in the draft bridge design code.

It is concluded that the study of isolated panel behaviour goes some of the way towards understanding the overall collapse behaviour of steel box girders but that, in particular, the problem of changing boundary conditions throughout the loading history of a critical panel limits the application of the approach formulated within this thesis. Interactive effects, such as redistribution, need further consideration than is currently possible using an isolated plate analysis.

ACKNOWLEDGEMENTS

The author would like to express his gratitude and thanks to the following:-

Dr. P.J. Dowling, for initially inviting the author to participate in the extensive box girder experimental programme and for his most generous and helpful guidance during this period, and subsequently for his suggestions and guidance regarding the theoretical work;

Dr. R.E. Hobbs, for his explanations of some of the intricacies of dynamic relaxation;

Bridges Engineering Design Standards Division of the Department of the Environment, for their sponsorship of both the experimental and theoretical work;

Mr. J. Neale and the staff of the Engineering Structures Laboratories, for their intensive and protracted efforts during the arduous testing programme, their willingness to co-operate with the author at all times was very much appreciated;

Mr. G.N. James of the Computer Centre, for his generous efforts and advice with technical aspects of programming;

Mr. F.M. Moolani, for his co-operation with the experimental work and for generously making available his computer program for the column analyses;

Mr. J.E. Harding, for allowing the author to use some of his results for comparisons and for his constructive discussions regarding the theoretical results;

Dr. M.A. Crisfield of the Transport and Road Research Laboratory, for his friendly and helpful exchange of ideas;

Mr. J.A. Dean, Mr. G.W. Owens and Mr. S. Chatterjee, for their useful discussions;

His wife, Maxine, for her excellent typing of this thesis and extreme patience and understanding during the past four years;

Mrs. F.H. Guile, for her high standard of draftsmanship;

and

Mrs. J. Slatford, for her help with the preparation of the manuscript.

CONTENTS

CHAPTER 1

INTRODUCTION

Background to Thesis

Until the end of 1969 the development of the steel box girder bridge had continued successfully. Early work on design methods for orthotropic decks in Germany using linear elastic theory had been rationalised[1] and was incorporated into national design guides in Germany[2] and the United States[3,4]. The remainder of the girder was designed by methods similar to those used for plate girders, although the enhanced torsional stiffness of the closed cross-section was taken into account in allowing for transverse distribution of eccentrically placed loads. It was common practice in Britain for bridge engineers to extrapolate the recommendations contained within the existing British Standard for steel girder bridges[5] to the design of box girders. A paper[6] by three of the major contributors to this specification was most useful in giving the background to the BS 153 clauses on web design, and alternative methods were available for the design of singly-stiffened[7] and multi-stiffened[8] girder webs.

The structural efficiency of the box girder resulted in the use of thinner plates than were generally used in plate girders. The slenderness of these plates was such that not only was instability a problem needing careful consideration in design, but imperfection sensitivity was also greatly increased. Where elastic

linear buckling theory was used as a basis for design, safety factors which were considered to be appropriate against buckling were used, such as the approach used in the German DIN 4114. However, the influence of imperfections on buckling was not clearly understood and this was one of the factors contributing to the series of collapses of box girder bridges in Britain, Australia, Austria and Germany between 1969 and 1971.

Following the collapse of two British designed bridges, a Committee of Inquiry into the basis of design and method of erection of steel box girder bridges was appointed. The Committee proposed a programme of short term research which incorporated and considerably extended a study already in progress in the Engineering Structures Laboratories at Imperial College for the new bridge code. A team of research workers at Imperial College of which the author was a member undertook the work.

Following the report of the Committee, which included interim appraisal[9] and design rules[10], a joint Department of the Environment and Transport and Road Research Laboratory Working Group on steel box girders was established. This Group was to continue the programme of research started by the Committee and to initiate further studies when suitable analytical methods became available. The general aim was to mould the interim design rules into a more suitable form for use in the bridge code currently under preparation.

The author was involved in both the earlier experimental work outlined above, and in the development of an analytical method for studying plate behaviour in the elasto-plastic range. The program was to be checked against the experimental results, and used for

parametric studies on plate behaviour. One such study undertaken for the Working Group is described within this thesis.

Aim of Thesis

The object of the work presented in this thesis is to show the relationship between component collapse and overall collapse of a box girder. To this end, the theoretically predicted capacities of isolated imperfect plates with various boundary conditions are compared with the experimentally observed strengths of related panels acting as components of box girders. In particular, it is hoped to establish under what circumstances isolated panel theory can be used to predict the strength of entire girders.

Scope of Thesis

In Chapter 2, experiments on five of the models in the series 'Short Term Box Girder Tests' are described. The models may be divided broadly into two groups: one where failure is dominated by collapse of the flanges, and the other in which web collapse is dominant. The relationship between the observed overall and plate component collapse is discussed in detail.

In Chapter 3, a method for analysing the elasto-plastic response of plate components of steel box girders is developed. Discussions on the yield function and associated flow rule and the numerical procedure adopted for the analysis are included. Comparisons with existing large deflection elasto-plastic solutions are made.

Chapter 4 describes the application of the analytical method to various plate components of the models treated in Chapter 2. The boundary conditions appropriate to the different panels are discussed and the relationship between component and overall behaviour is considered.

In Chapter 5 the results of a parametric study on the collapse behaviour of plates in compression is presented.

Chapter 6 contains the conclusions and recommendations for future work. In particular, the relationship between plate component behaviour on overall girder behaviour is discussed, and the conclusions of the parametric study are presented.

Note on Literature Survey

Practically no experimental information on the behaviour of box girders up to and beyond peak load was available when the work described in this thesis was undertaken[11]. It is only now that the results of current experimental work are beginning to filter through. No attempt has been made in this thesis to correlate the results of the experiments described here with these new results. This is a task which is currently being undertaken by another of the author's colleagues.

Available literature on related elasto-plastic analytical and experimental studies of plates is reviewed in the appropriate Chapters 3 and 5.

CHAPTER 2

EXPERIMENTAL PROGRAMME

2.1 BACKGROUND AND OBJECTIVES OF TESTS

The object of the programme was to collect as much experimental data as possible in the time available to help substantiate or modify the basis of the methods proposed by the Committee of Inquiry for initially, the appraisal (IDAR)[9] and subsequently, the design (IDWR)[10], of steel box girders[12].

The first part of the programme involved the testing of eight box girders. The proportions of these were varied so that failure would be initiated in each of the following ways:

in the compression flange by

(i) plate panel buckling,

(ii) stiffened panel buckling between transverse stiffeners, and

(iii) overall stiffened panel buckling;

and in the webs by

(i) plate panel buckling, with and without sturdy horizontal stiffeners, and

(ii) stiffened panel buckling between vertical stiffeners.

Some of the tests concerned with flange behaviour were carried out under both point load and pure moment conditions to compare the behaviour with and without shear (and consequently shear lag) present.

Finally, to study the redistribution capacity of a box section after failure of the web panels on one side only, one girder was tested under combined moment, shear and torsion.

Following this part of the programme a further investigation was carried out on two models to study the influence of shear lag in more detail. Although the earlier tests had indicated that this phenomenon did not significantly reduce the capacity of the box cross-section, the evidence concerning the redistribution of the direct stresses was far from conclusive. To ensure that shear lag would be pronounced the proposed models were made twice as wide as the earlier girders, and for a direct comparison one was tested under a point load and the other under uniform moment.

For the purposes of this thesis the following models from the ten outlined above are studied in detail:

Model 1 (stiffened and retested to collapse twice) - where failure was preceded twice by web panel buckling and finally appeared to occur by simultaneous collapse of both flange plate and web plate panels;

Model 2 (stiffened and retested to collapse once) - where failure appeared to be precipitated twice by flange plate buckling;

Model 5 - in which web panel buckling preceded collapse;

Model 7 - in which buckling was at first confined to one web through the application of eccentric loading; and

Model 9 - in which the presence of shear lag initiated buckling in the external flange plate panels followed by progressive collapse of the remaining panels.

2.2 DETAILS OF MODELS

2.2.1 Dimensions

The models represented to approximately 1/4 scale either the support section or the span section of a continuous box girder. The former was simulated by the use of a central point load which produced the high shears and moments expected at the support section, and the latter by applying equal end moments to produce, in an idealised way, the low shear conditions in the midspan region of a practical girder.

Models 1, 5 and 7 had identical layout dimensions except that an additional longitudinal stiffener was included in the tension region of the webs of the two outer bays in girders 5 and 7. The stiffening was necessary to prevent premature collapse of these panels which were found to be susceptible to buckling following the testing of Model 1. The models had a central diaphragm at which to apply the point load, and three equal length bays either side of this separated by ring-stiffeners. The end cross-frames were stiffened to support the reaction pads located at each end of the model. Figures 1d and 1e show typical compression flange and web layouts, and Table I a typical cross-section together with component sizes and material properties. Figure 1c shows modifications to the end ring-stiffeners of Model 7 used to provide a distortion free cross-section for final testing. Some preliminary tests on this model were conducted without the cross-bracing to study distortional effects.

Model 2 had a cross-section identical to that of Model 1, but the diaphragm was omitted as it was unnecessary in a girder to be loaded in pure bending. An elevation of the model (Fig. 2) shows

that only five equal bays were used here compared with six in the centrally point loaded girders, and the cross-section can be seen in Table I together with a list of component sizes and material properties. Note that in Models 1 and 2 simulated bulb flats were used as longitudinal stiffeners whereas flats were employed for the later models.

The compression flange of Model 9 had similar plate thicknesses, stiffener spacing and dimensions to the earlier models but was twice as wide. Also, the use of thicker web and tension flange plates avoided the need for longitudinal stiffeners in these elements. The model was subdivided equally by ring-stiffeners into only three bays as can be seen in Fig. 3. The diaphragm was omitted so that the effect of shear lag on flange panel behaviour would not be obscured by the restraining effect of a diaphragm on transverse straining of the flange. Its cross-section is shown in Table I together with the list of element sizes and properties.

Fabrication details of the models can be found in references 13 to 17 and detailed drawings of each of the girders in references 18 to 22.

2.2.2 Materials

The steel specified for the models was Grade 43A, BS 4360. Ultimate tensile tests were conducted on at least four specimens taken from every element of the models and the average results of some of these are shown in Table I. Only those elements of immediate interest have been included in the table, the remainder being omitted for clarity. As can be seen in the table a number of plates had yield stresses below that specified.

2.3 TEST RIGS AND INSTRUMENTATION

2.3.1 Strain Gauges

A demountable mechanical Demec strain gauge was used to measure residual strains caused by welding. Measurements were taken between fixed points on the plates at three stages during fabrication: namely, after cutting and butt welding to form the full length plates; after welding of the stiffeners; and after welding of the stiffened plate components together to form the final model. Readings were taken on both surfaces of the plating and the gauge points were distributed around the cross-sections where failure was expected to occur.

Electrical resistance strain gauges were used to record strains under load. Some 400 gauges of the rosette, cross and linear type were used on each model and their distribution was again generally centred around the regions of interest. References 13 to 17 contain details of both types of gauges and their layouts.

2.3.2 Transducers

Electrical resistance transducers were used to measure both initial distortions and deflections under load. The transducers were mounted on an inverted U-frame (Fig. 4) which straddled each girder. The U-frames traversed the length of the girder on rails and were positively located at the sections to be monitored by balls set into the top of the rails. The balls had been accurately levelled so that they generated a plane under the weight of the U-frame. The rails were supported directly onto the girders at three points. Recordings were made of the compression flange and webs in the first eight models, but only of the compression flanges in Models 9 and 10. In general,

the transducers were located over the longitudinal stiffeners, over the corners of the girder and over the centre-lines between stiffeners. In the case of large web panels two additional transducers were used at the quarter-points of the panels. The cross-sections at which transverse profiles were recorded varied from model to model. For Models 1, 5 and 7 they are shown in Fig. 1 by the letters A to U, for Model 2 in Fig. 2 by the letters A to W, and for Model 9 in Fig. 3 by the letters A to U.

A reference cross-section in the form of a three-sided frame with machined surfaces was provided for measuring the initial shape. This was positioned at one end of each model and its shape recorded prior to measuring the model. For recording the initial profiles the transducer shafts bore directly onto the model. However, because under test the model would move relative to the transducers, plates were fixed at the ends of the shafts normal to their direction of movement. The plates then bore on small steel balls stuck to the surface of the model.

2.3.3 Point Load Test Rigs

Central point load tests on Models 1 and 5 were carried out by applying jack loads at one end of the model, providing a central reaction by means of bearings located on an overhead cross-beam, and resting the far end of the girder on bearings supported by concrete blocks on the laboratory floor. The eccentric loading on Model 7 was produced by using one jack at each end at diagonally opposite corners. Diagrammatic layouts of these rigs are shown in Fig. 1. Longitudinal movement of the models was prevented by stops each side of the centrally placed cylindrical rockers. With the central point load on

top of the models they were upside down in relation to the conditions at the support of a continuous girder. This position was adopted, however, for ease of testing and observation of critical compression flange components.

Model 9 was tested under central point load conditions. However, since a diaphragm had not been included in its design an alternative method of applying the central reaction was required. This was accomplished by welding large plates to each web of the model and bolting these to the laboratory floor through hinged connections (Fig. 3). The loading and reacting arrangements at each end were similar to those used for Models 1 and 5.

2.3.4 Uniform Moment Test Rig

To help provide equal and opposite moments at each end of Model 2, special loading arms were welded to the extremities of the girder as shown in Fig. 2. Load was applied by jacks at the far ends of the arms and these were restrained against vertical movement at their junction with the model. The reactions were resisted by spherical bearings which allowed rotation of the model in all directions and which were bolted to the floor. Although the arrangement was self-stabilising, flexible stays were taken from the loading arms to the floor to restrict longitudinal movement.

Hydraulic jacks were used in all tests. Servo-mechanisms in the control cabinet enabled either load or displacement control to be employed as required. For the latter a transducer was suspended between the model and the laboratory floor. The point of contact on the girder was selected as that having the largest displacement under load relative to the floor.

2.4 TESTING PROCEDURE

2.4.1 Initial Measurements

Upon installation of each model, some residual strain gauge readings were re-recorded to check whether any relaxation of residual stress had occurred during transportation and erection. The initial shape of the compression flange and webs was also recorded at this stage.

Coupons for tensile test specimens had been cut from the various components prior to fabrication. Plate thicknesses, however, were determined from coupons cut from the model after testing. The spots selected for this purpose were well removed from the regions of plate which had yielded or distorted during testing. The tensile test specimens were not used for plate thickness determination as they were usually cut from near the edges of whole plates which under the action of rolling are generally thinner than the remainder of the panel. A later report[23] showed that specimens taken from the very edge of the plate overestimated the tensile yield stress for the remainder of the plate. This effect was noted at the time and the results from such specimens were not used unless no other results were available. After testing the model was surveyed to record accurately the 'as fabricated' dimensions such as the exact spacing of stiffeners, etc.

2.4.2 Preliminary Tests

The first loading cycle on each model was restricted to loads well within its estimated ultimate capacity. It was designed to provide information on the elastic behaviour of the model as well as check the satisfactory functioning of the rig and instrumentation.

Both strains and deflections were recorded during loading and unloading.

The preliminary tests on Model 7 were rather more complicated than those on the other girders because several cycles of loading were involved. Initially the box was tested in pure torsion without cross-bracing in the end frames which permitted distortion of the cross-section to occur. The bracing was then installed and the loading repeated on the stiffened cross-section. Subsequent loading on the model was under the central point load condition described previously for this model. An elastic analysis of the torsion tests on Model 7 has been reported in reference 24.

2.4.3 Ultimate Load Tests

Early stages of loading were by predetermined load increments. This was soon altered to deflection (or strain) control to enable the model to be loaded incrementally to maximum load and beyond: this type of control allows the tracing of unloading as well as loading paths. Once yielding had become significant some 30 to 40 minutes were required after application of a load increment to achieve steady state conditions. This is because the instantaneous level of load is influenced by the rate of loading and time is required for plastification to spread until a steady (sustained) load can be maintained. This sustained load was taken as corresponding to the measured deflected shape.

Models 1 and 2 first collapsed in regions which were not instrumented. In these cases the failed components were strengthened and the models reloaded to collapse. The stiffening was arranged to have as little effect as possible on the remaining elements. Subsequent calculations[25,26] showed such failures were not unexpected.

2.5 INITIAL IMPERFECTIONS

2.5.1 Out-of-Plane Deformations

Transverse and longitudinal profiles of both webs and the compression flange were obtained from the transducer recordings of the initial shape of each girder. Longitudinal profiles of the stiffeners, the plate centre-lines between stiffeners and the edges of the model were plotted, along with transverse profiles of the sections indicated in Figs 1 to 3. Some general comments will be made on features of the initially deformed plate and stiffened panels, but only those profiles of immediate interest will be presented here. Detailed reports on the initial deformations of the models under discussion can be found in references 19 to 22 and 27.

2.5.1.1 *Plate Panels:* Transverse profiles of both flanges and webs showed that plate panels in general bowed towards the stiffeners. Movement of the plate in this direction was expected under the action of the transverse shrinkage of the welds connecting the plate to the stiffeners. In the longitudinal direction the resulting profile was that of an overall bow with superimposed ripples. This was modified frequently at the transverse stiffener positions where the plate was influenced by both longitudinal and transverse welds. The net result of this was that the sharpest longitudinal plate curvature often occurred adjacent to the cross stiffening.

This pattern of distortion was extensive in the flange panels and web compression zone panels where the slenderness ratio varied between 25 and 90. However, in the web tension zone panels where the slenderness ratio was approximately 144 a number of panels deformed with two half waves in the longitudinal direction.

2.5.1.2 *Stiffeners:* Assuming the centroid of a stiffener and its associated effective plating lies within the stiffener then longitudinal shrinkage of welding between the stiffener and the plate will cause distortion of the stiffened plate in the direction of the stiffener outstand.

This pattern of deformation was observed in most of the longitudinal stiffeners except in end bays where frequently the bow was in the opposite direction. It was assumed that this was the result of the sequence and method of fabrication. Exceptions to this pattern were the small web stiffeners employed at the neutral axis and mid-height of the tension zone of Models 5 and 7. These stiffeners often bowed outwards in the internal bays, a feature which can probably be attributed to the centroid lying at the top of the outstand or within the effective plate.

The transverse stiffeners bowed inwards where they formed part of the internal ring-stiffeners. Their profiles were more regular in nature than those through the plate cross-sections. The end cross-frames showed only small out-of-plane distortions, but at the diaphragm irregularities in the profiles were not infrequent. The latter could have resulted from a small degree of misalignment during fabrication.

2.5.1.3 *Compliance with Fabrication Tolerances:* In Table II the maximum measured plate distortions for the models under study are listed as proportions of panel width or depths: the deformations were measured at the centre of the panels transverse to the longitudinal stiffeners. In the table a positive value indicates a deformation in the direction of the stiffener outstand.

Included in the table are the tolerance requirements of the IDAR[9]: these limits were applicable at the time of fabrication. Comparison of the measured distortions with the tolerances indicates that the plate panels as fabricated were well within the required limits.

In Table III maximum longitudinal stiffener distortions for the girders under consideration are indicated. The values shown are the maximum recorded off-sets with respect to the transverse stiffeners spaced a distance L apart. Initial bows for both the positive and negative directions are indicated.

The IDAR fabrication tolerances are included in the table and comparison with the measured flange distortions shows that these elements were fabricated within the required limits. However, although the web stiffeners which bowed inwards also satisfied the tolerance requirements the outward distortions of these elements were significantly greater than the permitted levels. In general, these large stiffener bows occurred in the end bays and therefore were expected to have little influence on the ultimate load behaviour of the models.

2.5.1.4 *Panels for Study:* Because the emphasis in this thesis is on plate panel behaviour, the initial distortions of the flange and web bays containing those elements under consideration will be described more fully.

In Models 1 and 2 panel collapse occurred at more than one cross-section. As can be seen in Figs 1 to 3 the initial shape was not measured in detail along the full length of each model since, in an effort to keep the number of readings down to a manageable size, only regions where failure was expected were monitored closely. Thus,

in Models 1 and 2 a detailed study of initial imperfections had only been carried out on those panels involved in the final collapse.

(a) Model 1: Transverse profiles of the initial deformations of both webs of this model are shown in Fig. 5. A longitudinal section of the web is shown at the top of the figure. The letters indicate the vertical gridlines on the webs across which recordings of the initial shape were taken. Transverse sections of each web are shown on the right of the figure. From these the locations of the horizontal gridlines can be determined. The positions of the longitudinal stiffeners are indicated by dashed lines.

Figure 5 shows that all plate panels have bowed towards the stiffeners although the magnitude of the deformation of the tension zone panel in bay JO of the north web is small.

Details of the initial deformations in bay DI of the compression flange are illustrated by transverse profiles in Fig. 6. The positions of the longitudinal and transverse gridlines can be related to the model by the sections above and to the left of the figure. The positions of the longitudinal stiffeners are indicated by long dashed lines. The records from one of the transducers, however, proved to be erratic and therefore have not been used. This has lead to the estimated shape shown in the figure by the short dashed lines[27]. Where data are available, the figure shows that nearly all the panels bowed towards the stiffener outstands.

Longitudinal profiles of this girder are not available because the initial shape of the diaphragm cross-section was not recorded.

(b) Model 2: Of the two bays in which plate buckling was observed in this model, only one had its initial shape thoroughly documented. This was bay OU for which transverse and longitudinal profiles of the compression flange initial deformations are presented in Fig. 7. Transverse and longitudinal sections of the girder are shown at the top and side of the figure to indicate positions of the longitudinal and transverse gridlines. The longitudinal stiffeners are indicated by long dashed lines.

With few minor exceptions the plate panels have bowed in the direction of the stiffener outstands. In the longitudinal direction the deformed shape of the plates tends to be a single overall bow with a superimposed ripple. The longitudinal profiles of the flange edges show distortions similar in nature and magnitude to those of the stiffeners and, indeed, of the plate panels. Lack of accurate fit-up during fabrication could account for this, although local distortions of the plate were clearly visible in the vicinity of the intermittent weld runs which would have contributed significantly to the resulting pattern. The local weld distortions were most obvious in the thinnest plate.

(c) Model 5: Transverse and longitudinal profiles of the initial deformed shape of the four centre web bays of this model are shown in Fig. 8. Longitudinal and transverse sections of the girder are included to indicate the positions of the gridlines. The locations of the longitudinal stiffeners are shown by the dashed lines.

In the compression regions of the webs, most of the plate panels have deformed towards the stiffener outstands (Fig. 8). The tension zone panels, however, were not so simply deformed. Two of the

panels, bay EK of the north web (Fig. 8a) and bay KQ of the south web (Fig. 8d), distorted into two half waves longitudinally. In bay KQ of the north web (Fig. 8b), three longitudinal half waves could be distinguished, all of small magnitude. For the fourth panel, bay EK of the south web (Fig. 8c), the deformed shape longitudinally was that of a single ripple superimposed on a larger overall bow.

(d) Model 7: During testing of this model, only two of the centre web bays were significantly overstressed. They were bay EK of the north web and bay KQ of the south web. Transverse and longitudinal profiles of the initial deformations of these bays are shown in Fig. 9. Longitudinal and transverse sections of the girder are included to indicate gridline locations. The positions of the longitudinal stiffeners are shown as dashed lines.

Figure 9a shows that parts of both the tension zone and intermediate panels have bowed outwards. The result is two asymmetrical half waves in each of these panels. The compression zone panel has deformed inwards along its entire length. A large outward bow (equal to length/397) can be seen in the midheight stiffener.

The plate panels have all bowed inwards in bay KQ of the south web (Fig. 9b). Longitudinally the tension zone panel has one ripple superimposed on a larger asymmetrical single bow.

(e) Model 9: Longitudinal and transverse profiles of the centre compression flange bay of this model are presented in Fig. 10. Sections of the girder are shown to indicate the gridline positions. Long dashed lines illustrate the longitudinal stiffener locations. Recordings of the deformations along two plate panel centre-lines were

inaccurate because faulty transducers were used. The profiles at these locations are shown either dashed (Fig. 10a) or have been omitted (Fig. 10b).

Transversely the plate panels have all deformed inwards although a significant outward bow has developed across the whole stiffened panel (Fig. 10a). This, however, is only equal to width/1200 for the transverse stiffener at E.

Longitudinally the plate panels are relatively flat. In fact, distortions in the longitudinal stiffeners and along the top of the webs are more pronounced than those in the plates.

2.5.2 Residual Stresses

Welding residual strains recorded in Models 1, 5, 7 and 9 are shown in Figs 11 to 14 respectively. The values are plotted around a cross-section of each girder the sides of which form the bases for the scales. Two scales are given for each flange and web element, one for strain and the other stress. The latter is related to the strain scale by assuming transversely unrestrained panels. The average value of residual strain (and stress) across each element is indicated.

The figures show that straining in the compression flange tends to be symmetrical. Also, the values in one web of a girder mirror approximately those of the opposite web.

Models 5 and 7 (Figs 12 and 13) have one distinctive feature of straining in their webs and that is the low value recorded adjacent to the tension flange. In the north web of Model 5, in fact, tensile residual strains were measured. Despite similarity of the

geometry, the weld details and the fabrication procedures of these two models, the level of welding strain in Model 7 is almost twice that of the other girder. This suggested that factors other than weld size and sequence of welding influenced the distribution and magnitude of welding residual strains[21].

2.6 BEHAVIOUR OF COMPONENTS UNDER LOAD

In the following sections the behaviour of each of the models during testing will be discussed in turn. The emphasis in each case will be on the response of the particular panels of interest and how their failure was related to collapse of the whole girder. Collapse will be defined as either the maximum sustained load in the case of models which exhibit a peak in the load-deflection response, or as the beginning of the plateau for girders which can continue to maintain load whilst undergoing increased deformation. Further details of the tests can be found in references 12, 18 to 22, 27 and 28.

2.6.1 Model 1

2.6.1.1 *Test 1:* During this test the first signs of distress were noted at a centre point load of 90.0 ton in the form of plate buckling in bay DI of the compression flange. The distortions grew only slowly with further loading when shear buckling occurred in the tension zone panels of the end bays at a load of 120.0 ton. A small increase in load resulted in buckling of the adjacent intermediate panels of the end bays and testing was terminated. The growth of the web buckles is shown diagramatically in Fig. 15, and their development in relation to the overall girder response can be seen on the appropriate curve of Fig. 16. First web panel buckling is seen to coincide with a signifi-

cant reduction in overall stiffness in the latter figure (load level a) and thereby marks the end of the useful load-carrying capacity of the model.

2.6.1.2 *Test 2:* After strengthening the end bays for shear, the model was tested again. Distortions were visible first in the web tension zone panels of the middle bays at a load of 118.6 ton (c in Figs 15 and 16). Further loading amplified this buckling and also initiated plate buckling in bay DI of the compression flange. A maximum load of 132.0 ton was reached when shear buckling spread across the middle bays and the load reduced to 123.2 ton. On applying further displacement to the girder a plateau in the overall load-deflection response was recorded.

In this test, there was only a small difference between the loads at which web buckles formed and at which the plateau developed (c and d Fig. 16). However, in this particular case, the overall response between these two stages was complicated by the appearance of compression buckles in the flange and a significantly higher peak capacity at an intermediate increment. Thus although failure in this model occurred again by web shear buckling, the overall response to this type of collapse was not as clearly defined as in Test 1.

2.6.1.3 *Test 3:* After further strengthening, the model was loaded to 128.0 ton when simultaneous failure of compression flange plates and web plates on opposite sides of the diaphragm occurred. The web response can be seen in Figs 15 and 16. They show that the first buckle appeared during the increment to maximum load with amplification and spreading of the buckling with loading beyond this stage.

The behaviour of the compression flange is illustrated in Fig. 17 by the curve marked location 1. This is the out-of-plane movement of the plate and indicates the initiating of buckling with the increment to maximum load. Stiffener failure (see curve marked location 2) which followed immediately produced the drooping load-deflection characteristic.

2.6.2 Model 2

2.6.2.1 *Test 1:* The cross-section of Model 2 was identical to that of the first girder but, in contrast to the earlier model, was loaded under pure moment conditions. While loading to collapse, a buckle first developed in the compression flange adjacent to the end cross-frame at a jack load of 62.5 ton (Fig. 18). Out-of-plane movement of flange plates in the adjacent bay OU was also noted. With the next increment to 64.5 ton, the remaining flange plates adjacent to the end cross-frame buckled with little recorded increase in the distortions of the adjacent bay. This was the maximum load recorded as the application of further jack displacement resulted in a reduction in the load response. The importance of first plate buckling in relation to maximum load in this model can be seen in the load-deflection curve in Fig. 19 through the proximity of the loads marked a and b.

Both end bays of the model were strengthened after unloading and the use of external stiffening prevented any further recording of deflections in these bays. Consequently, from the point of view of measured overall deflection the length of the model was reduced by 40 per cent. In Fig. 19 this has been compensated for by the use of different horizontal scales for each of the tests.

2.6.2.2 *Test 2:* Upon reloading, distortions were first noted at a jack load of 63.0 ton in bay OU at the positions at which out-of-plane movement had been observed in the previous test. With the next increment, to the maximum load of 64.5 ton, buckles appeared in the remainder of the flange plates at the midbay section. Additional loading amplified the plate buckling and produced strut failure (inwards) in this bay.

Figure 18 illustrates the growth of plate buckling and Fig. 19 shows the importance of this in relation to the overall girder response. Centre panel midplane strains and stiffener plate strains at the centre of bay OU have also been plotted against overall girder deflection in the latter figure. The location 1 curve illustrates development of the tensile component arising from stretching of the midplane of the plate with increasing out-of-plane movement. The location 2 plot shows the stiffener response and its close relationship with that of the plate is clearly seen.

However, although the first plate buckle did not occur at midbay, stiffener influence was noticeable in that the next phase of distortion of the plates occurred at this cross-section where the additional stresses that arose from stiffener movement were a maximum.

2.6.3 Model 5

Model 5 had a similar cross-section to the first two models except that the flange plate thickness had been increased to prevent any failure within the compression flange. Also, an additional longitudinal stiffener had been positioned at midheight of the web tension zone panels in the middle and outer bays to preclude shear failure of these components: this action was taken following the behaviour of Model 1.

From the onset of loading, out-of-plane movement of the web tension zone panel in bay EK of the north web was noted (dashed curve, Fig. 20). However, this only became pronounced with the increment to 110.0 ton together with a spread of buckling to the intermediate panel of the same bay (Fig. 21). Visible buckling of the remaining centre bays occurred also at this load. Maximum load was reached with the next increment when buckles developed in the intermediate panel of the adjacent bay CE: only a small increase in load was noted. The overall load-deflection characteristic developed a plateau for displacements applied beyond this stage (Fig. 20).

An important aspect of behaviour exhibited by this model is the proximity of the load of 110.0 ton at which component buckling occurred to the maximum load of the whole girder of 112.0 ton.

2.6.4 Model 7

This model was nominally identical to Model 5 but was loaded in torsion in addition to the flexure and shear imposed on the earlier model. The response of the directly loaded half of each web was similar to that of the webs of Model 5, the indirectly loaded half being relatively unaffected. The load in the webs could be proportioned using simple bending and torsion theory[21] up to the level of failure of the directly loaded half web. Redistribution between the web halves was noted beyond this stage which occurred with the increment to maximum load.

The overall response of the girder and out-of-plane movement of the tension panel in the north web centre bay can be seen in Fig. 22. The growth of buckles with load in the north web is illustrated in Fig. 23. The response of the south web was similar but because of the

torsional component of loading the buckles developed on the opposite side of the diaphragm.

In comparison with Model 5 (Fig. 20), out-of-plane movement of the critical component of this model grew more rapidly from the onset of loading. Two more increments, however, were required before panel buckling was initiated (b Fig. 22). It may be[21] that the load level achieved with the next increment does not reflect the true capacity of the directly loaded web since redistribution between webs had commenced with this increment. However, because of the difficulty in assessing what reduction, if any, should be made to account for this phenomenon the maximum load recorded has been used for determining the ultimate capacity of the web panel.

2.6.5 Model 9

The compression flange plate panels of this model were very similar to those of Models 1 and 2, but the stiffeners were of more slender proportions. The model was also twice as wide as its predecessors and as it was loaded under point load conditions, the influence of shear lag on the distribution of elastic stresses in the flange was very pronounced[22].

The behaviour of selected compression flange plates is illustrated in Fig. 24 together with the overall load-deflection response. Although in the figure out-of-plane movement is noted earliest in an internal panel, buckling occurred first in the plates adjacent to the webs (Fig. 25). The response of the edge plate (location 1) has probably been inhibited by the effective 'clamping' action of the thick web to which it was connected. Little loss of girder stiffness is noted with the appearance of the first buckle.

The spread of buckling to location 2 (Fig. 24) still has little influence on the overall response, but this alters with the appearance of buckles in the centre plate (location 3). The deflection of this plate appears to be in two stages. This is probably due to the difference in behaviour of the longitudinal stiffener on each side of the panel. It was noted during the test that one of the stiffeners moved very little out of its plane until maximum load was reached; whilst for the other, deflections grew slowly with load.

In contrast with the earlier models, the appearance of the earlier buckles in Model 9 had little direct influence on overall girder response. However, at peak load, out-of-plane deflection of the centre panel was not large indicating that it was not as strained as the outer flange plates.

2.7 ANALYTICAL TREATMENT

For comparison with the experimental capacities of the models just described, the theoretical strengths of the components were determined using a large deflection elasto-plastic method of analysis. Details of the method are presented in the next chapter and the comparison is presented in Chapter 4.

CHAPTER 3

THEORY

3.1 INTRODUCTION

A numerical method for solving the large deflection plate equations for elastic-perfectly plastic materials is presented in this chapter. Initial imperfections are included and behaviour in the elasto-plastic range is determined by a single-layer yield function and an associated flow rule.

The yield function, and application of the flow rule to this function which leads to a set of rigidities appropriate to flow in the elasto-plastic range, are discussed first. The numerical method and the manner in which the initial imperfections are incorporated are then outlined followed by a discussion on some details of the program. Finally, the results of the present analysis are compared with those of other large deflection elasto-plastic solutions.

3.2 YIELD FUNCTION AND APPLICATION OF FLOW RULE

3.2.1 Yield Function

The yield function adopted for the present analysis was developed by Ilyushin[29] for the case of thin shells obeying von Mises' yield criterion. It proposes yield as a sudden full-depth phenomenon, determined on the basis of values of the stress resultants rather than the stresses, and as such ignores the surface yield

that normally occurs in advance of membrane yield. The gradual spread of plasticity through the depth can be accounted for by using a layered analysis. However, because far less computer storage is required for a single-layer approach than for a multi-layer solution, there is a significant advantage in using the former.

By defining an equivalent strain at a distance z from the centre plane in terms of the midplane strain components and the curvature components, Ilyushin determined values of equivalent strain for the lower surface (e_{i_2} at $z = t/2$), for the upper surface (e_{i_1} at $z = -t/2$), and for a plane $z = z_o$ (e_{i_0}) such that the minimum value of equivalent strain e_{i_0} occurred in this plane. Depending on whether $-t/2 \leqslant z_o \leqslant t/2$ or $|t/2| < z_o$ the condition was described as 'bending dominant' or 'in-plane dominant' accordingly.

Two fundamental parameters were defined in terms of equivalent strain ratios, namely, $\alpha = \frac{e_{i_2}}{e_{i_1}}$, and $\rho = \frac{e_{i_0}}{e_{i_1}}$, and an exact function was then developed in the form:

$$f(Q_t, Q_m, Q_{tm}) = 0 \qquad \ldots\ 3.1$$

where $$Q_t = \frac{1}{\omega^2}(\rho^2 \psi^2 + \kappa^2)$$

$$Q_m = \frac{4}{\omega^4}(\rho^2(\rho^2 + \gamma^2)\psi^2 + (4\rho^2 + \gamma^2)\kappa^2 + 2\rho^2\gamma\kappa\psi - 2\rho^2\psi\chi + 2\gamma\kappa\chi + \chi^2)$$

$$Q_{tm} = \frac{2}{\omega^3}(\rho^2\gamma\psi^2 + \gamma\kappa^2 + \rho^2\kappa\psi + \kappa\chi)$$

and $$\gamma = \sqrt{1 - \rho^2} \pm \sqrt{\alpha^2 - \rho^2}$$

$$\omega = \frac{1 - \alpha^2}{\gamma}$$

$$\kappa = \alpha - 1$$

$$\psi = \left| \ln \frac{1 + \sqrt{1 - \rho^2}}{\rho} \pm \ln \frac{\alpha + \sqrt{\alpha^2 - \rho^2}}{\rho} \right|$$

$$\chi = \left| \sqrt{1 - \rho^2} \pm \alpha\sqrt{\alpha^2 - \rho^2} \right|$$

In these equations, the positive and negative signs indicate the 'bending dominant' and the 'in-plane dominant' conditions respectively.

By varying α and ρ in the range $0 \leqslant \rho \leqslant \alpha \leqslant 1$, Q_t, Q_m and Q_{tm} can be determined and when plotted as variables in three dimensional space generate the surface shown in Fig. 26a for the 'bending dominant' case and in Fig. 26b for the 'in-plane dominant' condition. The figures show the two states are separated by the curve $\alpha = \rho$ but are in fact continuous across the interface. This feature is illustrated in Fig. 26d where the surface is shown for $\rho = .1$ in the vicinity of the junction.

By considering the two limiting conditions of pure in-plane action and pure bending, and then how the surface varied with Q_{tm}, Ilyushin proposed an approximation to the exact surface in the form:

$$Q_t + Q_m + \frac{1}{\sqrt{3}} |Q_{tm}| = 1 \qquad \ldots\ 3.2$$

Comparisons between the surfaces generated by equation 3.2 and the exact criterion can be seen in Figs 26c and 26d. For the approximate surface, Q_t and Q_m were determined from equation 3.1 and Q_{tm} then calculated satisfying equation 3.2.

The suitability of this particular function for thin shell analysis has been discussed by Robinson[30], who concludes that it is a very good approximation to the exact solution and is superior to other linear approximations. It has been used for plates by

Crisfield[31] who finds that the simplified form of the equation:

$$Q_t + Q_m = 1 \qquad \ldots\ 3.3$$

is more accurate for the limiting cases of uniaxial direct force and uniaxial moment and consequently, he adopts this reduced form for the surface when $Q_{tm} \to 0$. This has the advantage that it not only satisfies the limits in question, but also removes the discontinuity that appears in the differential of equation 3.2 when $Q_{tm} \to 0$.

3.2.2 Flow Rule

Although Ilyushin's work was based on a deformation theory stress-strain law, it is concluded by Mikeladze[32] (and accepted by Onat[33]) and Robinson[30] that it should still be applicable even when a flow rule is employed. Crisfield[34] acted on this conclusion when he used the Prandtl-Reuss flow rule in conjunction with the approximate yield criterion as the basis of his 'area approach' method of solution for the large deflection elasto-plastic analysis of isolated plates.

The Prandtl-Reuss flow rule was originally intended for application to materials which yielded according to the von Mises' yield criterion. Although the proposed yield function was derived on the basis of such a material, the resulting single-layer formulation represents a departure (approximation) from the original approach. The present application of the Prandtl-Reuss flow rule, therefore, needs further examination.

3.2.3 Elasto-Plastic Tangential Rigidities

The derivation of these rigidities, shown below, is similar to that given by Crisfield[34]. It is presented here in more general

terms through the use of the orthotropic in-plane and bending elastic rigidities given respectively by:

$$\underset{\sim}{C} = \begin{bmatrix} C_x & C_1 & 0 \\ C_1 & C_y & 0 \\ 0 & 0 & C_{xy} \end{bmatrix} = \begin{bmatrix} \dfrac{F_x t}{1-\mu_x\mu_y} & \dfrac{\mu_y F_x t}{1-\mu_x\mu_y} & 0 \\ \dfrac{\mu_x F_y t}{1-\mu_x\mu_y} & \dfrac{F_y t}{1-\mu_x\mu_y} & 0 \\ 0 & 0 & F_{xy} t \end{bmatrix} \quad .. \ 3.4$$

and

$$\underset{\sim}{D} = \begin{bmatrix} D_x & D_1 & 0 \\ D_1 & D_y & 0 \\ 0 & 0 & D_{xy} \end{bmatrix} = \begin{bmatrix} \dfrac{E_x t^3}{12(1-\nu_x\nu_y)} & \dfrac{\nu_y E_x t^3}{12(1-\nu_x\nu_y)} & 0 \\ \dfrac{\nu_x E_y t^3}{12(1-\nu_x\nu_y)} & \dfrac{E_y t^3}{12(1-\nu_x\nu_y)} & 0 \\ 0 & 0 & \dfrac{E_{xy} t^3}{12} \end{bmatrix} \quad .. \ 3.5$$

The inclusion of the orthotropic rigidities was to study the behaviour of plates in the elastic range. It was not intended that the elasto-plastic response of a stiffened plate could be analysed by using idealised orthotropic properties.

Replacing the parametric form of Ilyushin's approximate yield criterion, equation 3.2, by the definitive set of six stress resultants produces the following equation:

$$f = \frac{1}{t^2\,\sigma_o^2}\left(N_1^2 - N_1N_2 + N_2^2 + 3N_3^2\right) +$$

$$\frac{16}{t^4\,\sigma_o^2}\left(M_1^2 - M_1M_2 + M_2^2 + 3M_3^2\right) +$$

$$\frac{4}{\sqrt{3}\,t^3\,\sigma_o^2}\left|M_1N_1 + M_2N_2 - \tfrac{1}{2}M_1N_2 - \tfrac{1}{2}M_2N_1 + 3M_3N_3\right| \leq 1 \quad .. \ 3.6a$$

where subscripts 1 and 2 refer to the primary orthogonal directions on the centre-plane of the plate, and 3 to the shear or twist component. Subscript notation will be used in this part of the formulation with i, j, k and l referring to the in-plane components, and p, q, r and s to the moment components. Unless indicated otherwise, each subscript will adopt in turn the values 1, 2 and 3 and a repeated subscript indicates summation. A comma is used to indicate differentiation with respect to the generalised stress resultant corresponding to the succeeding subscript.

The corresponding terms in equations 3.2 and 3.6a are:

$$Q_t = \frac{1}{t^2 \sigma_o^2} (N_1^2 - N_1 N_2 + N_2^2 + 3N_3^2)$$

$$Q_m = \frac{16}{t^4 \sigma_o^2} (M_1^2 - M_1 M_2 + M_2^2 + 3M_3^2)$$

and $$Q_{tm} = \frac{4}{t^3 \sigma_o^2} (M_1 N_1 + M_2 N_2 - \tfrac{1}{2} M_1 N_2 - \tfrac{1}{2} M_2 N_1 + 3M_3 N_3)$$

Equation 3.6a can now be rewritten in the form:

$$f = Q_t + Q_m + \frac{S}{\sqrt{3}} Q_{tm} = 1 \qquad \ldots. \quad 3.6b$$

where $S = Q_{tm}/|Q_{tm}|$ the significance of which is discussed in Section 3.5.3.

The onset of yield is determined by equation 3.6. For flow within a perfectly plastic material to remain on the yield surface, any variation in the generalised stress resultants must be such that no variation occurs in f, that is,

$$f,_i \Delta N_i + f,_p \Delta M_p = 0 \qquad \ldots. \quad 3.7$$

The plastic strain increments can be found using the Prandtl-Reuss flow rule as:

$$\Delta\varepsilon''_j = \lambda f,_j$$
$$\Delta\phi''_q = \lambda f,_q \qquad \ldots\ 3.8$$

where λ is the plastic strain multiplier.

The elastic increments in the stress resultants are determined from:

$$\Delta N_i = C_{ij}(\Delta\varepsilon_j - \Delta\varepsilon''_j)$$
$$\Delta M_p = D_{pq}(\Delta\phi_q - \Delta\phi''_q) \qquad \ldots\ 3.9$$

where C_{ij} and D_{pq} are the subscripted versions of the rigidities given by equations 3.4 and 3.5 respectively (the first index indicates the corresponding row in the matrix), and $\Delta\varepsilon_j$ and $\Delta\phi_q$ are the total increments of midplane strain and curvature. After substitution from equation 3.8, these become:

$$\Delta N_i = C_{ij}(\Delta\varepsilon_j - \lambda f,_j)$$
$$\Delta M_p = D_{pq}(\Delta\phi_q - \lambda f,_q) \qquad \ldots\ 3.10$$

Making use of equation 3.7, the plastic strain multiplier is found as:

$$\lambda = \frac{f,_i\ C_{ij}\ \Delta\varepsilon_j + f,_p\ D_{pq}\Delta\phi_q}{f,_k\ C_{kl}\ f,_l + f,_r\ D_{rs}\ f,_s} \qquad \ldots\ 3.11$$

so that the generalised stress resultant increments given in terms of the generalised total strain increments are:

$$\Delta N_i = C^*_{ij}\ \Delta\varepsilon_j + R^*_{iq}\ \Delta\phi_q$$
$$\Delta M_p = R^*_{pj}\ \Delta\varepsilon_j + D^*_{pq}\ \Delta\phi_q \qquad \ldots\ 3.12$$

where C^*_{ij} and D^*_{pq} are the elasto-plastic equivalents to the elastic

axial and flexural rigidities, C_{ij} and D_{pq}, and, R^*_{iq} (= R^*_{pj} for i=j and p=q) is the interaction rigidity. The elasto-plastic tangential rigidities are given by:

$$C^*_{ij} = C_{ij} - \frac{C_{im}\, f_{,m}\, f_{,n}\, C_{nj}}{f_{,k}\, C_{kl}\, f_{,l} + f_{,r}\, D_{rs}\, f_{,s}}$$

$$D^*_{pq} = D_{pq} - \frac{D_{pt}\, f_{,t}\, f_{,u}\, D_{uq}}{f_{,k}\, C_{kl}\, f_{,l} + f_{,r}\, D_{rs}\, f_{,s}} \quad \ldots\ 3.13$$

$$R^*_{iq} = - \frac{C_{im}\, f_{,m}\, f_{,v}\, D_{vq}}{f_{,k}\, C_{kl}\, f_{,l} + f_{,r}\, D_{rs}\, f_{,s}}$$

where m and n apply to the in-plane components and t, u and v to the flexural components.

3.3 NUMERICAL METHOD

3.3.1 Introduction

The numerical method adopted here for the study of plate behaviour is 'dynamic relaxation'. It is a quasi-dynamic iterative procedure for solving two dependent sets of non-homogenous differential equations.

In the application of dynamic relaxation to plates, the plate equilibrium equations constitute one of these sets. They are incorporated into three equations of motion representing the three orthogonal plate displacements and, as such, are treated as out-of-balance forces which impart components of accelerations to each of the displacements. By integrating the acceleration components twice with respect to time the displacements can be calculated. The exact response at any period of time is governed by the values of the damping factors and either the densities or the time increments which arise through the use of the equations of motion.

After application of any displacement boundary conditions, strains can be calculated and the out-of-balance forces found from the second set of differential equations which relate strains to stresses through the appropriate elastic or elasto-plastic rigidities. Stress boundary conditions are then applied after which displacements are recalculated and the cycle repeated.

The iterative procedure is pursued until the total kinetic energy calculated as the sum of the squares of the velocities reaches an acceptably low level. This convergence can also be checked by monitoring displacement and stresses at critical regions of the plate to ensure they have achieved essentially stationary values.

Dynamic relaxation lends itself conveniently to the analysis of the finite difference form of the basic equations and here the central difference formulation has been used.

Dynamic relaxation has been discussed in detail by Rushton[35] and Cassell[36] and, therefore, only aspects of the current method which differ significantly from these earlier approaches will be discussed in detail here. The previous authors differ in their procedures when dealing with densities and time increments and that suggested by Cassell[36] will be the one adopted for this analysis.

Rushton[35] solved the von Karman[37] form of the large deflection plate equations using dynamic relaxation, and Williams[38] extended it to include initial distortions (based on the work of Marguerre[39]) and orthotropy.

Lowe[40] incorporated material non-linearity with an associated flow rule into the small deflection plate equations, and Rushton[41]

recently extended his solution to include material non-linearity, but without a flow rule.

Williams'[38] form of the equilibrium and stress-strain equations has been used in this analysis to determine behaviour in the elastic range.

3.3.2 Fictitious Densities

Through the use of a unit time increment it has been shown[36] that a fictitious density at node i can be given by:

$$\frac{1}{4} \sum_{j} |S_{ij}|$$

where S_{ij} are the elements of the stiffness matrix written in displacement terms. Strictly, only deflections that vary within the iterative loop should be included in these expressions, indicating that separate density formulations should be made for boundary nodes, and for adjacent nodes when displacement boundary conditions are used. In the present approach the same density expressions were used throughout the plate and to date no refinement has appeared necessary.

In the elastic range, each generalised stress resultant is a function of at most two strain components, for example $\Delta N_1 = f(\Delta\epsilon_1, \Delta\epsilon_2)$. Therefore, for each stress resultant, the contribution to a fictitious density involves displacement terms from one or two strain components. However, as illustrated by equation 3.12, for behaviour in the plastic range, each stress component is a function of all six strain variables. Ideally, the density expressions should be extended to include the additional terms when post-elastic behaviour is being analysed but this has proved unnecessary.

3.3.3 Boundary Conditions

The fundamental difference when dealing with boundary conditions for the post-elastic range compared with the elastic region is that the option of using either stress or displacement conditions is no longer readily available. Unless a stress resultant is to remain at zero throughout the full loading schedule, the use of such a boundary criterion is precluded since it would eventually require violation of equation 3.7, that is, the generalised stresses must remain on the yield surface. However, if a hardening material were used in place of the perfectly plastic one adopted here this restriction would no longer be necessary.

An appreciation of the differences in edge formulation that occur when plastic flow occurs can be seen in the simple support condition. For a non-deflecting boundary in the elastic range, this reduces to zero curvature transverse to the edge; or, in finite difference terms, $w_{ext} = - w_{int}$.

In the plastic regime, however, the governing equation is, (equation 3.12):

$$\Delta M_p = R^*_{pj} \Delta\varepsilon_j + D^*_{pq} \Delta\phi_q = 0 \qquad p = 1 \text{ or } 2$$

which for, say $\Delta\phi_1 = 0$, still leaves the edge curvature expression $\Delta\phi_2$ a function of four strain components. Consequently, the external w displacement is not simply the negative of the first internal out-of-plane displacement, and generalising, a more complex formulation is required for boundary elements in the elasto-plastic range compared with that necessary for the purely elastic problem.

3.3.4 Interlacing Meshes

Interlacing meshes were used in the analysis and the lay-out is illustrated in the figure below. The arrangement is that recommended by Cassell[36] for the calculation of stresses from displacements when a finite difference formulation is used.

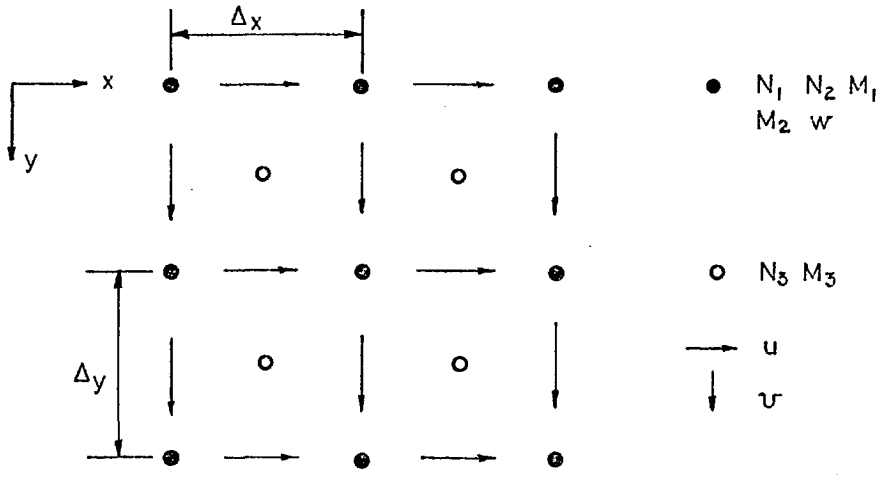

The alternative is a non-interlacing mesh in which all the stress and displacement variables are calculated at each node. The interlacing mesh has an advantage over the non-interlacing mesh in that displacements required for the calculation of stress resultants normally lie within half a grid width ($\Delta x/2$, $\Delta y/2$) of the stress node rather than at the full grid width as in the single mesh system. Consequently, for the same degree of accuracy, the number of nodes required in either direction for interlacing meshes is only some two-thirds of that needed for the alternate system. This leads to a considerable saving in computer time and storage.

The above argument applies only in the case of nodes that are elastic when each stress resultant is dependent on one or two

strain components. In the plastic range, however, the six generalised strains influence behaviour at each stress node and their influence can be assessed in either one of two ways. Firstly, the strains can be determined from the basic finite difference equations derived for each node: this would result in two groups of generalised strains, one for each of the sets of N_1 and N_3 nodes. Secondly, for say, an N_3 node, the strains calculated at the four adjacent N_1 nodes can be averaged and this value used at the shear node. In this approach only one set of strains has to be generated so that it has a storage advantage over the first method. Consequently, the second approach has been adopted in the current analysis.

When calculating the stress resultant from one grid appropriate to a point on the interlacing mesh, the average of the values at the four adjacent nodes has been used.

The N_1 nodes were normally selected as edge nodes. However, N_3 nodes were adopted wherever symmetry was used to reduce the amount of computing, as for example, across the centre-lines of plates in compression. This arrangement was preferred since N_3, M_3 and u or v are zero at such locations and provide uniquely defined boundary conditions. This probably contributes to a more rapid convergence of the solution.

The number of nodes required to achieve a sufficient degree of accuracy without recourse to the use of excessive computational time and storage is illustrated in Fig. 27. For an increasing number of nodes, the same in each direction, the maximum out-of-plane deflection and average stress ratio are plotted against applied strain for a square plate in uniaxial compression (Fig. 27a) and pure shear (Fig.

27b). The results for the plate in compression show little difference between the solutions with 10 and 14 nodes indicating the suitability of a 9 × 9 mesh (10 nodes per edge) for plates under this type of loading. Figure 27b shows that shear loading does not produce such satisfactory results for a similar number of nodes. However, because the lack of symmetry for plates in shear leads to a significant increase in computational time it was decided to use the 8 × 8 mesh (9 nodes) for these panels and accept that the maximum loads could be in error by up to 4 per cent.

3.4 INITIAL IMPERFECTIONS

3.4.1 Out-of-Plane Deformations

Plate initial deformations are accounted for in the analysis by the Marguerre[39] modifications to the von Karman[37] large deflection equations.

3.4.2 Residual Stress

For a given level of compressive residual stress in an initially flat plate the necessary width of idealised tensile yield zone (Fig. 28) can be determined by considering equilibrium, and vice versa. However, with the finite difference formulation of stresses, nodal values represent average stresses on a width of plate equal to the node spacing. Since the mesh length rarely corresponds to the width of the tensile yield zone, the idealised residual stress pattern cannot always be represented exactly in finite difference formulations. Thus the residual stress attributed to a node is determined by averaging the total force under the idealised pattern acting on a width of plate equal to half the mesh length on either side of the node (see Fig. 28).

The idealised welding residual stresses are in equilibrium only in the case of perfectly flat plates, so that in combination with initial bows, a relaxation procedure is required to restore equilibrium. During this process which is accompanied by additional out-of-plane movement, the compensatory longitudinal shrinkage is restricted so that the ends are free to pull-in but remain straight. Subsequent loading is taken relative to the shortened plate.

Residual stress is incorporated as an additional component directly into the expression for the longitudinal stress resultant to give:

$$N_1 = \Delta N_1 + N_1^p + N_R \qquad \ldots\ 3.14$$

where ΔN_1 = increment in the longitudinal stress resultant as given by equation 3.12,

N_1^p = value of the longitudinal stress resultant at the end of previous increment, and

N_R = residual stress resultant.

This approach is similar to the use of an initial plastic strain in finite element and related formulations.

The residual stress distribution was assumed to be uniform along the length of the plate to eliminate end effects (high in-plane shears) and so represent more accurately actual conditions of continuity in a plate being treated analytically in isolation.

3.5 NUMERICAL PROCEDURE

3.5.1 Flow Chart

A flow chart of the program is shown in Fig. 29. Application of the yield criterion and calculation of the appropriate rigidities is shown in Fig. 29a, and the residual stress relaxation procedure is illustrated in Fig. 29b. The former shows that application of the yield function and the subsequent calculation of elasto-plastic rigidities is outside the dynamic relaxation iterative loop, and that the rigidities calculated at the end of one load application apply without modification throughout the next increment. Consequently, as each increment is a linear step only small increases in load (applied displacement) are permitted, especially when significant changes in the rigidities are occurring such as at first yield, if the behaviour is to be traced with acceptable accuracy.

The chart also illustrates the use of the plastic strain multiplier λ. This variable is a function of strain as well as stress (equation 3.11) and is used to check loading or unloading from the yield surface. For a negative λ the elastic rigidities replace the elasto-plastic tangential rigidities, otherwise the latter are modified in accordance with equation 3.13.

3.5.2 Finite Increments

The use of finite steps to approximate the infinitesimal increments assumed in the theory introduces errors into the differentials such that the variation of f is no longer zero. This is compensated for after each increment by factoring the stress resultants, for every node at yield, normal to the surface. The resultants are immediately recorded as N_i^p and M_p^p so that at the beginning of the next

increment at every node $f \simeq \sigma_o^2$. This procedure for preventing accumulation of errors has no effect upon the magnitudes of the elasto-plastic rigidities since it is the relative and not absolute values of the stress resultants that determines a particular rigidity (see equation 3.13).

The result of using different increment sizes can be seen in Fig. 30 where the usual pattern of strain increments is compared with two other cases, one with twice as many and the other with half as many steps, for behaviour in the elasto-plastic range. As can be seen in the figure, the out-of-plane deflection was identical in all three cases. From the average stress-strain curves, the effect of using twice as many increments as normal can be seen to make little difference to the result, whereas halving the number introduces significant differences at various positions along the plots. The 'normal' increment size was generally dictated by the number of nodes yielding within any increment: this was restricted to a relatively small proportion of the number already plastic.

Factoring the stress resultants can lead to the situation where a node at yield during the previous increment is apparently no longer so, according to the yield criterion, for the current load level. When such a situation arises, the sign of the plastic strain multiplier is checked and accordingly designated as either elastic or plastic (see flow chart, Fig. 29a).

No particular account is taken of nodes that are elastic at the beginning of an increment but plastic at the end other than to ensure that increments are generally kept small so that penetration of the yield surface is minimal.

3.5.3 Incorporation of Elasto-Plastic Rigidities

If the denominator in equation 3.13 is expanded, it is found to be of the form:

$$G_1 N_1^2 + G_2 N_1 N_2 + G_3 N_2^2 + \ldots\ldots$$

where G_1, G_2, G_3 ..... are linear combinations of the orthotropic elastic rigidities (constants). The unspecified terms of this expression contain the remainder of the set of products of stress resultants that appear in equation 3.6a and, for example, G_1 is given by:

$$G_1 = \frac{1}{t^4}\left(4C_x - 4C_1 + C_y\right) + \frac{S^2 4}{3t^6}\left(4D_x - 4D_1 + D_y\right) \quad .. \quad 3.15$$

where $S = Q_{tm}/|Q_{tm}|$.

Similarly, expanding the numerators in equation 3.13 leads to another set of equations for each element of the elasto-plastic rigidities. For instance, the numerator corresponding to C^*_{11} is

$$G_{14} N_1^2 + G_{15} N_1 N_2 + G_{16} N_2^2 + \ldots\ldots$$

where G_{14}, G_{15}, G_{16} ..... are further combinations of elastic orthotropic rigidities. Also, when the equation for λ is developed similar groupings arise. In fact, when all components of the elasto-plastic rigidities and of λ are written in full some 290 constants are required to completely describe the set of stress resultant products. However, it was found that all the constants were linear combinations of a basic set of ten linear expressions in the elastic axial and flexural stiffnesses so that the complete set of constants could be calculated readily.

Thus the relative ease with which these constants could be generated, together with the fact that nearly all the products of the stress resultants were needed in the determination of f, suggested that matrix formulation of the problem was not necessary and in any case would be computationally time consuming. Consequently, all the elasto-plastic rigidity expressions were fully expanded and used directly in that form which also had the distinct advantage that it was consistent with the way the dynamic relaxation part of the problem was formulated.

The variable S appearing in equations 3.6b and 3.15 was introduced by Crisfield[34] so that the magnitude of the interaction expression could be monitored and set equal to zero if $\frac{1}{\sqrt{3}} |Q_{tm}| < 10^{-4}$. This was proposed because of the discontinuity that occurs in the partial derivatives of f as $Q_{tm} \to 0$ and because, for either in-plane dominant or bending dominant conditions, f is more accurately represented by assuming $Q_{tm} = 0$ (see equation 3.3).

However, if the expressions for the elasto-plastic rigidities are examined for either limiting load condition, then further justification for adopting this constraint can be found. From equation 3.15, the coefficient for N_1^2 in the denominator of the rigidity equations, it can be seen that its magnitude is influenced by both the axial and flexural elastic constants. It seems unlikely, however, that the axial stiffness of a perfect plate under pure in-plane loading would be influenced by flexural stiffnesses, so that S should be equal to zero for this limiting case. Consequently, although setting S equal to zero is necessary for defining the onset of yield more satisfactorily and ensuring continuity of the differentials, it is also essential in the

present flow rule application to the yield function to ensure that, in the limit, the elasto-plastic rigidities are correctly assessed. If this restriction is not applied then it has been found that the average stress-strain curve for a perfect plate of low slenderness is of bi-linear form with the plateau having an apparent 'hardening' factor of some 10 per cent.

3.5.4 Interlacing Meshes

Although interlacing meshes offer both computational time and store advantages particularly in the elastic range, there is a small disadvantage in their use for behaviour in the elasto-plastic range. This arises from the duplication of some elasto-plastic tangential rigidities on both N_1 and N_3 meshes since, although averaging stresses is justified to cater for the interlacing meshes, the averaging of rigidities is not acceptable. Consequently, although 21 rigidities are necessary to define completely behaviour beyond yield, this has been increased through duplication to 29, which represents an increase of nine per cent in the total number of arrays stored by the program.

3.5.5 Computer Requirements

The program has been written in Fortran IV and on the CDC6400 computer occupies some 27600 words of core: the maximum array size corresponding to this store requirement is 18 × 10. For one increment using 200 cycles of the dynamic relaxation loop and analysing one-quarter of a square plate (9 × 9 mesh for whole plate), nine seconds of computer time are required. The time is only slightly dependent on whether the increment is elastic or elasto-plastic since calculation of the elasto-plastic rigidities takes a relatively short period of time.

After the first increment and just prior to application of each further increment, convergence has been accelerated by factoring all the displacements by an amount equal to the ratio of the current load level to the previous load level. As a result fewer dynamic relaxation cycles are necessary with a corresponding saving in total computational time.

3.6 COMPARISONS WITH EXISTING ANALYSES

3.6.1 Multi-Layer Solutions

Few large deflection elasto-plastic solutions for plates under even simple loading conditions are available. Moxham[42] produced results for a simply supported plate in uniaxial compression with edges unrestrained in-plane. These were determined using a Rayleigh-Ritz approach in which the three orthogonal plate displacements were represented by eight Fourier coefficients. The energy was calculated at five layers through the plate with 18 stations along each edge (symmetry was employed to reduce the analysis to one-quarter of the plate). Initial imperfections were incorporated by assigning initial plastic strain values equal and opposite to those calculated for an 'unloaded' plate into which the imperfections had been set.

More recently Crisfield[34], in addition to his 'area approach', also developed a 'volume approach' but provided few solutions using this method. Both approaches were incorporated into a finite element program in which the total potential energy was minimised, convergence being assisted by the use of Newton-Raphson or modified Newton-Raphson iterations.

The most extensive set of multi-layer solutions available are those provided recently by Harding[43]. His formulation is similar to that adopted here in that dynamic relaxation is used to solve large deflection elasto-plastic equations in which the rigidities are calculated outside the main iterative loop. The rigidities, however, are determined on a multi-layer basis by subdividing the plate into five layers and calculating the strain in each layer from the single-layer strains determined within the dynamic relaxation loop. The layered stresses can then be found from the stored elasto-plastic rigidities and a new set of rigidities calculated and saved. The rigidities were derived by application of the Prandtl-Reuss flow rule to the von Mises' yield criterion, an approach similar to Crisfield's 'volume approach'[34]. The new layered rigidities are then integrated to give single-layer values which are used in the next iterative loop.

Comparisons made by Harding[43] with other multi-layer solutions, in particular that developed by Crisfield, show that similar peak loads are predicted by all methods, but beyond this the solutions tend to slowly diverge. The load-end shortening curves for four plates in compression resulting from Harding's multi-layer solution and the present single-layer analysis are shown in Fig. 31. They show that peak load is predicted within some $3\frac{1}{2}$ per cent but that behaviour beyond this point is more conservatively predicted by the single-layer approach. The largest difference in estimating maximum load occurs in the case of the b/t = 55 panel (curve B, Fig. 31) the slenderness for which, in an ideally flat mild steel plate, the elastic critical buckling stress coincides with yield stress. The behaviour of such a plate will be particularly sensitive to surface

yield, and since this is ignored in the present analysis the single-layer solution will predict that yield occurs at a later stage than that predicted by the multi-layer approach. The occurrence of yield will also be depicted more suddenly in the single-layer solution since the elasto-plastic rigidities influence the full depth of the plate rather than just part of the depth as in the multi-layer method. The combination of the delay in predicting yield and of the more dramatic influence at the onset of plasticity causes the pronounced 'peaky' behaviour in the b/t = 55 plate seen in Fig. 31. For plates of different slenderness where critical buckling and yield do not coincide, the difference between the single and multi-layer solutions near first yield will be less marked: this can be seen in curves A, C and D of the figure.

3.6.2 Single-Layer Solutions

Crisfield[34] has provided the only other single-layer solutions which can be compared with the results of the current analysis. The comparisons are shown in Fig. 32 where two versions of Crisfield's solutions are presented. The curve marked 'original' is that presented in reference 34 and those designated 'current' can be found in reference 31. The modified results arose through improvements to the finite element aspects of his program.

In Fig. 32, it can be seen that the results from the Crisfield 'current' solution and from the present analysis are in good agreement.

Crisfield has further modified his single-layer approach in an attempt to allow for surface yielding[44]. However, the results produced by this appear less satisfactory than this earlier approach when compared with a multi-layer solution[43].

CHAPTER 4

COMPARISON OF EXPERIMENTAL AND THEORETICAL RESULTS

4.1 INTRODUCTION

The satisfactory correlation of theoretical results derived for isolated components with the results of experiments on practical steel structures incorporating such members presents many problems. Assumptions made in the theory relating to such parameters as material properties, boundary conditions, etc. are generally over-simplifications of the real conditions. For example, in the cases under discussion the plate panel boundaries in the theoretical model are assumed to lie in the same plane, whereas the real panel boundaries almost certainly do not; furthermore, the actual plate which is continuous over stiffener supports is idealised in the theory as an isolated panel with edge restraints only approximating those provided by plate continuity. In the case of residual stresses, apart from the general fact that the distribution is far from clearly understood, the idealised pattern used in the theory is a very simplified model of that which occurs in practice. It is useful to be aware of these difficulties when considering the correlation of theory and test results described in the remainder of this chapter.

4.2 COMPRESSION FLANGE PLATES

4.2.1 Boundary Conditions

The out-of-plane boundary conditions selected for the isolated panel to represent a plate forming part of a wide stiffened

flange were the simple support and the non-deflecting edge. The former accounts for the possibility of the plate panels deforming in the elastic critical buckling mode in which no rotational restraint is provided between adjacent panels, whilst the latter was selected not only because of the difficulty in establishing the appropriate vertical spring stiffness to be used to represent the support provided by the longitudinal stiffener, but also on the supposition that it approximated closely the true situation.

The tangential in-plane boundary condition considered appropriate for compression plates is that of zero shear stress: this arises from the symmetry exhibited by plates in the critical buckling mode. In the longitudinal direction uniform displacement was selected for the in-plane loading condition normal to the end of the plate. This was chosen for three reasons. Firstly, in the critical buckling mode, symmetry dictates that this is the correct condition. Secondly, and more importantly from the numerical analysis point of view, applying displacement rather than stress boundary conditions enables the unloading part of the average stress-average strain curve to be followed. Thirdly, stress boundary conditions other than a zero stress value cannot readily be used where an elastic-perfectly plastic material is being analysed because penetration of the yield surface could happen which would conflict with one of the basic assumptions of the analysis. The choice of the in-plane boundary condition normal to the longitudinal edge depends upon the position of the plate within the compression flange. Plates at the edge of a wide stiffened flange, or anywhere within a narrow flange with only one or two longitudinal stiffeners, are

treated as unrestrained. Those at the centre of a wide multi-stiffened panel can be considered from symmetry to have edges free to translate but forced to remain straight.

For the analysis of the test results, most of the plate panels were assumed to have edges free to move in but constrained to remain straight. The only exception was the edge panel of Model 9 which was treated as unrestrained.

4.2.2 Initial Imperfections

Models 1 and 2 were subjected to more than one cycle of loading to collapse. The initial imperfections in panels involved in failure during the second and third tests were modified during the preceding load cycles. In the case of Model 1, however, insufficient deflection records were available from the first test to determine the modified profiles for the subsequent tests. This was not the case for Model 2, so this model is considered first.

The procedure for establishing the initial imperfections for use in the compression plate analysis will be discussed in some detail for Model 2: less detail will be presented on the other models.

4.2.2.1 *Model 2:* During the first test on Model 2, collapse was precipitated by plate buckling in the end bay adjacent to the end cross-frame. Initial imperfections had not been measured at this cross-section so that an analysis of this plating was not possible. During this test, however, out-of-plane movement of the compression flange plate in the direction opposite to the stiffener outstand was noted in the adjacent bay. Inspection of the initial

deformations in this region (Fig. 7) showed that at the position of the buckle, i.e. section Q between the two stiffeners closest to the south web, the plate had distorted inwards transversely, but longitudinally an outward bow was apparent. An analysis was undertaken on a square section of plate, the centre-line of which coincided with section Q. A doubly-sinusoidal initially deformed shape was assumed with a maximum amplitude equal to the off-set at Q relative to a line joining P and R on the longitudinal centre-line of the plate. Since residual stresses had not been recorded at this particular cross-section, the average value of residual stress measured in the centre bay was used in the analysis. The resulting average stress-strain curve is shown as the upper plot in Fig. 33 and the particular values of initial bow and residual stress used are listed in Table IV in the column headed "measured initial imperfections". The analysis was repeated using values for the initial imperfections which included the residual out-of-plane deflections and strains noted at completion of the first test: the modified values are also listed in Table IV. The lower curves shown in Fig. 33 relate to this case. Material and geometrical properties used in the analysis are shown on the figure and also listed in Table I: Poisson's ratio was assumed to be 0.3.

The most convenient experimental value with which to compare the theoretical result is the average midplane stress in the flange at maximum load assuming a fully effective cross-section. However, this underestimates the plate strength because amplification of the applied stress occurs through out-of-plane movement of the stiffened panel between cross-panels: the P-Δ effect. Inter-

action with the stiffener has been treated theoretically in three ways. These are discussed in detail in Section 4.3 but the Model 2 results will be considered here to confirm the use of the particular orientation of measured initial bow and also aspect ratio which is discussed in Section 4.2.3.

The strut analysis results are presented in Table V and the Model 2 values are all seen to be similar and equal to some 94 per cent of the experimental result. The theoretical and test results show good agreement although some enhancement of the experimental value can be expected through continuity of the strut over the transverse stiffeners.

The longitudinal orientation of plate initial bow indicated correctly the direction of movement under load. Also the use in the analysis of the value of initial distortion measured longitudinally gave a theoretical strength which showed good correlation with the experimental capacity. As a result, it was decided to use the longitudinal rather than transverse profile of compression plates to calculate the magnitude of initial bow for use in the analysis.

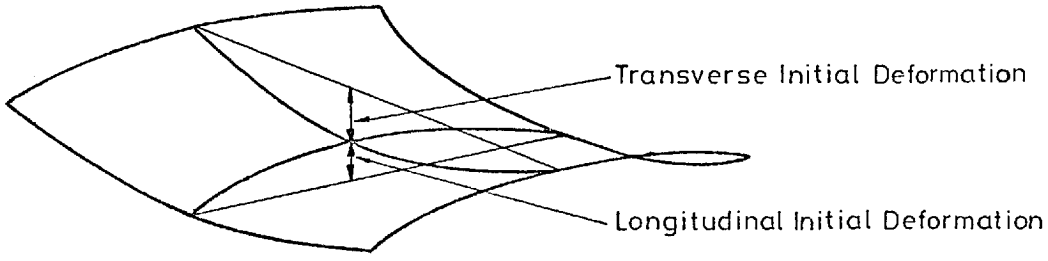

4.2.2.2 *Model 1:* The compression flange plate at Section H of this model moved most during testing. This section was situated one-third of the bay length from the centre diaphragm. During the second test the centre panel had initially deflected inwards but towards the end of the test the direction of movement had reversed. Since the adjacent plates had both deformed inwards throughout their loading history, the one with the larger initial bow was selected for study. The initial bow and residual stress measured in this panel (south of centre) are listed in Table IV.

No records of the residual deflections of Test 1 are available. Thus only the residual deflections and strains of Test 2 have been added to the measured imperfections to give the corresponding values listed in Table IV.

4.2.2.3 *Model 9:* The three panels whose experimental behaviour was presented earlier were selected for analysis. They were positioned on the transverse centre-line of the model.

After the preliminary test, which was terminated just as yield occurred at the flange-web junction, residual strains were recorded in the outer flange panels. Deflections were not measured at the sections on either side of the centre-line so that no modifications to the initial bows could be made. The magnitude of the residual distortions was less than .005 in. which, although small, was larger than the measured initial deformation of all three panels. Thus in Table IV the only imperfection shown modified is that of residual stress in the outer panel.

From Table IV, it can be seen that plates 2 and 3 were extremely flat. For plate 3 with the larger bow, the initial deformation is only equal to width/11800 or thickness/240.

4.2.3 Aspect Ratio

Because of the good agreement between the experimental and theoretical strengths shown by Model 2 (Table V) it was decided to adopt a square plate for the remainder of the compression flange panel studies. It had been expected that an analysis of the whole panel between transverse stiffeners might be necessary although such an approach would present several difficulties. Firstly, in the longitudinal direction some 26 nodes would be required in the analysis since advantage could not be taken of symmetry: this would be extremely expensive on computer time. Furthermore, for the models subjected to moment gradient the variation of direct stress along the long plate would have to be incorporated. This would complicate the analysis compared with that of a square plate since the latter can reasonably be represented longitudinally by a uniform stress.

4.3 THEORETICAL COMPRESSION FLANGE STRENGTHS

Interaction with the stiffener has been treated theoretically in two basic ways. Both methods involve the analysis of an isolated strut pin-ended between transverse stiffeners. The strut section is formed by a longitudinal stiffener and an associated section of plate equal in width to the stringer spacing.

The first method used is that described by Moolani[28] in which the response of the plate is calculated from the appropriate

average stress-strain curve and that of the stiffener is found from the bilinear stress-strain relationship. An initial shape is assumed for the strut and internal and external moments are then matched iteratively at a number of stations along the length. Load is applied through the effective centroid at each end of the strut and failure is usually marked by lack of convergence of curvature near midspan. This normally occurs when the tangent stiffness of the plate average stress-strain curve is approaching zero but can be due to tension yield at the tip of the stiffener.

The second strut analysis used is a method described by the author[57]. In this single-step approach the additional stress at midspan due to initial bowing of the strut is amplified by a factor of the form $1/(1 - P/P_{cr})$. The stress at midspan is then limited to tensile yield at the tip of the outstand, or to the level of stress at midplane of the plate corresponding to the secant stiffness used to calculate the effective width of plating acting with the outstand; the effective width of plate is assumed to be constant along the length of the column.

In this second approach[57] a variation of the basic method was proposed to avoid the need to consider both types of initial imperfections. In this case, an equation was derived for converting residual stress into an equivalent geometrical deformation. The concept of a 'limiting stress' and a corresponding 'limiting secant stiffness' was introduced for use in conjunction with this equivalent deformation where the limiting values were determined from the plate average stress-strain curve when the tangent stiffness reached an arbitrarily low value.

4.3.1 Model 2

The average stress-strain curves for both the measured initial imperfections and for those modified by Test 1 are shown in Fig. 33. Total central out-of-plane deflection for the latter imperfections is also shown plotted against average applied strain. The imperfections are listed in Table IV and the material properties indicated on the figure are also presented in Table I.

The maximum stress ratios predicted for the compression flange of Model 2 by the above methods are compared with the experimental result in Table V. The strut initial bow consists of the measured distortion (initial plus residual after Test 1) and the effective eccentricity of the flange force due to the stress gradient through the depth of the stiffener caused by overall bending. The latter was calculated assuming a fully effective plate as this represents the conditions existing at the ends of a strut. For the simplified approach discussed by the author[57], the strength was calculated using both the plate average stress-strain curve (Fig. 33) and the limiting stiffness-stress concept based on the calculation of an equivalent deformation. Table V shows that the theoretical strengths are in good agreement with the experimental ones.

4.3.2 Model 1

The average stress-strain curves for both the initial imperfections and those measured after Test 2 are presented in Fig. 34. The effect of the large initial bow and level of residual stress can be seen in the reduced secant stiffness of the latter curve throughout the full loading history.

The results of the strut analyses are presented in Table V. Since the stiffener initial bow and deflections under load were not measured, the value of strut distortion used has been assumed to be twice that of Model 2. Two of the results show reasonable agreement with the experimental value bearing in mind that continuity effects will be greater here than for Model 2. This arises from the use of bearing pads over the central diaphragm of the earlier model which have the effect of restricting outward movement of the stiffeners in the adjacent bay thereby providing some rotational restraint to the ends of the stiffeners in question.

The value obtained using the equivalent deformation and limiting stiffness-stress approach[57] considerably underestimates the experimental result. However, the equivalent deformation was derived for levels of residual stress up to 0.33 times yield stress and as the present value is twice this limit, it is not surprising that the agreement is less satisfactory.

4.3.3 Model 9

Both average stress and out-of-plane deflection have been plotted against average strain for the three plates shown in Fig. 35. The effect of the flatness of plates 2 and 3 can be seen in both the average stress and out-of-plane deflection curves. The former are linear until yield occurs just before peak load after which a rapid unloading is noted, and the latter are very similar to the classical elastic buckling curve. Although plate 2 is the flatter, the higher residual stress in this panel causes it to yield first and then buckle.

Of the plates analysed, plate 3 had the highest capacity. It was also probably the strongest of the Model 9 plates because of those not analysed all had an initial bow at least three times that of plate 3 and, where recorded, residual stresses greater than those found in this panel. Only the stiffeners associated with plate 3 have been considered because they were the last to undergo out-of-plane movement in the test. Each had an outward initial bow but the addition of the eccentricity due to the stress gradient through the depth of the stiffener produced a net inward distortion in both struts. The stiffener with the smaller initial bow was analysed and the results are presented in Table V. The equivalent deformation approach[57] gives the lowest estimate of strength but since the plate initial deformation was outside the range for which this method was established good agreement is not necessarily expected. The other approaches estimate the strength within 8 per cent. Although some enhancement of the experimental strength through continuity is expected suggesting good agreement with the theoretical result, the influence of the unusual longitudinal stress gradient, which has been ignored in the strut analysis, is far from certain.

Another aspect of the behaviour of this model which needs further consideration is that of redistribution of direct stresses within the compression flange. It was noted during the test that the outer plates and stiffeners moved out-of-plane prior to collapse of the entire cross-section. Presumably some of these components are on the unloading part of their load-end shortening curve thereby increasing the thrust on the components still retaining a positive tangent stiffness. Assuming that this is the case then

the experimental result listed in Table V will underestimate the strength of the centre strut of this model. A more thorough analysis of the entire compression flange is needed to deal satisfactorily with this problem.

4.4 WEB PLATES

Because extensive experimental data was available on the panels which appeared to precipitate collapse of Models 5 and 7, these will be dealt with in some detail in the following sections. Model 1 will then be considered in the light of the theoretical results of these models.

4.4.1 Loading

Although the webs of the models were subjected to longitudinal direct stress gradients, this variation was ignored in the analysis and the distribution on the transverse centre-line was assumed to be uniform along the panel. The value of extreme fibre direct stress at midbay was calculated from the cross-sectional properties determined assuming the shear lag effective widths contained in reference 45. The close proximity of the neutral axis to the midheight stiffener enabled a zero direct stress to be assumed for the top edge of the tension zone panels. The extreme fibre direct stress to shear stress ratio given in Table VI was calculated assuming a uniform shear stress distribution over the web depth.

4.4.2 Boundary Conditions

The edges of the web plates were assumed to be simply supported and fixed against out-of-plane movement. The appropriate in-plane boundary conditions for web panels are more difficult to determine than in the case of compression plates. The latter generally have the advantage of symmetry which exists unchanged both in the pre- and post-buckling states, whereas the former not only have no symmetry prior to buckling but also some of the in-plane restraints appear to alter with load and, more particularly, with buckling.

Two in-plane boundary restraints seem to be applicable throughout the complete loading history. These are the tangential or v displacements along the vertical edges and the normal restraint at the bottom edge of the tension zone panel. They are illustrated in Fig. 36 together with the other boundary conditions used in combination with these two restraints.

The use of displacements tangential to the vertical edges of the panels is required for applying the shear loading beyond yielding. The displacements were considered to be uniform along the edges because of the relatively high axial stiffness of the vertical stiffening along these boundaries. This condition remains constant provided failure of the vertical stiffeners or diaphragms does not occur: none was observed in the models reported herein.

The bottom edge of the panel was assumed to be unrestrained normally, that is, $N_2 = 0$, because of the low flexural rigidity of the tension flange. The magnitude of the self inertia of the flange is one feature which distinguishes the box from the plate girder. At

the top edge the normal restraint seems dependent on the state of buckling of both the panel in question and the adjacent panel. Prior to buckling of either panel, the top edge displacements are a combination of the linear shear and the circular bending displacements given by linear elastic theory (see a, Fig. 36). However, after buckling the large membrane forces produced by out-of-plane movement induce non-uniform displacements normal to the edge which can only be determined by an analysis of at least the whole web bay. Here the post-buckled condition is represented by zero normal stress, $N_2 = 0$ (b and c, Fig. 36). Both conditions were considered separately and therefore each was applied throughout the complete loading history. This was necessary because it is difficult to determine during which part of the loading each should apply.

The tangential boundary condition adopted for the top and bottom edges was that of uniform displacement. At the lower boundary the in-plane shear stiffness of the tension flange ensures the displacements will be reasonably uniform. At the upper edge the longitudinal stiffener will not be nearly as effective but since the direct stress is zero here it is probably still a reasonable assumption.

The normal boundary condition at each end of the panel is influenced by both the state of buckling of the plate in question and of the longitudinally adjacent panels, and by the longitudinal position of the panel within the girder. For those adjacent to a diaphragm, symmetry in both the pre- and post-buckling states dictates a linear distribution of displacements normal to the ends. For other internal edges prior to buckling, a non-linear variation should be used because

the assumption 'plane sections remain plane' does not strictly apply in the presence of high shear stresses. After buckling the membrane forces between adjacent panels introduce significant non-linearity along the interface which can only be studied by incorporating more than one bay into the analysis. For web bays at the ends of a girder, the plates can be taken as unrestrained along the external boundary, that is, $N_1 = 0$. Thus for panels adjacent to a diaphragm or at the end of a girder, each end has a different boundary condition. This has not been taken into account in an effort to keep the parameters within manageable limits and the same boundary condition was used for each end of the panels analysed. Consequently internal panels were assumed to have a linear distribution of normal or u displacements along each vertical boundary (a and b, Fig. 36), while external panels were treated as unrestrained (c, Fig. 36).

4.4.3 Initial Imperfections

It was noted earlier that some tension zone panels had deformed with two half waves in the longitudinal direction. Thus to suit the assumed doubly-sinusoidal waveform within the analysis, a 'best fit' sine wave in each direction was determined for those panels where extensive initial deformation data was available. The magnitudes of the waves in both directions were averaged to give the value listed in Table VI. The plates were analysed with this value of initial bow together with the number of longitudinal half waves determined from the 'best fit' curves in this direction (see Table VI). A single half wave was used in the transverse direction.

Residual stresses were generally determined from the values recorded in the panel in question. In Model 1 residual strains were not measured in the two outer bays. Thus for the middle bay the residual stress was assumed to be equal to that in the adjacent centre bay, while for the end bay half this value was used.

Relaxation of both imperfections arising from earlier tests was checked in Models 5 and 7. No modifications were required for Model 5, but after the preliminary test on Model 7 relaxation of the residual stresses was noted. Only out-of-plane deflections of the centre bays of Model 1 were checked upon completion of Tests 1 and 2. However, because not all the available cross-sections were recorded during the earlier test only changes in the central out-of-plane deformation could be assessed. Where available, the modified initial imperfections are listed in Table VI.

When analysing the web plates, it was found that during relaxation the correct value of initial bow could not be obtained for some of the panels. Calculations showed that for these plates the measured value of residual stress was in excess of the elastic critical buckling stress in compression. A value of residual stress equal to some 90 per cent of the theoretical critical value was tried and the analysis proceeded satisfactorily. These reduced values of residual stress are shown in parenthesis in Table VI.

4.5 THEORETICAL WEB STRENGTHS

4.5.1 Models 5 and 7

The web plates of Models 5 and 7 were analysed with the elastic proportions of shear and triangular bending tension (Section

4.4.1) applying throughout the full loading history. The panels were assumed to have the in-plane boundary conditions appropriate to the pre-buckled state, that is, linear displacements along each vertical edge and linear shear plus bending curvature displacements at the upper edge (a(i), Fig. 36). The results are shown as curves of average shear stress against average shear strain in Figs 37 to 39 (solid curves marked a) which can be seen to exceed the experimental results by between 11 and 23 per cent. They also have a softening characteristic beyond the knee of the curves.

The analyses were repeated with the upper edges unrestrained, that is, $N_2 = 0$, to represent the post-buckled condition along this boundary (b(i), Fig. 36). These results are indicated by the solid curves marked b in Figs 37 to 39 and are in excess of the test values by between 6 and 18 per cent. The average shear stress-shear strain characteristics beyond the knee are again falling but not to the same extent as for the previous boundary condition.

In order to establish a lower limit for the results of the shear plus bending loading cases, the panels were analysed with their vertical boundaries unrestrained, that is, $N_1 = 0$, (c(i), Fig. 36). For this, in-plane bending was applied by means of tangential or u displacements at the top and bottom edges. The resulting average shear stress-shear strain curves are shown as the solid curves marked c in Figs 37 to 39. They have pronounced falling characteristics and overestimate the experimental strengths by between 0 and 8 per cent.

The results presented above were considered unsatisfactory from two points of view. Firstly, the theoretical predictions of

maximum strength were always non-conservative and in some cases quite significantly so, and secondly, the average shear stress-shear strain curves all had softening characteristics. Apart from boundary conditions and the plate parameters, maximum strength and the degree of softening are influenced by a number of factors. The type of loading will probably have the greatest effect on the maximum value but will also influence the extent of softening. It was noted earlier (Section 3.3.4) that the mesh size adopted for the web panel analyses would produce values of the peak strength which were some 4 per cent non-conservative. The use of strain hardening and an alternative yield function (Section 3.6.1) in the analysis would reduce the degree of softening and would possibly even reverse the response in the case of the longitudinally restrained and vertically unrestrained panels. Reflecting on the experimental behaviour of the box girder models, it was observed that once the shear stiffness fell to a low level any further application of jack displacement produced only shear displacements of the models. This was shown by the fact that during this period of the tests the direct strains in the flanges remained essentially constant[20]. Consequently, since the type of loading influenced the entire average stress-strain curve and only shear displacements were noted during the final stages of the model tests, it was decided to repeat the web plate analyses with pure shear loading.

The boundary conditions appropriate for the pure shear cases are shown in Fig. 36 a(ii), b(ii) and c(ii). They are identical to the previous examples except that the longitudinal or u displacements at the lower edges are now equal to zero. The resulting average shear stress-shear strain curves are shown as dashed lines in Figs 37 to 39.

The response of the partly vertically and longitudinally restrained plates (dashed curves a, Figs 37 to 39) seems dependent on the geometrical imperfection. The panels with single and three half wave initial bows all have softening characteristics but those with two half waves have both hardening and softening responses. The maximum capacities of these panels are in excess of the test results by between 4 and 13 per cent.

Removing the part vertical restraint leads to the dashed curves marked b in Figs 37 to 39. They have either a plateau or a slight hardening characteristic and predict capacities greater than the test values by between 0 and 10 per cent.

The results for the completely unrestrained panels (dashed curves c, Figs 37 to 39) again show significant softening responses which suggest this boundary condition is not appropriate for internal web plates. It thus appears that some normal restraint as well as tangential restraint is required to support the diagonal tension forces generated by shear buckling if the plateau type of response characteristic of plates failing in shear is to be obtained.

Bearing in mind the influence of mesh size on the peak values and of the single-layer yield function on the degree of hardening or softening, the best correlation with the experimental results is obtained when the panels are assumed to be vertically unrestrained and longitudinally restrained and loaded in shear only. However, it is not easy to appreciate how all the direct stress could be shed from the webs to the flanges. Indeed both the current experimental evidence and the concept of movement of stresses on the yield surface suggest this only applies to additional direct stresses

once yielding has occurred. If the minimum theoretical result for each of the models is considered (Table VII), the average of these varies from 1.02 to 1.11 times the experimental result for the pure shear and shear plus bending loading cases respectively. Thus, if direct stress shedding could be accounted for, the current approach would estimate strengths intermediate to these limits.

4.5.2 Model 1

The tension zone web panels of this model were analysed with shear loading only. Because of the limited geometrical imperfection data, the plates were all assumed to have a single half wave bow so that for the middle and end bays only the panels with the largest initial distortion were analysed. For the centre bays, collapse occurred experimentally in bay JO so again the plate with the larger initial bow in this bay was analysed. For Tests 2 and 3, the measured initial imperfections were used only if the relaxed values had not been measured. Unfortunately, satisfactory numerical convergence could not be achieved with the relaxed value of initial bow for the Test 3 panel and twice the plate thickness was therefore assumed in the analysis.

The average shear stress-shear strain curves for Model 1 are presented in Fig. 40. Since the Test 1 plate was at the end of the model it was treated as unrestrained (c(ii), Fig. 36), but the Tests 2 and 3 plates were assumed to be restrained at each end (b(ii), Fig. 36). The Test 1 result has a softening characteristic and the ratio of theoretical strength to experimental strength is 1.038. Both the other results show a hardening characteristic and the ratios of theoretical to experimental strength are .989 and .995 for Tests 2

and 3 respectively. The kink in the Test 3 plate curve appears to be associated with the development of the diagonal tension field.

The experimental load-deflection curve for Test 1 (Fig. 16) seems to be forming a plateau, but in the absence of further experimental evidence it should be treated as unrestrained. The load-deflection curve for Test 2 (Fig. 16) has an unusual characteristic prior to the development of a plateau. It is to be expected, therefore, that the theoretical curve would show little correlation with the experimental plot in the vicinity of the peak in the latter. The plateau in the experimental curve, however, is closely predicted by the theoretical result. For the third test, the experimental maximum load is accurately predicted by the theoretical result although the experimental plot was almost linear up to peak load in contrast with the continuing drop in stiffness observed in the analytical curve. Of course, the two previous tests to which Model 1 was subjected cannot be reproduced analytically so that significant differences in the theoretical and experimental load-deflection responses are to be expected.

4.6 INFLUENCE OF COMPONENT BEHAVIOUR

4.6.1 Compression Flanges

If stiffened compression flanges are treated as a set of independent isolated struts supported by transverse stiffeners, failure can occur in either the plate or the outstand mode: only plate collapse is considered here. For slender struts, Euler buckling will precipitate failure and plate strength will have no

effect on the result. For stocky stiffeners with both plate and outstand material of similar yield stress, strut behaviour will be dominated by the response of the plate and, therefore, influenced by the plate parameters such as slenderness and initial imperfections. For struts of intermediate slenderness, failure will be influenced by both plate and stiffener parameters.

The proximity of the strut strengths to the maximum plate strengths of Models 1 and 2 reflects the fact that the stiffeners of these girders are in the stocky range where behaviour is dictated by plate response. In Model 9, despite the small initial bow of span/2140, the reduction in strength below peak plate capacity due to interaction between the plate and the stiffeners caused by strut out-of-plane movement is proportionally greater than in the other two girders. The increased influence of stiffener factors on the response of this model is not surprising since the slenderness ratio, L/r, of the fully effective strut, 75.4, lies close to the value of 78.0 at which the Euler buckling stress equals the plate yield stress.

From Table V it can be seen that the method described by the author[57] using the plate average stress-strain curve provides the best estimate of the experimental strengths. In this approach, however, compression yield at the base of the stiffener is ignored. The method described by Moolani[28] accounts for the reduction in in-plane stiffness which is initiated by this yielding but it was noted this phenomenon was not a criterion for collapse. This is presumably because the base of the outstand lies close to the centroid of the stiffener-plate combination so that loss of stiffness here will not have a large effect of on overall behaviour. The correlation

shown by the equivalent deformation approach[57] with the other methods is good only where the plate initial imperfections lie within the formers' limitations such as in the case of Model 2.

All the methods for determining compression flange strut strengths are conservative in comparison with the experimental results. However, continuity has been ignored and this will enhance the test values. For Models 1 and 9 the effect of a non-uniform stress gradient has been ignored in all the analyses and, in the case of Model 9, the influence of redistribution of the direct stresses within the flange has not been considered: both these phenomena require further study.

4.6.2 Webs

The strength of vertically and longitudinally stiffened webs of plate girders has been found to be dependent upon the buckling stress of the weakest sub-panel[46]. The same criterion seems to apply to box girders although it has been shown[21] the buckling stress is not that given by the combination of stresses determined from linear elastic theory. Following buckling, according to the 'collapse mechanism' approach[47], tensile membrane forces develop which when combined with the buckling stress produce yield on a diagonal band. The inclination of the yielded band is dependent in part on the plastic moment capacity of the flanges about their own axis and for the box girders studied here would appear to be negligible. For both longitudinally stiffened and unstiffened girders the diagonal membrane field is considered acting over the full depth of the web bay.

The present analysis accounts for both the buckling and the membrane forces and also for the initial imperfections which in the collapse mechanism approach are accounted for by means of a reduced buckling stress. Reasonable estimates of the shear strengths of Models 1, 5 and 7 have been obtained by using boundary conditions appropriate to the post-buckled condition and bounding the values between those obtained by loading the plates in pure shear and in shear plus in-plane bending. Thus satisfactory results have been obtained without need to resort to an analysis of the complete stiffened bay.

The parameters studied in the present work were limited. The in-plane bending component of loading considered was that of tension only. Whether this approach can be extended to panels in the compression zone of webs or to longitudinally unstiffened webs is yet to be confirmed. Also, the ratio of extreme fibre direct stress to shear stress determined from linear elastic theory was limited to 1.91. Additional test evidence is necessary to establish an upper limit to this ratio. The plates analysed all had an aspect ratio of 1.72 and a depth to thickness ratio of approximately 140. Further experimental data is required to confirm extension of the present approach to plates with significantly different values of these parameters.

CHAPTER 5

PARAMETRIC STUDY

5.1 INTRODUCTION

The established design methods for the buckling of plates in the inelastic range are largely empirical. More recently analytical techniques have been developed which can investigate the problem on a rigorous analytical basis[42,34]. However, none of these procedures has been used in a systematic way, either to provide information for the design of such panels, covering the range of practical parameters, or to confirm or modify the existing empirically based methods. This chapter describes a parametric study of the behaviour of plates in compression in which, in particular, the influence of practical levels of initial deformation and residual stress on both strength and stiffness was studied.

A major part of the work was directed towards plates with boundary conditions appropriate to internal panels of stiffened steel compression flanges of box girders. A smaller part was devoted to plates that could be used in stocky box columns, as edge panels of stiffened flanges, or as compression flanges of unstiffened box girders. The application of these results to the design of plates with rigid supports, such as stocky box columns and the ends of stiffened compression panels, is presented.

The program described in Chapter 3 was used in the analysis, and the equivalent of a 9 × 9 interlacing finite differ-

ence mesh on a square panel was adopted throughout, although symmetry was employed to reduce the actual analysis to only one-quarter of each plate.

A report on this study has been prepared and submitted to the sponsors[48].

5.2 PRELIMINARY STUDIES

5.2.1 Effect of Aspect Ratio

5.2.1.1 *High Aspect Ratio:* The average stress-strain curves for plate panels with an aspect ratio of three and with single half-sine wave initial deformations of amplitude 1/80 b/t mm and 1/10 b/t mm are shown in Fig. 41. They are compared with curves for square plates with the same magnitude of initial out-of-flatness and the same slenderness, namely, b/t = 60. The figure shows that in both cases the initial stiffness and the peak load are considerably enhanced for the longer plate compared with the square panel of the same initial bow. This even occurred in the 3 to 1 panel with the smaller initial deformation despite the fact that it underwent a mode change (to three half-waves) while still elastic. Although for this panel the final capacity was less than could be sustained by the equivalent square panel, it is the maximum load and corresponding secant stiffness that are the important factors.

A similar comparison was undertaken for panels with a slenderness ratio of 20. All cases produced the same average stress-average strain plot, one that was similar to the elastic-perfectly plastic material stress-strain curve. No mode change was observed for either level of initial distortion in these panels.

These results indicated that although the effect of large aspect ratio was dependent both on the level of initial deformation and the slenderness, nonetheless the square plate would generally provide conservative estimates of panel strength and stiffness. It is appreciated, however, that in panels which form part of the stiffened compression flange of a box girder or the bottom plating of a ship, or indeed in many test panels, the aspect ratios will normally be greater than three, and also that the level and form of the initial distortions in these plates will differ significantly from those adopted here. Nevertheless, since these deformations are generally basically cylindrical in nature the stiffness and strength derived from square panel analyses will be conservative and thus appropriate for design.

5.2.1.2 *Low Aspect Ratio:* For a slenderness ratio of 60 and initial deformation magnitudes of 1/10 b/t mm and 1/80 b/t mm, the aspect ratio was varied between 0.67 and 1.0. The resulting average stress-strain curves are shown in Fig. 42a (note the use of a non-zero origin) and the insert shows how the maximum average stress ratio varies with aspect ratio for the smaller deformation. It indicates that a minimum value of peak stress occurs at an aspect ratio of 0.74. In contrast, it is clear that for the larger initial deformation no such minimum occurs within the range of aspect ratios studied.

Figure 42b shows the effects of the same parameters but now the non-planarity varies with length instead of width. Similar comments can be made for these panels as for the preceding ones.

A similar preliminary study on panels with a b/t = 20 again indicated that the influence of aspect ratio was dependent upon the magnitude of the initial deformation. In this case, no minimum was observed for the panel with the smaller amplitude of initial bow leading to the conclusion that the effect of aspect ratio was different for panels of different slenderness ratios. The importance of b/t when considering the effect of aspect ratio had been noted earlier by Moxham[42]. It was concluded, therefore, that since the effect of aspect ratio was dependent upon the level of initial deformation as well as slenderness ratio, there was no conclusive evidence for selecting a particular aspect ratio as a basis for a study on compressed plates which would have general application to all compression panels.

5.2.2 Effect of In-Plane Restraint

The influence of different in-plane restraints along the unloaded edges was studied. The three boundary conditions considered were zero transverse displacements ("restrained"), free to pull-in but remain straight ("constrained") and stress free ("unrestrained"). Curves showing the effect of the varying transverse restraint are given in Fig. 43 (note the non-zero origin).

Results for the stocky plate (Fig. 43a) show the beneficial effect on strength of the biaxial compressive stress associated with the restrained condition, although this effect decreases with increasing initial deformation. There is no significant difference between the constrained and unrestrained cases at this slenderness ratio.

In the case of the b/t = 60 panel with the smaller initial deformation (Fig. 43b), the constrained edge maximum capacity was greater than that of the restrained panel although the latter could sustain a higher load for straining beyond 1.3 times yield strain. However, for the largerinitial deformation, the restrained case had a significantly higher capacity. At this slenderness the capacity of the constrained panel was at all times well above the unrestrained case reflecting the restraint afforded by enforcing zero relative transverse displacements along the unloaded edges.

Comparing Figs 43a and 43b shows that the pattern of influence of edge restraint is different for each slenderness ratio. The conclusion from this particular study was, therefore, that the influence of in-plane restraint along the unloaded edges was dependent upon slenderness ratio as well as the magnitude of initial deformation.

5.2.3 Elimination of Some Parameters

In view of the fact that both aspect ratio and in-plane boundary restraint effects are dependent upon the magnitude of initial deformation as well as slenderness ratio, it was decided not to pursue their influence beyond this preliminary point, but to select a square plate with edges constrained to remain straight as the most appropriate for the major part of the remainder of the study. The constrained boundary condition was considered to represent most closely that relating to a typical internal panel of a multi-stiffened flange plate. For edge panels, compression flanges of unstiffened box girders, or box columns, unrestrained edges are considered to be appropriate.

5.3 PRESENTATION OF STUDY

5.3.1 Panel Definition

The plate panel used in the main part of the study had the following features:

(i) simple supports fixed against out-of-plane movement,

(ii) unloaded edges constrained in-plane to remain straight but free to pull-in,

(iii) loaded edges held straight and displaced uniformly,

(iv) zero shear stress along all edges,

(v) an aspect ratio of unity,

(vi) an elastic-perfectly plastic material stress-strain curve,

(vii) doubly-sinusoidal initial deformations,

(viii) an idealised rectangular residual stress pattern (see Section 3.4.2), and

(ix) plate slendernesses in the range $0.7 \leqslant \beta \leqslant 2.8$ ($20 \leqslant b/t \leqslant 80$ for mild steel).

With the reference plane oriented so that the x-axis corresponds to the direction of applied loading, condition (ii) is analogous to ensuring that the (uniform) transverse displacement of the y edges is such that $\int_0^a N_2 \, dx = 0$.

A smaller study was carried out on panels complying with all the above conditions except (ii). On this occasion the unloaded edges were free to pull-in.

5.3.2 Initial Imperfections

The values of initial bow and residual stress used in this study were primarily selected to encompass those given in the Interim Design and Workmanship Rules[10]. For initial deformations the limits were selected to represent the minimum and twice the maximum assumed in the Rules, whilst for residual stress values up to a maximum of one-third of yield stress were selected. The particular values selected are listed in Table VIII together with their non-dimensionalised equivalents. Note that the selected values of initial deformation are not expressed in non-dimensional terms but in mm despite the use of b/t in their formulation. A panel width of 240 mm was used throughout the study.

5.3.3 Average Stress-Strain Curves

Average stress-strain curves were determined in the analysis by averaging the longitudinal stresses at the end of a panel for each level of applied strain. They are shown in Figs 44 to 83 where for each value of β, firstly, the effect of increasing residual stress on each selected value of initial bow, and secondly, the influence of varying the magnitude of initial deformation upon the selected values of residual stress are presented. In the curves the abscissa represents the average strain applied to the panel divided by the strain corresponding to uniaxial yield, whilst the ordinate is the average stress recorded at the ends of the panel non-dimensionalised with respect to yield stress. The IDWR[10] values of initial imperfection corresponding to those indicated on the curves can be found in Table VIII.

All of the plate panel average stress-strain curves were obtained using an elastic modulus of 205000 N/mm^2 and a yield stress of 245 N/mm^2. (These particular values were recommended in the brief from the Overall Behaviour Sub-Group.) However, a number of cases were re-run with the latter parameter increased to 355 N/mm^2 and with b/t revised so that the value of the expression $b/t\sqrt{\sigma_o/E}$ (=β) remained unaltered. It was found that, provided stresses were expressed relative to yield stress and deformations relative to thickness, unique values of $b/t\sqrt{\sigma_o/E}$, σ_R/σ_o and δ_o/t produced unique average stress-strain and average stress versus out-of-plane deformation curves. Consequently, all the average stress-strain curves have been presented in these non-dimensional terms.

Although δ_o/t proved to be the non-dimensionalised form for initial bow, in assessing the effect of this parameter over the range of slenderness ratios under study its direct use was not entirely satisfactory. By choosing to keep b constant for all the panels in the study (and varying t), it was found the δ_o/t values varied with $(b/t)^2$ so that the linear form δ_o/t was not appropriate to embrace the range of initial deformations actually considered. Also, Faulkner[49] found earlier that the best fit to data of δ_o/t varied with β^2, and Dawson and Walker[50] came to a similar conclusion, albeit for cold-rolled sections, when they found that for the most satisfactory agreement to existing data, δ_o/t varied with σ_o/σ_{cr}. As both β^2 and σ_o/σ_{cr} are functions of $(b/t)^2$ it was concluded that presenting δ_o/t as a function of β^2 would be the most appropriate way of incorporating the initial deformations into the

study. Consequently, the selected values of initial out-of-flatness as factors of β^2 are included in Table VIII.

The secondary study on unrestrained panels involved levels of initial distortion which differed slightly from those used in the main work. The reasons for this will be discussed in a later section.

5.3.4 Secant and Tangent Stiffnesses

From the average stress-strain curves for initially stress-free plates, secant (K_s) and tangent (K_t) stiffnesses were determined for any stress level as the ratio of stress to strain and as the slope of the curve at that particular point respectively. They were plotted (Figs 84 and 85) for the various values of δ_o' against $\sigma_x' \beta^2$ which, apart from a multiplying constant, is equivalent to the uniaxial version of the variable adopted in IDWR Part III[10]. The elastic critical buckling coefficient adopted for the Part III variable was that appropriate to simply supported square plates in compression. Curves of secant and tangent stiffness for elastic plates have been presented in IDWR Part III. These were based on the work of Falconer and Chapman[51] and show that for any δ_o' the secant and tangent stiffnesses are independent of slenderness.

Secant and tangent stiffness curves for elastic plates with initial bows of $\delta_o' = .001$ and 1.0 have been included for comparison in Figs 84 and 85.

5.3.5 Constrained Panel Results

5.3.5.1 *Average Stress-Strain Curves:* Except for slender plates with large residual stresses, the effect of increasing initial bow is to reduce in-plane stiffness and the load-carrying capacity of

the plate over its full strain range. In general, the largest reduction occurs in the vicinity of the maximum stress ratio.

In contrast, the effect of residual stress initially has little influence on the average stress-strain curve. However, once yield occurs due to the combination of applied loading and initial stress a reduction in stiffness occurs: the higher the level of residual stress the earlier yield is initiated. While its edges remain elastic (due to the weld tension zone) the capacity of an initially stressed plate is able to increase until it converges on that of the initially stress-free panel. This happens when the edges of the plate yield in compression and it occurs at a strain greater than that corresponding to maximum strength for the initially stress-free plate: in the presence of large residual stresses convergence is observed at strains approaching twice yield strain. Thus, although for panels that can achieve 'squash' conditions, no reduction in strength is noted when residual stresses are present, in general, the loss in stiffness that occurs with the earlier yielding also leads to a reduction in the maximum load capacity. This reduction is not readily apparent in the cases of slender panels with large initial deformations since in this range the detrimental effect of residual stress is completely swamped by the influence of initial bow.

5.3.5.2 *Maximum Load-Slenderness Curves:* For each level of residual stress, including the initially stress-free plates, the maximum average stress has been plotted against slenderness for the various initial bows. Figure 86a shows the curves for σ'_R = 0 and .102 and Fig. 86b for σ'_R = .033 and .327 (note the non-zero origin). Included on Fig. 86a for σ'_R = 0 are curves for δ'_o = .022 and .697,

but these extend only over part of the slenderness range. The IDWR Part III values of initial deformation corresponding to those shown on the figures can be found in Table VIII.

Originally, average stress-strain curves for b/t = 80 (β = 2.766 for σ_o = 245 N/mm^2) were not included in the study. However, as can be seen in Figs 86a and 86b the shape of the plots between slendernesses of 40 and 60 (β = 1.383 and 2.074) would be uncertain without a further point in this range. Therefore, since it was necessary to include an additional b/t ratio, it was decided to extend the slenderness range beyond b/t = 60.

Both Figs 86a and 86b show that an increase in initial bow results in a decrease in capacity: the effect is most pronounced around β = 1.4. Extrapolating the curves into the lower β range indicates that unless δ_o' is greater than .5 β^2 then the magnitude of the initial deformation will have negligible effect on capacity for β less than about 0.55. This corresponds to b/t = 16 for a yield stress of 245 N/mm^2 when δ_o' = .15.

5.3.5.3 *Comparison with IDWR Part III Ultimate Plate Strengths:* For plate panel initial deformations corresponding to the minimum and twice the maximum expected in the Interim Design and Workmanship Rules[10] and for residual stress levels of 0 and 80 N/mm^2, the ultimate strength of plates in compression was calculated in accordance with Part III of these Rules. Their variation with slenderness is shown as Curve 2 in Fig. 87 together with the corresponding curves from the present single-layer analysis. In deriving the Part III predictions residual stress was treated as an additional deformation since in all cases the capacity so derived was greater than

that obtained by treating it as an applied stress. The discontinuity which occurs in these curves for $\beta \simeq 2.6$ is due to the change from using the basic strength equation to using the minimum strength part of the clause.

The Part III curves in Fig. 87 show that except in the case of the smaller deformation in the stress-free plate the plate strengths show very little variation. Chatterjee and Dowling[52] came to the same conclusion after studying the influence of a wide range of imperfections on the Part III ultimate strength predictions. The curves also indicate that for β greater than 2.0 the presence of significant residual stresses enhances the capacity of a plate. This is in contrast with the results from the present analysis particularly in the case of small levels of initial bow. Again for β greater than 2.0 the Part III predicted strengths are greater for panels with the larger initial deformation. As discussed in Section 5.3.5.2 this is contrary to the results of the present analysis. Comparison of the two sets of curves in Fig. 87 shows very little correlation between the pairs of results and at worst the Part III predictions overestimate by some 27 per cent the present single-layer solutions.

5.3.5.4 *Secant and Tangent Stiffnesses:* Each of the curves in Figs 84 and 85 showstwo distinct phases. The first phase which relates to the elastic behaviour of the panel originates from the vertical axis (at zero stress) and continues more or less parallel to the stress axis until the development of yield becomes critical. This is signified by a rapid deterioration, particularly of the tangent stiffness,as the second phase develops. This phase appears

as a curve of reducing stiffness at more or less a constant stress level.

The elastic parts of the curves confirm that for any δ_o' stiffness is independent of slenderness. In contrast the post-elastic phases are slenderness dependent as can be seen by the groupings of the curves for the different values of β. For each β the effect of increased initial out-of-flatness can clearly be seen to reduce the stress ratio at which yielding is initiated.

The tangent stiffness curves (Fig. 85) clearly indicate the maxima in the average stress-strain curves when they cross the horizontal axis, that is, the tangent stiffness is zero at peak plate strength. Beyond this point although in general the tangent stiffnesses were close to zero they varied in a haphazard manner and have been omitted for clarity. The secant stiffness curves (Fig. 84) showed no such irregular behaviour and have been plotted up to the limits of the stress-strain curves.

Comparison of the elastic part of these curves with those in Part III of the Rules for the edges kept straight condition shows reasonable agreement for small δ_o' but an overestimate of some 15 per cent by the Part III values for large δ_o'.

5.3.6 Unrestrained Panel Results

This secondary study on unrestrained plates followed the major work on constrained panels and was more particularly tied to design imperfections than the earlier study. Consequently, only a few average stress-strain curves have been obtained and the parameters were mainly limited to include initial deformations of $\delta_o' = .145\beta$ and residual stresses of $\sigma_R' = 0$, .102 and .327. Where

the panel slenderness was such that the load-end shortening response was relatively unaffected by the unloaded edge boundary condition, the result for the constrained panel have been used.

5.3.6.1 *Average Stress-Strain Curves:* The load-end shortening response was obtained for panels with slendernesses in the range $1.037 \leqslant \beta \leqslant 2.766$, although for panels with $\beta < 1.4$ the results were more or less identical to those of the constrained panels with the same imperfections. The only noticeable difference for these plates was at strains approaching three times yield strain where the capacity of the unrestrained case was some 97 per cent of that of the constrained plate.

The curves are shown in Figs 88 to 90 and overall no basic difference in behaviour is observed in comparison with the constrained panels except for the drop in strength and stiffness for plates with $\beta > 2.0$.

5.3.6.2 *Maximum Load-Slenderness Curves:* Because of the limited number of unrestrained panel results, the maximum strength-slenderness curves have been expressed directly in a form suitable for design (Fig. 91). Results have been plotted for one magnitude of initial distortion, $\delta_o' = .145\beta$, and for three levels of residual stress, namely, zero, 10 per cent and 33 per cent of yield stress. For $\beta < 0.7$ (b/t = 20 for mild steel) residual stress has no detrimental influence on strength.

5.4 APPLICATION TO DESIGN

5.4.1 Existing Recommendations

5.4.1.1 *Strength:* In reference 53, Chatterjee and Dowling present a critical appraisal of recently proposed design methods for stiffened compression flanges. All the approaches discussed in the report make use of plate strength curves in one form or another. Although the curves were intended for use in stiffened panel component design they were generally based on data from isolated plates or box columns and therefore are directly comparable with the present results.

The first method is that contained in the Interim Design and Workmanship Rules and for which plate strength curves have already been compared with the present analysis. It will not be considered again here.

Methods two and three are based on Faulkner's panel strength curve (equation (13), or generalised form equation (14), in reference 49) although they differ in their treatment of the limiting stress (reduced yield stress) allowed in the formula. The maximum strength equation which was derived on the basis of being a good fit with experimental data is presented in Fig. 92. Comparison with the curve for $\delta_o' = .087\ \beta^2$ from the present analysis indicates close agreement for slendernesses up to $\beta = 2.5$. Beyond this point the present analysis provides higher strengths presumably due to the condition along the unloaded edges: here the edges are constrained whereas Faulkner's equation has been derived for unrestrained plates. However, from the study undertaken on unloaded edge boundary restraint (Fig. 43) it might have been expected that divergence of the

two conditions would have become obvious from a lower slenderness and have been more pronounced for $\beta \geq 2.5$.

Faulkner's treatment of residual stresses is initially based on the use of a constant ratio of width of tensile yield zone to plate thickness for the whole slenderness range which produces residual stresses of 40 per cent and 8 per cent of yield at the extremes of the practical plate range. However, modifications to this influence of residual stress in the stocky panel region leads finally to a reduction of strength over the full range of slendernesses, compared with initially stress-free panels, but with the maximum difference occurring at $\beta = 2.4$. These results conflict with the findings of the present study where for $\beta > 2.5$ and an initial deformation corresponding to Faulkner's basic strength curve, viz. $\delta_o' = .087\ \beta^2$, very little loss of strength was noted in the presence of residual stress.

At the lower end of the slenderness range, Faulkner finds little loss in plate panel strength for initially stressed plates. His proposed strength curves show good correspondence with existing data from box column and simply supported panel tests. The test arrangements provided non-deflecting edge supports to the panels in question and therefore enabled the full strength of the plates to be developed. This is in agreement with the present analysis. However, the full panel strength is only achieved at strains approaching twice yield strain whereas in conjunction with stiffeners 'column type' failure may occur at strains well below this level.

The fourth approach discussed in reference 53 is that based on plate strength curves developed by Little[54]. The curves were

developed partly from experimental data and partly from the average stress-strain curves obtained from an elasto-plastic program and apply to plates with unrestrained edges. In that work a doubly-sinusoidal initial out-of-flatness was assumed with a magnitude $\delta_o' = .001$ b/t and the curve for zero residual stress is shown on Fig. 92. For $\beta < 1.5$, the enhanced strength arising from the use of a smaller original bow than that adopted in the current work is to be expected. However, considering that the initial deformation is increasing linearly with β for Little's curve and with β^2 in the present solution, the depreciation in capacity as depicted in the former case for $\beta > 1.5$ is greater than the current analysis would indicate for the combined effects of using unrestrained edges (Fig. 43) and a reduced aspect ratio (0.875 compared with unity - see Fig. 42).

Little's treatment of residual stress has a similar influence on plate strength as that proposed in reference 49. However, the large strains required to achieve maximum strength in initially stressed plates were noted by Little and some reductions in strength are proposed for application to the design of stiffened plates.

The final method discussed by Chatterjee and Dowling is that proposed by Walker and Murray[55]. Their approach involves the use of two empirical equations which have been derived from an elastic analysis and predict the maximum stress along the edge of a plate. Maximum plate strength is then assumed to occur when this peak edge stress reaches yield. The first equation is for the maximum panel strength of unrestrained plates and includes a general imperfection factor, the proposed form of which is a linear function

of β. By comparison with available test data on isolated steel plates a coefficient of 0.158 was recommended as most appropriate. The coefficient was determined for panels both with and without residual stresses, so that these do not have to be treated separately, and consequently probably overestimate the influence of initial bow in the absence of welding stresses.

The second empirical formula introduced caters for unloaded edges remaining straight but free to pull-in. It is assumed that the above imperfection still applies to this condition and its substitution into the new formula results in the final equation for plate strength: the equation is shown plotted in Fig. 92. Also plotted on this figure is a curve for the present analysis for $\delta_o' = .145\beta$, and comparing it with Walker and Murray's curve shows good agreement for $\beta < 1.8$. Beyond this slenderness ratio, however, the present analysis is significantly underestimated and would only be more so if the graphs in reference 55 were used instead of the equation. A disparity was found between the equation as given and as plotted which amounted to some 7 per cent at $\beta = 2.77$. No reason could be found for the higher value given by the formula.

It should be noted that the first of Walker and Murray's empirical relationships is supposed to be restricted to plates in which the average stress is greater than the elastic critical buckling stress. This condition was violated in nearly all the panels considered by them and in the absence of any alternative formulation for plates in the stocky range the validity of their approach to the problem at hand must be questioned.

5.4.1.2 *Stiffness:* Plate stiffness is particularly important in the context of interactive local and overall buckling such as might occur in slender box columns or at mid-panel of a stiffened plate. Here the concern is with plates in isolation or with rigid supports where maximum plate strength can be achieved, and where any loss of in-plane rigidity has little influence on overall stability until nearly the full plate strength is realised.

5.4.2 Initial Imperfections Appropriate in Design

5.4.2.1 *Initial Deformations:* In Section 5.4.1.1 it was shown that the strength-slenderness curve from the present analysis for an initial bow of $.087\ \beta^2$ compared favourably with a 'good fit' curve to available test data. However, a distortion proportional to panel width/thickness is more practical from the tolerance point of view and, with this in mind, an initial bow of $.145\beta$ might be more appropriate. Although this particular value is less than the maximum anticipated by the IDWR, as indeed is $\delta_o' = .087\ \beta^2$, it does make some allowance for the additional strength expected from plates where the initial bow is not in the lowest critical buckling mode but rather more cylindrical in nature. It also has the advantage of providing a strength curve, based on the present analysis, that lies close to the curve for $\delta_o' = .087\ \beta^2$ over the slenderness range considered, having identical values at $\beta = 1.7$ (Fig. 92).

5.4.2.2 *Residual Stress:* Apart from initially stress-free plates, two broad classifications seem necessary to describe the levels of residual stress likely to be encountered in practice. "Lightly welded" would apply to intermittently welded stiffeners and could be represented by a $\sigma_R' = .1$ (25 N/mm^2 for mild steel),

and "heavily welded" would apply to continuous welding where residual stresses up to 30 per cent of yield could be expected. These particular values were recommended in reference 56 and it would appear that similar conclusions were reached during preparation of the brief for this parametric study.

5.4.3 Constrained Panels

The plating at the end of a stiffened panel can be more critical than that elsewhere for two reasons. Firstly, for a girder which has a moment gradient or a cross-section that varies longitudinally, the stress in the plate adjacent to the orthogonal stiffening can be higher than that near the centre of the panel even in the case where the effects of stiffener bending are additional to the primary loading. Secondly, when a stiffener bows in the direction opposite the outstand the net stress in the plate at mid-panel could be less than at the panel ends. (In the context of stiffener deflections, it is normally assumed that adjacent panels will buckle in alternate modes so that the plate at the transverse stiffener is subjected only to the primary loading.) In either situation the plate at the end of the panel can be treated as an isolated plate with longitudinal edges constrained to remain straight. Recommendations for the analysis and design of such panels are contained in the following paragraphs.

Maximum plate strengths can be obtained from Figs 86a and 86b for panel slendernesses in the range $0.7 \leqslant \beta \leqslant 2.8$. They are suitable for residual stresses up to $\sigma'_R = .33$ and for initial deformations of $.04\ \beta^2 \leqslant \delta'_o \leqslant .4\ \beta^2$. Within these limits of the latter imperfection, extrapolation is permitted beyond the curves presented.

For the case of zero residual stress, two other levels of initial bow are provided within certain slenderness limits. These are for deformations as small as $\delta_o' = .015\ \beta^2$ in the range $2.0 \leqslant \beta \leqslant 2.8$, and up to $\delta_o' = .75\ \beta^2$ in the range $0.7 \leqslant \beta \leqslant 1.4$: a certain degree of extrapolation has again been permitted.

For design, the maximum strength curves relating to $\delta_o' = .087\ \beta^2$ and $\sigma_R' = 0$, .102 and .327 are recommended: they have been redrawn for clarity in Fig. 93 under the residual stress classification of unwelded, lightly welded and heavily welded respectively. The non-dimensionalised slenderness ratio has been replaced by a set of curves which indicate b/t for different levels of yield stress, σ_o. The derivation and use of the curves adjacent to the left-hand axis in Fig. 93 are discussed in Section 5.4.5.

5.4.4 Unrestrained Panels

Unrestrained panels can be found as compression flanges in unstiffened box girders, as edge panels in stiffened flanges, and as the plate components of box columns. It is assumed in these applications that there is no interaction with overall buckling.

For design, the maximum strength curves relating to $\delta_o' = .145\ \beta$ and $\sigma_R' = 0$, .102 and .327 have been recommended: they are shown in Fig. 91 with the residual stress classification of unwelded, lightly welded and heavily welded respectively. The abscissa shows how b/t varies with yield stress and the curves adjacent to the strength axis are discussed in the next section.

5.4.5 Co-existing Shear Stress

In reference 43 an interaction curve for uniform shear and uniform compression has been presented for a plate with an aspect

ratio of unity, b/t = 60 and δ'_o = .5. The curve can be conveniently and closely represented by the equation:

$$\left(\frac{\sigma'_x}{\sigma'_{xm}}\right)^2 + \tau'^2 = 1 \qquad \ldots\ 5.1$$

where σ'_x and τ' are the co-existing direct and shear stresses non-dimensionalised with respect to their yield stress, and σ'_{xm} is the peak stress ratio for the panel in pure compression. Equation 5.1 has been assumed to be valid over the range of slenderness and initial bow considered here and was used to derive the curves shown adjacent to the vertical axis in Figs 91 and 93; levels of shear stress up to two-thirds shear yield are permitted. An example, indicated by dashed lines, shows how the curves are to be used: in this case a σ'_{xm} of .825 and a τ' of .4 give a co-existing direct stress ratio of .755.

For unequal values of shear stress along two edges the use of a value of shear stress equal to two-thirds the sum of the edge values is recommended.

CHAPTER 6

CONCLUSIONS AND FUTURE WORK

CONCLUSIONS

1. Experimental results relating to the ultimate load behaviour of five model box girders have been presented. The models were constructed from structural steel of minimum thickness 1/8 in and were fabricated using normal welding techniques. Consequently, realistic imperfections were introduced into the plate and stiffener components of the model girders. The results show that in these models collapse was initiated by plate buckling in either the web or the compression flange but that in the case of flange failure, interaction between the plate and the stiffener occurred prior to collapse of the entire cross-section.

2. The formulation of a theoretical method for analysing the large deflection elasto-plastic response of plates typical of box girders has been presented. A single-layer yield function and an associated flow rule were adopted and dynamic relaxation was used to solve the plate equations. Comparisons with more expensive finite element and other finite difference methods have confirmed the soundness of the technique.

3. The theory has been used to establish whether the strength of complete stiffened box girders subjected to both pure bending and combined bending and shear can be related to the strength of isolated plate components. The plate boundary conditions assumed constant during the complete loading cycle were chosen to represent

the effects of continuity with the remainder of the structure. Both flange elements failing mainly in compression and web components failing predominantly in shear have been considered by generating average stress-strain curves in compression and shear, as appropriate, for the box girder model panels in which buckling was initiated.

4. The following conclusions were drawn in relation to compression flanges subjected to both pure bending and bending plus shear.

4.1 Use of the plate average stress-strain curves in conjunction with rigorous inelastic column theory gave satisfactory correlation with the experimental results. Good correlation was also achieved using a simple elastically based strut approach to calculate amplification of the stresses in the plate due to out-of-plane bending of the longitudinal stiffeners between cross-frames. Only in the cases where the longitudinal stiffening was extremely stocky was the plate strength information alone sufficient to predict flange collapse. This condition was approached in Models 1 and 2 where the effects of amplification were small.

4.2 In the case of a wide stiffened girder subjected to point load conditions (Model 9), the initiation of plate buckling in an edge panel did not lead directly to collapse of the entire cross-section. This was in contrast with other models suffering compression flange failure and reflected the redistribution capacity of this model in the presence of pronounced shear lag. Indeed, failure of the longitudinal stiffeners at the edge of the model also did not constitute overall collapse. The strength of the model appeared to be determined by that of the plate and stiffeners

at the centre of the flange suggesting that redistribution occurs progressively rather than uniformly across the as yet undistorted panels.

4.3 For the present comparisons, the average stress-strain curves were all derived assuming a uniformly loaded square panel. The satisfactory correlation with experimental results indicates this can be used to represent long plates subjected to stress gradients. Also, the magnitude of the initial bow used in the analyses of the plates was that determined from the profile of the initially deformed shape on the longitudinal centre-line of the square panel.

5. The experimental data relating to the girders loaded in bending and shear and failing by shear of the webs, that is, Models 1, 5 and 7, suggested that collapse of the entire cross-section was precipitated, and indeed limited, by the strength of the weakest panel in shear. Thus the possibility of predicting longitudinally stiffened web strength using an isolated panel analysis looked attractive. However, the choice of the appropriate boundary conditions and type of loading proved a major difficulty. Several combinations of these parameters were tried using an isolated panel and the following conclusions were drawn from the study.

5.1 The idealised welding residual stress block is unsuitable for use in the analysis of panels where the level of residual stress is greater than the elastic critical buckling stress of the plate in compression.

5.2 When the plates were loaded in pure shear and in shear plus in-plane bending estimates of web strengths varied between 1.02

and 1.11 times the experimental results respectively. Allowing for possible post-yield direct stress redistribution indicates a theoretical result which included direct stress shedding would lie intermediate to these values. Since the coarseness of the mesh adopted for the web analyses produces a 4 per cent non-conservative error in the shear strength results, the correlation between the experimental and theoretical results is reasonable.

5.3 Because the experimental data available was not extensive the following limitations on the conclusions relating to webs failing in shear should be noted.

(a) Only tension zone plates have been considered. Extension of this approach to compression zone plates and longitudinally unstiffened webs needs to be checked.

(b) The ratio of direct to shear stress determined by linear elastic theory was limited to 1.91. Additional test evidence is needed to establish an upper limit to this parameter for which the post-yield direct stress component may apparently be redistributed.

(c) The analysis was restricted to plates with an aspect ratio of 1.72 and depth to thickness ratio of approximately 140. Further test data is required to confirm the suitability of the present method for plates with significantly different values of these parameters.

6. The theory was also used to undertake a parametric study on plates suited to stiffened and unstiffened flanges of box girders and box columns. The data generated has since formed the basis of

a new design method to be incorporated in the bridge design code. The following conclusions can be drawn from this study.

6.1 The results from a pilot study on the influence of aspect ratio showed that it was dependent upon both slenderness and level of initial bow. It was also found that the strength and stiffness of long panels could be conservatively estimated using square panel results.

6.2 A parametric study on compression plates with edges free to pull-in but constrained to remain straight has been presented. The range of panel slendernesses considered was particularly suited to the stiffened plating in steel box girder bridges and the parameters studied were initial bow and residual stress. The following aspects of plate behaviour were noted.

(a) Increasing the initial bow of a panel reduces both its stiffness and capacity from the onset of loading, the maximum reduction being in the vicinity of peak load.

(b) The effect of initial bow is most pronounced at $\beta = 1.4$. For $\delta_o' < 0.5\ \beta^2$ initial distortion has no detrimental effect on strength when $\beta < 0.55$.

(c) The presence of residual stress has no obvious initial influence on plate behaviour. However, once yielding is initiated both strength and stiffness are reduced: the higher the residual stress the earlier the onset of plasticity. After yielding the plate retains a positive stiffness until the edge yields. This occurs at a capacity equivalent to that of the initially stress-free

plate so that beyond this point the behaviour of both plates is more or less identical.

(d) For $\beta < 0.7$ residual stress ratios up to 33 per cent of yield have no detrimental effect on maximum strength for $\delta_o' < .35\ \beta^2$.

6.3 Comparing the present solutions with the IDWR Part III predictions of ultimate panel strength and elastic stiffnesses showed that the Part III values are up to 27 per cent and 15 per cent non-conservative respectively over the slenderness range $0.6 \leqslant \beta \leqslant 2.8$.

6.4 The results from a short study on unrestrained plates are presented: the imperfections studied were generally limited to those appropriate to design. Little difference was noted in the response between the constrained and unrestrained plates for $\beta < 1.4$.

6.5 Design curves for maximum strength for both unrestrained and constrained plates are presented. One initial bow and three grades of residual stress namely, unwelded, lightly welded and heavily welded, were adopted for the imperfections. Reductions in strength to allow for co-existent shear were determined from an interaction formula and are given by curves on the design charts.

7. In general, it can be concluded that the study of isolated panels up to and beyond peak load goes some way (although only part of the way it must be emphasised) towards understanding the overall collapse behaviour of box girders. In only a few instances is the study of an isolated panel alone strictly sufficient to

determine the limit of the load-carrying capacity, for example, box girders with unstiffened compression flanges. In all other situations some interaction with adjacent components must be considered as, for example, in the case of flanges, between plate and stiffeners, and, additionally in the case of webs, between the webs and the flanges. Nevertheless, the current studies have contributed towards our understanding of the ultimate load behaviour of box girders.

FUTURE WORK

As further experimental data on box girders becomes available it would be useful to correlate the results with the theoretical strengths predicted by the current theory. In this way the limits at present imposed on the various parameters could be confirmed or modified.

However, the current approach only goes part of the way to providing an understanding of interaction. More benefit would be derived from a method which looks directly at the problem rather than relying on the extrapolation of isolated plate analysis results. The present theory has been used to study elastically interaction between flanges and webs and it is intended to extend this into the elasto-plastic range. Such an approach will lead to a clearer understanding of interaction and, in particular, provide information on the redistribution of stresses between webs and flanges. It is hoped this will lead to a more complete understanding of the ultimate load behaviour of box girders so that simple but rational rules can be developed for the design of these structures.

REFERENCES

1. Pelikan, W. and Esslinger, M. "Die Stahlfahrbahn, Berechnung und Konstruktion", MAN Forschungsheft Nr 7, 1957.

2. German Standard DIN 1073, "Stählerne Strassenbrüchen: Berechnungsgrundlagen", Deutscher Normenausschus, Beuth-Vertrieb, Berlin.

3. Wolchuk, R. "Design manual for orthotropic steel plate deck bridges", AISC, New York, 1963.

4. Troitsky, M.S. "Orthotropic bridges, theory and design", James F. Lincoln Arc Welding Foundation, Cleveland, Ohio, 1967.

5. British Standard 153, Specification for steel girder bridges, British Standards Institution, London.

6. Kerensky, O.A., Flint, A.R. and Brown, W.C. "The basis for design of beams and plate girders in the revised British Standard 153", Proc. ICE, Part III, Vol. 5, 1956, pp396-461.

7. Rockey, K.C. "Web buckling and the design of web plates", Structural Engineer, Vol. 36, February 1958, pp45-60.

8. Richmond, B. "Approximate buckling criteria for multi-stiffened rectangular plates under bending and compression", Proc. ICE, Vol. 20, 1961, pp141-150.

9. Committee of Inquiry into the basis for design and method of erection of steel box girder bridges. Appendix A - Interim design appraisal rules, Department of the Environment, September 1971.

10. Committee of Inquiry into the basis for design and method of erection of steel box girder bridges. Report of the Committee - Appendix 1. Interim design and workmanship rules, Department of the Environment, London, 1973.

11. Committee of Inquiry into the basis for design and method of erection of steel box girder bridges. Report of the Committee, Department of the Environment, London, 1973.

12. Dowling, P.J., Chatterjee, S., Frieze, P.A. and Moolani, F.M. "Experimental and predicted collapse behaviour of rectangular steel box girders", Proc. Int. Conference on Steel Box Girder Bridges, ICE, 1973.

13. Guile, P.J.D. and Dowling, P.J. "Steel Box Girders. Model 1 - Progress Report 1", Engineering Structures Laboratories, Civil Engineering Department, Imperial College, London. CESLIC Report BG1, July 1971.

14. Guile, P.J.D. and Dowling, P.J. "Steel Box Girders. Model 2 - Progress Report 1", Engineering Structures Laboratories, Civil Engineering Department, Imperial College, London. CESLIC Report BG3, November 1971.

15. Guile, P.J.D. and Dowling, P.J. "Steel Box Girders. Model 5 - Progress Report 1", Engineering Structures Laboratories, Civil Engineering Department, Imperial College, London. CESLIC Report BG12, June 1972.

16. Guile, P.J.D. and Dowling, P.J. "Steel Box Girders. Model 7 - Progress Report 1", Engineering Structures Laboratories, Civil Engineering Department, Imperial College, London. CESLIC Report BG14, August 1972.

17. Guile, P.J.D., Moolani, F.M. and Dowling, P.J. "Steel Box Girders. Models 9 and 10 - Progress Report 1", Engineering Structures Laboratories, Civil Engineering Department, Imperial College, London. CESLIC Report BG33, February 1975.

18. Mittleman, M.L. and Dowling, P.J. "Steel Box Girders. Model One - Progress Report 2", Engineering Structures Laboratories, Civil Engineering Department, Imperial College, London. CESLIC Report BG2, September 1971.

19. Frieze, P.A. and Dowling, P.J. "Steel Box Girders. Model 2 - Progress Report 2", Engineering Structures Laboratories, Civil Engineering Department, Imperial College, London. CESLIC Report BG11, June 1972.

20. Frieze, P.A. and Dowling, P.J. "Steel Box Girders. Model 5 - Progress Report 2", Engineering Structures Laboratories, Civil Engineering Department, Imperial College, London. CESLIC Report BG23, June 1973.

21. Frieze, P.A. and Dowling, P.J. "Steel Box Girders. Model 7 - Progress Report 2", Engineering Structures Laboratories, Civil Engineering Department, Imperial College, London. CESLIC Report BG20, February 1975.

22. Moolani, F.M. and Dowling, P.J. "Steel Box Girders. Models 9 and 10 - Progress Report 2", Engineering Structures Laboratories, Civil Engineering Department, Imperial College, London. CESLIC Report BG34, August 1975.

23. DoE - TRRL working group on long-term research into steel box girder bridges. Report of the panel for standard practices for testing, January 1975.

24. Billington, C.J., Ghavami, K. and Dowling, P.J. "Steel Box Girders. Parametric study of cross-sectional distortion due to eccentric loading", Engineering Structures Laboratories, Civil Engineering Department, Imperial College, London. CESLIC Report BG16, September 1972.

25. Chatterjee, S. and Dowling, P.J. "Steel Box Girders. Model 1 - Progress Report 4", Engineering Structures Laboratories, Civil Engineering Department, Imperial College, London. CESLIC Report BG7, May 1972.

26. Chatterjee, S. and Dowling, P.J. "Steel Box Girders. Model 2 - Progress Report 3", Engineering Structures Laboratories, Civil Engineering Department, Imperial College, London. CESLIC Report BG9, May 1972.

27. Mittleman, M.L. and Dowling, P.J. "Steel Box Girders. Model One - Report 3", Engineering Structures Laboratories, Civil Engineering Department, Imperial College, London. CESLIC Report BG4, January 1972.

28. Moolani, F.M. "Ultimate load behaviour of steel box girder stiffened compression flanges", Ph.D. Thesis, University of London, 1975.

29. Ilyushin, A.A. "Plasticite". Editions Eyrolles, Paris, 1956.

30. Robinson, M. "A comparison of yield surfaces for thin shells", Int. J. Mech. Sci., Vol. 13, No. 4, 1971, pp345-354.

31. Crisfield, M.A. "Some approximations in the non-linear analysis of rectangular plates using finite elements", Department of the Environment, TRRL Report SR 51UC, Crowthorne, 1974, (Transport and Road Research Laboratory).

32. Mikeladze, M.Sh. "Theory of perfectly plastic thin shells", Proc. Symp. I.A.S.S. Warsaw (1963), Ed. Olszak and Sawzuk, North-Holland, Amsterdam, 1964, pp722-731.

33. Onat, E.T. "Plastic shells, general report", Proc. Symp. I.A.S.S Warsaw (1963), Ed. Olszak and Sawzuk, North-Holland, Amsterdam, 1964, pp649-659.

34. Crisfield, M.A. "Large-deflection elasto-plastic buckling analysis of plates using finite elements", Department of the Environment, TRRL Report LR593, Crowthorne, 1973, (Transport and Road Research Laboratory).

35. Rushton, K.R. "Large deflection of variable thickness plates", Int. J. Mech. Sci., Vol. 10, 1968, pp723-735.

36. Cassell, A.C. "Shells of revolution under arbitrary loading and the use of fictitious densities in dynamic relaxation", Proc. Inst. Civ. Engineers, Vol. 45, January 1970, pp65-78.

37. Von Karman, Th. "Festigkeitsprobleme in Maschenembau", Encyklopädie der Mathematischen Wissenschaften, 1910 IV.

38. Williams, D.G. "Some examples of the elastic behaviour of initially deformed bridge panels", Civil Eng. & Pub. Wks Rev., October 1971, pp1107-1112.

39. Marguerre, K. "Zur Theorie der gekrümmten Platte grosser Formänderung", Proc. 5th. Int. Cong. appl. Mech., Cambridge, 1938.

40. Lowe, P.A. "Prediction of loading causing unserviceability of reinforced concrete and composite highway bridges", Ph.D. Thesis, University of London, 1969.

41. Rushton, K.R. and Hook, P.M. "Large deflection of plates and beams obeying non-linear stress-strain laws", J. Strain Analysis, Vol. 9, No. 3, July 1974, pp178-184.

42. Moxham, K.E. "Theoretical prediction of the strength of welded steel plates in compression", Cambridge University Report No: CUED/C - Struct/TR.2 (1971).

43. Harding, J.E. "Bolted spliced panels and stress redistribution in box girder components up to collapse", Ph.D. Thesis, University of London, 1975.

44. Crisfield, M.A. "Collapse analysis of box-girder components using finite elements", paper presented at Symposium on Non-Linear Techniques and Behaviour in Structural Analysis, Transport and Road Research Laboratory, Crowthorne, December 1974.

45. Moffatt, K.R. and Dowling, P.J. "Steel Box Girders. Parametric study on the shear lag phenomenon in steel box girder bridges", Engineering Structures Laboratories, Civil Engineering Department, Imperial College, London. CESLIC Report BG17, September 1972.

46. Rockey, K.C., Evans, H.R. and Porter, D.M. "Ultimate load capacity of stiffened webs subjected to shear and bending", Proc. Int. Conference on Steel Box Girder Bridges, ICE, 1973.

47. Rockey, K.C., Evans, H.R. and Porter, D.M. "The ultimate shear-load behaviour of longitudinally reinforced plate girders", paper presented at Symposium on Non-Linear Techniques and Behaviour in Structural Analysis, Transport and Road Research Laboratory, Crowthorne, December 1974.

48. Frieze, P.A., Dowling, P.J. and Hobbs, R.E. "Steel Box Girders. Parametric study on plates in compression", Engineering Structures Laboratories, Civil Engineering Department, Imperial College, London. CESLIC Report BG39, January 1975.

49. Faulkner, D. "A review of effective plating to be used in the analysis of stiffened plating in bending and compression", Report No. MITSG73-11, Massachusetts Institute of Technology, Cambridge, 1973.

50. Dawson, R.G. and Walker, A.C. "Post-buckling of geometrically imperfect plates", Journal of the Structures Division, ASCE, Vol. 98, No. ST1, January 1972, pp.75-94.

51. Falconer, B.H. and Chapman, J.C. "Compressive buckling of stiffened plates", The Engineer, June 5, 1953.

52. Chatterjee, S. and Dowling, P.J. "Steel Box Girders. A review of the stability clauses in the Merrison Rules for steel box girders", Engineering Structures Laboratories, Civil Engineering Department, Imperial College, London. CESLIC Report BG38, January 1974.

53. Chatterjee, S. and Dowling, P.J. "Steel Box Girders. Strength of stiffened compression flanges", Engineering Structures Laboratories, Civil Engineering Department, Imperial College, London. CESLIC Report BG37, October 1974.

54. Little, G.H. "Plate failure in stiffened steel compression panels", Cambridge University Report No. CUED/C - Struct/TR.33 (1973).

55. Walker, A.C. and Murray, N.W. "Analysis for stiffened plate panel buckling", Monash University, Civil Engineering Research Report No. 2/1974.

56. Dwight, J.B., Little, G.H. and Rogers, N.A. "An approach to stiffened steel compression panels", Cambridge University Report No. CUED/C - Struct/TR.32 (1973).

57. Frieze, P.A., Dowling, P.J. and Hobbs, R.E. "Steel Box Girders. A contribution to the design of stiffened compression flanges", Engineering Structures Laboratories, Civil Engineering Department, Imperial College, London. CESLIC Report BG42 (in preparation).

NOTATION

a	Plate length in x-direction
b	Plate width in y-direction
C_{ij} ($\equiv \underset{\sim}{C}$)	Generalised elastic in-plane rigidities
C^*_{ij}	Generalised elasto-plastic in-plane tangential rigidities
C_x, C_y, C_1, C_{xy}	Elastic in-plane rigidities
D_{pq} ($\equiv \underset{\sim}{D}$)	Generalised elastic flexural rigidities
D^*_{pq}	Generalised elasto-plastic flexural tangential rigidities
D_x, D_y, D_1, D_{xy}	Elastic flexural rigidities
e_{i1}, e_{i2}	Equivalent strain at upper and lower surfaces of plate
e_{i0}	Minimum value of equivalent strain
E	Modulus of elasticity (isotropic)
E_x, E_y, E_{xy}	Orthotropic flexural moduli of elasticity
f	Yield function
F_x, F_y, F_{xy}	Orthotropic in-plane moduli of elasticity
G_1, G_2, G_3 ...	Constants of multiplication in the elasto-plastic tangential rigidities
K_s	Secant stiffness ($= \sigma'_x/\varepsilon'_x$)
K_t	Tangent stiffness ($= d\sigma'_x/d\varepsilon'_x$)
L	Transverse stiffener spacing
M_p	Generalised flexural stress resultant (increment ΔM_p)
M_p^P	Total generalised flexural stress resultant at end of an increment
M_1, M_2, M_3	Flexural stress resultants
N_i	Generalised in-plane stress resultant (increment ΔN_i)

N_i^p	Total generalised in-plane stress resultant at end of an increment
N_R	(Longitudinal) residual stress resultant
N_1, N_2, N_3	In-plane stress resultants
Q_t, Q_m, Q_{tm}	Non-dimensionalised quadratic stress intensities for single-layer yield function
r	Radius of gyration of strut with respect to axis parallel to plate
R^*_{iq}, R^*_{pj}	Generalised elasto-plastic interaction tangential rigidities
S	$= Q_{tm}/\lvert Q_{tm}\rvert$
S_{ij}	Stiffness matrix in displacement terms
t	Plate thickness
u	In-plane displacement in x-direction
u_a, u_b	In-plane displacements applied at upper and lower edges of plate
v	In-plane displacement in y-direction
w	Out-of-plane deflection in z-direction
x, y, z	Longitudinal, transverse and normal cartesian co-ordinates
Δx, Δy	Node spacing in x- and y-directions
α	Ratio of equivalent strains at lower and upper surfaces
β	Plate non-dimensionalised slenderness ratio $(= b/t \sqrt{\sigma_o/E})$
γ'	Shear strain (non-dimensionalised with respect to shear yield strain)
δ	Measured out-of-plane deflection
δ_o	Maximum amplitude of doubly-sinusoidal initial deformation

δ'_o	$= \delta_o/t$
ε_x	Longitudinal average strain
ε'_x	$= \varepsilon_x/\varepsilon_o$
ε_o	Yield strain
$\Delta\varepsilon_j$	Generalised in-plane total strain increment
$\Delta\varepsilon''_j$	Generalised in-plane plastic strain increment
λ	Plastic strain multiplier
μ_x, μ_y	In-plane Poisson's ratios
ν_x, ν_y	Flexural Poisson's ratios
ρ	Ratio of minimum equivalent strain to equivalent strain at upper surface
σ	Direct stress
σ_{cr}	Elastic critical buckling stress for ideally flat plate
σ_R	Average compressive residual stress
σ'_R	$= \sigma_R/\sigma_o$
σ_x	Average longitudinal stress
σ'_x	$= \sigma_x/\sigma_o$
σ_{xm}	Maximum average longitudinal stress
σ'_{xm}	$= \sigma_{xm}/\sigma_o$
σ_o	Yield stress
τ	Shear stress
τ'	Shear stress (non-dimensionalised with respect to shear yield)
$\Delta\phi_q$	Generalised flexural total strain increment
$\Delta\phi''_q$	Generalised flexural plastic strain increment
η	Width of residual stress tension zone as proportion of plate thickness

ABBREVIATIONS

CF	Compression Flange
LS	Longitudinal Stiffener
NW	North Web
SW	South Web
TF	Tension Flange

Cross-section of Model

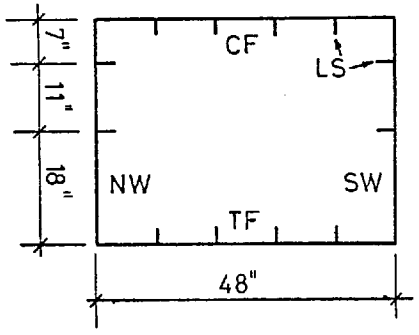

Models 1,2,5 and 7

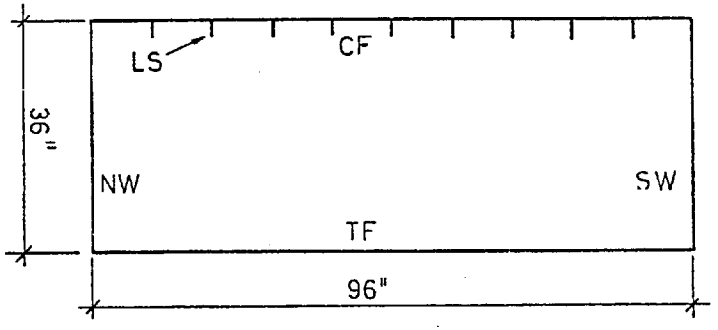

Model 9

Model No.	Component Sizes and Material Properties				
	Component	Nominal Size (in)	t (in)	σ_o (ton/in^2)	E (ton/in^2)
1	CF	3/16	.195	16.0	12970
	TF	3/16	.195	16.0	12970
	NW + SW	1/8	.133	17.7	13880
	LS	2 × 5/8 × 3/16L	-	21.3	12990
2	CF	3/16	.192	19.3	13530
	TF	3/16	.192	19.3	13530
	NW + SW	1/8	.133	13.5	13900
	LS	2 × 5/8 × 3/16L	-	17.9	12400
5	CF	5/16	.321	17.2	13400
	TF	5/16	.320	17.0	13420
	NW	1/8	.124	14.8	13190
	SW	1/8	.125	15.4	13330
	LS(CF + TF)	2 × 1/4 fl	-	18.7	13360
	LS(NW + SW)	{1 1/2 × 1/4 fl 1 × 1/4 fl}	-	19.2	13490
7	CF	5/16	.307	17.7	13370
	TF	5/16	.313	15.7	13040
	NW	1/8	.124	14.9	13370
	SW	1/8	.123	15.8	14740
	LS(CF + TF)	2 × 1/4 fl	-	20.0	12950
	LS(NW + SW)	{1 1/2 × 1/4 fl 1 × 1/4 fl	-	19.0	13380
			-	21.2	13200
9	CF	3/16	.192	21.6	13300
	TF	1/4	.268	20.4	13860
	NW + SW	1/2	.500	18.0	13460
	LS	2 3/4 × 5/16 fl	.312	18.5	13300

TABLE I. MODEL DETAILS AND MATERIAL PROPERTIES

Model	Plate Panel	Width (or depth) (in)	Deformation (× width)	Fabrication tolerance (IDAR)
1	Compression Flange Web	9.5 18.0	1/202 1/144	1/112 1/43
2	Compression Flange	9.5	1/330	1/111
5	Compression Flange Web	9.5 18.0	1/405 1/156	1/185 1/40
7	Compression Flange Web	9.5 18.0	1/490 1/162	1/176 1/40
9	Compression Flange	9.5	1/360	1/139

TABLE II. MAXIMUM PLATE PANEL INITIAL DEFORMATIONS

Model	Component	Towards Outstand		Away from Outstand	
		Measured	IDAR	Measured	IDAR
1	CF Web	L/1550 L/1100	L/450 "	- L/620	L/700 "
2	CF	L/1300	"	L/1150	"
5	CF Web	L/1760 L/775	" "	L/1900 L/248	" "
7	CF Web	L/2210 L/564	" "	L/1150 L/230	" "
9	CF	L/2700	"	L/1480	"

Notes: 1. L is spacing of transverse stiffeners.

TABLE III. MAXIMUM LONGITUDINAL STIFFENER INITIAL DEFORMATIONS

Model	Section	Initial Imperfections					
		Measured		After Test 1		After Test 2	
		δ_o (in)	σ_R (ton/in^2)	δ_o (in)	σ_R (ton/in^2)	δ_o (in)	σ_R (ton/in^2)
2	Q	-.0144*	3.39	-.0483	2.63	-	-
1	H	.055	2.67	n.m.**	n.m.	.233	10.82
9	K - 1†	.0036	4.92	n.m.	6.37	-	-
	K - 2	.0003	3.09	-	-	-	-
	K - 3	.0008	2.02	-	-	-	-

* Negative sign indicates a deformation away from the stiffener outstand.

** n.m. indicates residual imperfections were not measured at completion of test.

† Number refers to particular panels in this cross-section (see Fig. 35).

TABLE IV. INITIAL IMPERFECTIONS AS USED IN ANALYSIS OF COMPRESSION FLANGE PLATES

Model	Experimental Strength ($\times \sigma_o$)	Stiffener Initial Bow (in)	Theoretical Strength ($\times \sigma_o$)		
			Rigorous Approach[28]	Simplified Approach[57]	
				Aver. stress-strain curve	Equivalent deformation
2	.689	.090	.651	.650	.652 (-.108)*
1	.700	.180+	.610	.664	.442 (.468)
9†	.838	.029	.775	.803	.757 (.052)

*Equivalent deformation in inches (compare with values in Table IV).

+Assumed value, see text.

†Section K-3, see Table IV.

TABLE V. EXPERIMENTAL AND THEORETICAL STRENGTHS FOR COMPRESSION FLANGES

Model	Web	Bay	$\frac{\sigma}{\tau}$	Initial Imperfections						Long. Half-Waves
				Measured		After Test 1		After Test 2		
				δ_o (in)	σ_R (ton/in^2)	δ_o (in)	σ_R (ton/in^2)	δ_o (in)	σ_R (ton/in^2)	
5	NW	EK	1.14	.033	1.53	-	-	-	-	2
		KQ	1.14	.008	1.09	-	-	-	-	3
	SW	EK	1.14	.074	1.83	-	-	-	-	1
		KQ	1.14	.062	2.43 (2.1)*	-	-	-	-	2
7	NW	EK	0.83	.013	4.20	.013	2.86 (2.0)	-	-	2
	SW	KQ	0.83	.062	3.96	.062	2.51	-	-	1
1	SW	AB	0.35	.044	2.02**	-	-	-	-	1
	NW	BD	1.04	.070	2.12**	n.m.†	n.m.	-	-	1
	SW	JO	1.91	.049	5.04 (2.1)	.084	n.m.	.498	n.m.	1

* Value of residual stress used in the analysis since measured value is in excess of elastic critical buckling stress in compression.

** Assumed value (see Section 4.4.2).

† n.m. indicates residual imperfections were not measured at completion of test.

TABLE VI. INITIAL IMPERFECTIONS AS USED IN ANALYSIS OF WEB PLATES

Model	Web	Bay	Theoretical Strength/Experimental Strength Boundary Conditions as Fig. 36			
			a(i)	a(ii)	b(i)	b(ii)
5	NW	EK	1.176	1.110	1.150	1.050
		KQ	1.202	1.076	1.166	1.032
	SW	EK	1.235	1.108	1.184	1.070
		KQ	1.198	1.132	1.183	1.102
7	NW	EQ	1.110	1.041	1.061	1.003
	SW	KQ	1.175	1.072	1.123	1.044

TABLE VII. RATIOS OF THEORETICAL TO EXPERIMENTAL SHEAR STRENGTHS FOR MODELS 5 AND 7

Out-of-Plane Deformations							Residual Stress	
IDWR values of δ_o (mm)	δ_o' for b/t (β) of					δ_o' ($\times\beta^2$)	IDWR values of σ_R (N/mm^2)	σ_R'
	20 (0.691)	30 (1.037)	40 (1.383)	60 (2.074)	80 (2.766)			
$\frac{1}{80}\frac{b}{t}$	0.021	0.047	0.083	0.188	0.333	.044	0	0
$\frac{1}{40}\frac{b}{t}$	0.042	0.094	0.167	0.375	0.667	.087	8	.033
$\frac{1}{20}\frac{b}{t}$	0.083	0.188	0.333	0.750	1.333	.174	25	.102
$\frac{1}{10}\frac{b}{t}$	0.167	0.375	0.667	1.500	2.667	.349	80	.327

Notes: 1. δ_o was calculated using b = 240 mm.

2. σ_R was non-dimensionalised using σ_o = 245 N/mm^2.

TABLE VIII. INITIAL IMPERFECTIONS USED IN PARAMETRIC STUDY

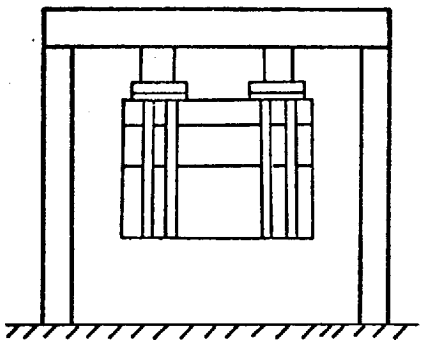

CROSS SECTION AT DIAPHRAGM
Showing overhead reaction frame

(a)

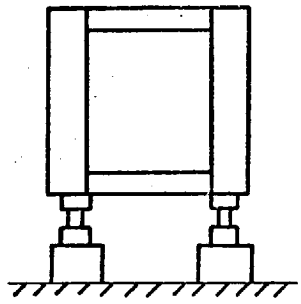

END ELEVATION
FOR MODELS 1&5

(b)

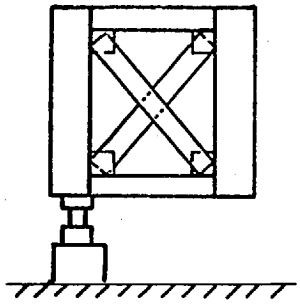

END ELEVATION FOR MODEL 7
Showing cross-bracing used
for distortion free tests.

(c)

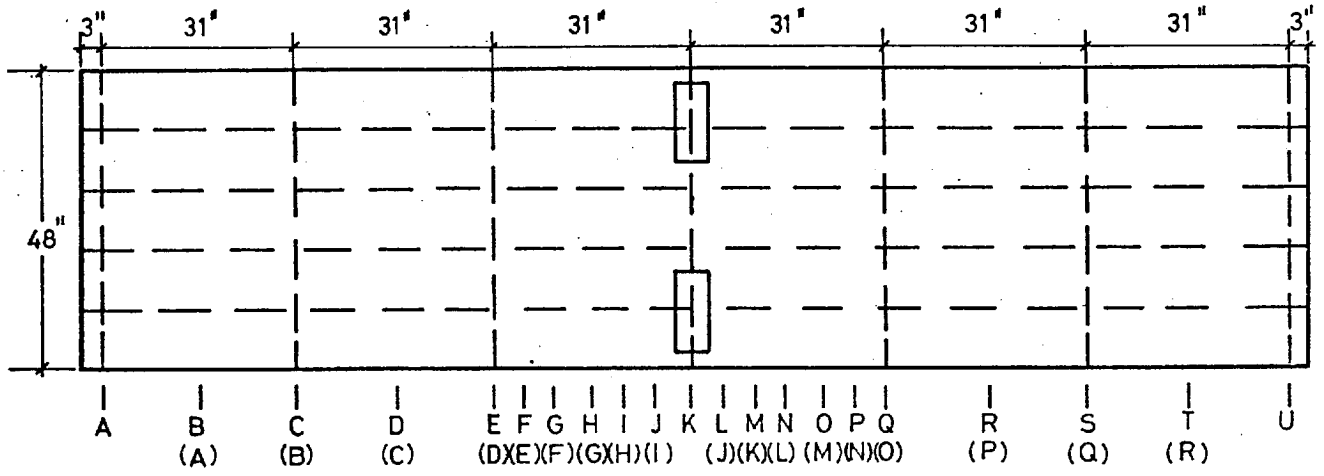

PLAN OF COMPRESSION FLANGE

(d)

The letters indicate the sections at which initial deformations and deflections under load were measured The Model 1 sections are indicated by the brackets.

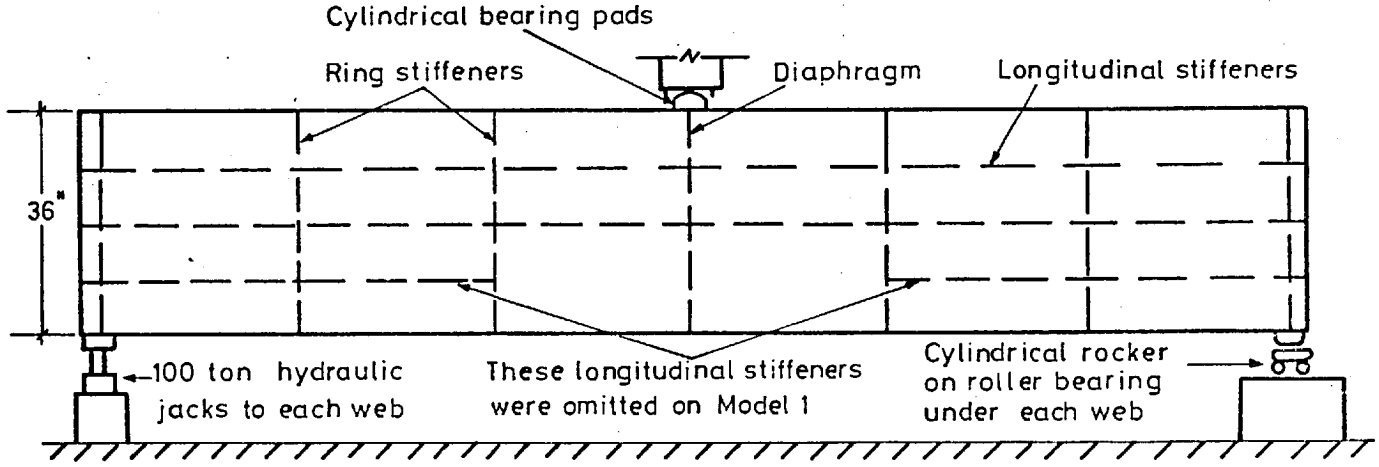

ELEVATION OF WEB

(e)

Fig. 1. Arrangement of Rig used for Point Load Tests

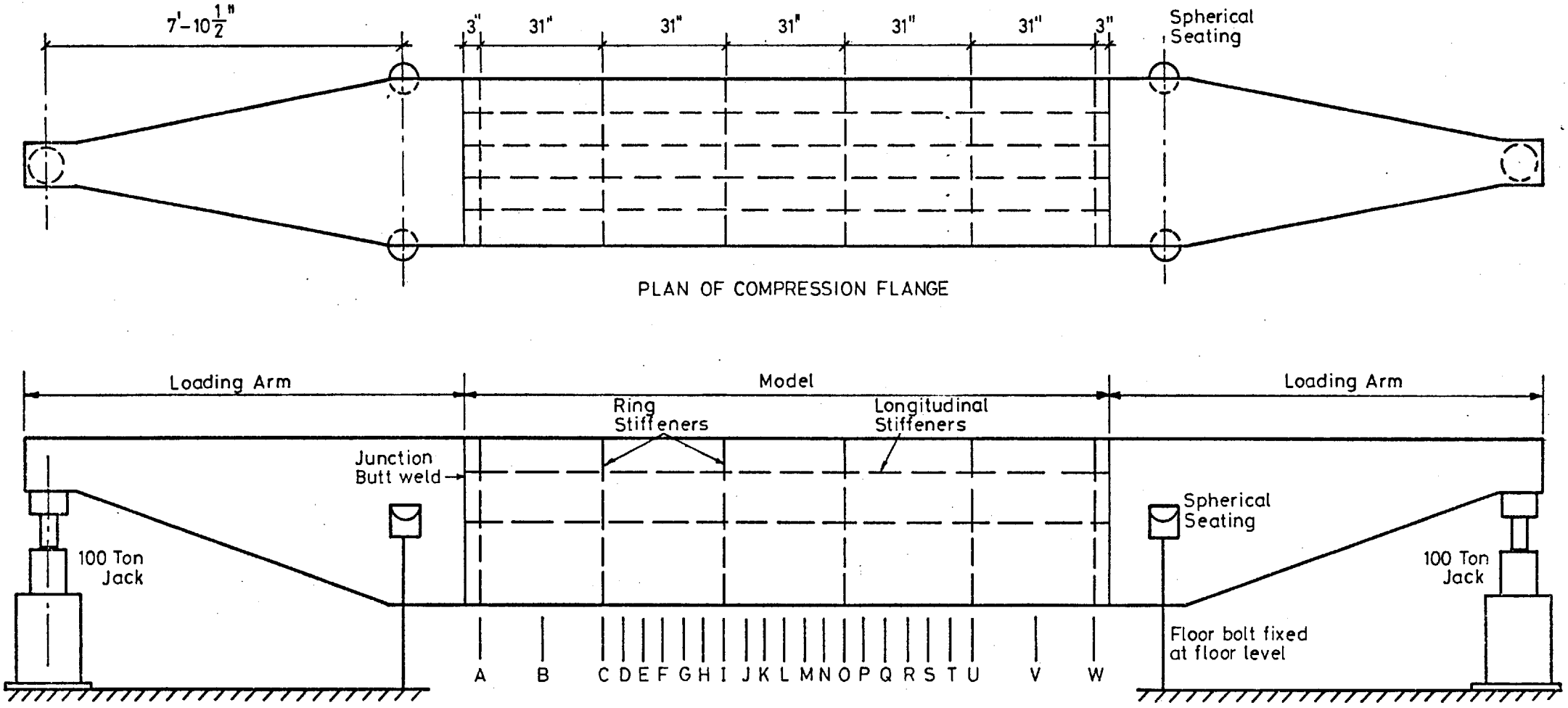

Fig. 2. Arrangement of Rig used for Pure Moment Test

The letters indicate the sections at which initial deformations and deflections under load were measured.

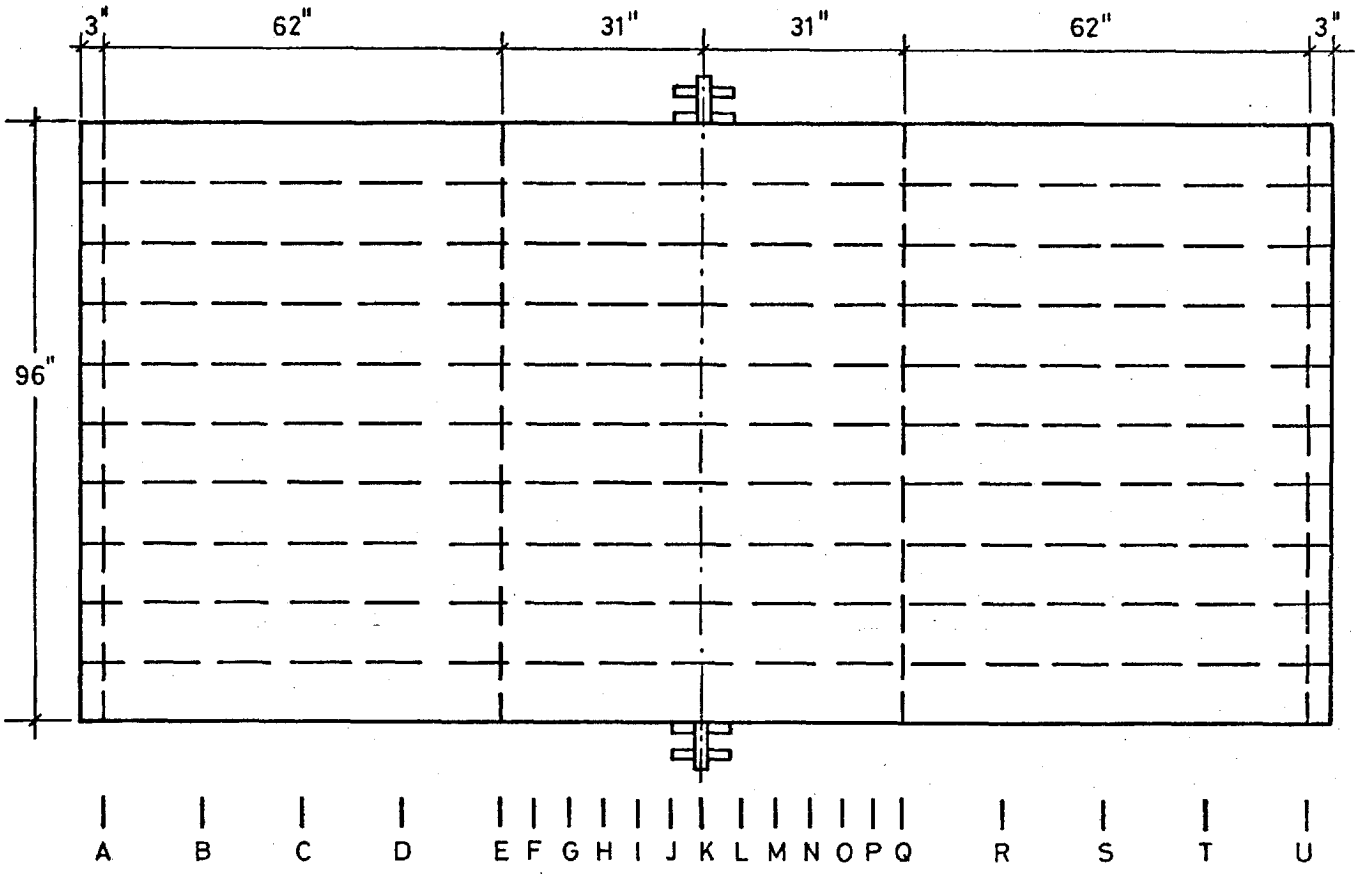

(a) PLAN OF COMPRESSION FLANGE
The letters indicate the sections at which initial deformations and deflections under load were measured.

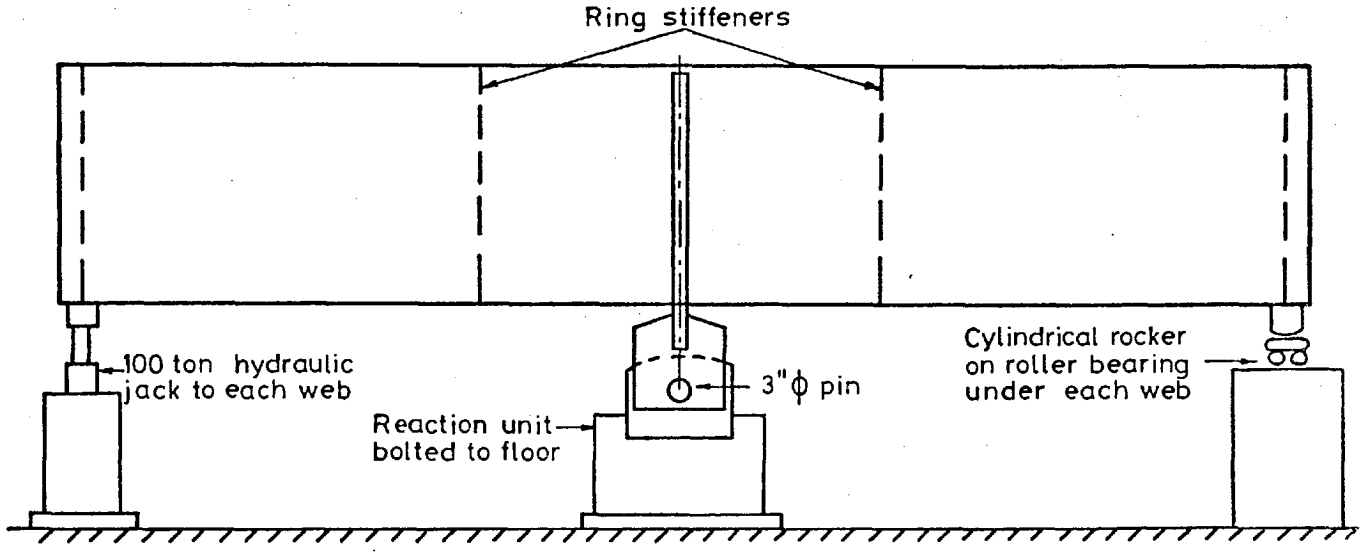

(b) ELEVATION OF WEB

Fig. 3. Arrangement of Model 9 Test Rig.

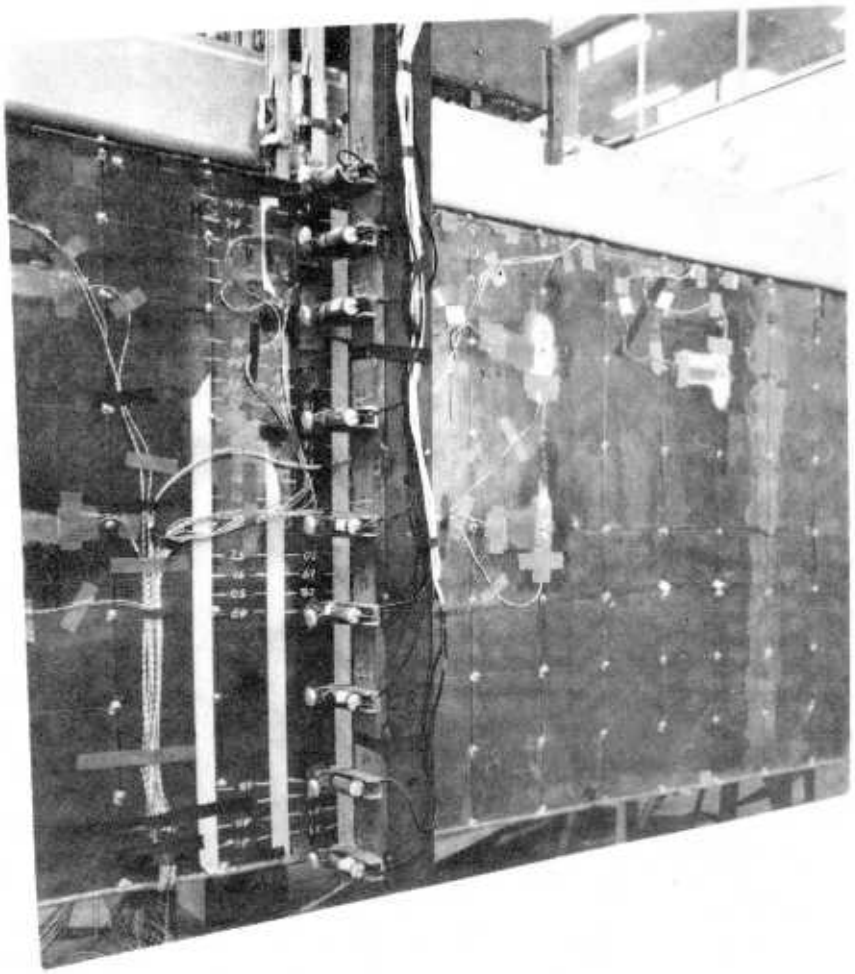

FIG. 4. TRANSDUCER U-FRAME ON RAILS.

Balls for locating U-frame can be seen on top of rails. Plates on transducer stems bare onto the small balls stuck to surface of the model.

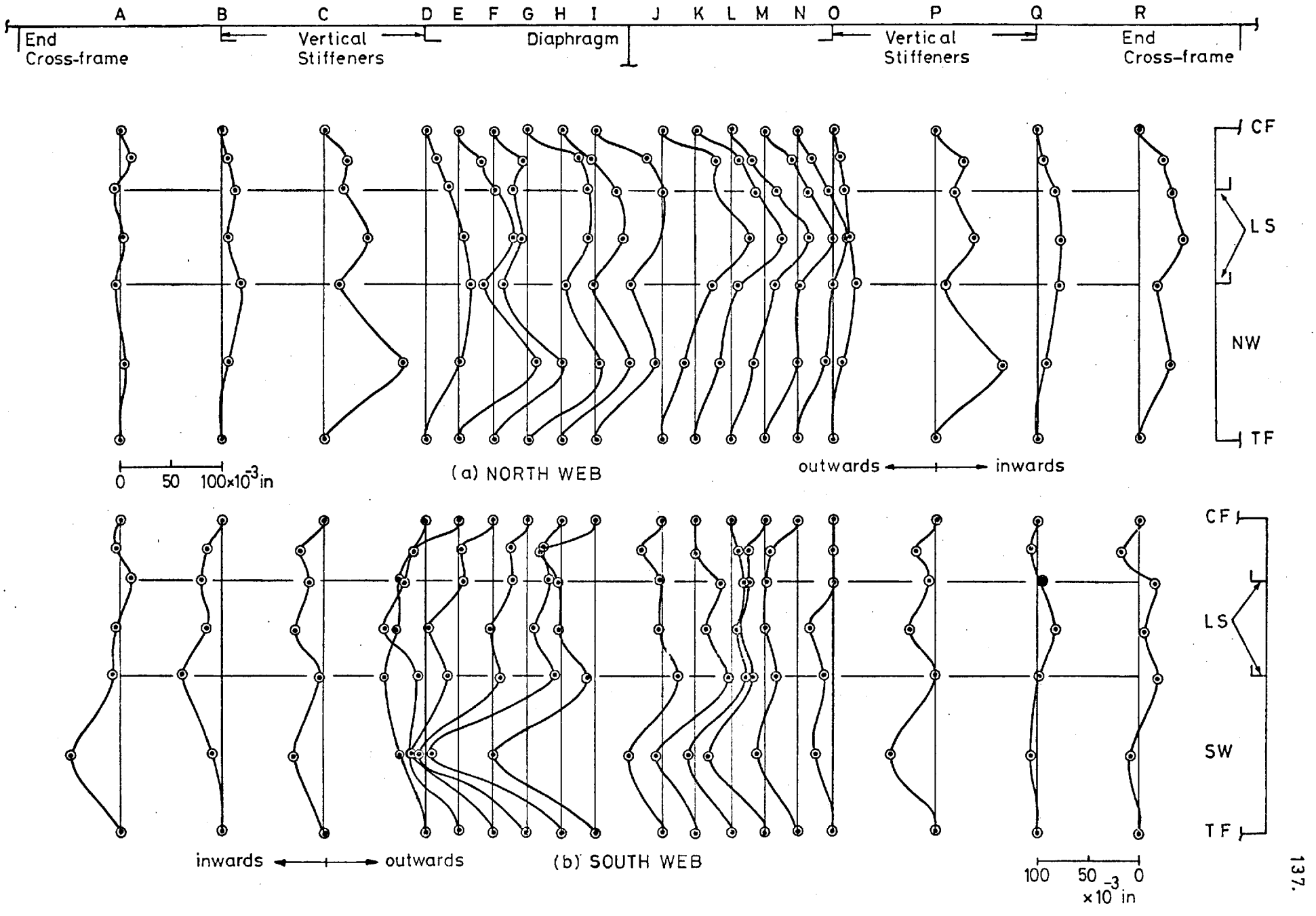

Fig. 5. Model 1: Transverse Profiles of Initial Deformations of Webs

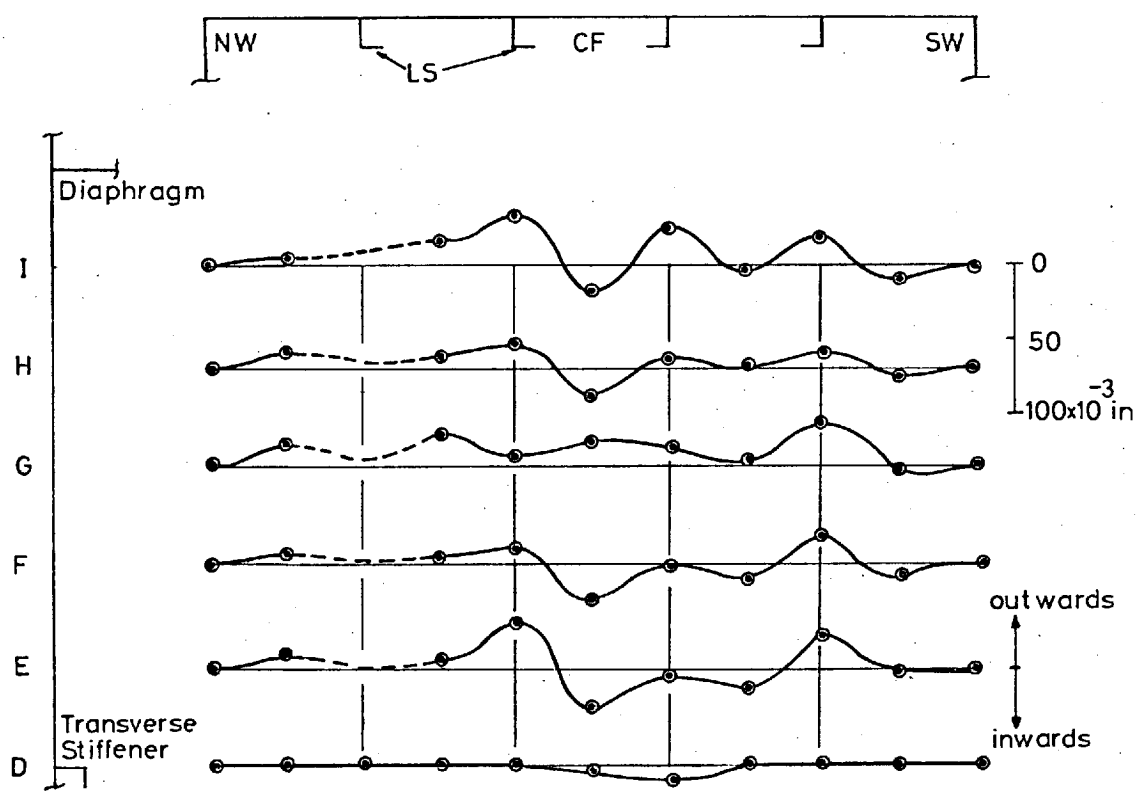

Fig. 6. Model 1 : Transverse Profiles of Initial Deformations of Compression Flange, Bay D I

Dashed lines indicate approximate shape only. A faulty transducer gave incorrect readings along this section.

Note that initial shape of diaphragm was not recorded so that no longitudinal profiles are available.

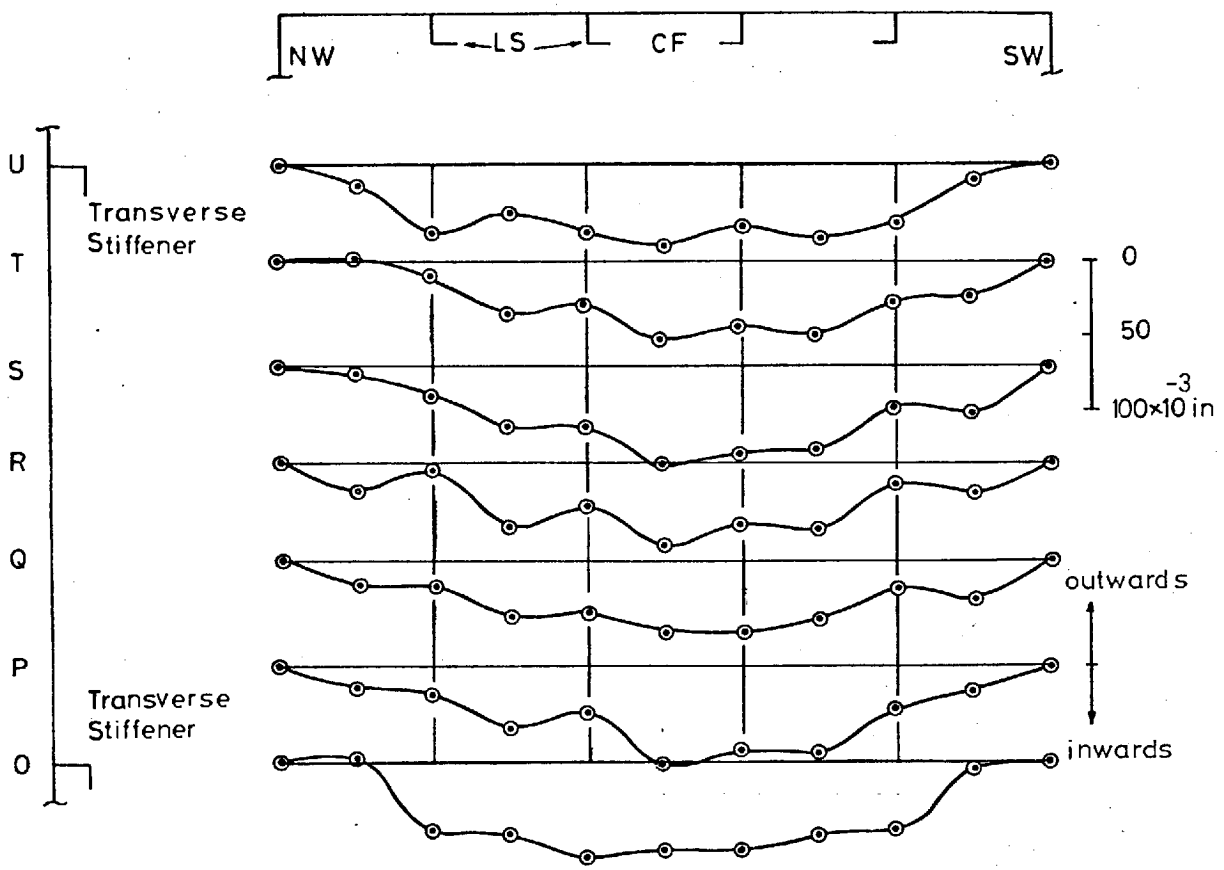

(a) TRANSVERSE PROFILES

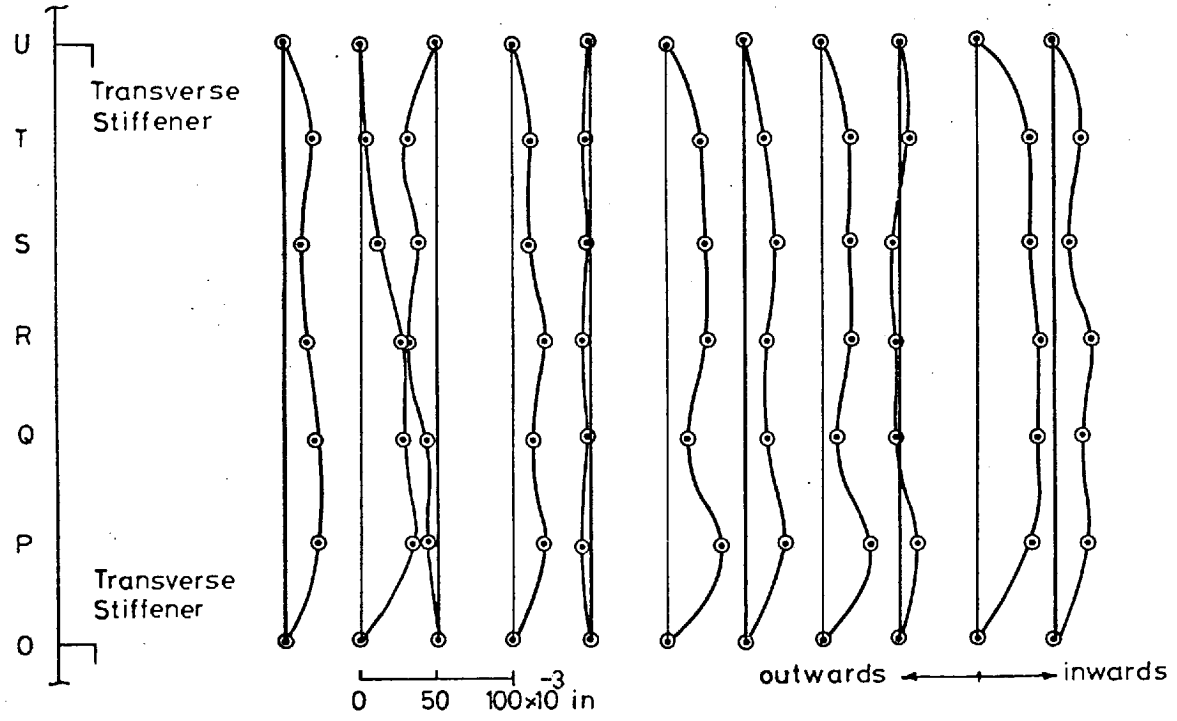

(b) LONGITUDINAL PROFILES

Fig. 7. Model 2: Initial Deformations of Compression Flange, Bay 0U

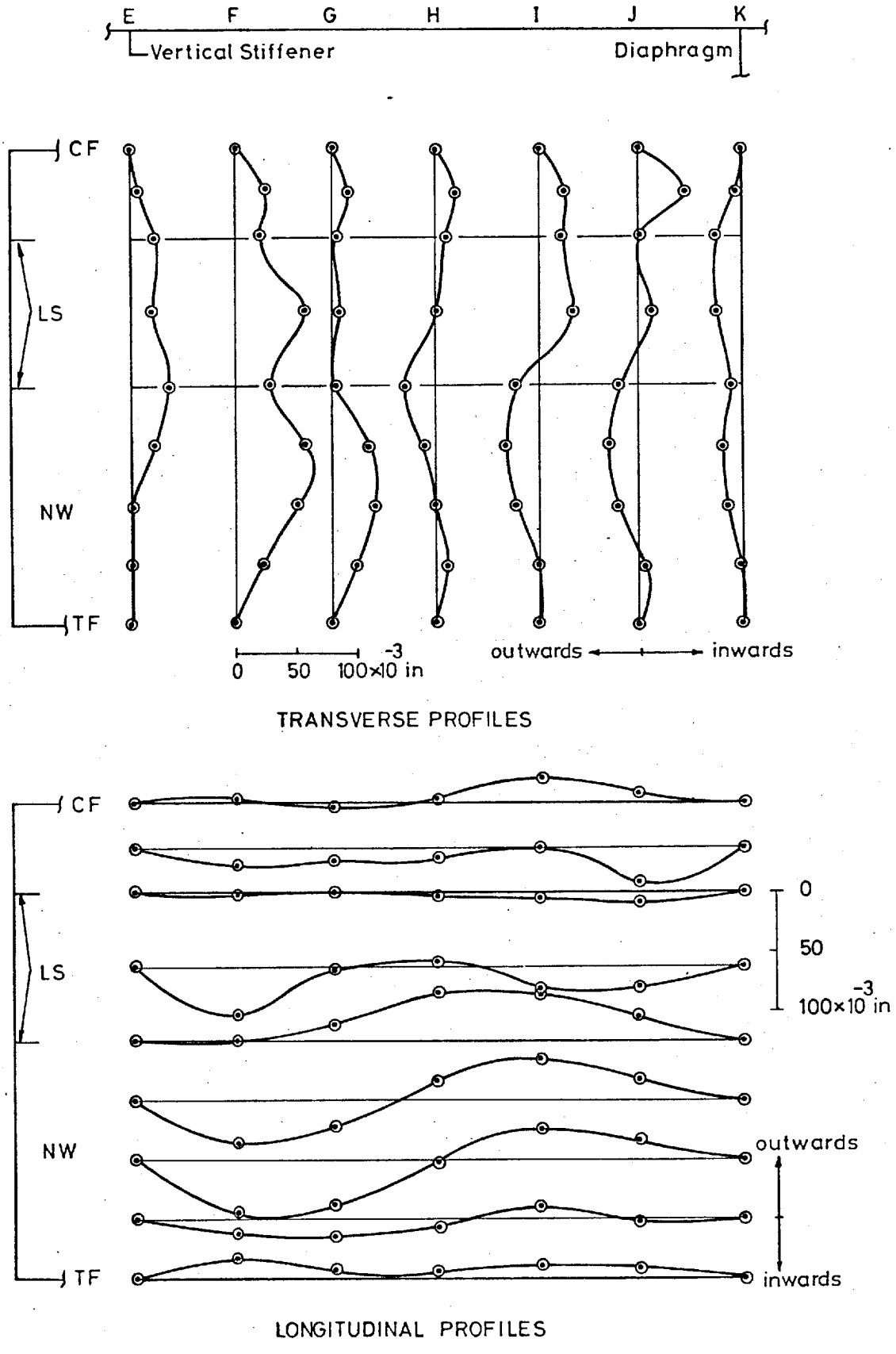

Fig. 8a. Model 5: Initial Deformations of North Web, Bay EK

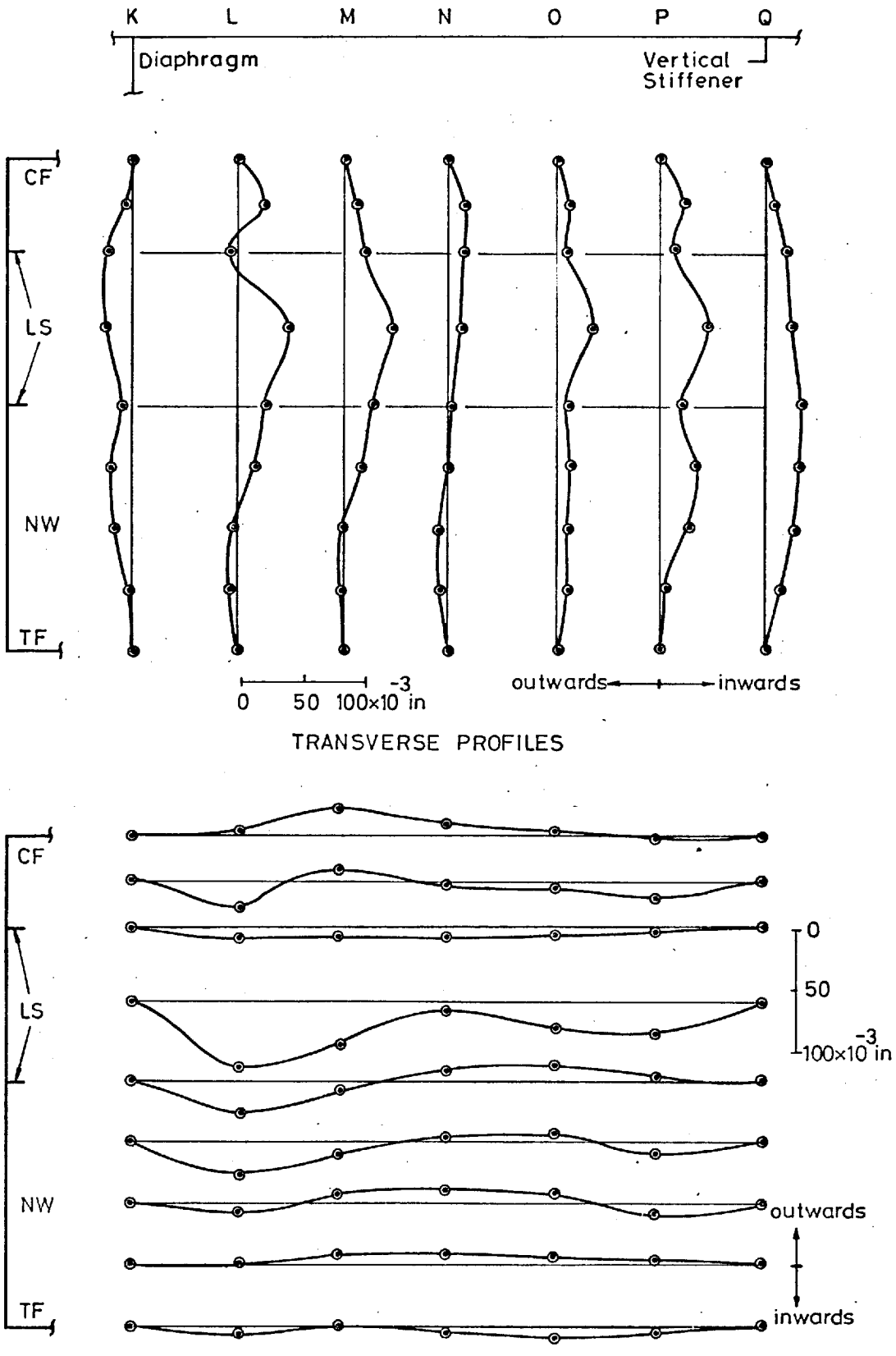

Fig.8b. Model 5 : Initial Deformations of North Web, Bay KQ

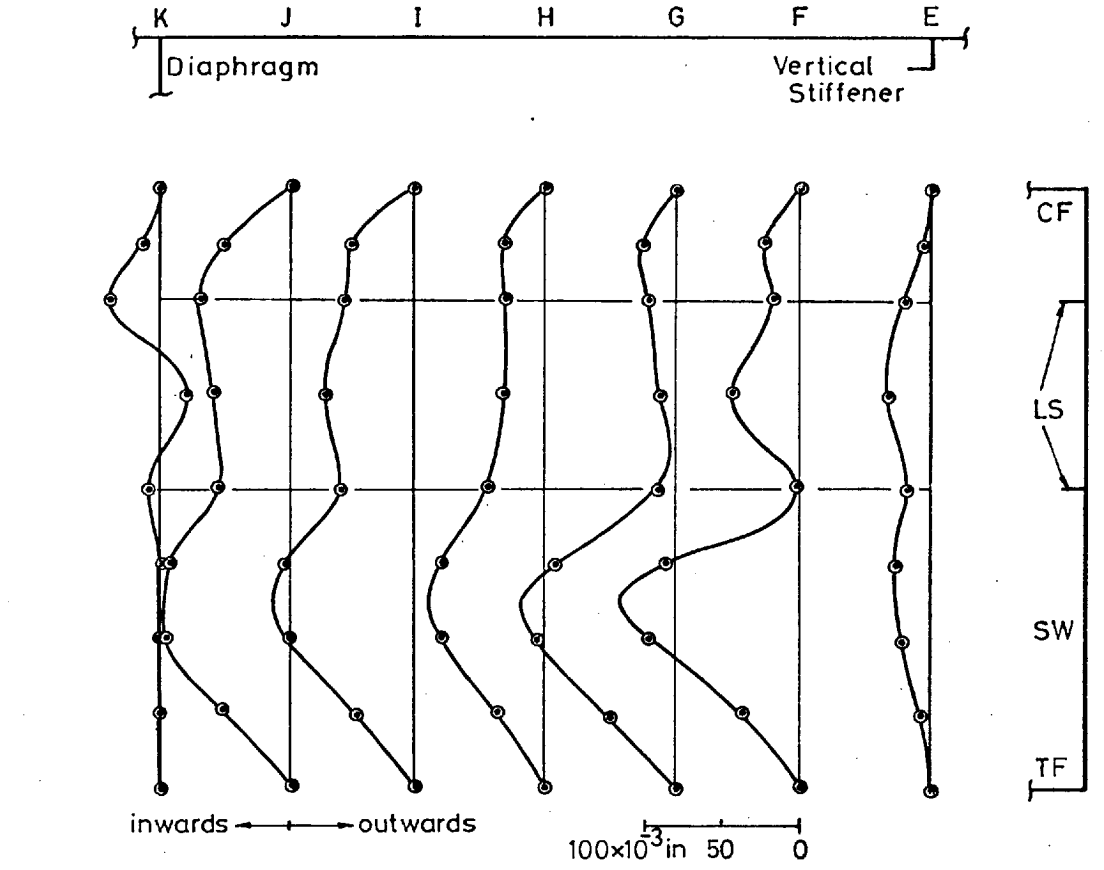

TRANSVERSE PROFILES

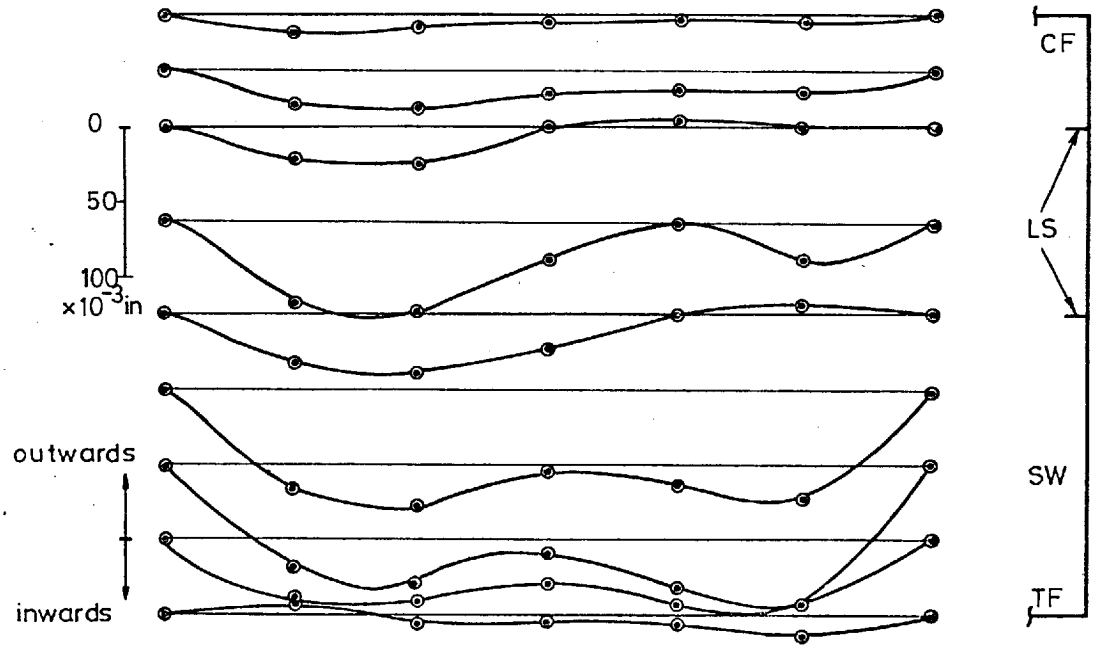

LONGITUDINAL PROFILES

Fig.8c. Model 5 : Initial Deformations of South Web, Bay E K

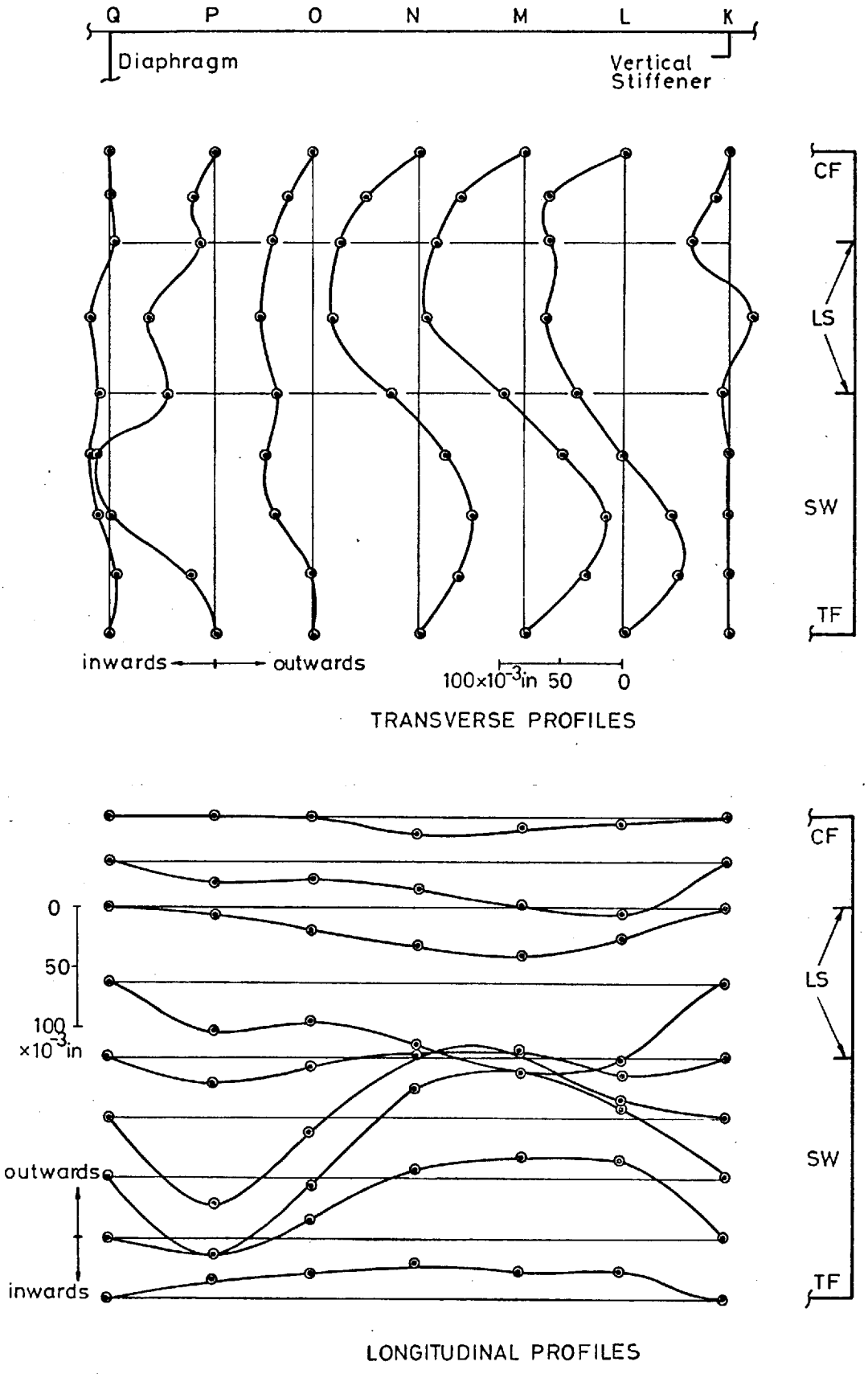

Fig.8d. Model 5: Initial Deformation of South Web, Bay KQ

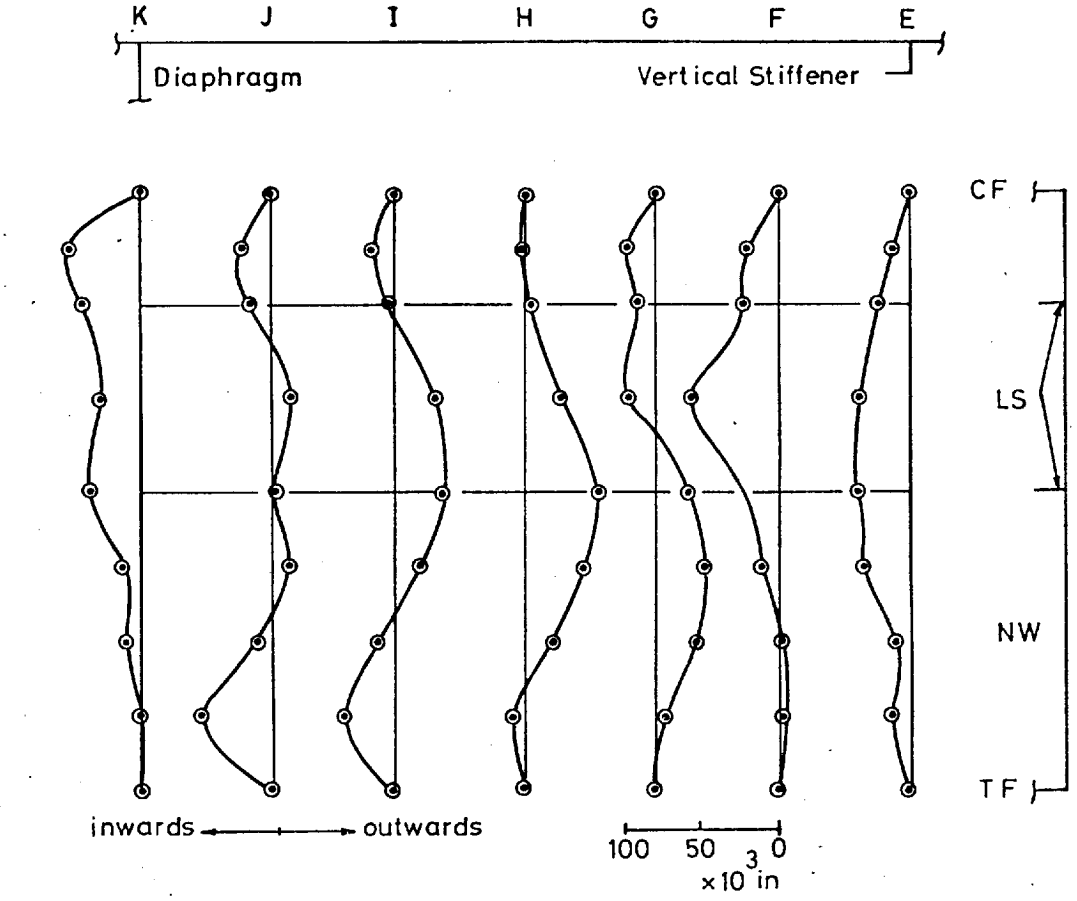

TRANSVERSE PROFILES

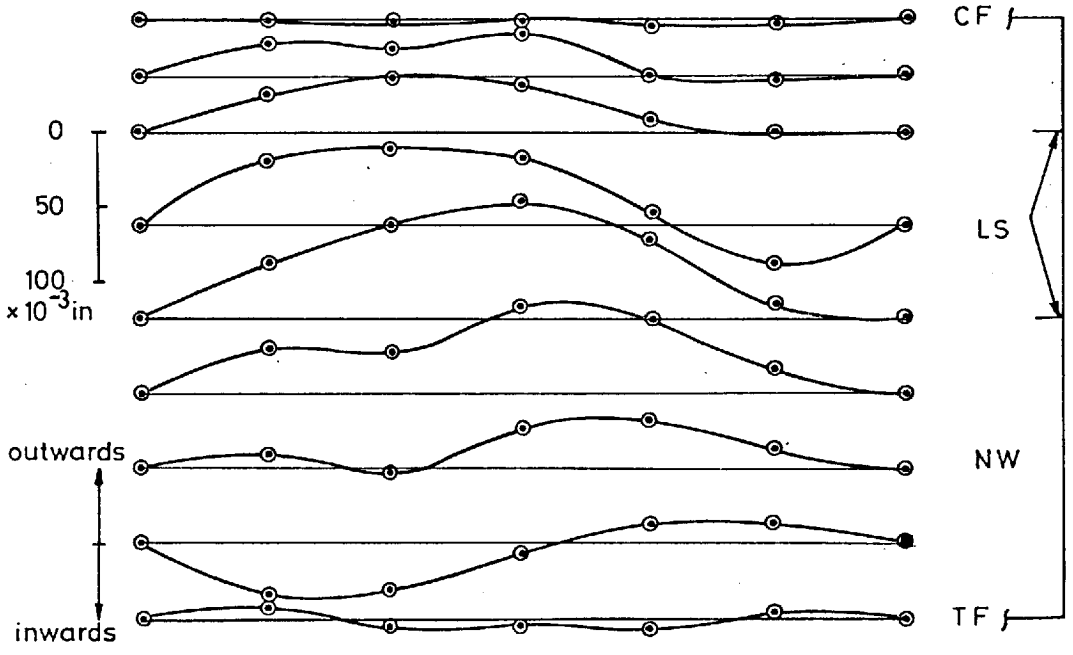

LONGITUDINAL PROFILES

Fig. 9a. Model 7: Initial Deformations of North Web, Bay E K

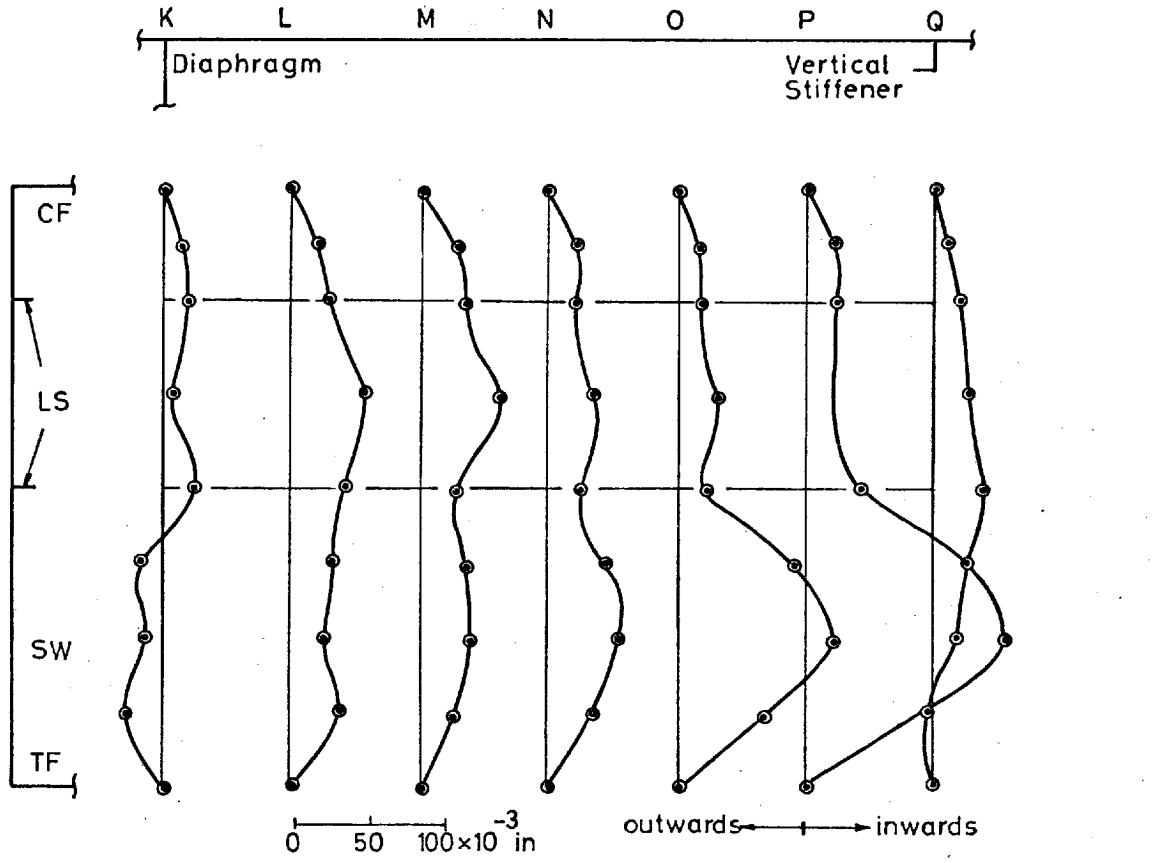

TRANSVERSE PROFILES

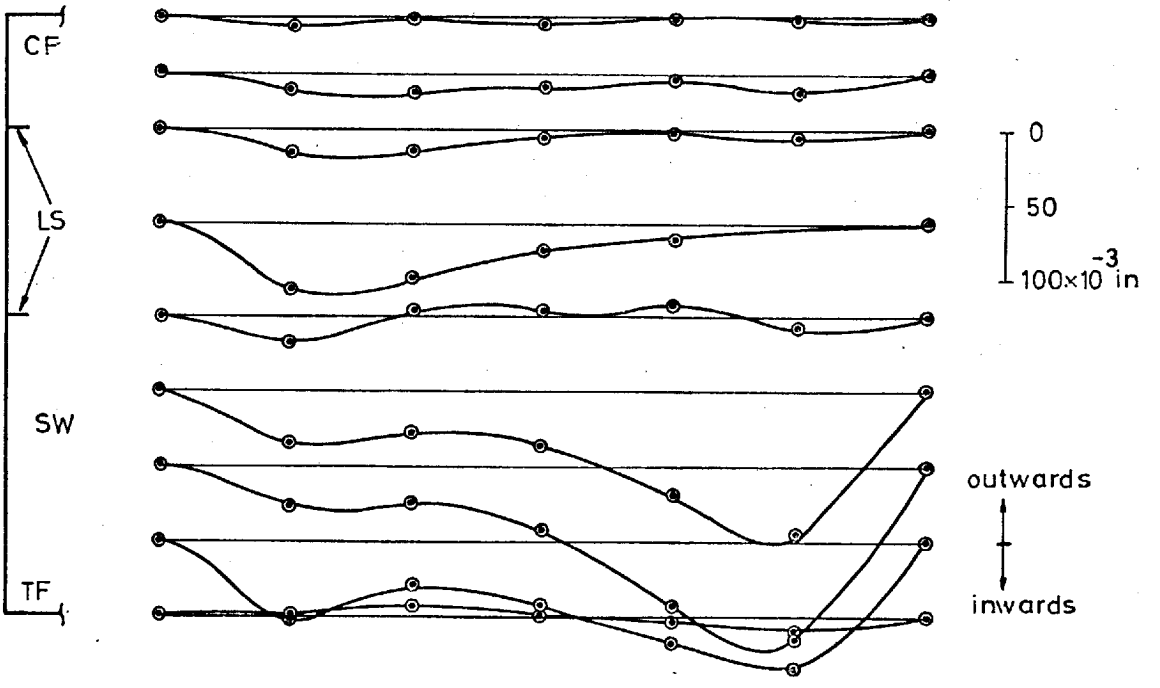

LONGITUDINAL PROFILES

Fig.9b. Model 7: Initial Deformations of South Web, Bay K Q

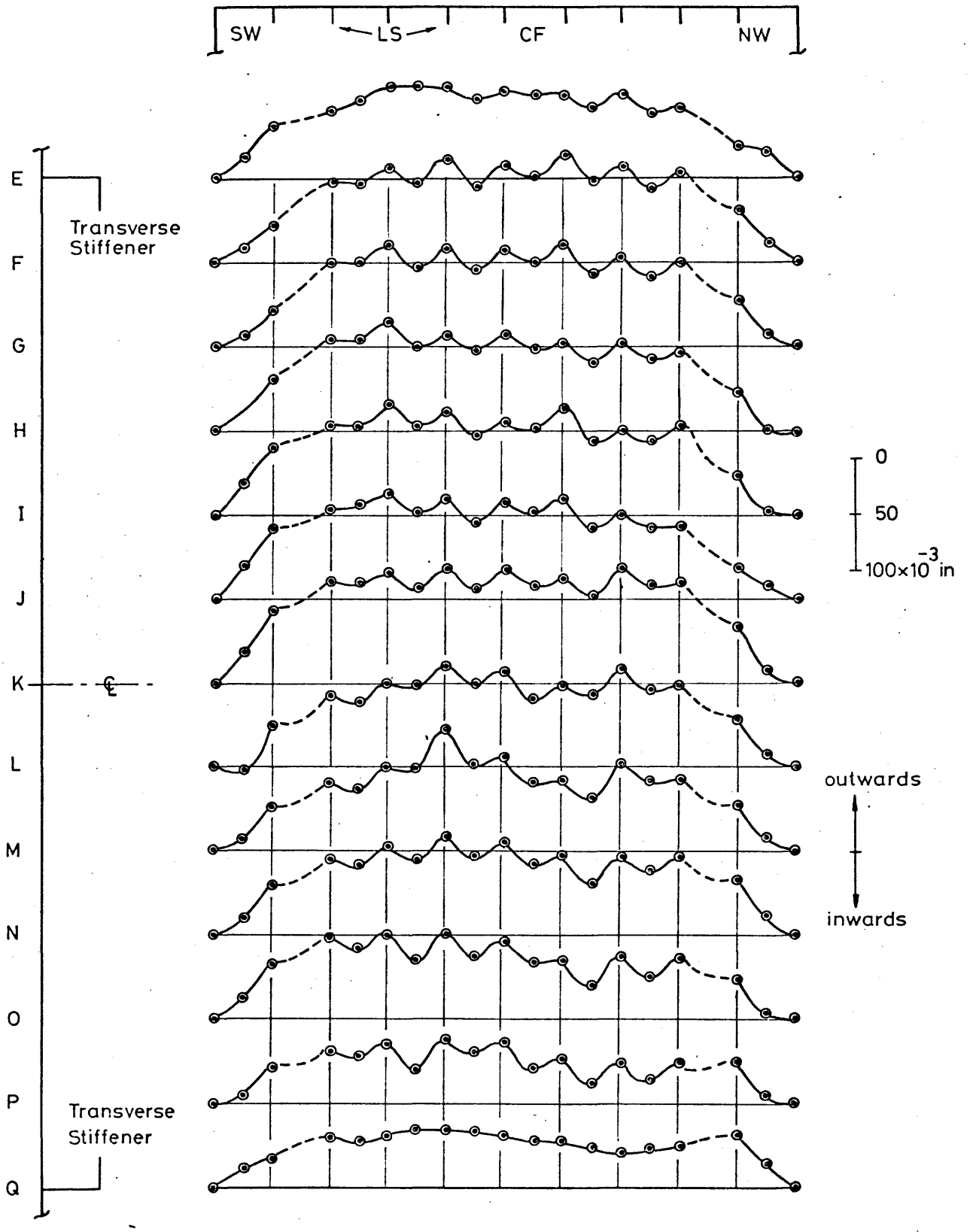

Fig.10a. Model 9: Transverse Profiles of Initial Deformations of Compression Flange, Bay EQ

Dashed lines indicate approximate shape only. Faulty transducers gave incorrect readings at these locations.

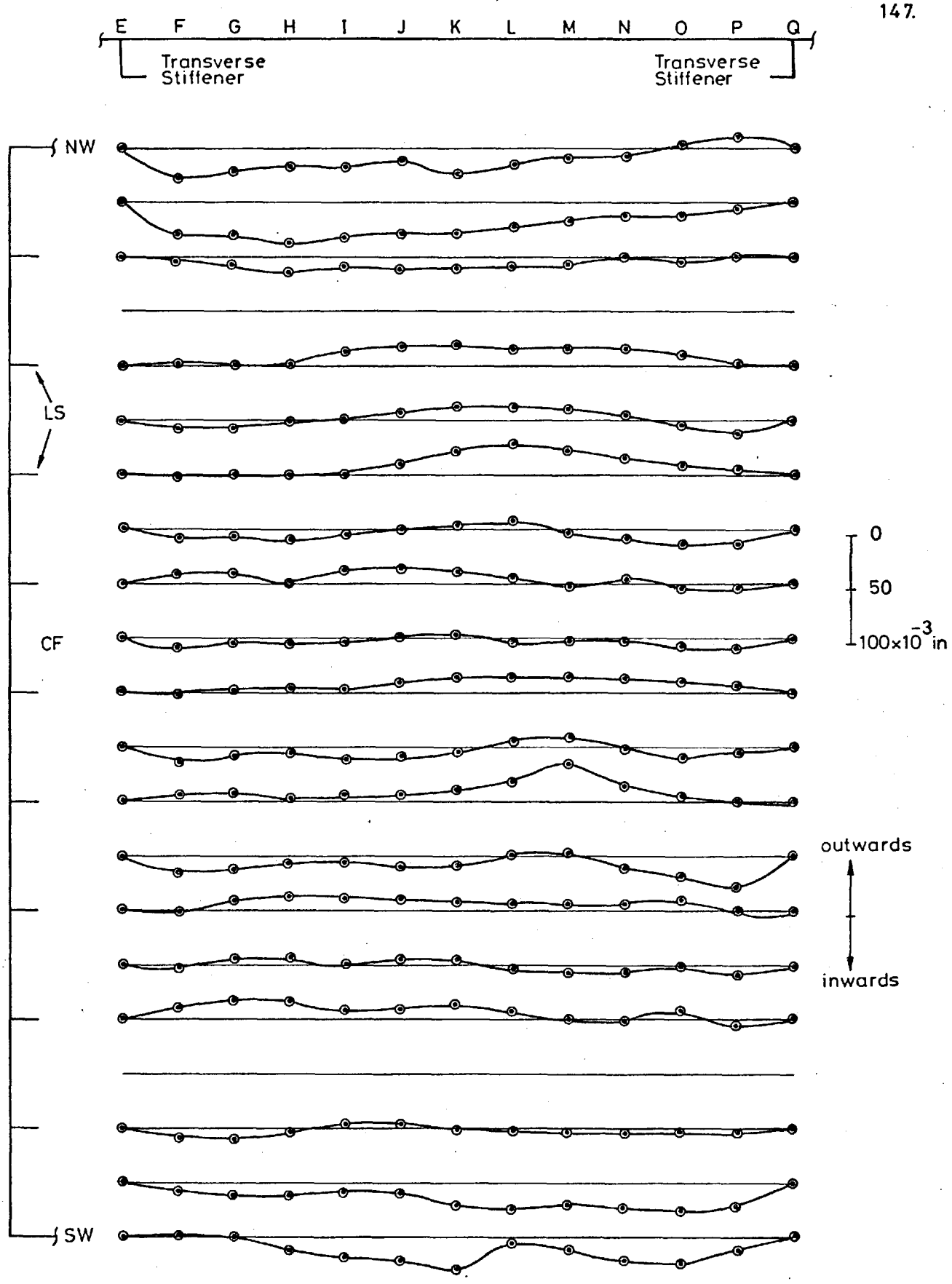

Fig.10b. Model 9: Longitudinal Profiles of Initial Deformation of Compression Flange, Bay EQ.

Profiles of two sections have been omitted. Faulty transducers gave incorrect readings at these locations

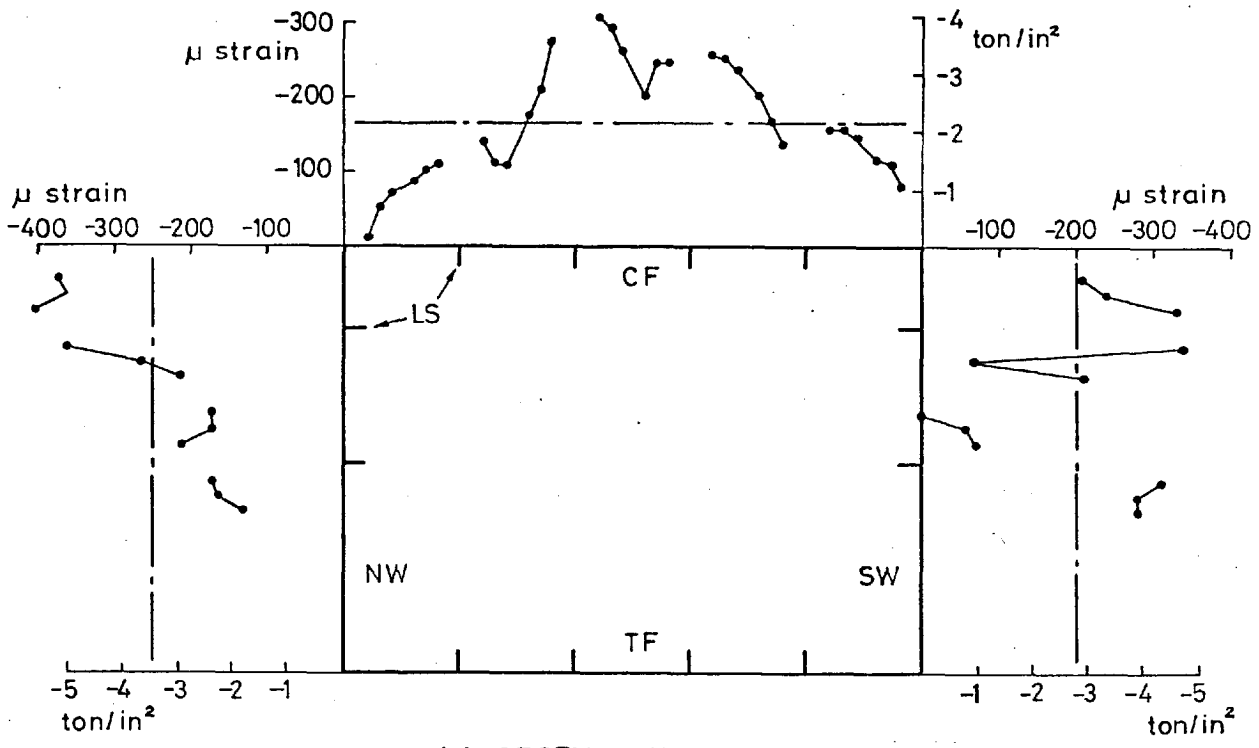

(a) SECTION H

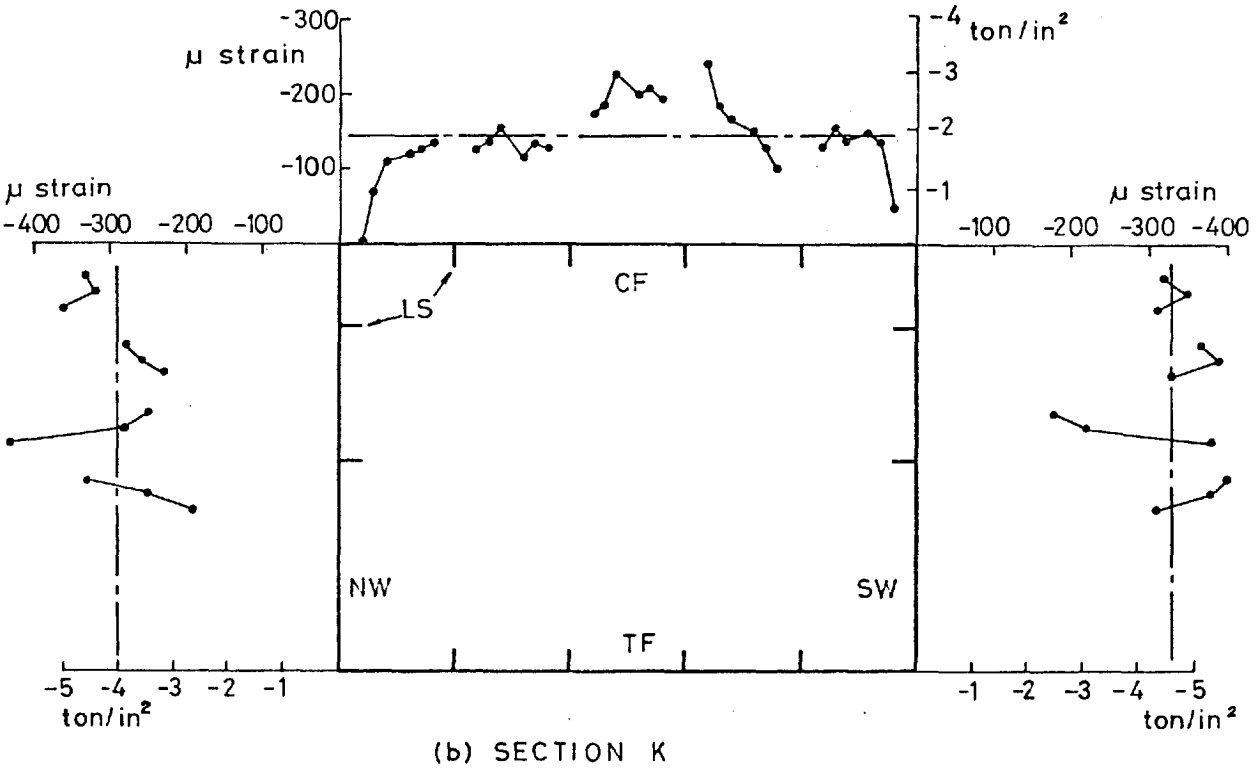

(b) SECTION K

Fig.11. Model 1: Plate Welding Residual Strains

Stresses calculated assuming transversely unrestrained panels. The average strain across an element is indicated by —·—·— (compressive negative)

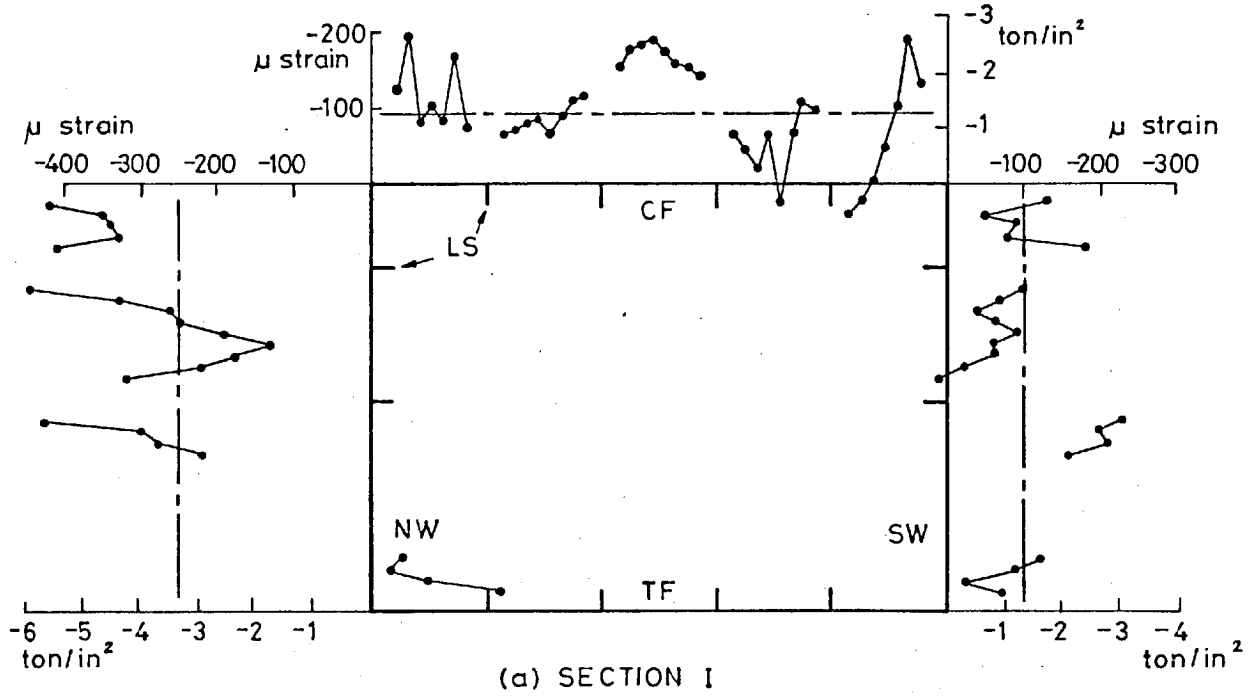

(a) SECTION I

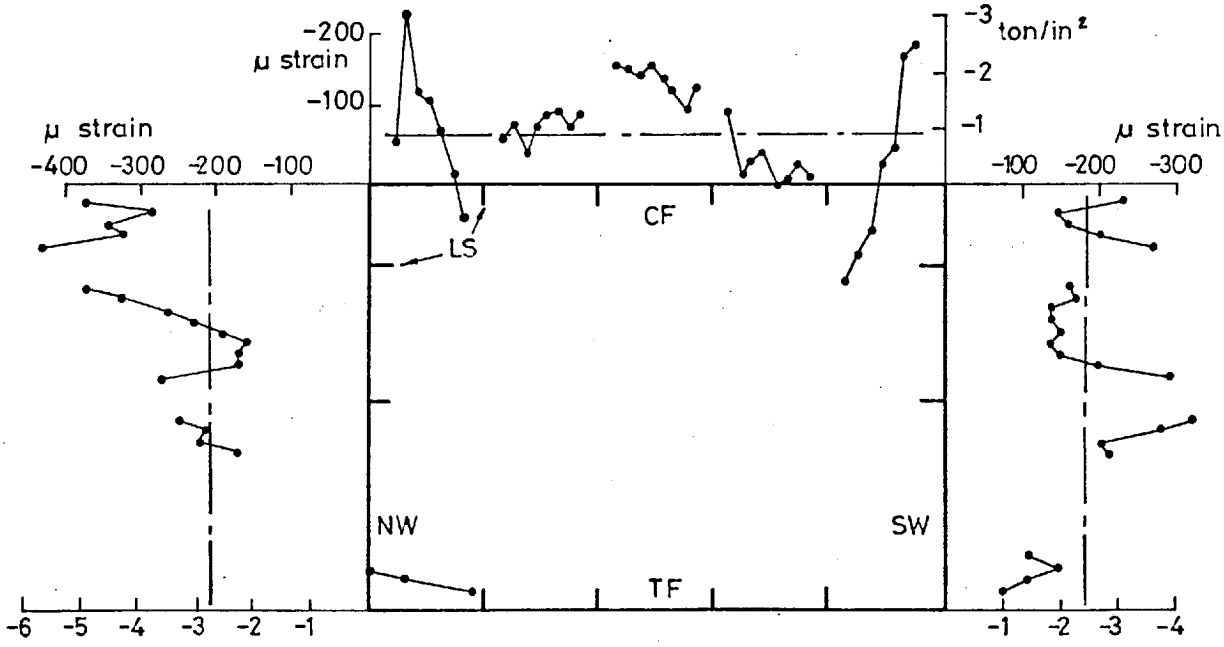

(b) SECTION M

Fig. 12. Model 5: Plate Welding Residual Strains

Stresses calculated assuming transversely unrestrained panels. The average strain across an element is indicated by —·—·— (compressive negative)

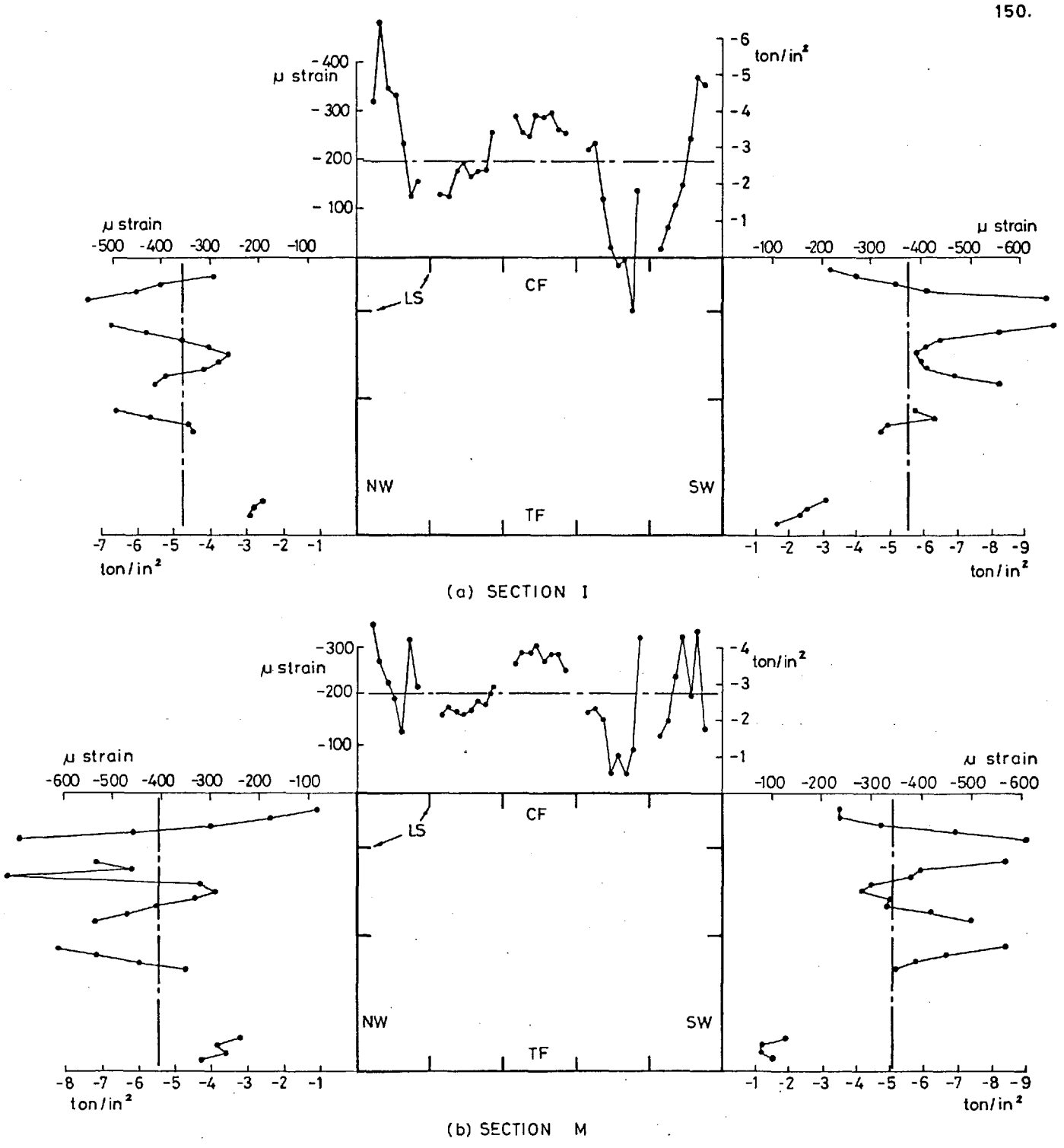

Fig. 13 Model 7: Plate Welding Residual Strains

Stresses calculated assuming transversely unrestrained panels. The average strain across an element is indicated by ——·—— (compressive negative)

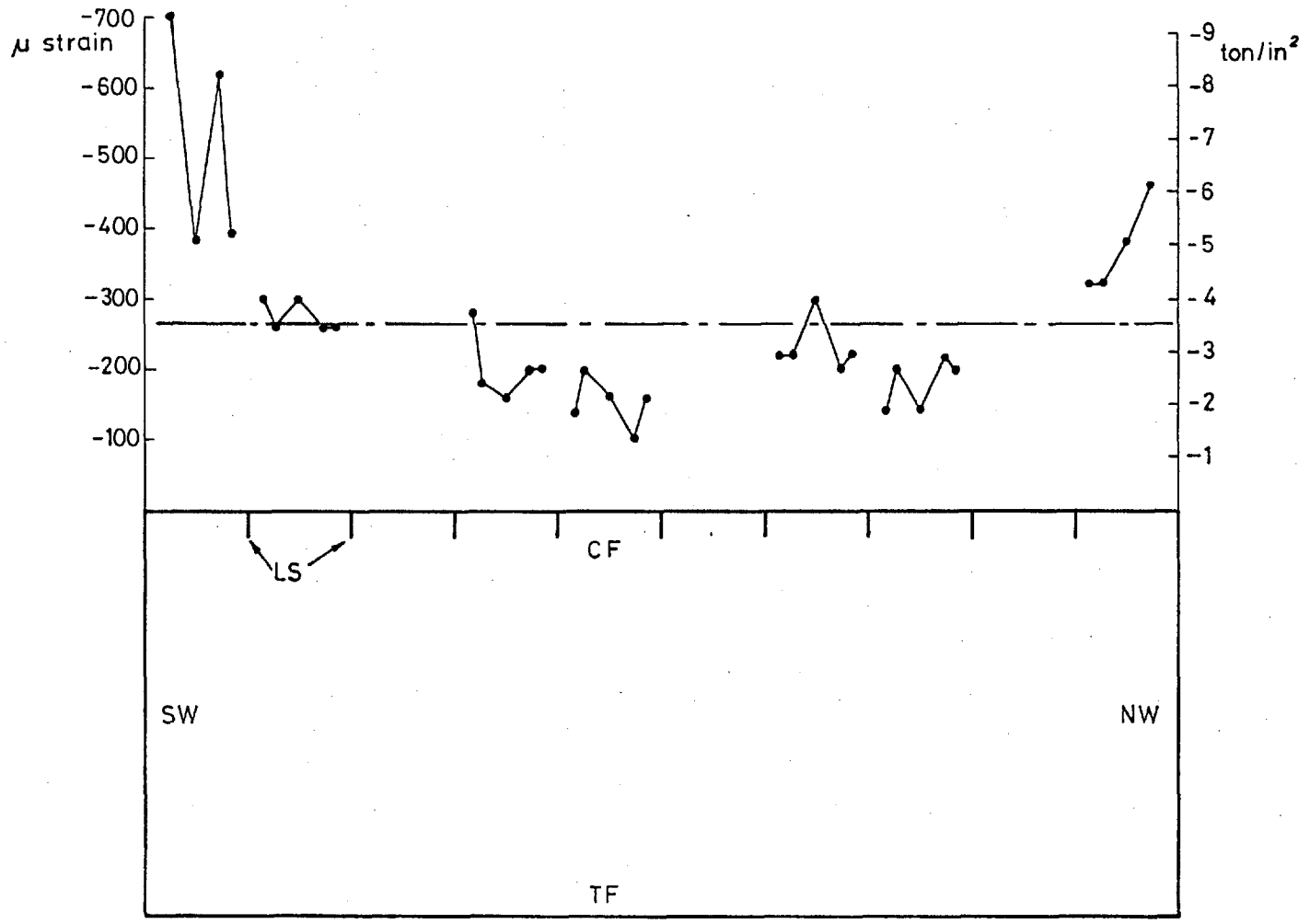

Fig.14. Model 9: Plate Welding Residual Strains, Section K.
Stresses calculated assuming transversely unrestrained panels. The average strain across an element is indicated by —·—·— (compressive negative)

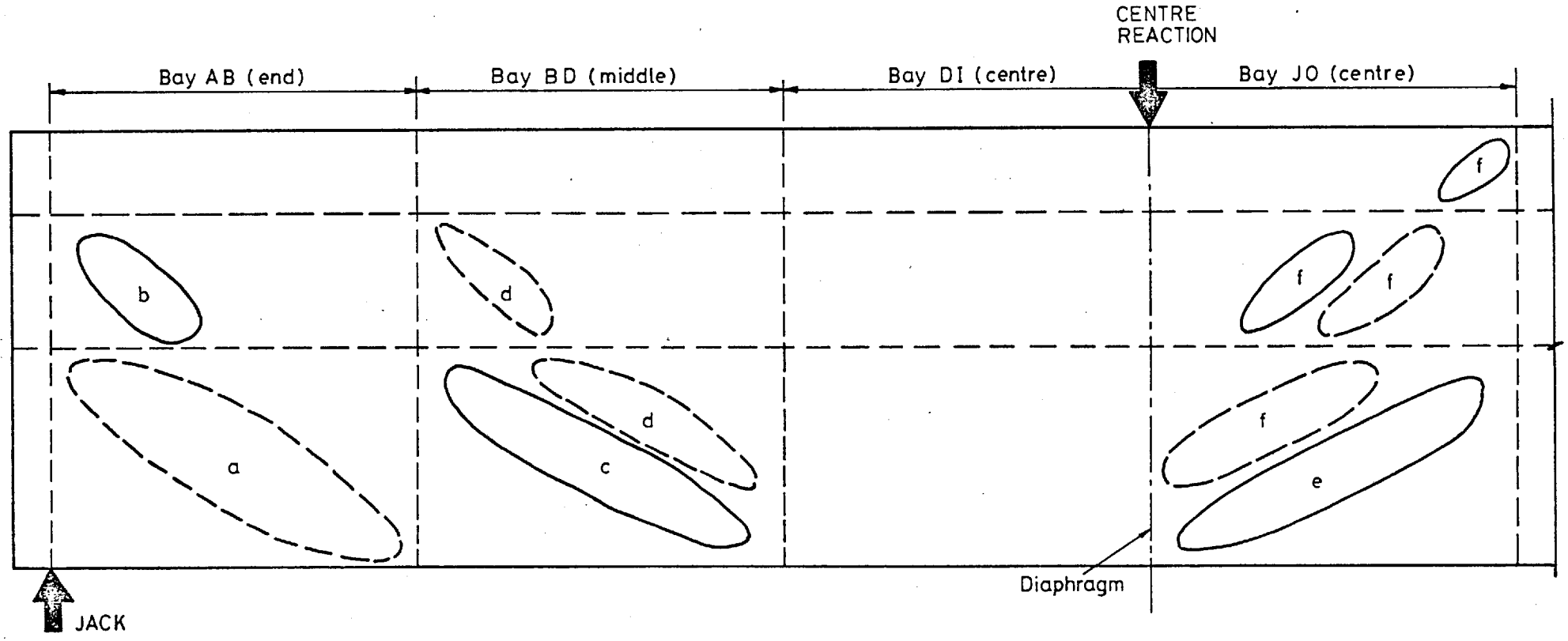

a. Test 1, 120·0 ton
b. Test 1, 120·4 ton
c. Test 2, 118·6 ton
d. Test 2, 123·2 ton
e Test 3, 128·0 ton
f. Test 3, with deformation applied beyond collapse load.

Fig. 15. Model 1: Development of Shear Buckles in the South Web During the Three Ultimate Load Tests.
The dashed lines indicate outward deflections, the full lines inwards. The load referenced against each deformation indicates the level at which it first developed. In Tests 1 and 2, buckling was symmetrical about the central diaphragm. The behaviour of the north web was similar.

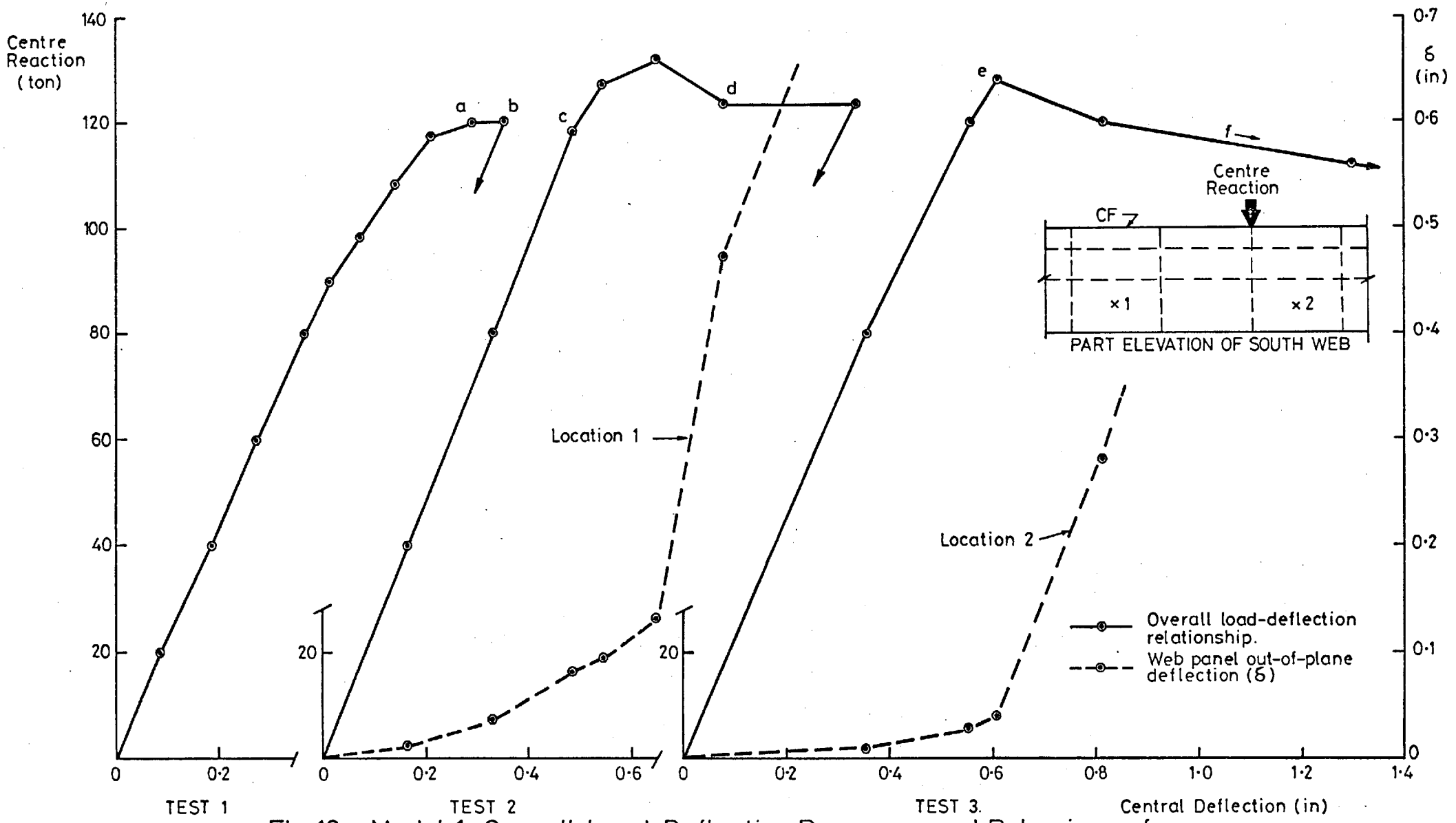

Fig. 16. Model 1: Overall Load-Deflection Response and Behaviour of Selected Web Panels during the Three Ultimate Load Tests.

The locations indicated on the curves of panel behaviour are shown on the elevation. The letters indicate the loads at which the buckles shown in Fig 15. developed.

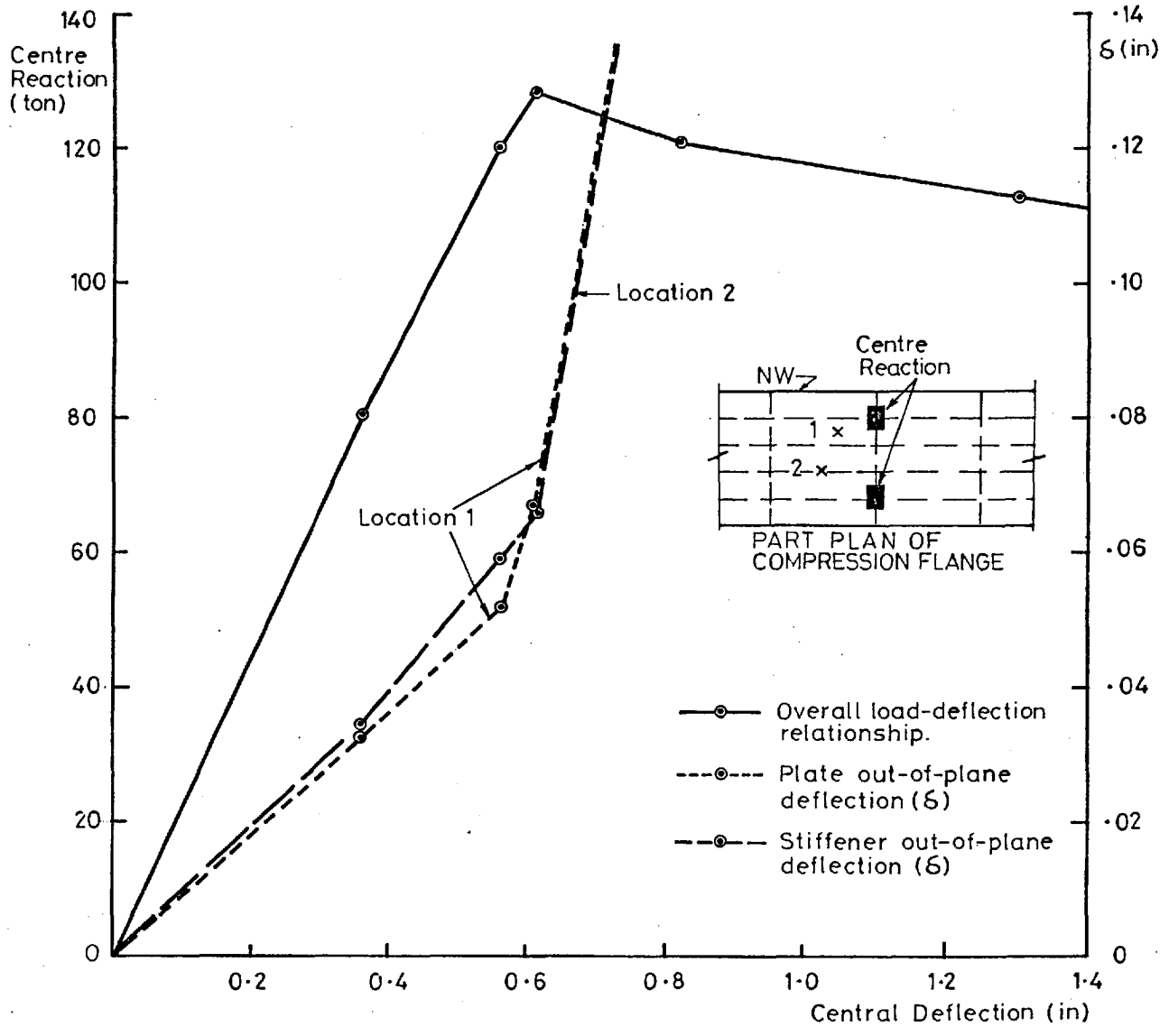

Fig. 17. Model 1: Overall Load-Deflection Response and Behaviour of Compression Flange during Test 3.

The locations indicated on the curves of flange behaviour are shown on the plan. Note that the stiffener deflected after peak load was reached.

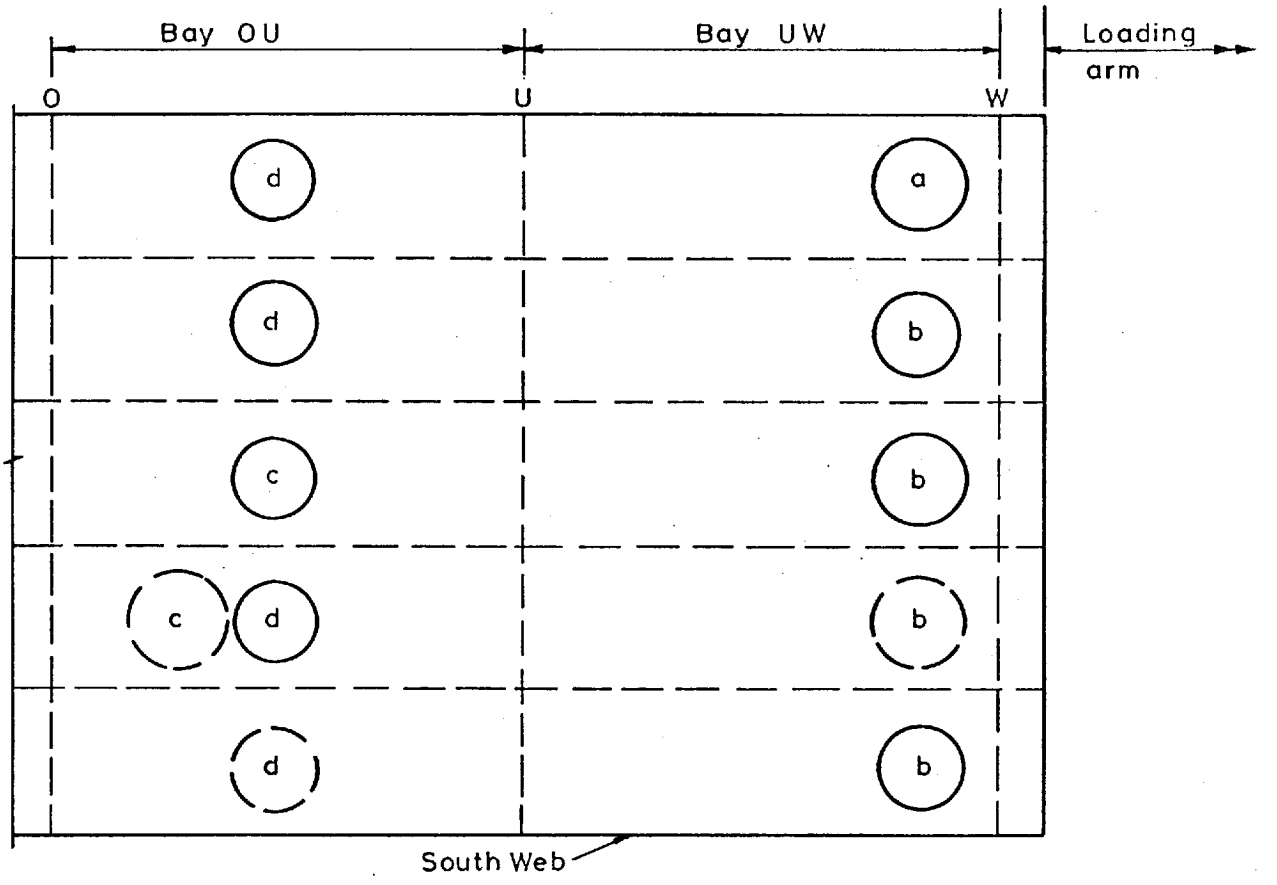

a. Test 1, 62·5 ton
b. Test 1, 64·5 ton
c. Test 2, 63·0 ton
d. Test 2, 64·5 ton

Fig. 18. Model 2: Development of Compression Flange Plate Panel Buckles during the Two Ultimate Load Tests.

The dashed lines indicate outward deflections, the full lines inward. The load referenced against each deformation indicates the level at which it first developed.

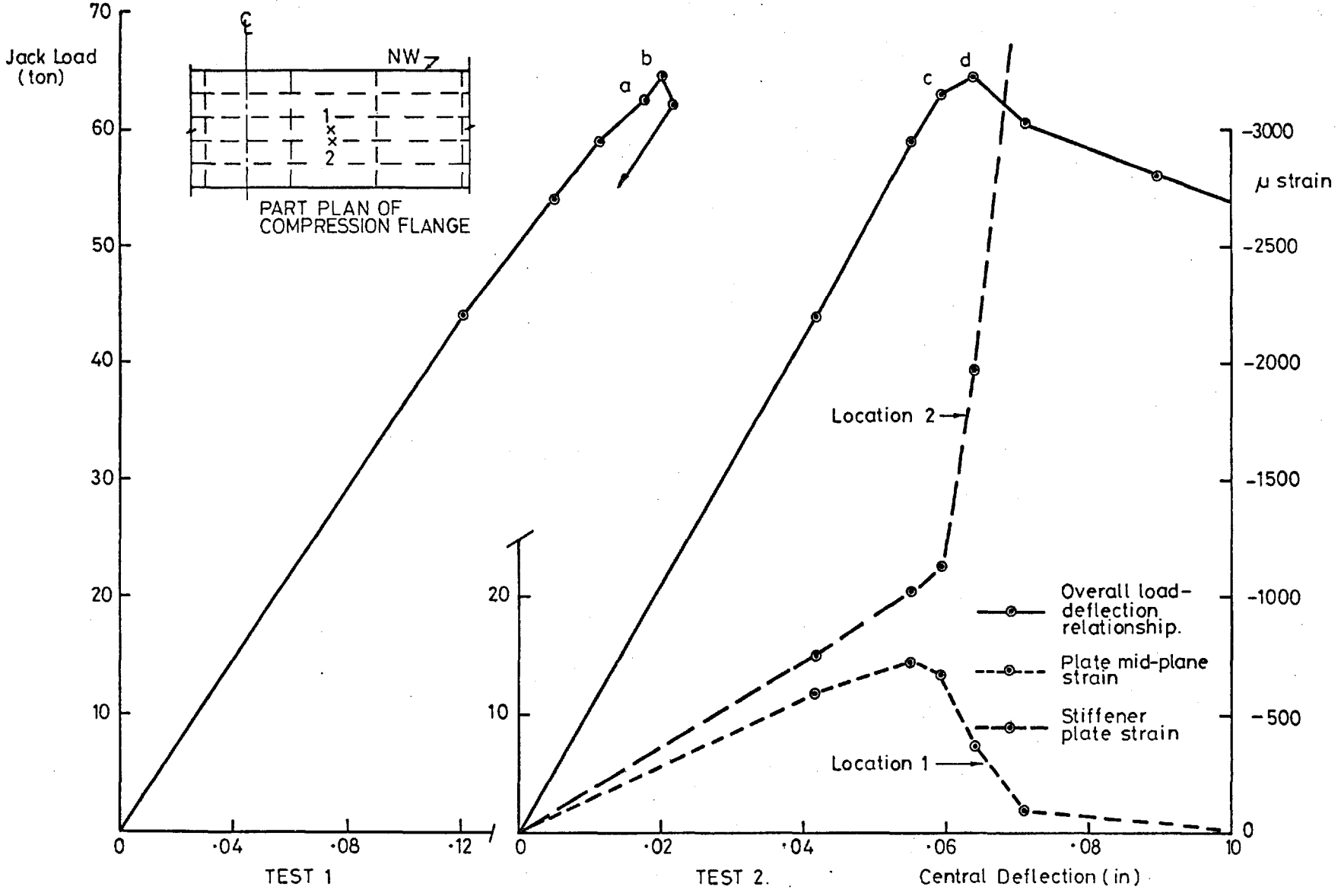

Fig. 19. Model 2 : Overall Load-Deflection Response and Behaviour of Compression Flange during the Two Ultimate Load Tests.

The locations indicated on the curves of flange behaviour are shown on the plan.
The letters indicate the loads at which the buckles shown in Fig. 18. developed.
Note the different central deflection scales for the two tests see text.
Note jack lever arm was 94·5 in.

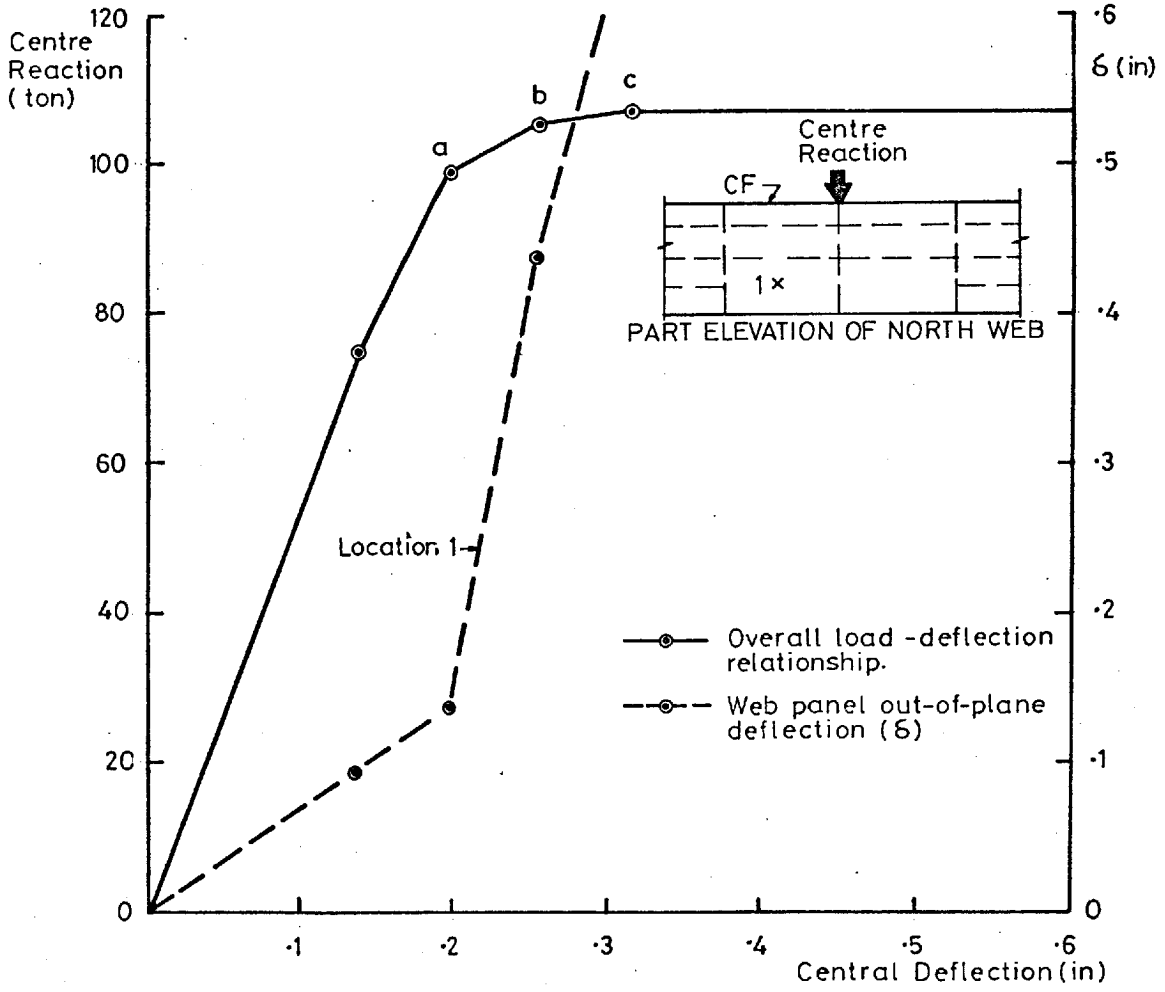

Fig.20. Model 5: Overall Load-Deflection Response and Web Panel Behaviour during Ultimate Load Test.

The location indicated on the curve of panel behaviour is shown on the elevation. The letters indicate the loads at which the buckles shown in Fig 21. developed.

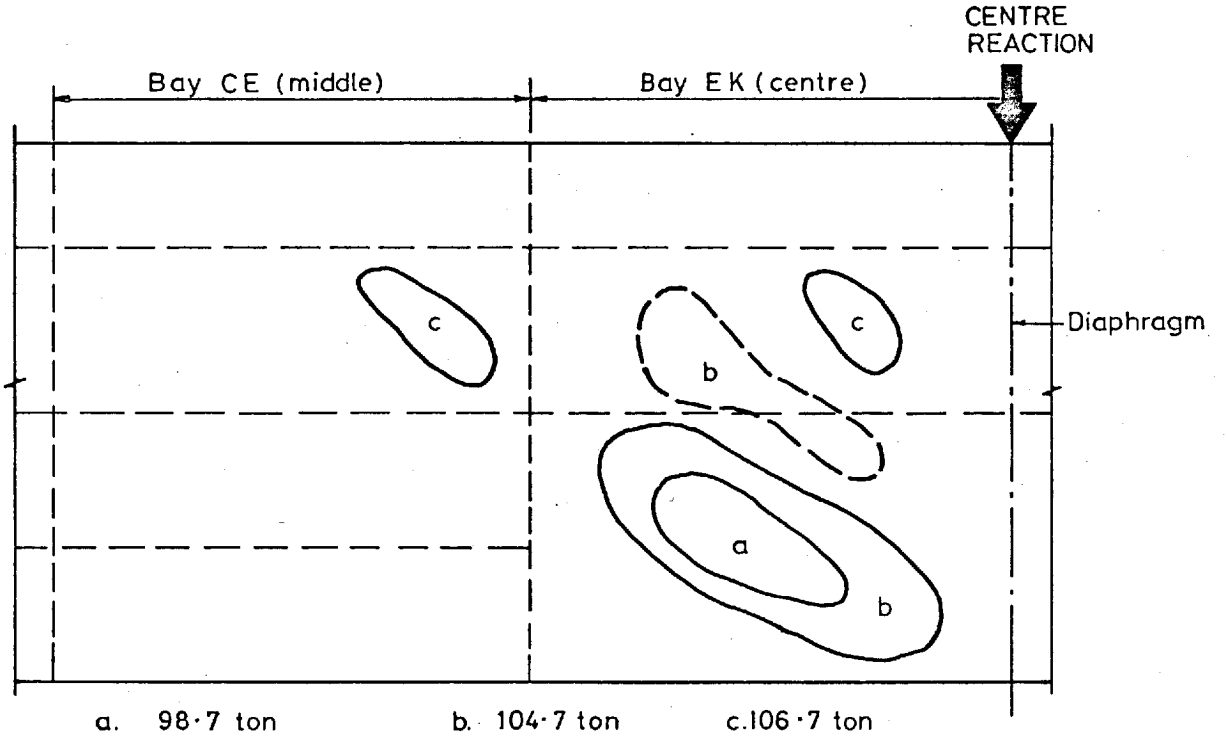

Fig. 21. Model 5: Development of Shear Buckles in the North Web during Ultimate Load Test.

The dashed lines indicate outward deflections, the full lines inwards. The load referenced against each deformation indicates the level at which it first developed. Distortions in all centre bays were similar at end of test, although buckles observed first in bay shown above

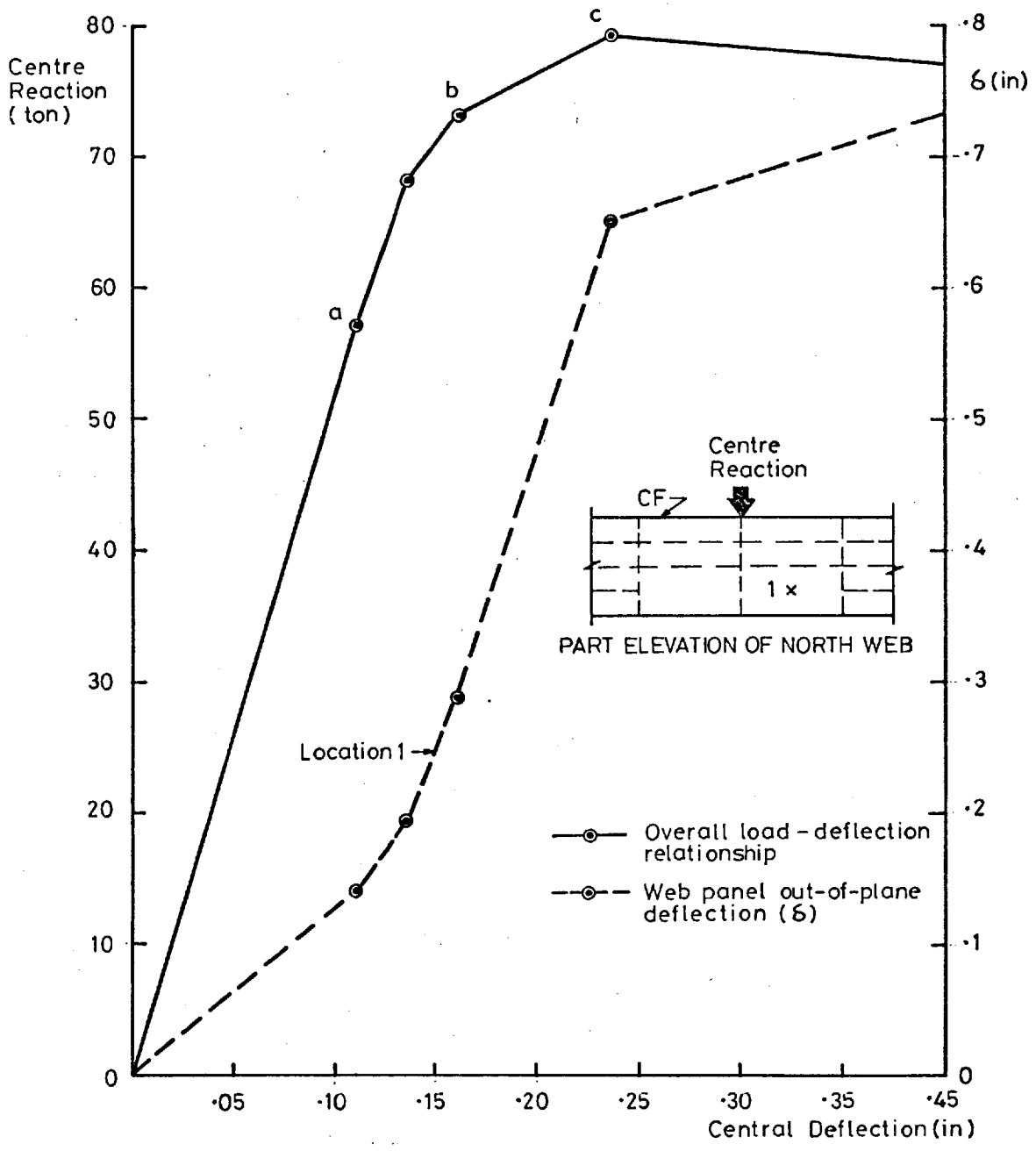

Fig.22. Model 7 : Overall Load-Deflection Response and Web Panel Behaviour during Ultimate Load Test.

The location indicated on the curve of panel behaviour is shown on the elevation. The letters indicate the loads at which the buckles shown in Fig.23. developed.

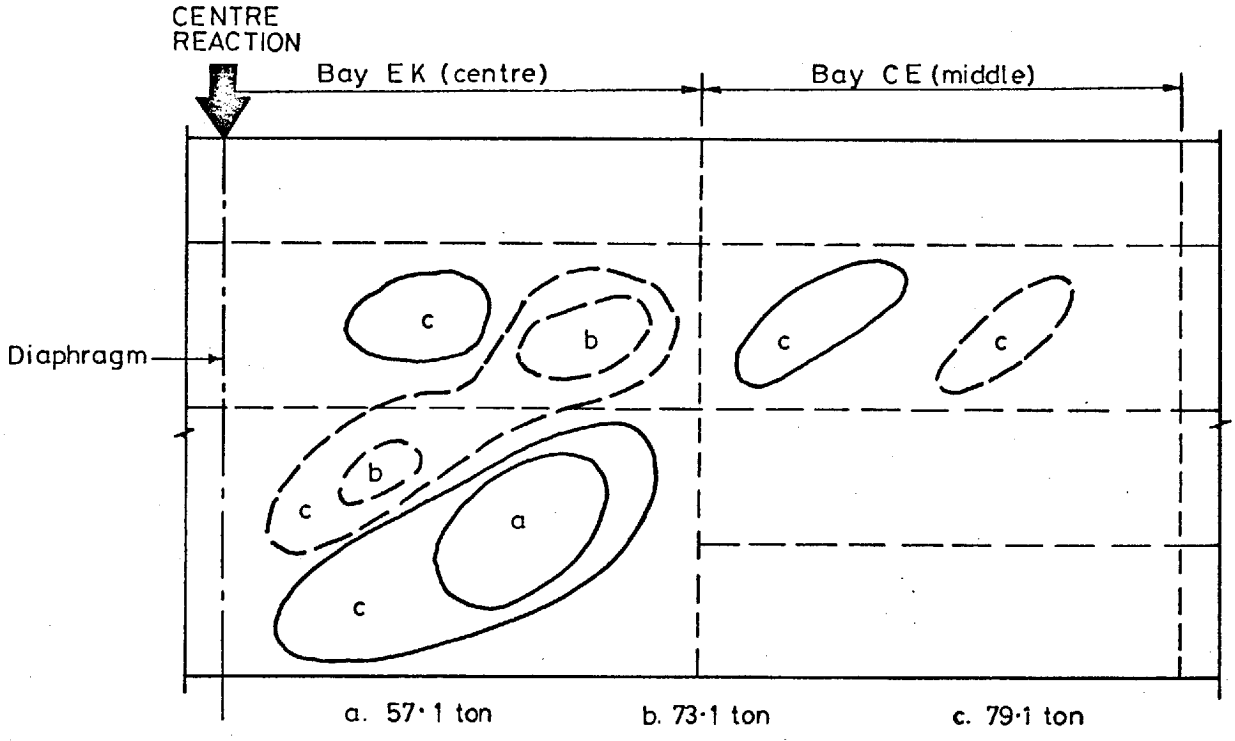

Fig. 23. Model 7: Development of Shear Buckles in the North Web during Ultimate Load Test.

The dashed lines indicate outward deflections, the full lines inwards. The load referenced against each deformation indicates the level at which it first developed. Similar buckles formed in the south web on the opposite side of the diaphragm.

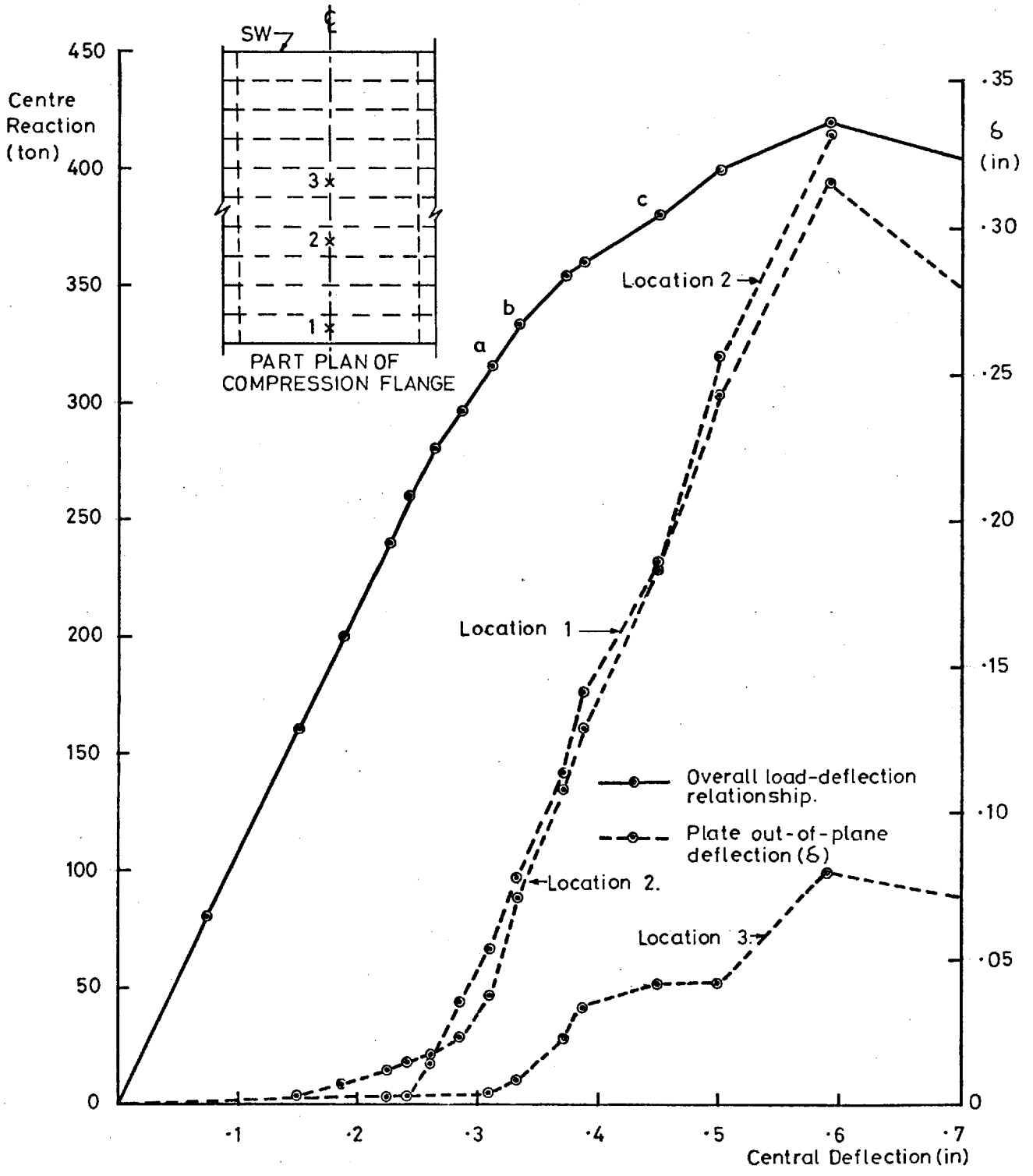

Fig. 24. Model 9: Overall Load-Deflection Response and Behaviour of Compression Flange during Ultimate Load Test.

The locations indicated on the curves of flange behaviour are shown on the plan. The letters indicate the loads at which the buckles shown in Fig. 25. developed

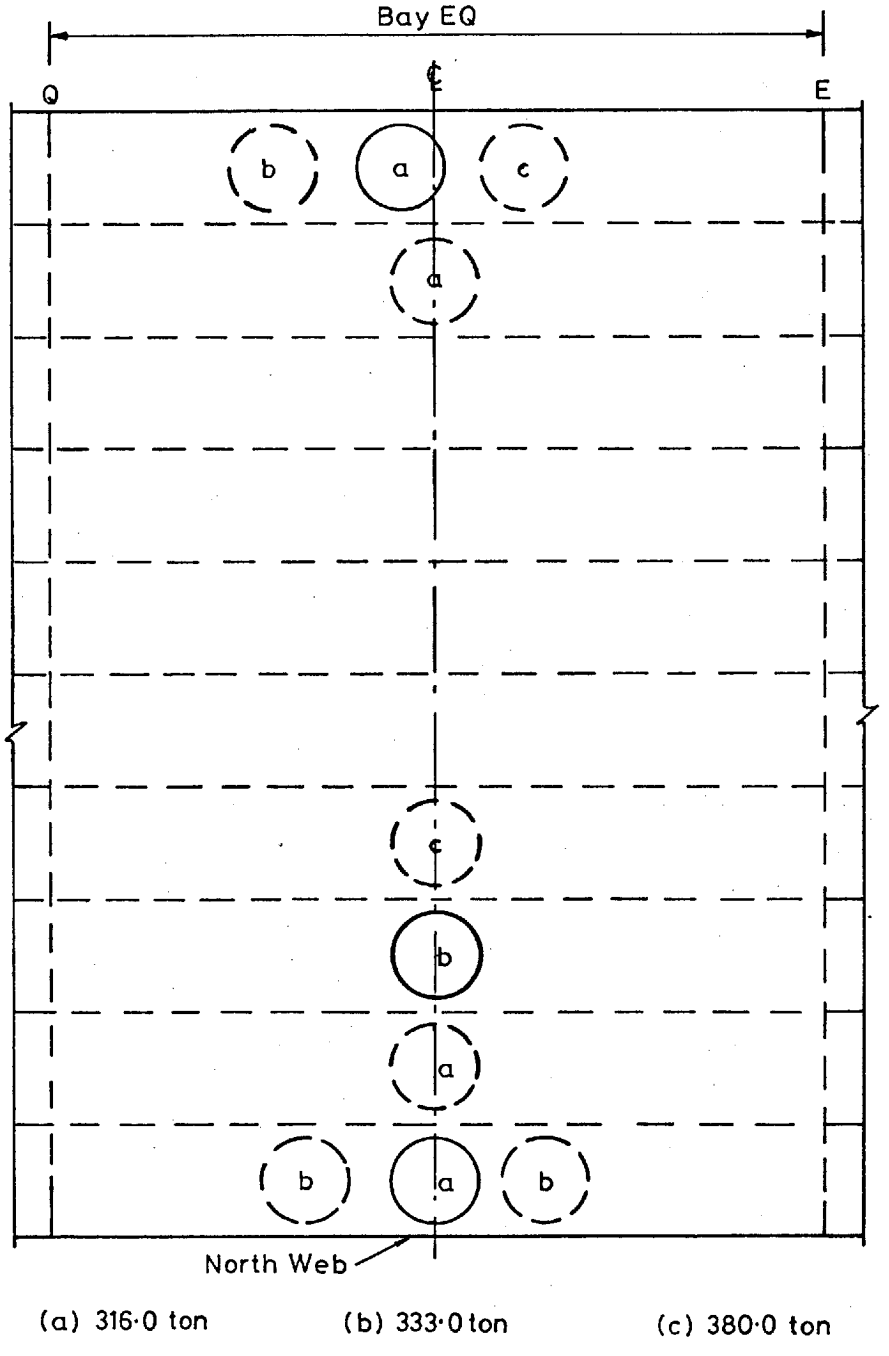

Fig.25. Model 9: Development of Compression Flange Plate Buckles during Ultimate Load Test.
The dashed lines indicate outward deflections, the full lines inward. The load referenced against each deformation indicates the level at which it first developed.

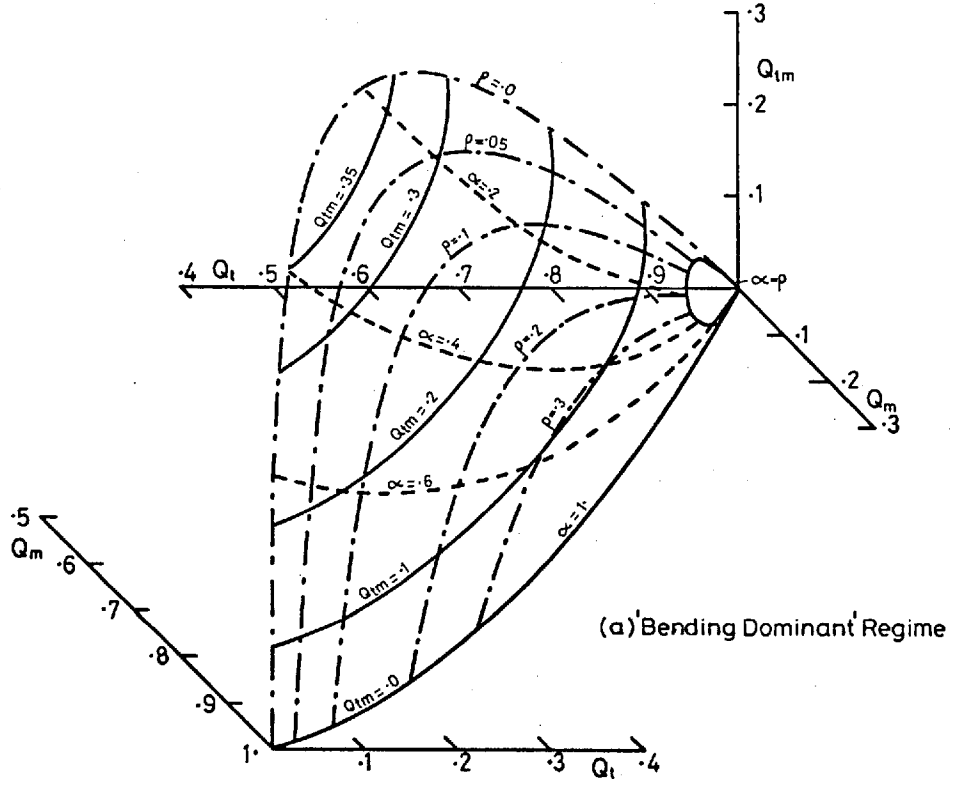

(a) 'Bending Dominant' Regime

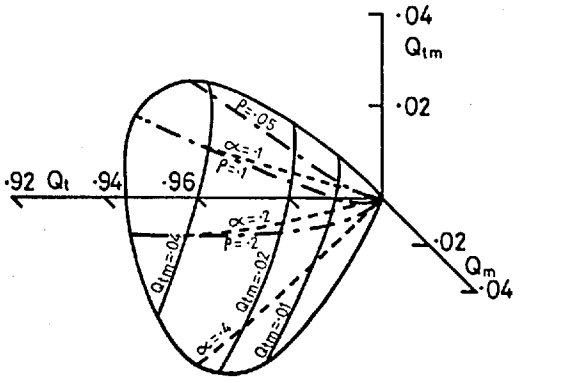

(b) 'In-plane Dominant' Regime

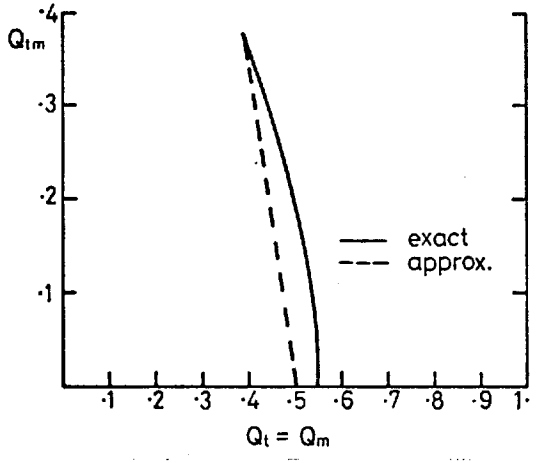

(c) Comparison between exact and approximate surfaces on plane $Q_t = Q_m$ (bending dominant)

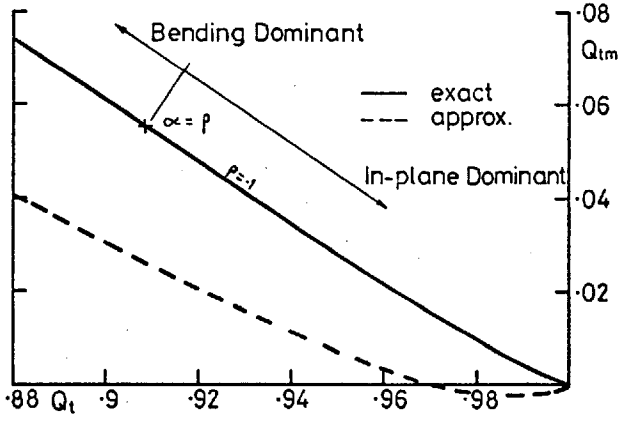

(d) Junction between bending dominant and in-plane dominant regimes.

Fig.26 Ilyushin's Yield Surface

Q_t, Q_m and Q_{tm} are the quadratic stress intensities.

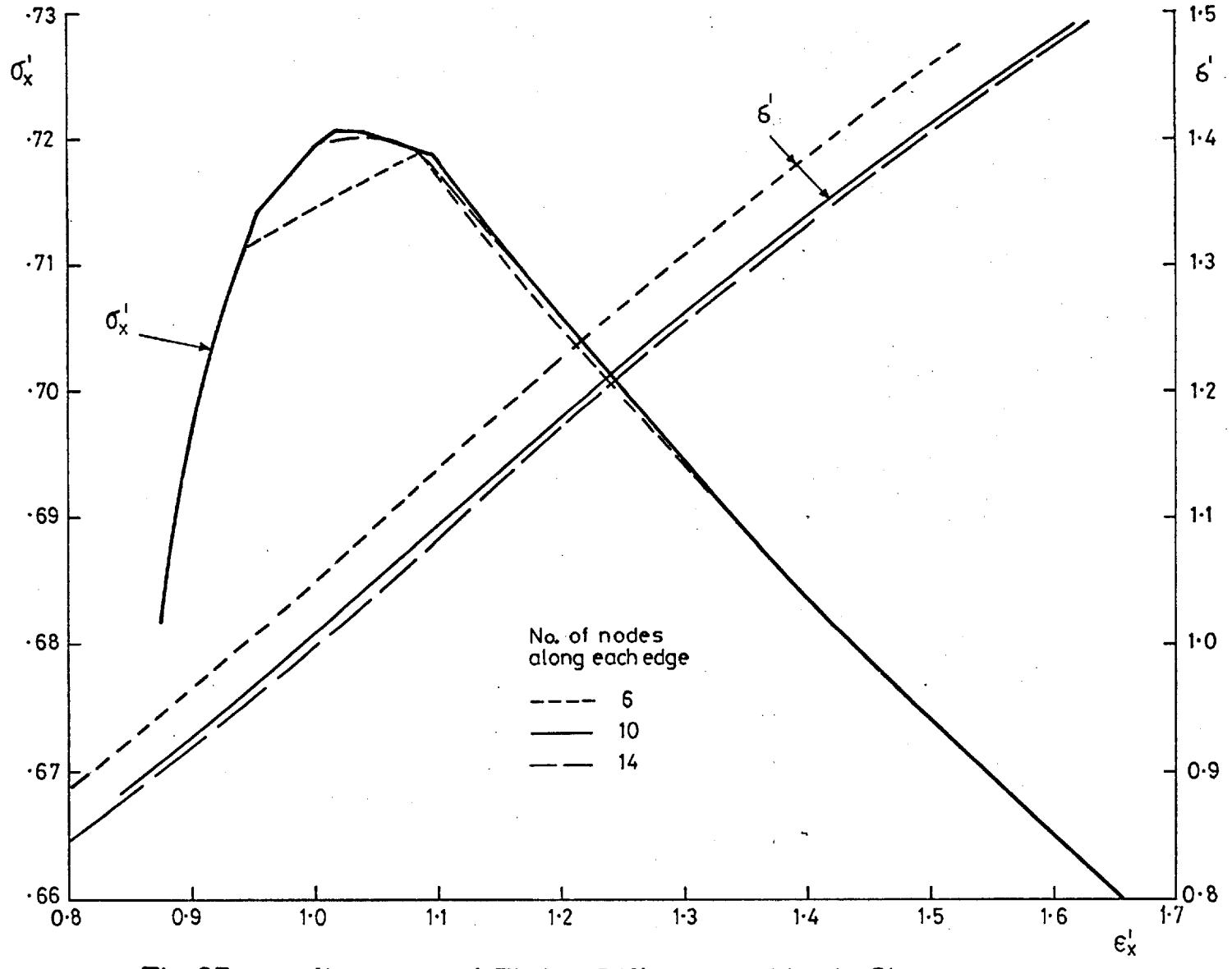

Fig. 27 a. Influence of Finite Difference Mesh Size on Solution for Plate in Compression.

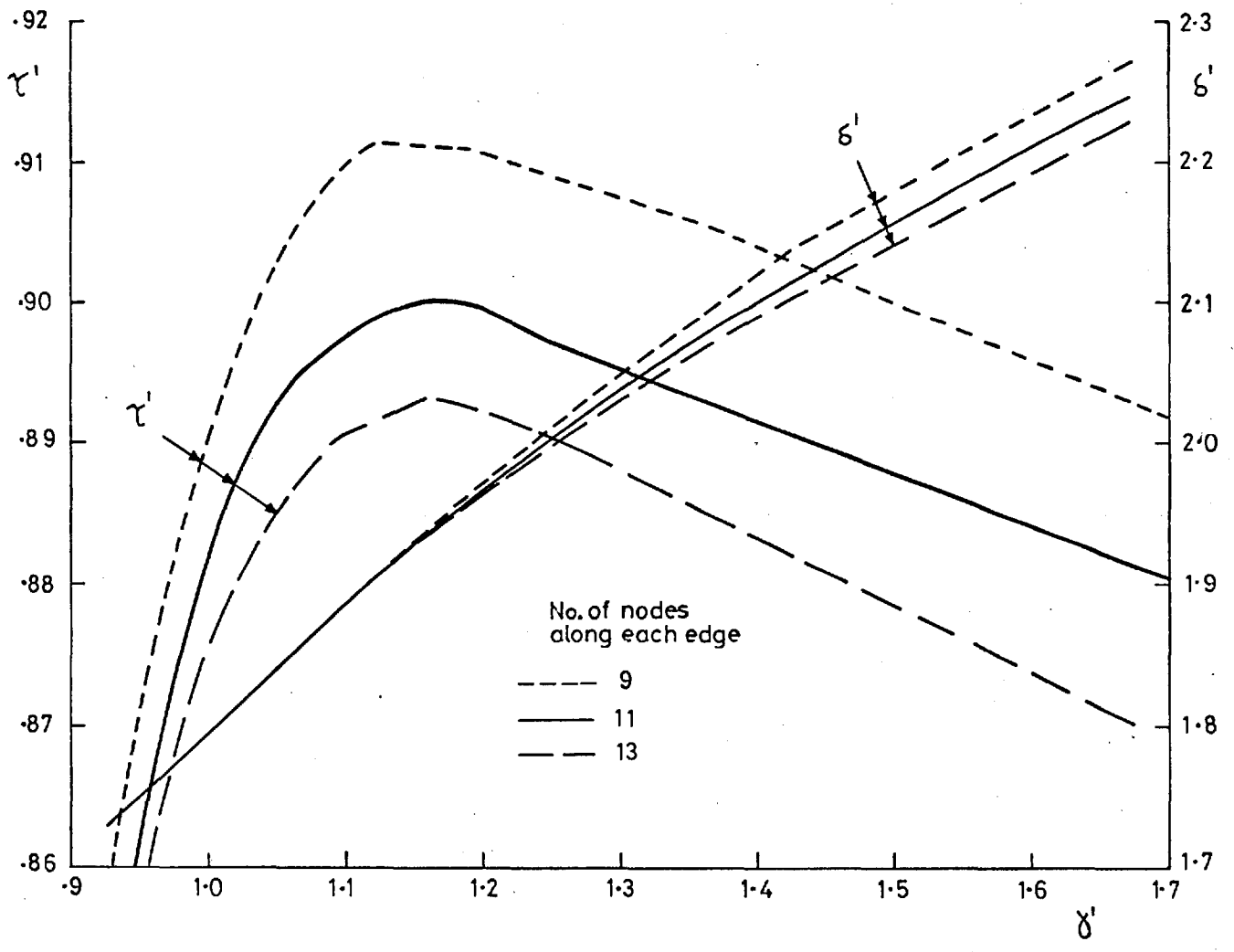

Fig. 27b. Influence of Finite Difference Mesh Size on Solution for Plate in Shear.

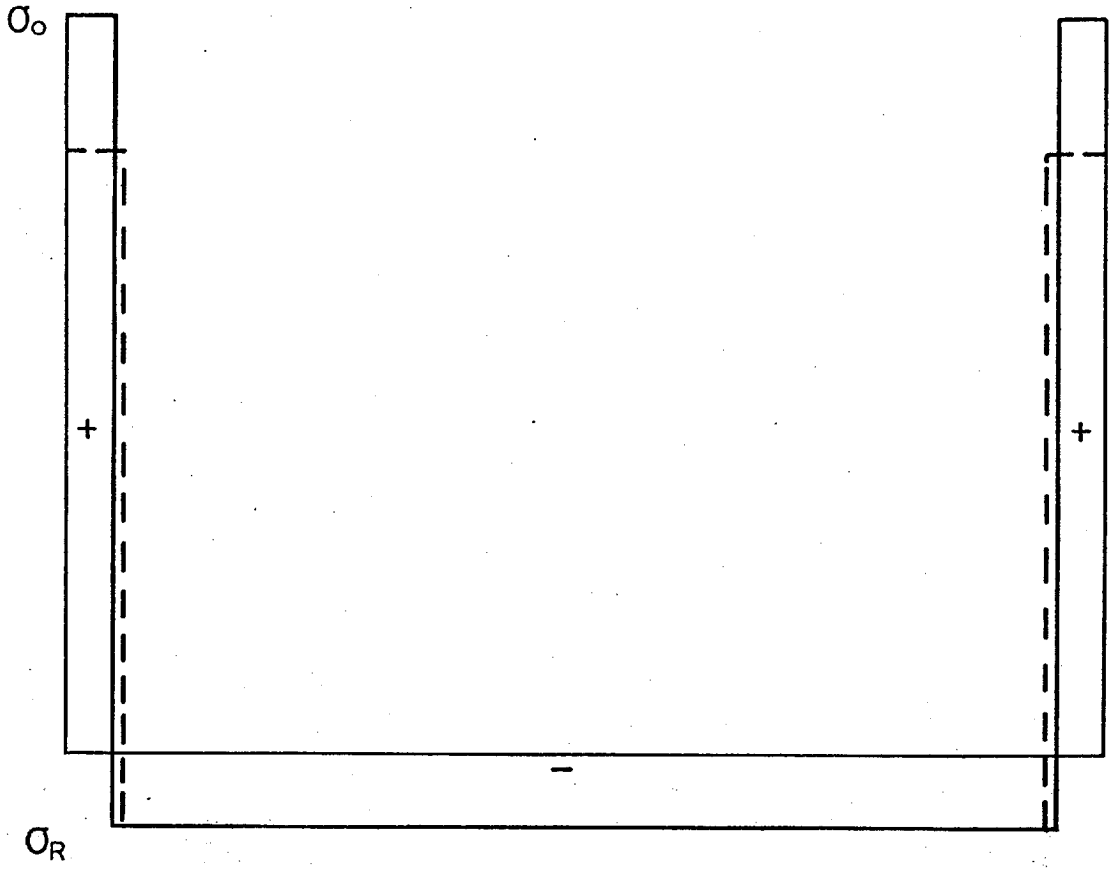

Idealised residual stress block

Stress block to suit finite difference mesh

σ_o Uniaxial yield stress

σ_R Required level of compressive residual stress

Fig.28. Finite Difference Form of Idealised Residual Stress Block.

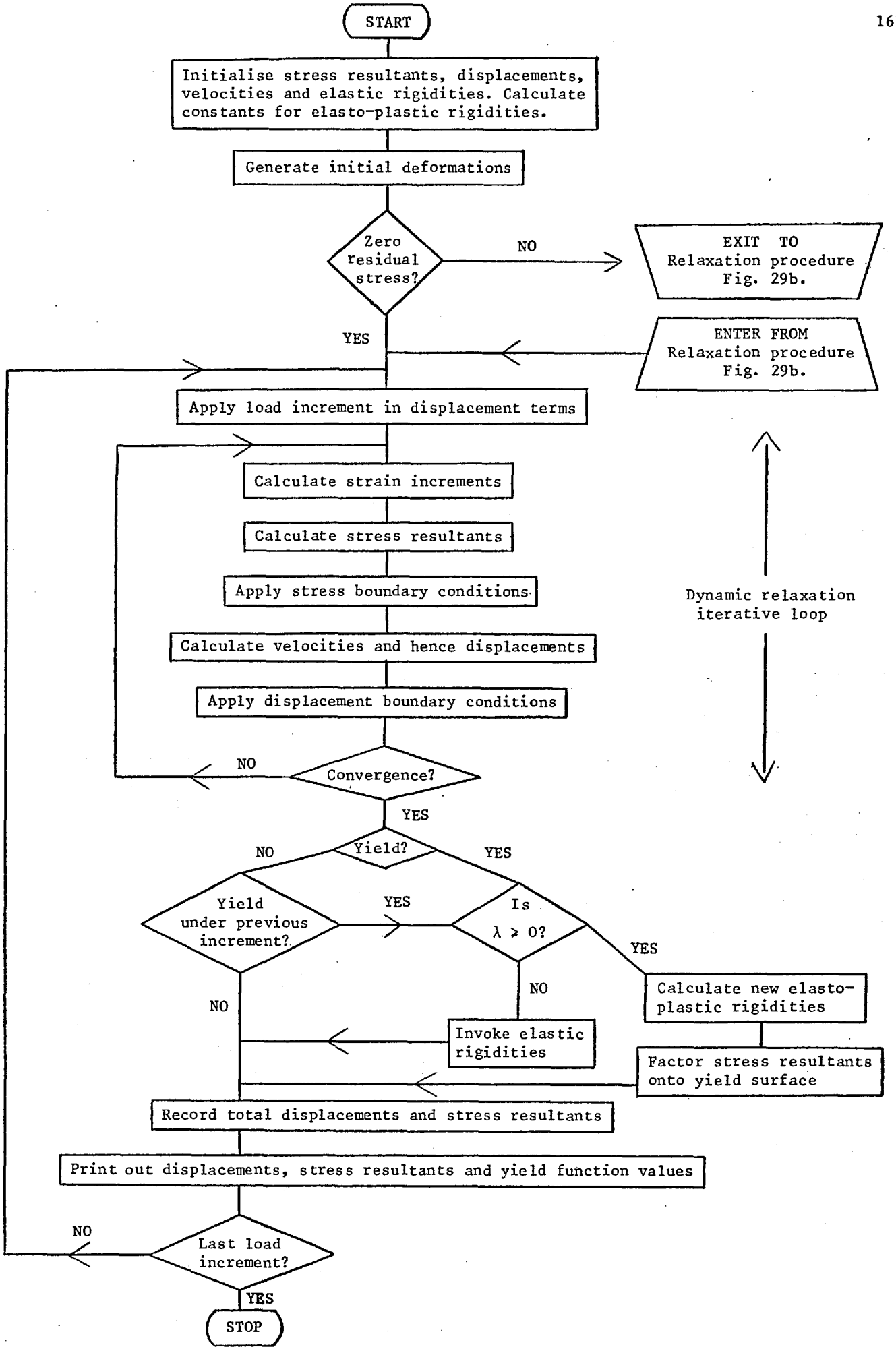

Fig. 29a. Flow Chart of Dynamic Relaxation Iteration Loop and Calculation of Elasto-Plastic Rigidities

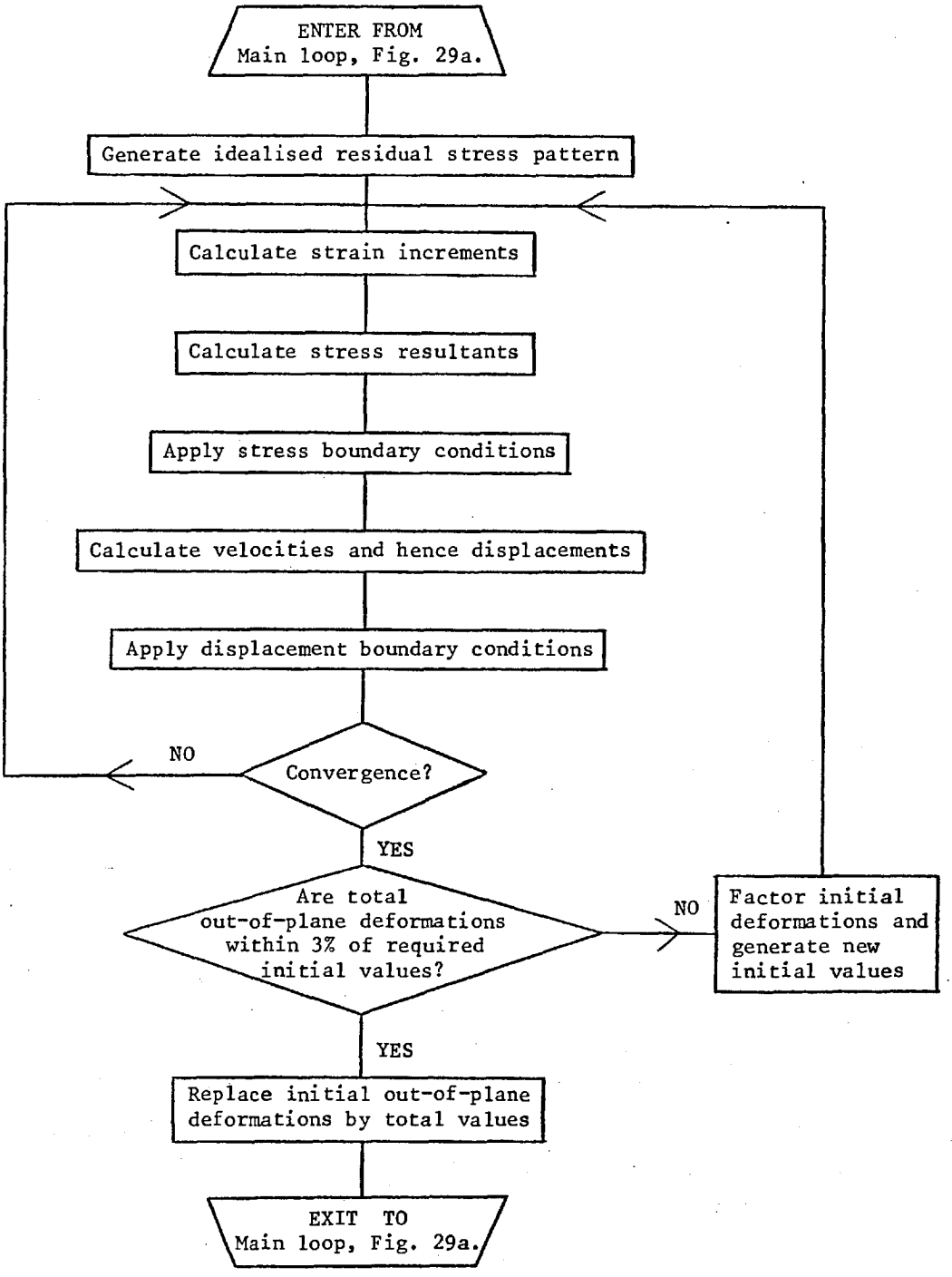

Fig. 29b. Flow Chart of Relaxation Procedure for Initial Out-of-Plane Deformations

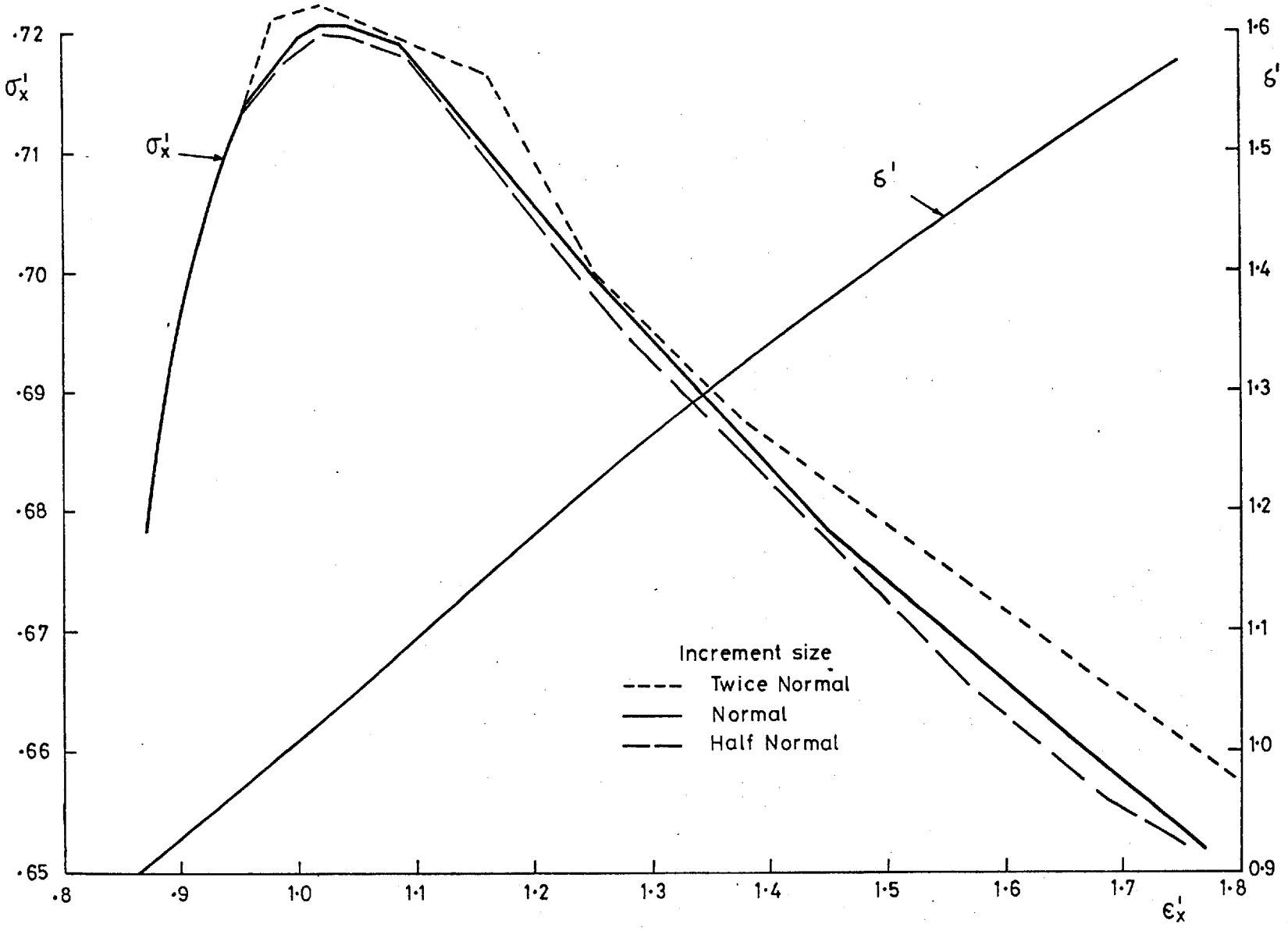

Fig.30. Influence of Increment Size on Solution for Plate in Compression

See text for defination of 'normal' increment.

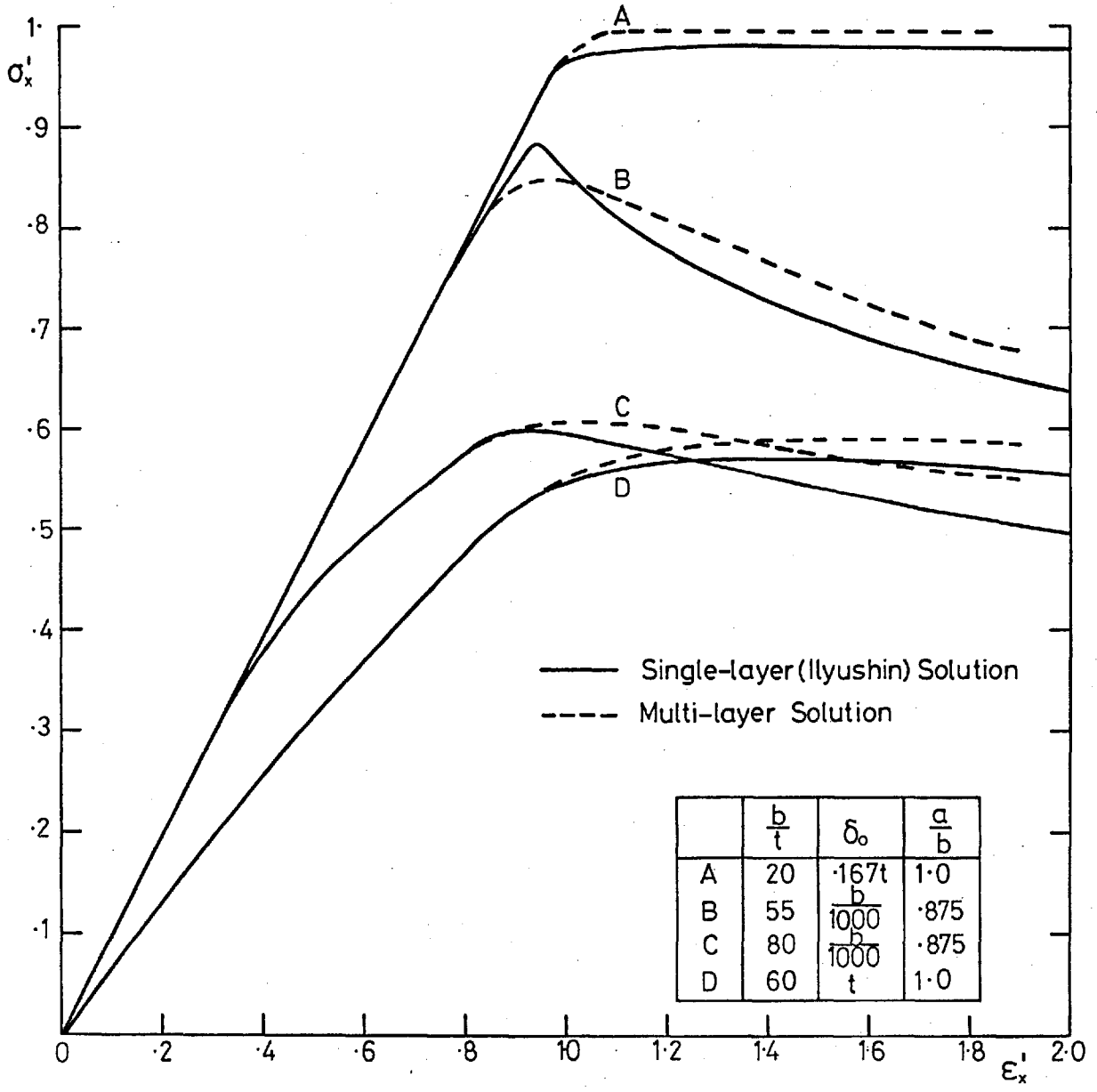

	$\frac{b}{t}$	δ_o	$\frac{a}{b}$
A	20	·167t	1·0
B	55	$\frac{b}{1000}$	·875
C	80	$\frac{b}{1000}$	·875
D	60	t	1·0

Fig.31 Comparison Between Single and Multi-Layer Solutions For Plates in Compression.

Edges unrestrained: zero residual stress.

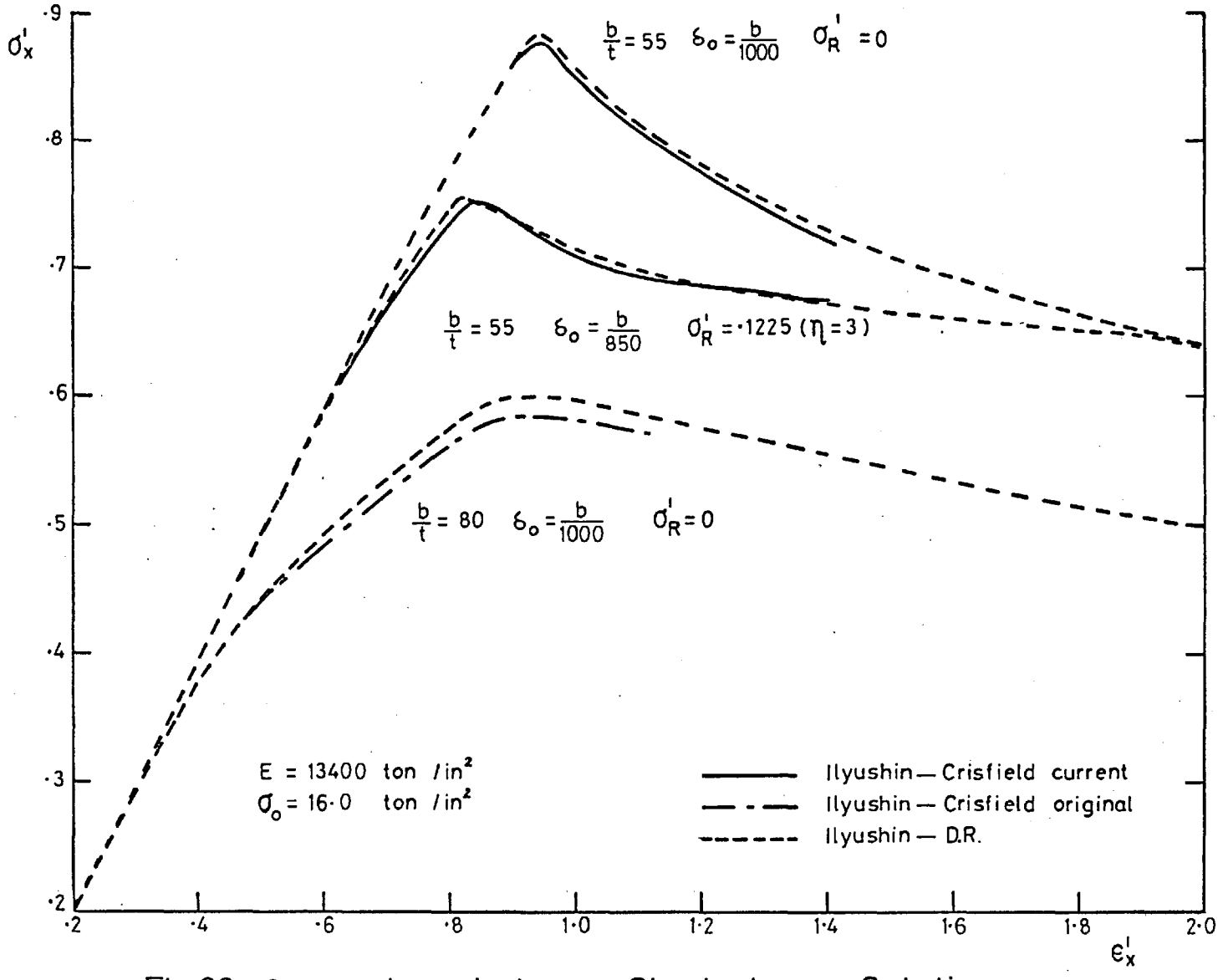

Fig.32. Comparison between Single-Layer Solutions for Plates in Compression.

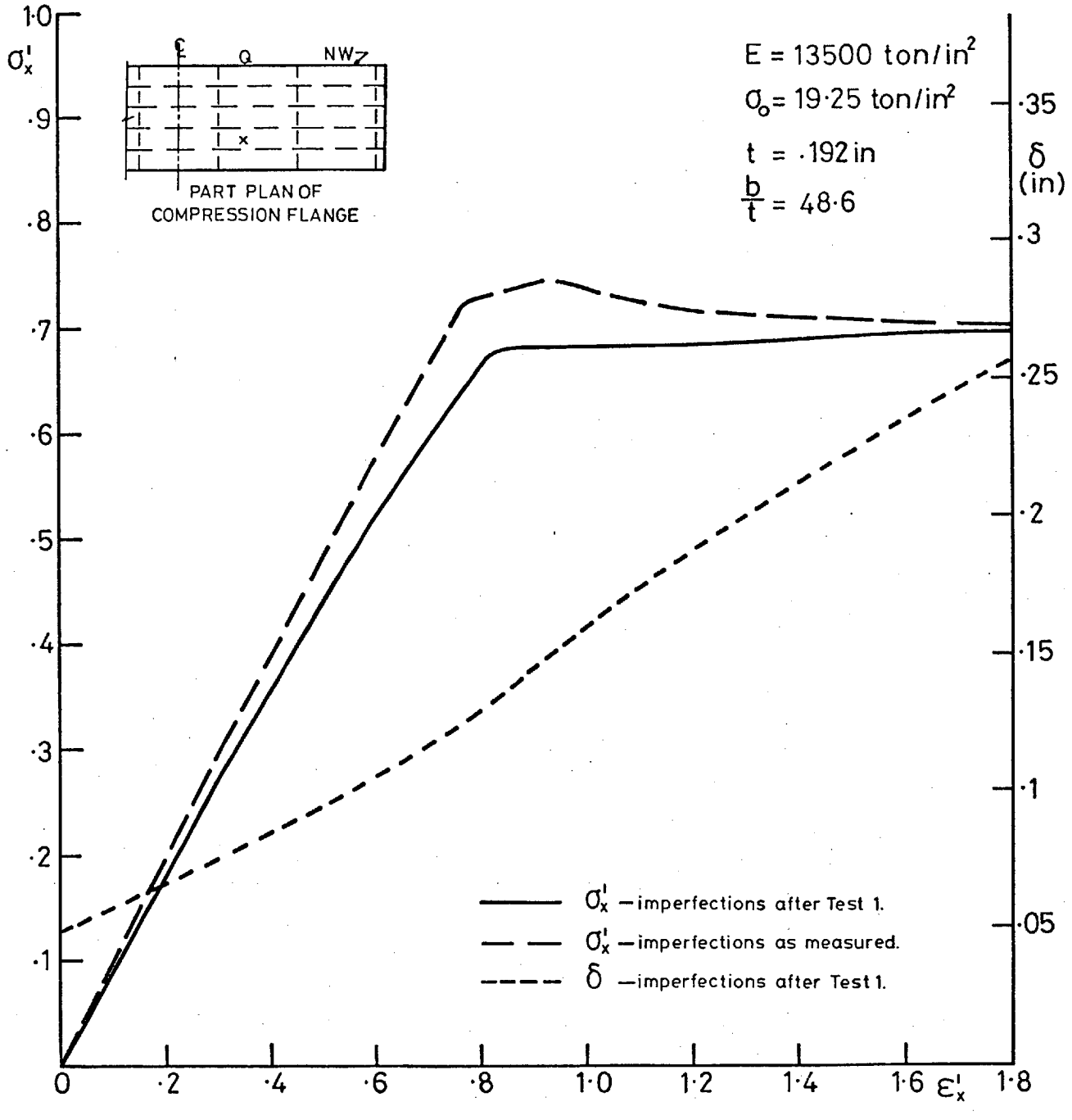

Fig.33. Model 2: Average Stress-Strain Curves for Compression Flange Plate.
Location of panel analysed is shown on insert.

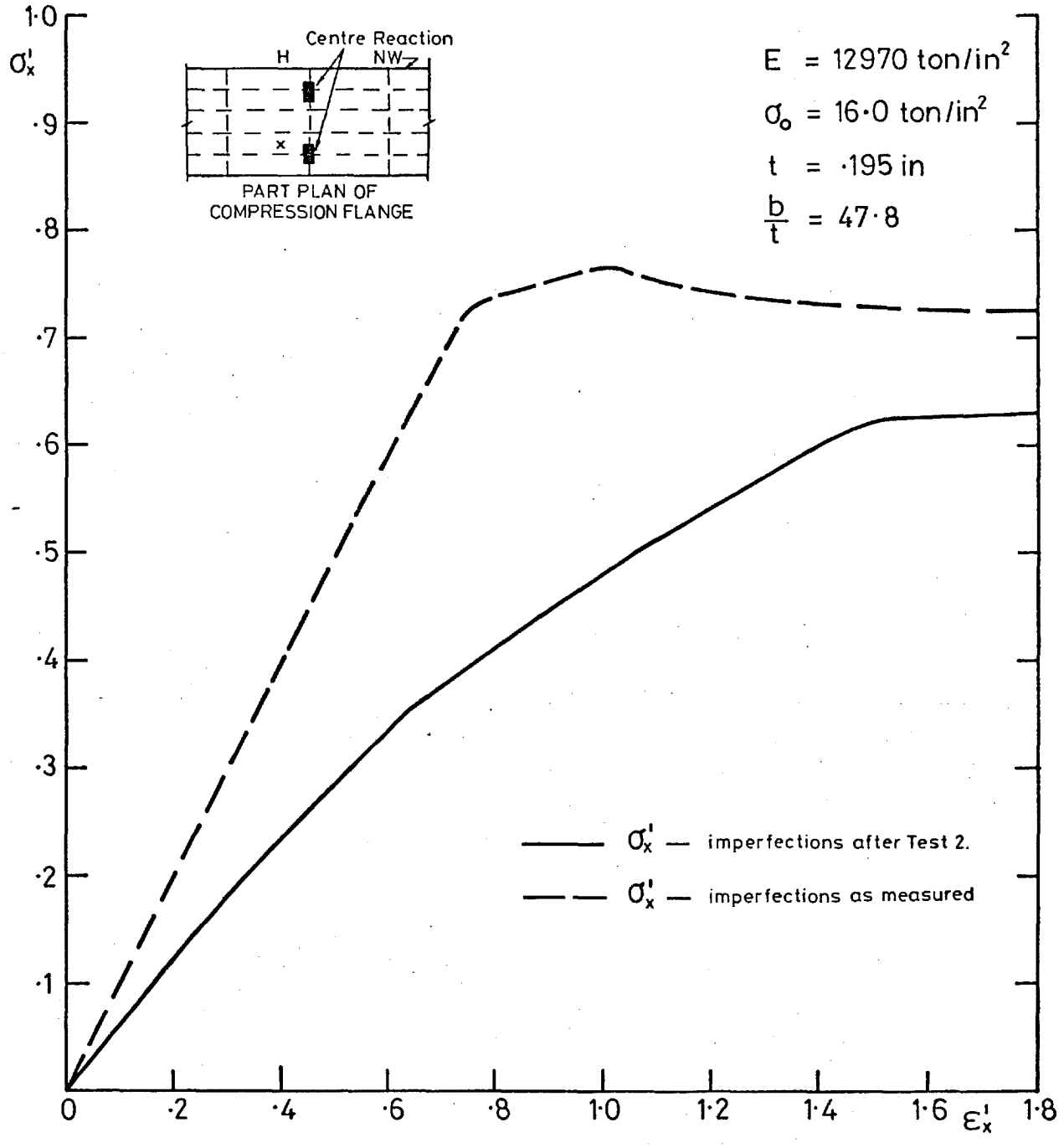

Fig.34. Model 1: Average Stress-Strain Curves for Compression Flange Plate.

Location of panel analysed is shown on insert.

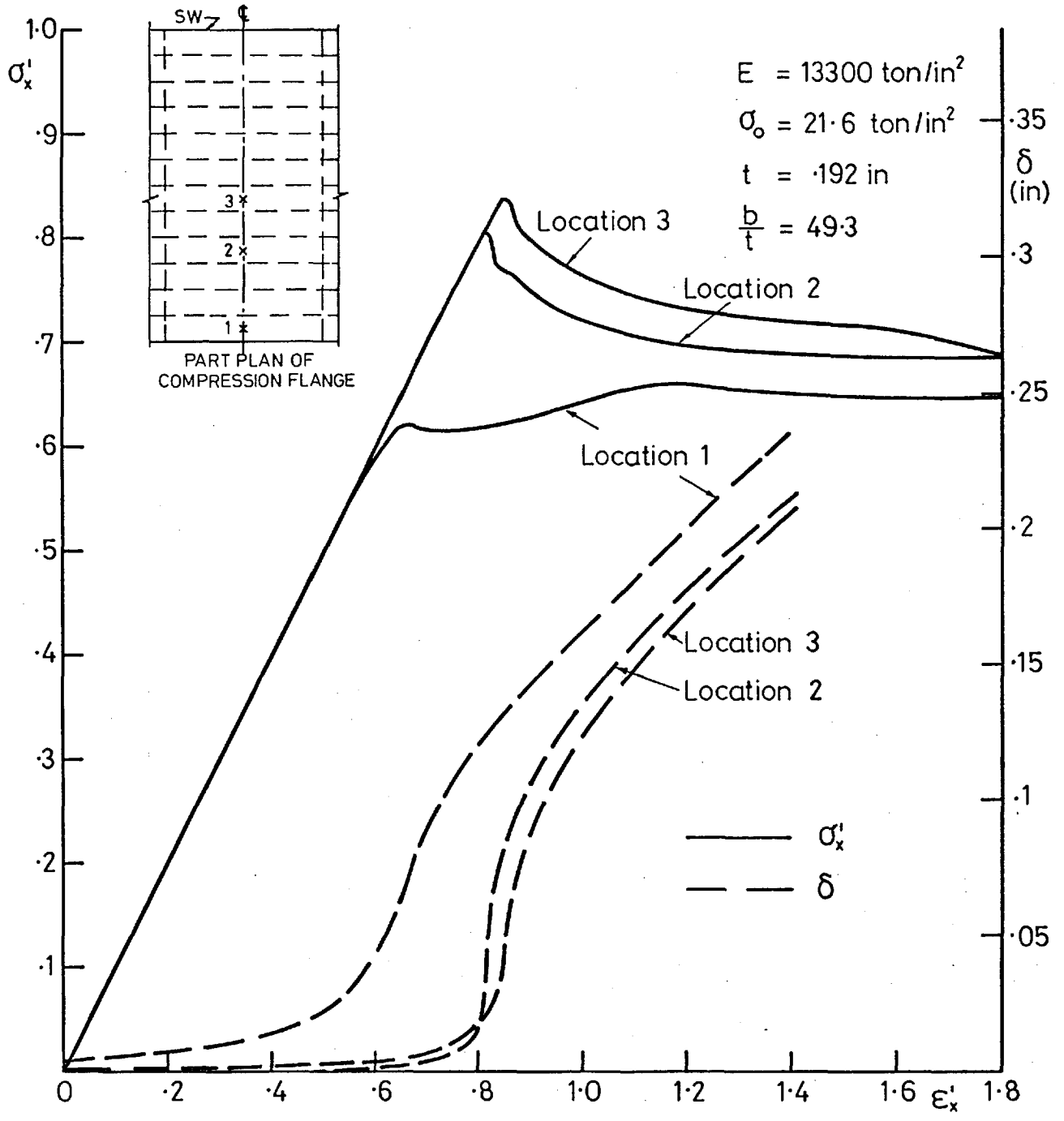

Fig.35. Model 9: Average Stress–Strain Curves for Compression Flange Plates.

Location of panels analysed is shown on insert.

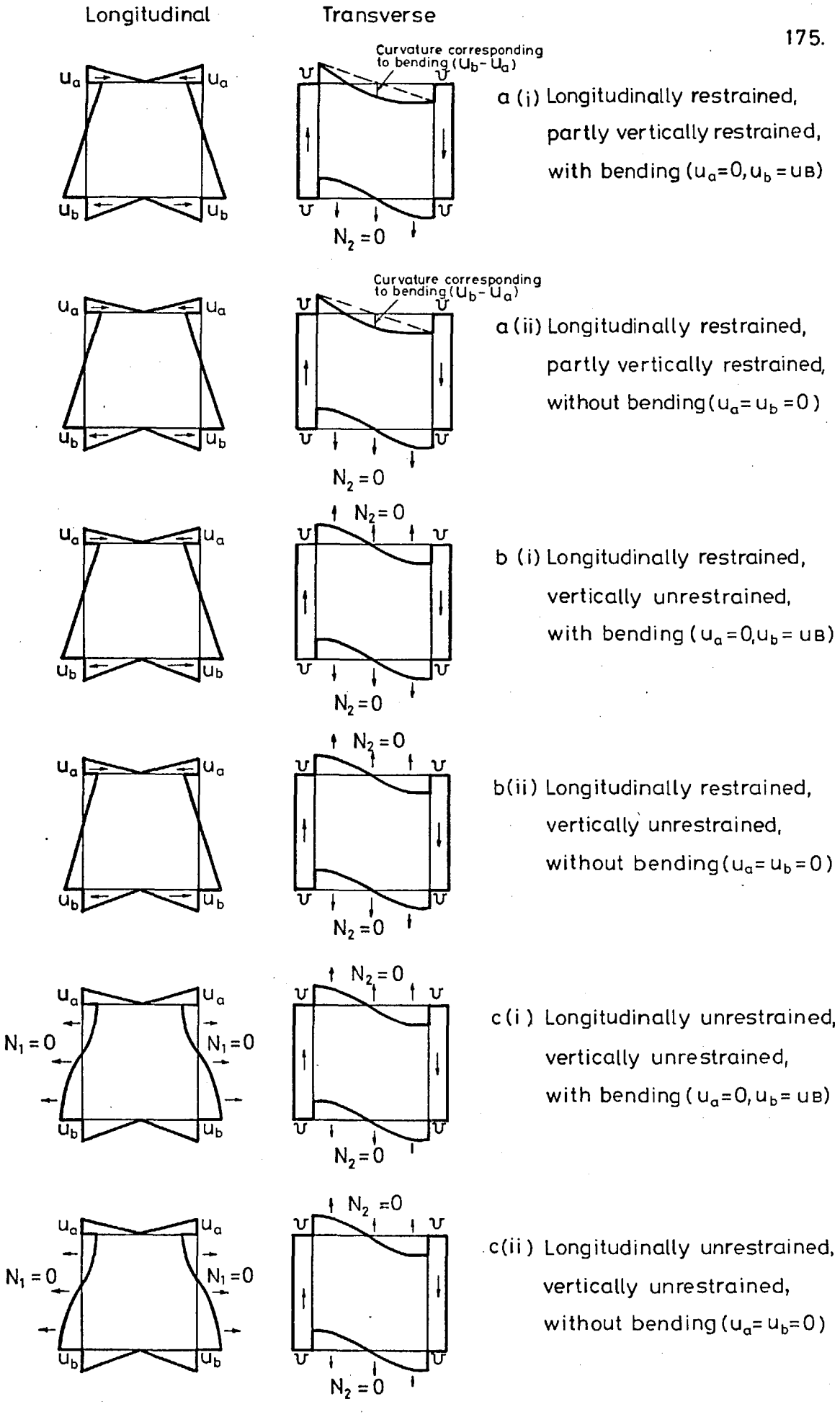

a (i) Longitudinally restrained, partly vertically restrained, with bending ($u_a = 0, u_b = u_B$)

a (ii) Longitudinally restrained, partly vertically restrained, without bending ($u_a = u_b = 0$)

b (i) Longitudinally restrained, vertically unrestrained, with bending ($u_a = 0, u_b = u_B$)

b(ii) Longitudinally restrained, vertically unrestrained, without bending ($u_a = u_b = 0$)

c (i) Longitudinally unrestrained, vertically unrestrained, with bending ($u_a = 0, u_b = u_B$)

c(ii) Longitudinally unrestrained, vertically unrestrained, without bending ($u_a = u_b = 0$)

Fig. 36 In-Plane Boundary Conditions for Plates Loaded in Shear

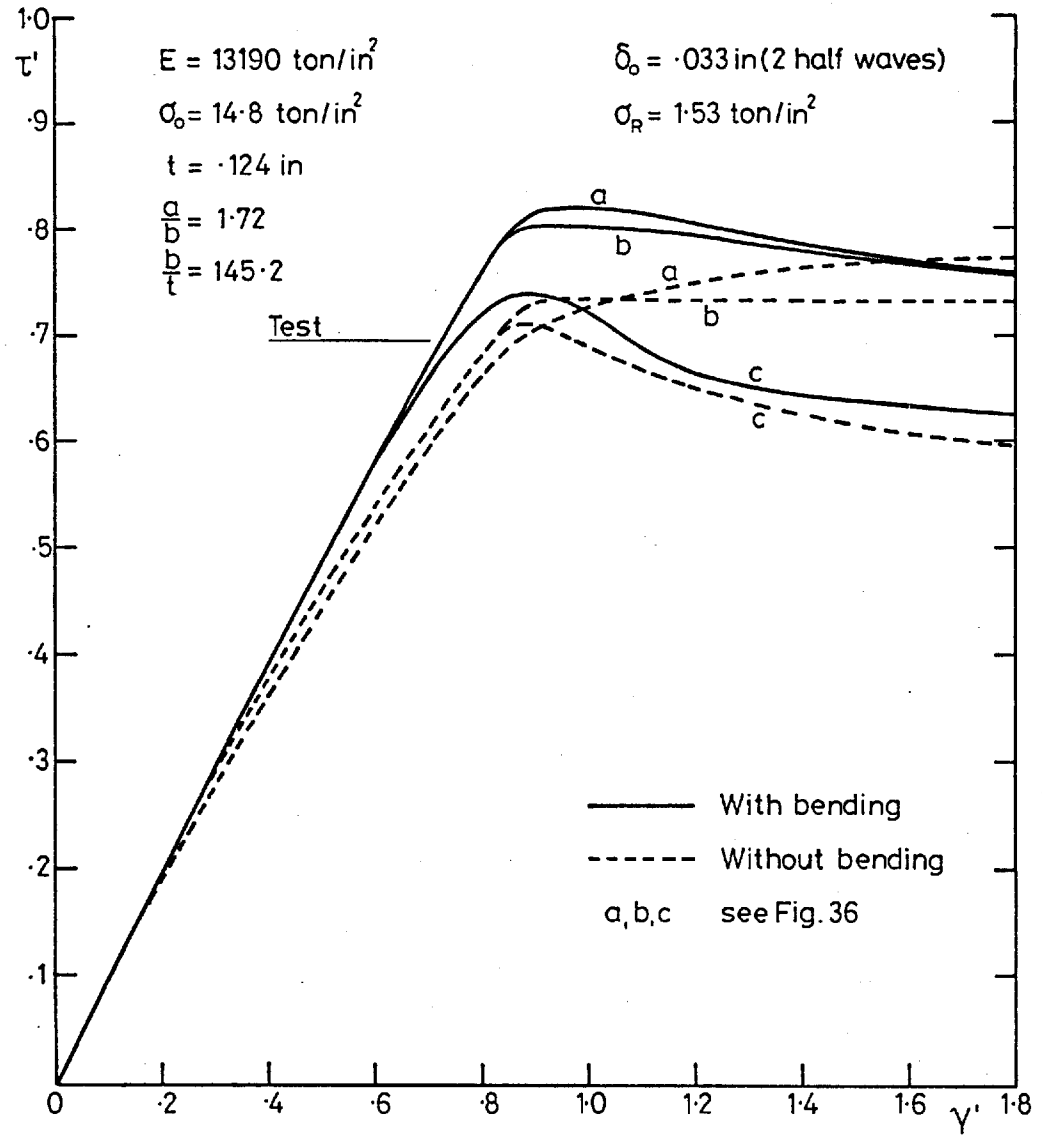

(a) North Web, Bay EK

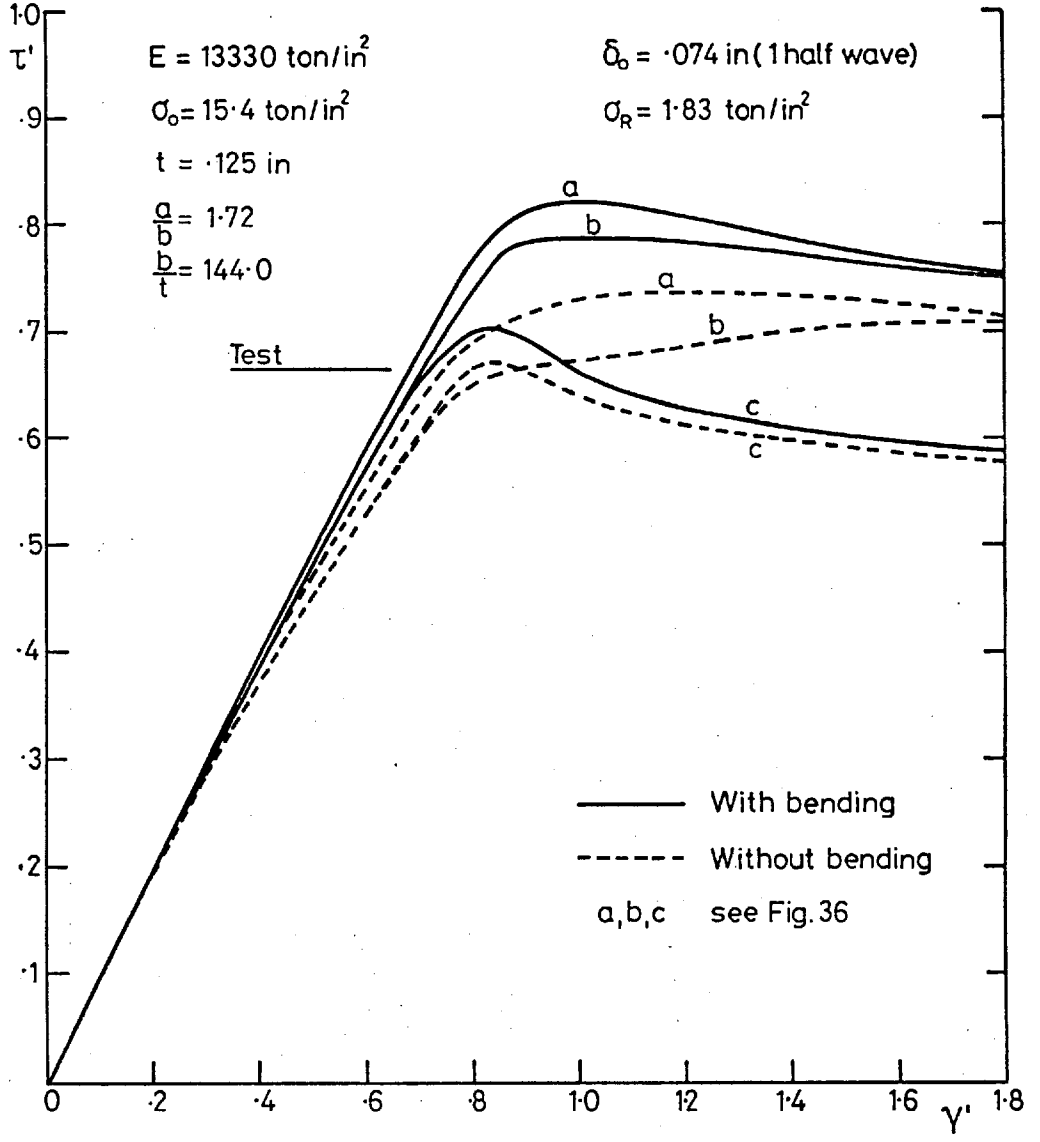

(b) South Web, Bay EK

Fig.37. Model 5: Comparison between Theoretical and Experimental Capacities of Web Plates

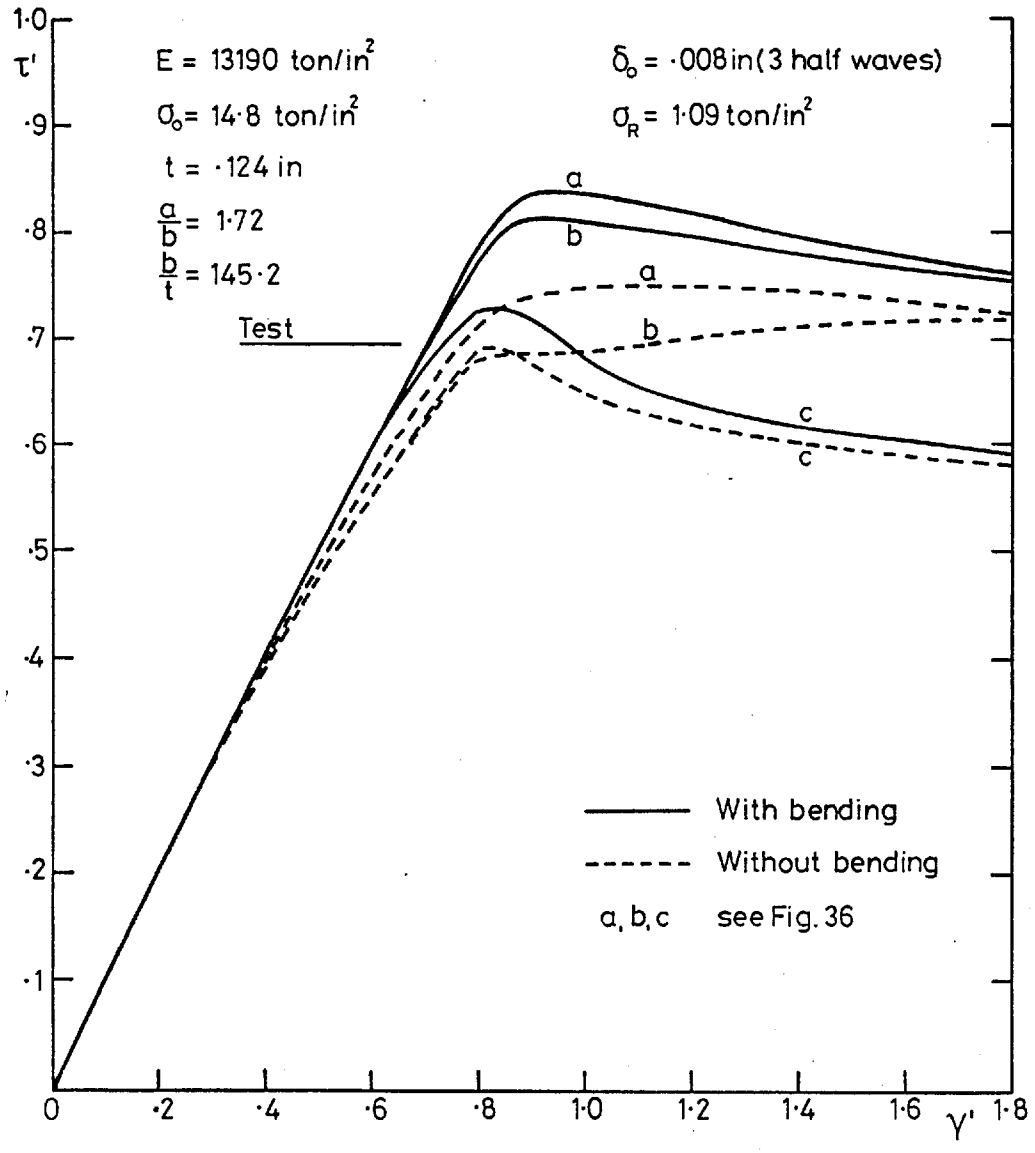

(a) North Web, Bay KQ

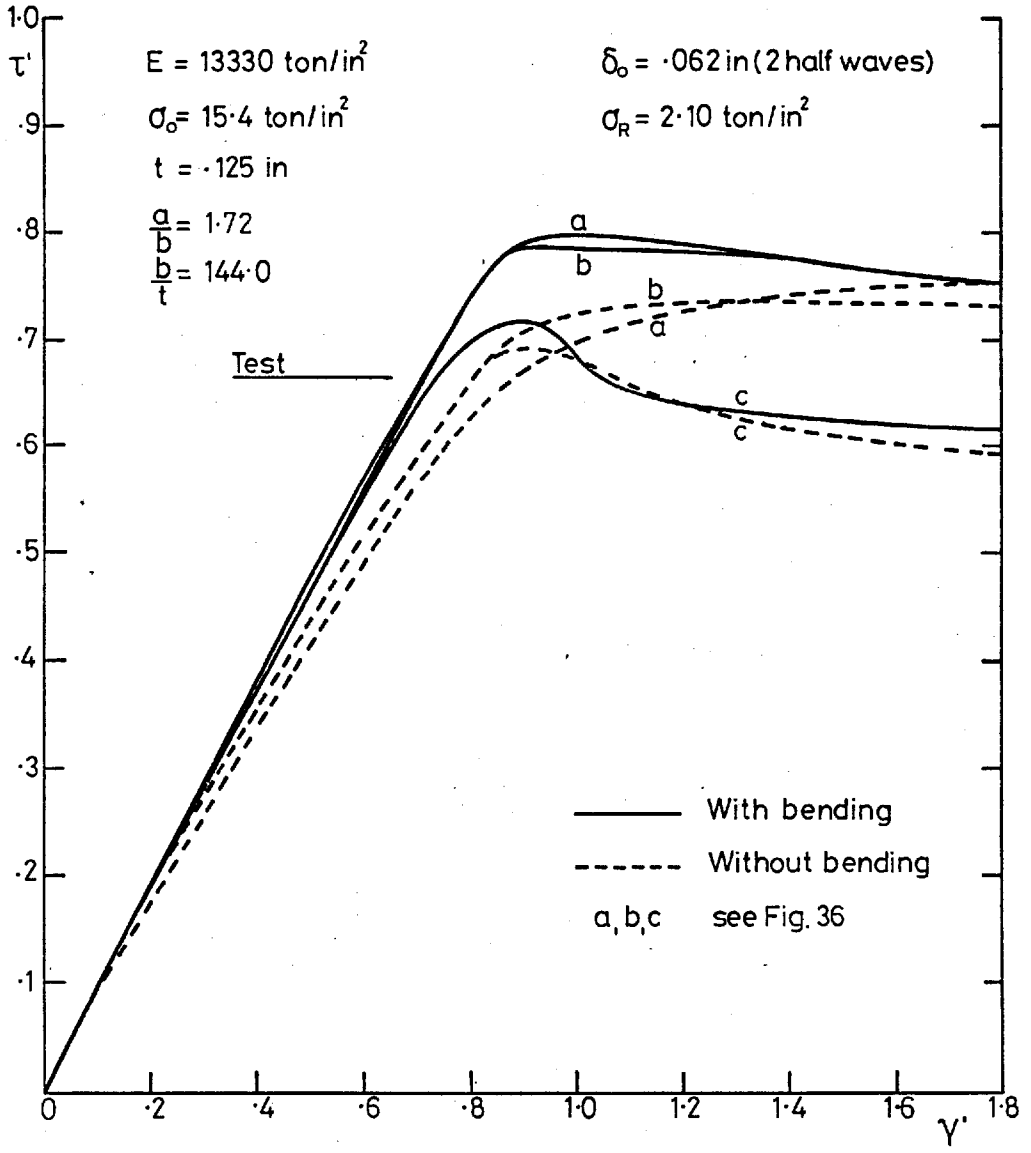

(b) South Web, Bay KQ

Fig.38. Model 5: Comparison between Theoretical and Experimental Capacities of Web Plates

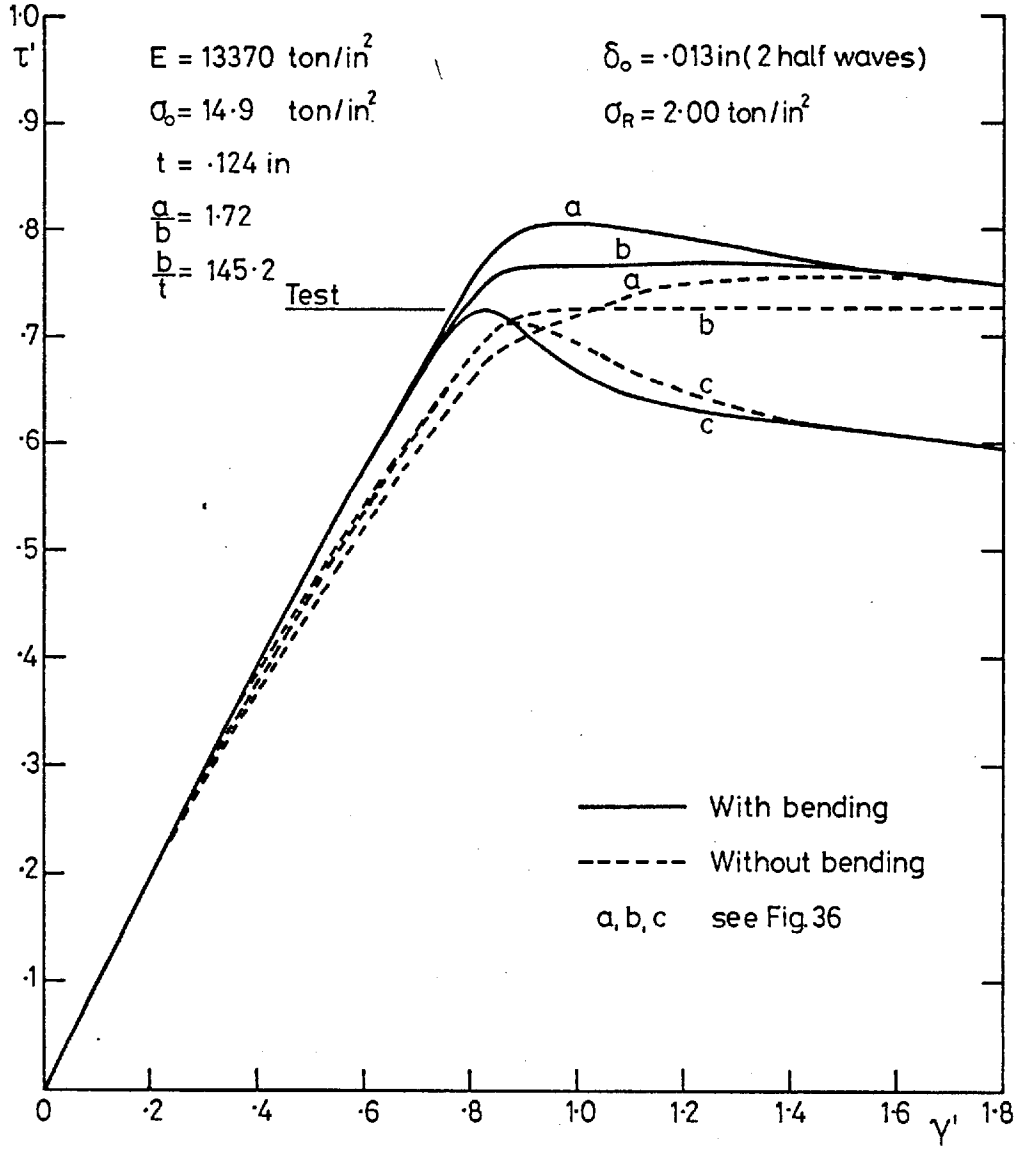

(a) North Web, Bay EK

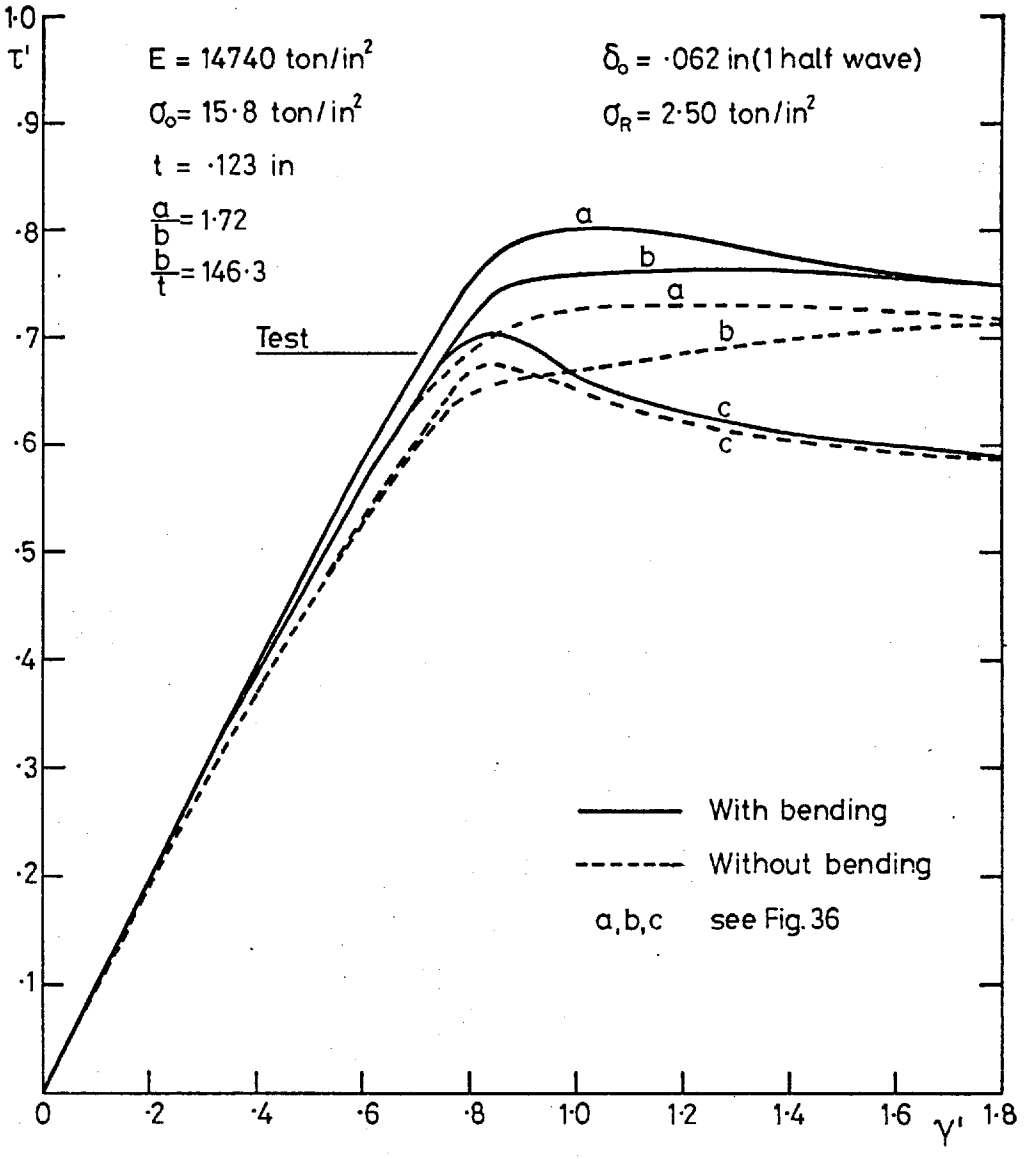

(b) South Web, Bay KQ

Fig. 39. Model 7: Comparison between Theoretical and Experimental Capacities of Web Plates

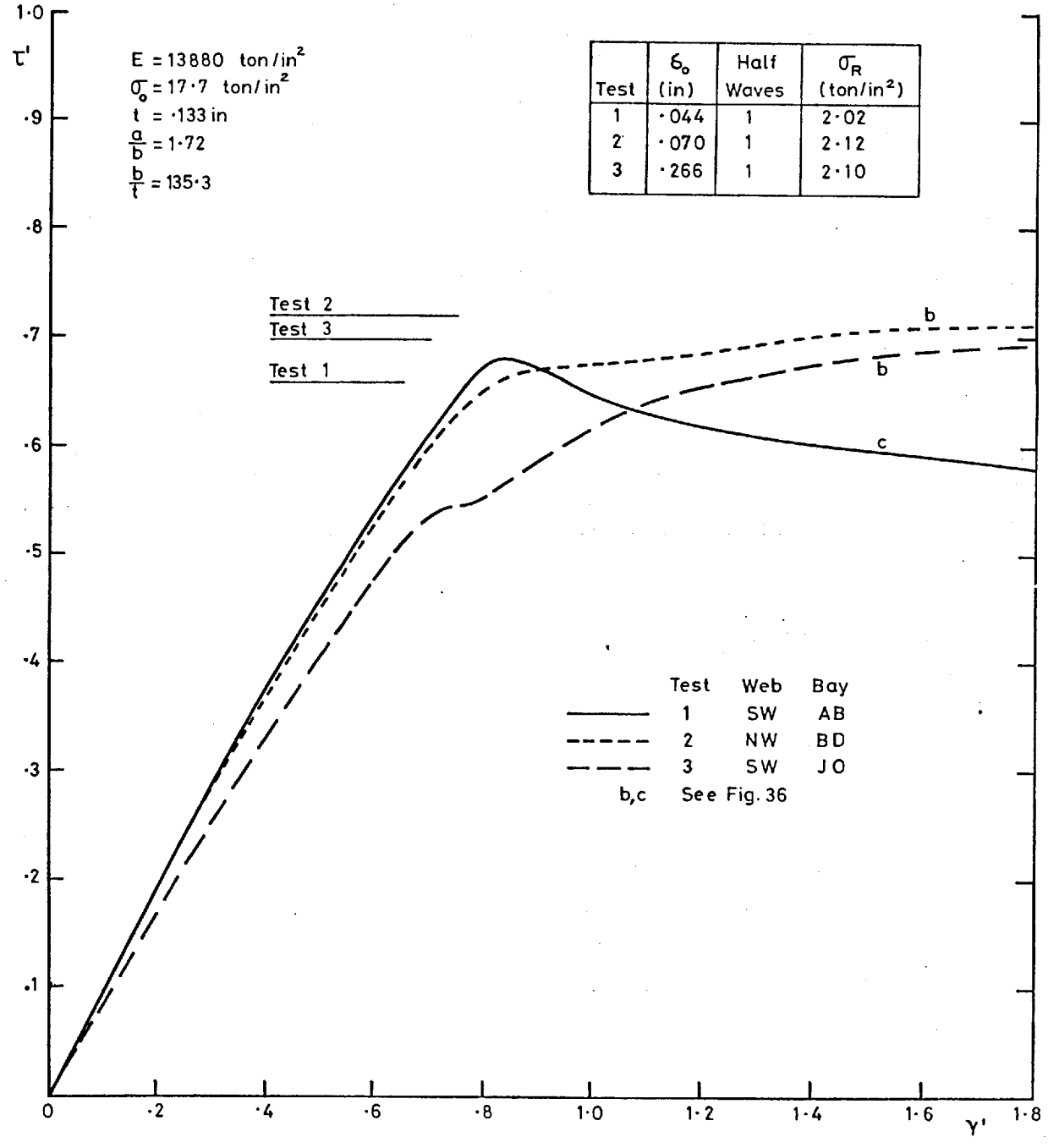

Fig.40. Model 1: Comparison between Theoretical and Experimental Capacities of Web Plates.

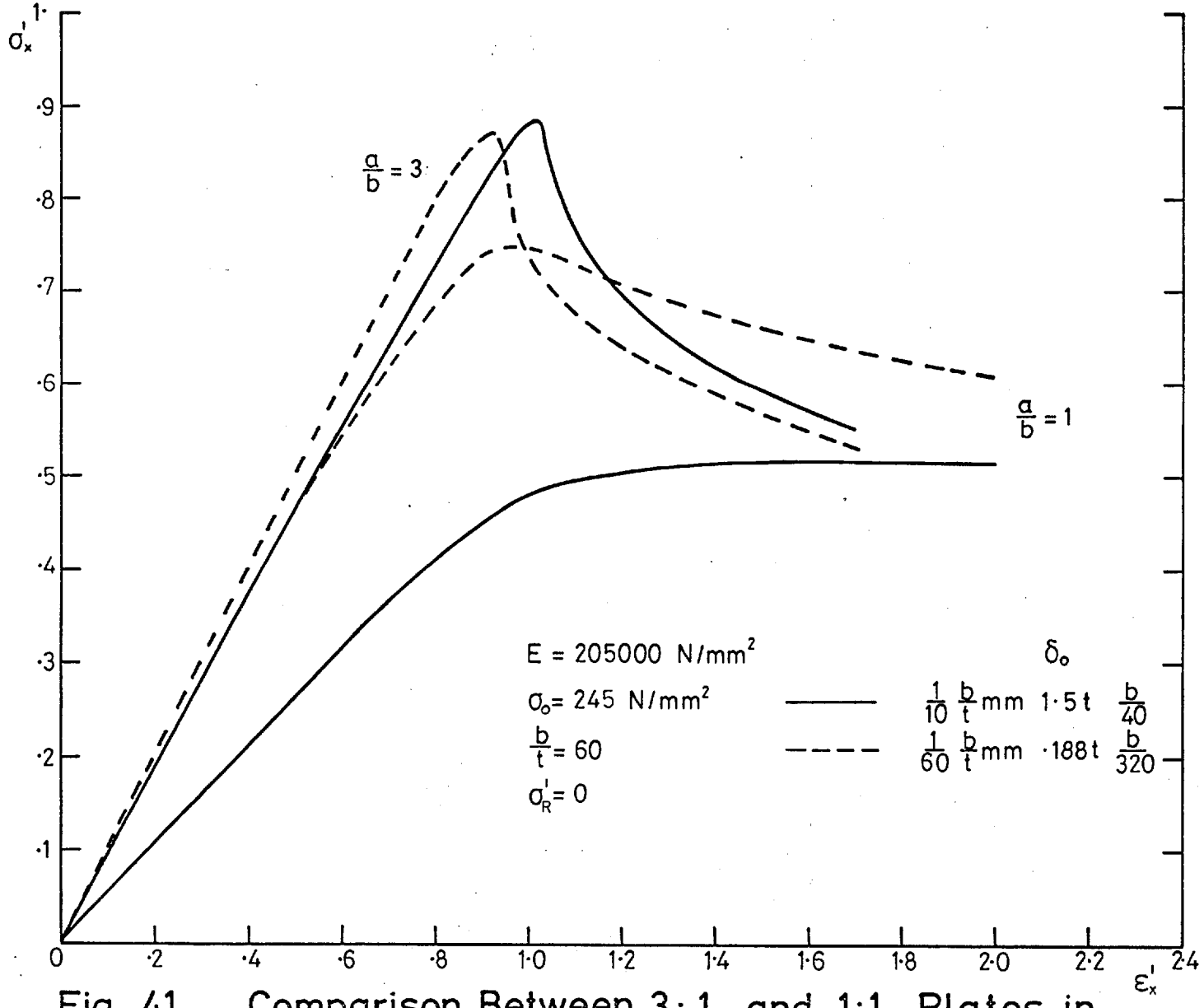

Fig. 41. Comparison Between 3:1 and 1:1 Plates in Compression with Single Half-Sine Wave Initial Deformation.
Edges Unrestrained.

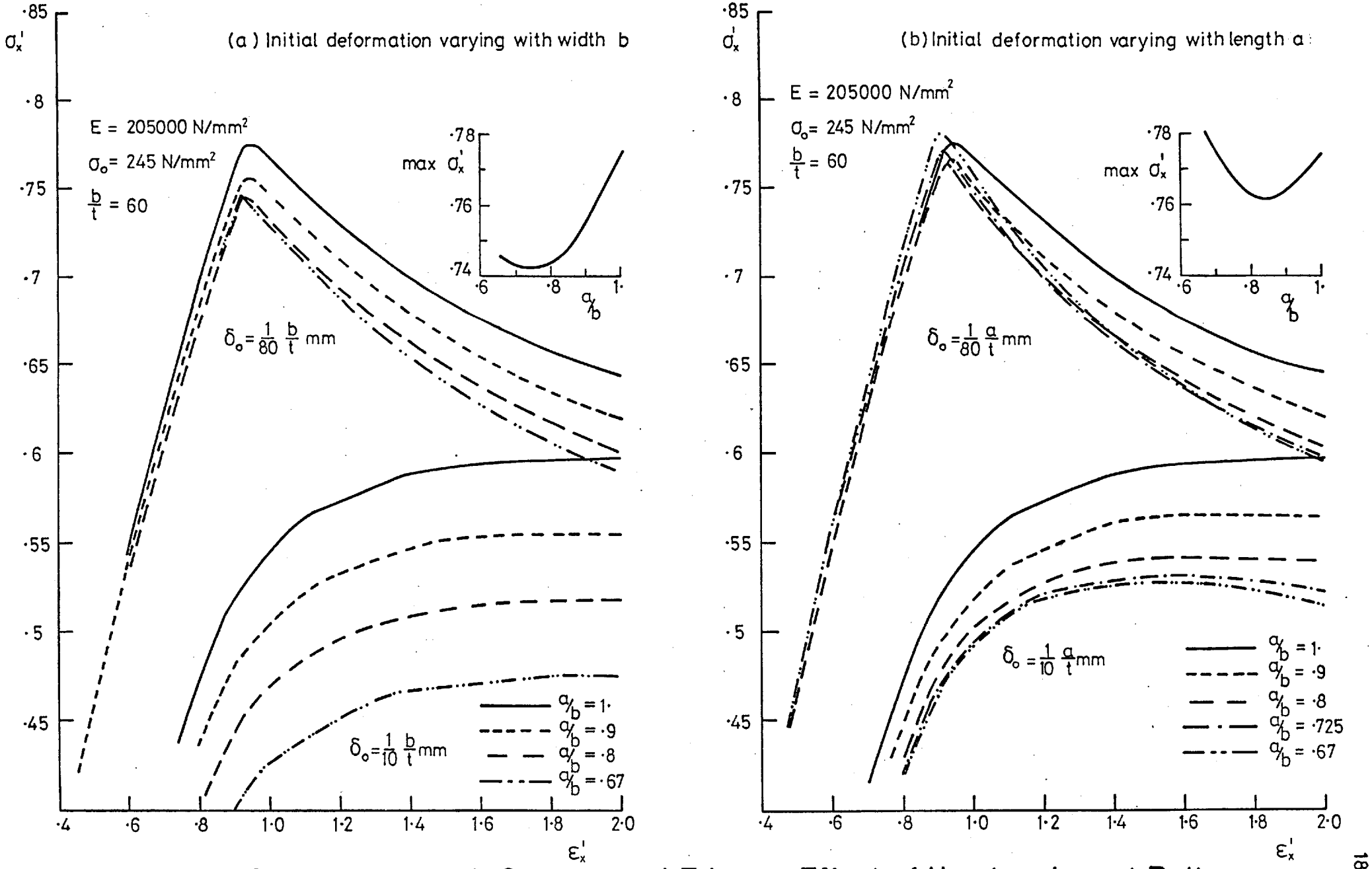

Fig.42. Plate in Compression with Constrained Edges—Effect of Varying Aspect Ratio

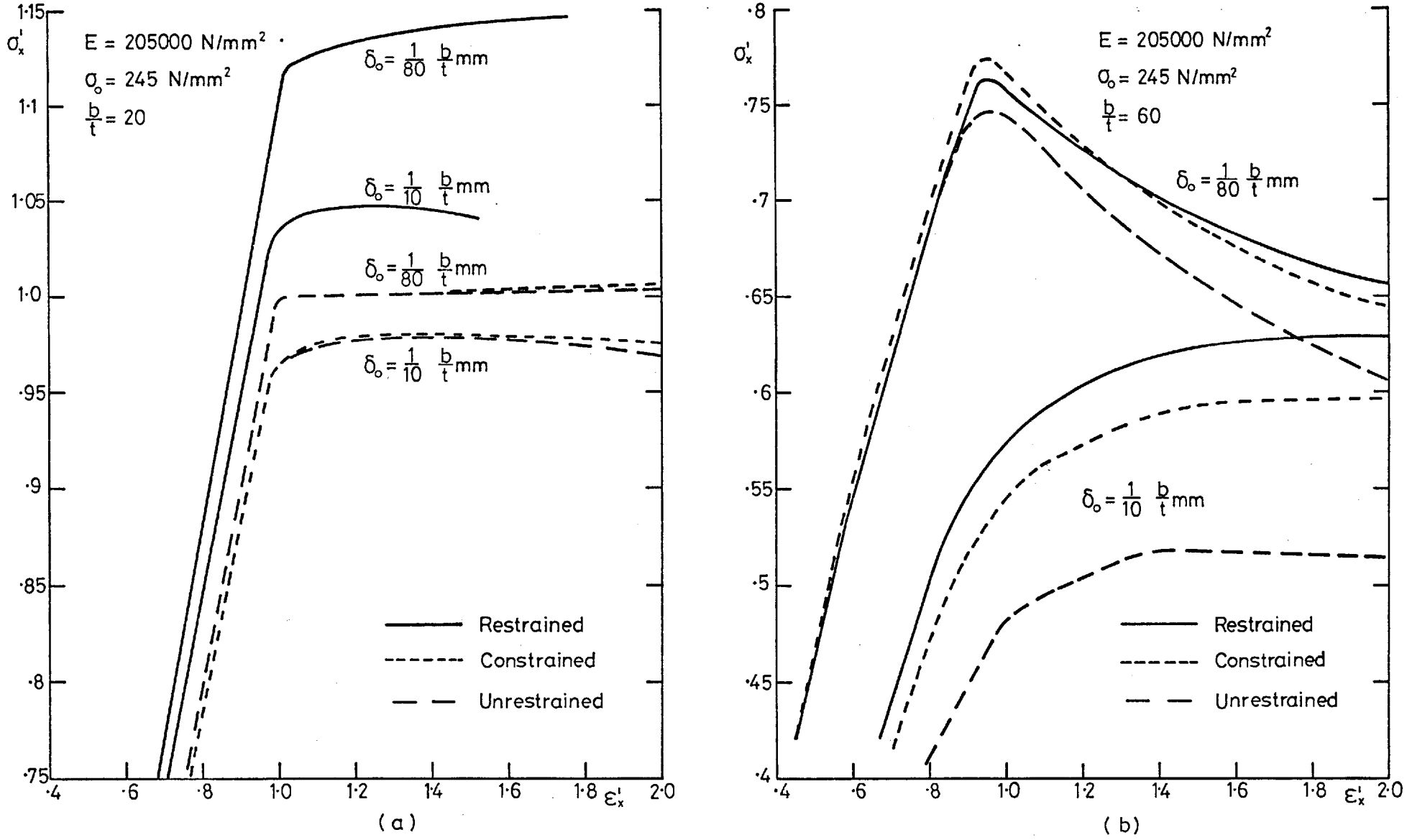

Fig. 43. Effect of In-Plane Restraint on Plates in Compression

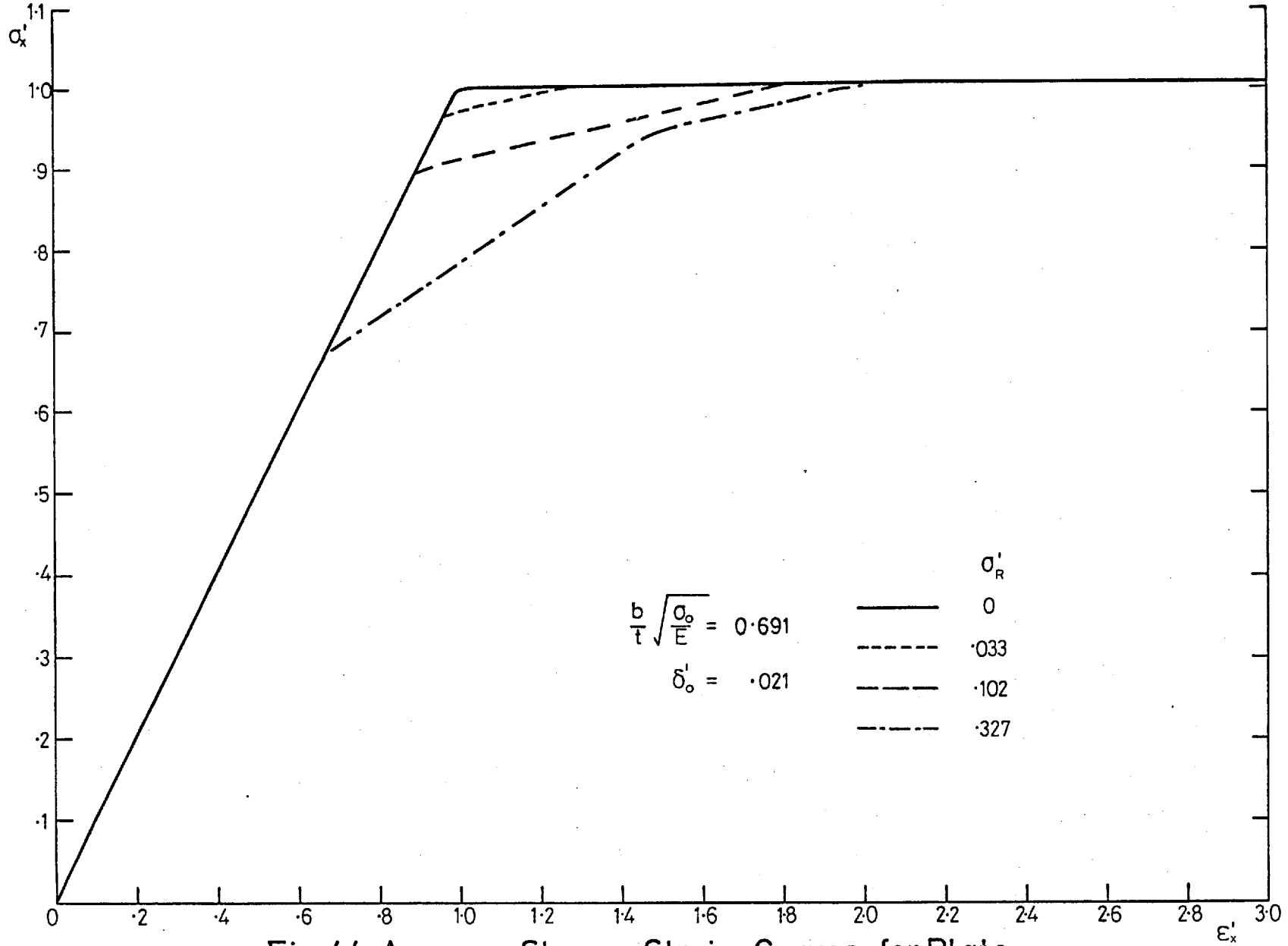

Fig.44. Average Stress–Strain Curves for Plate in Compression with Constrained Edges

Effect of Var ing Residual Stress

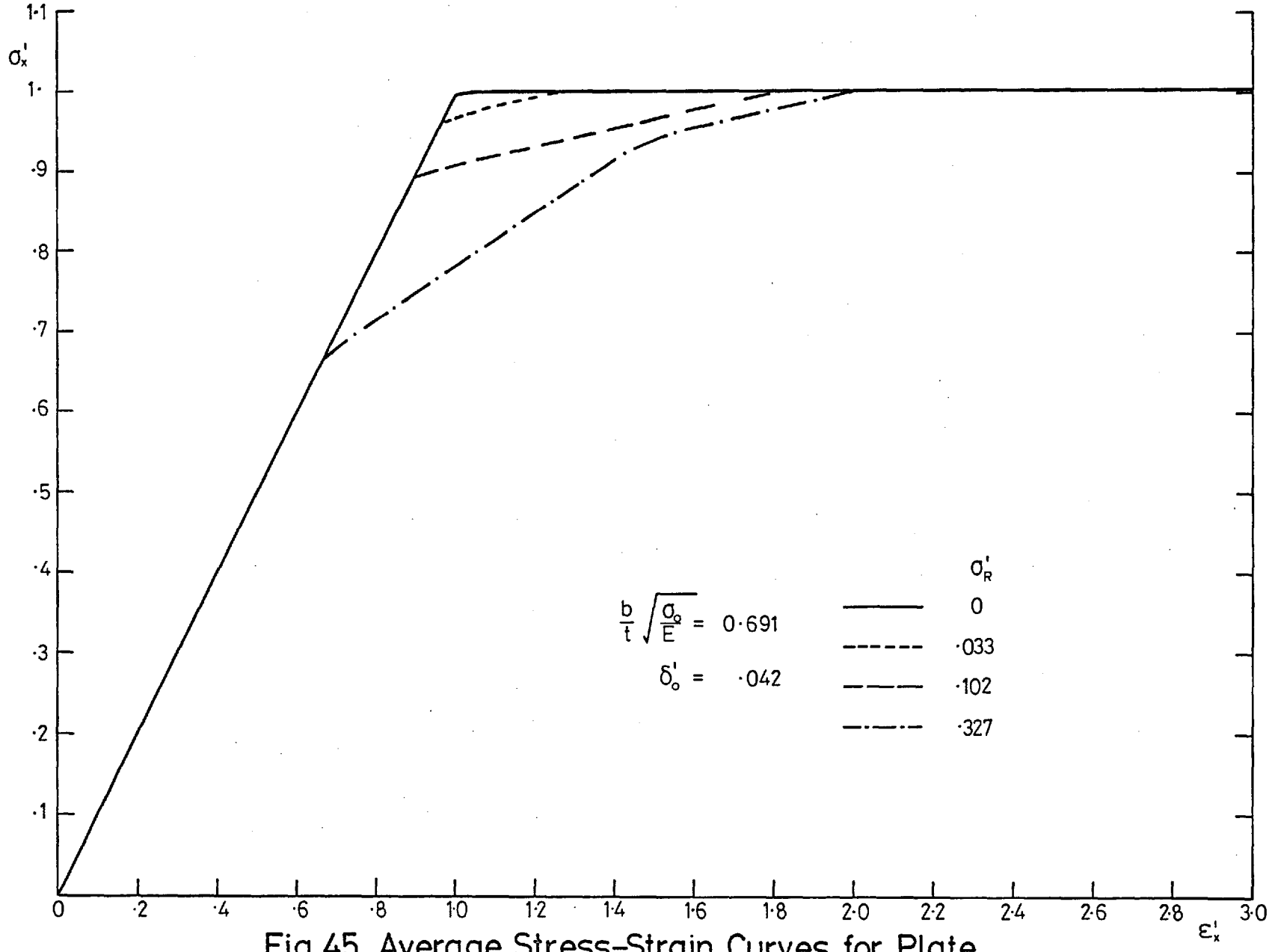

Fig.45. Average Stress-Strain Curves for Plate in Compression with Constrained Edges

Effect of Varying Residual Stress

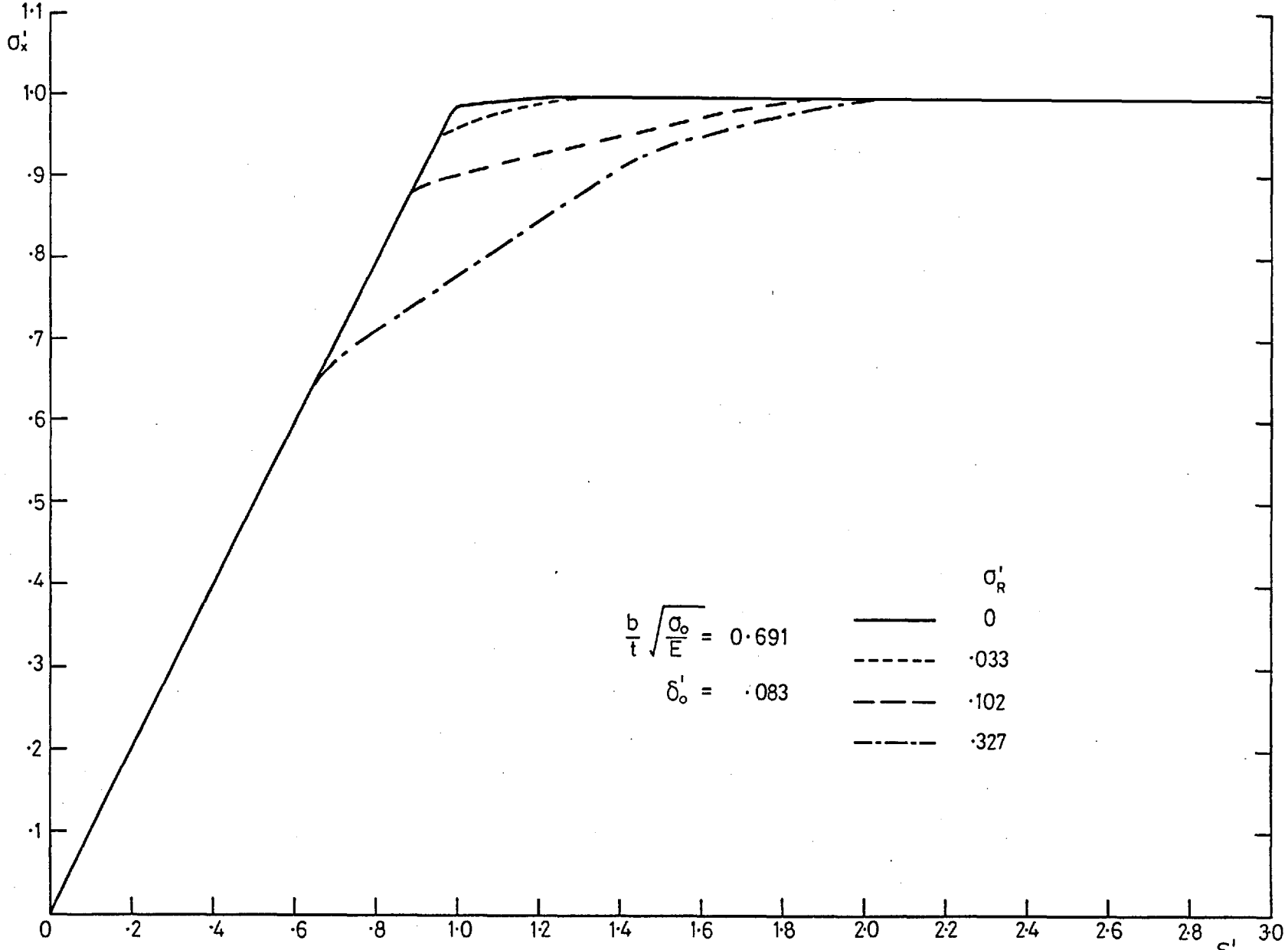

Fig. 46. Average Stress-Strain Curves for Plate in Compression with Constrained Edges

Effect of Varying Residual Stress

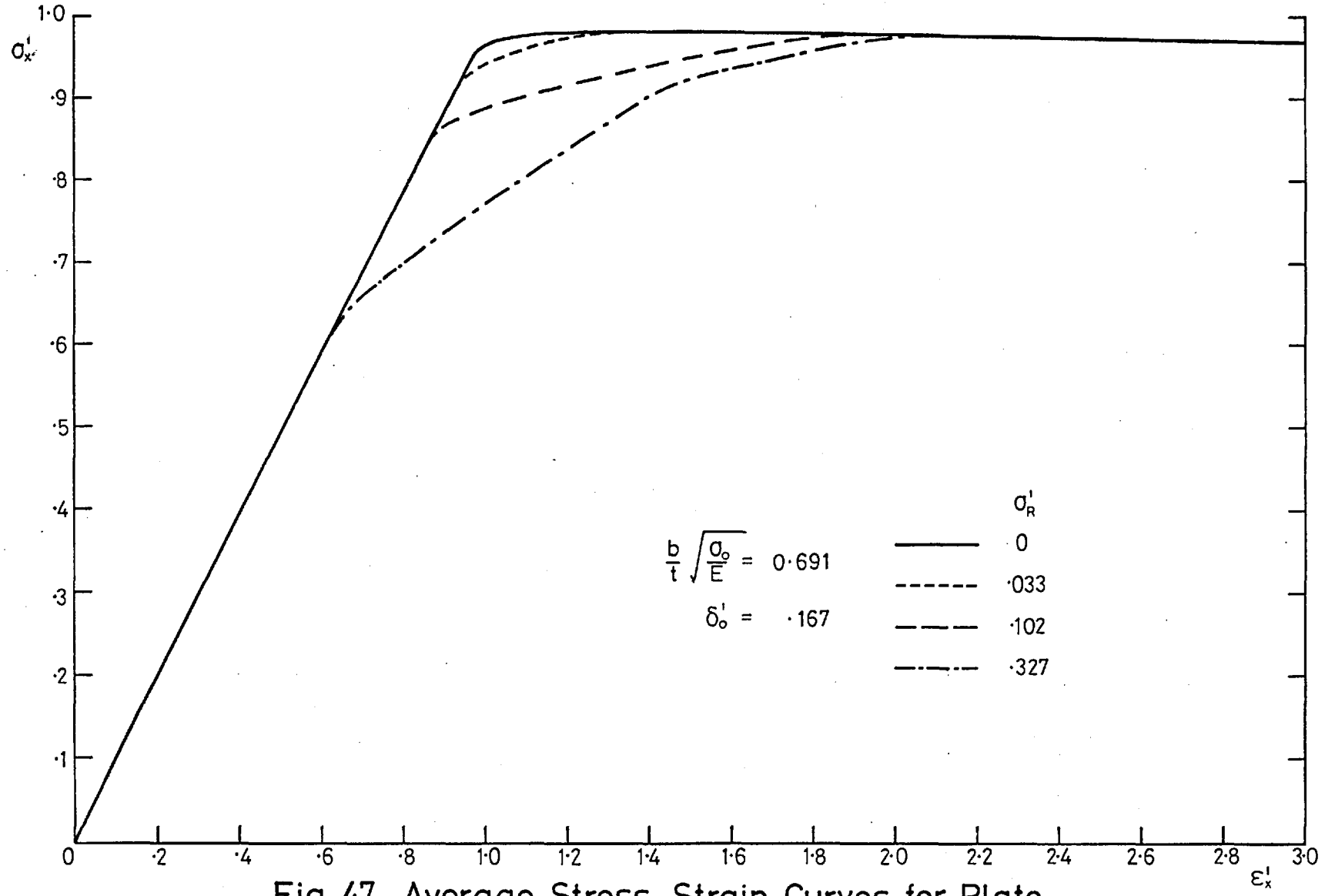

Fig. 47. Average Stress–Strain Curves for Plate in Compression with Constrained Edges
Effect of Varyin Residual Stress

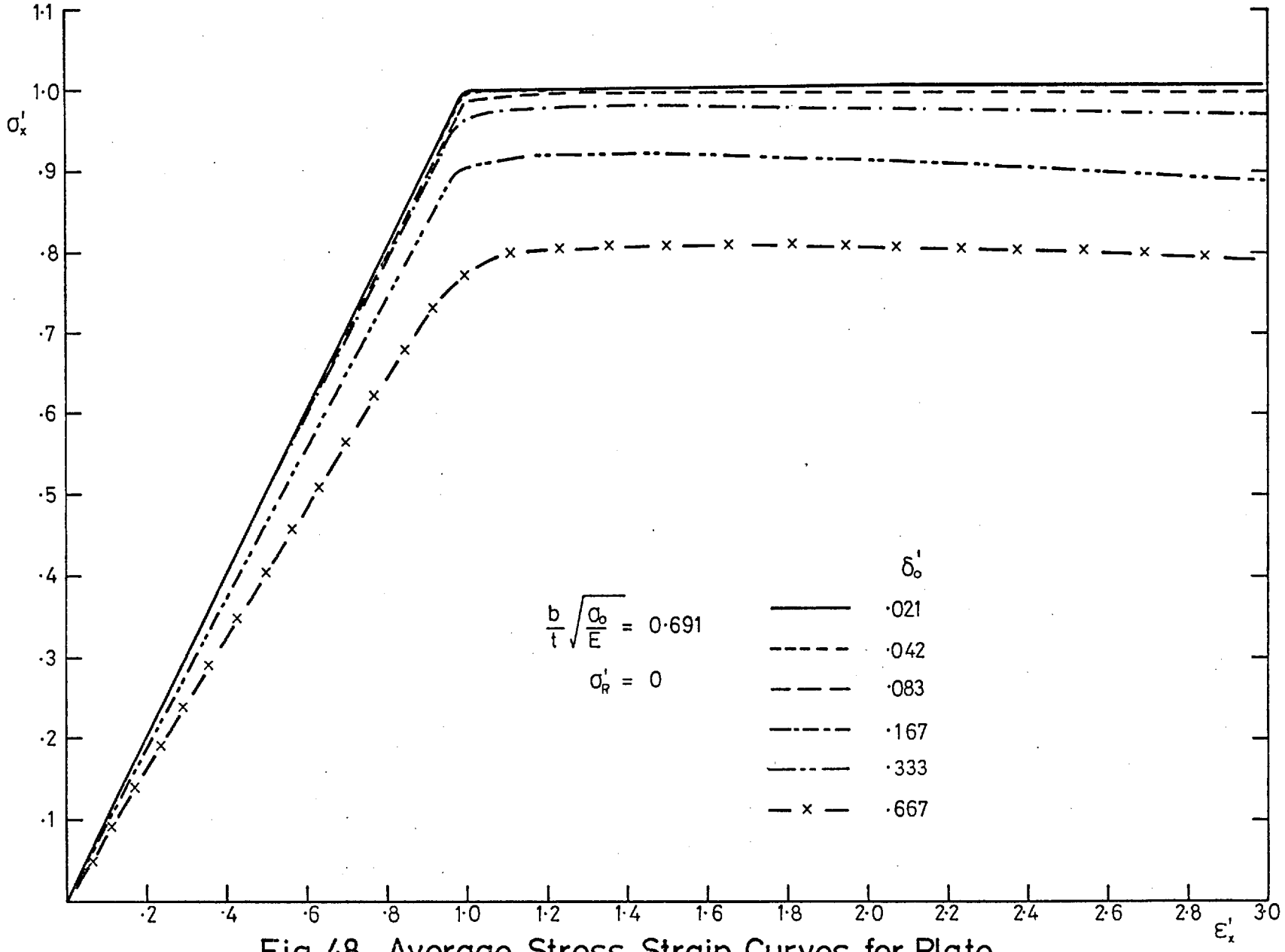

Fig. 48. Average Stress-Strain Curves for Plate in Compression with Constrained Edges

Effect of Var in Initial Deformation

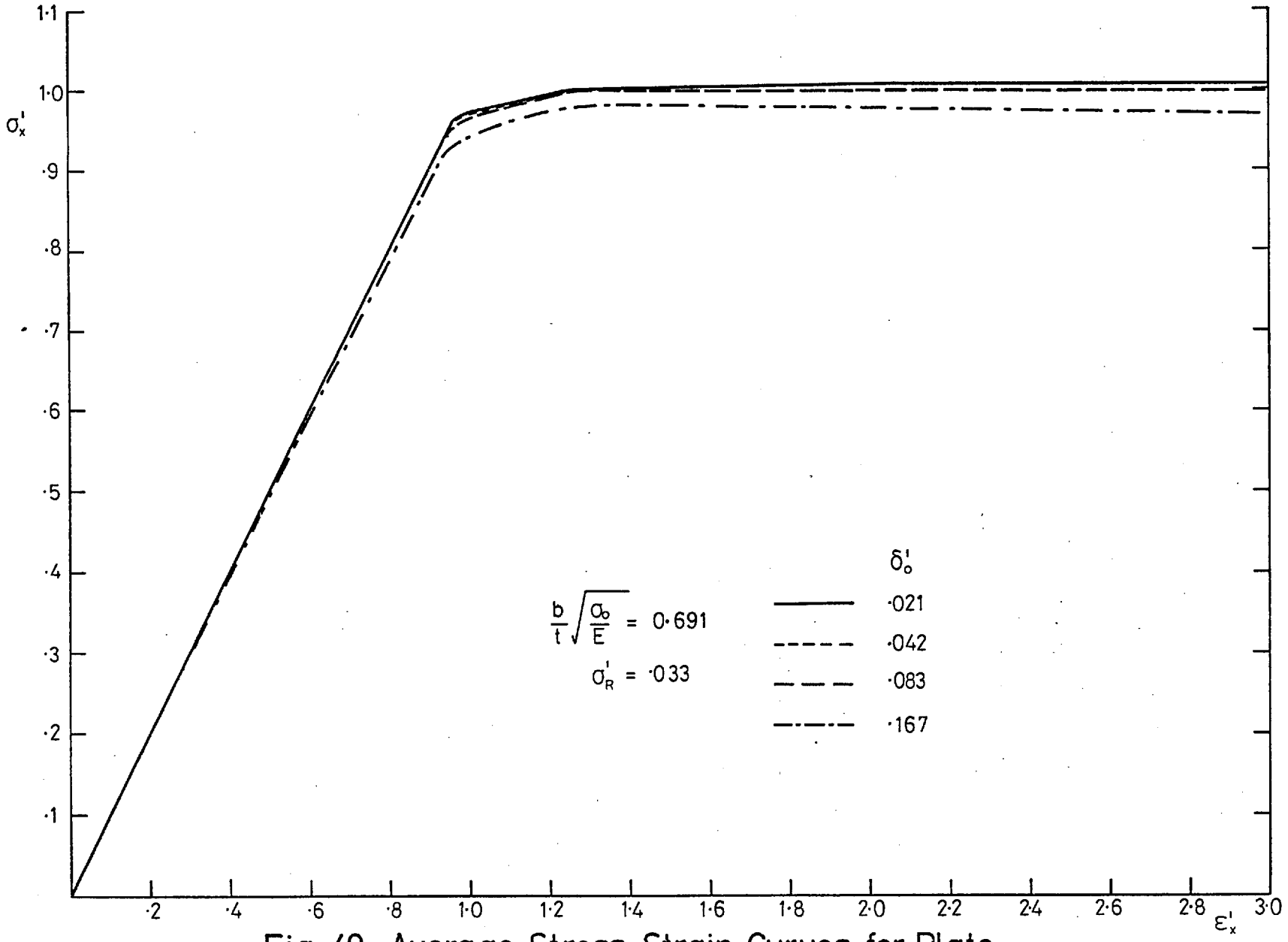

Fig. 49. Average Stress-Strain Curves for Plate in Compression with Constrained Edges

Effect of Varying Initial Deformation

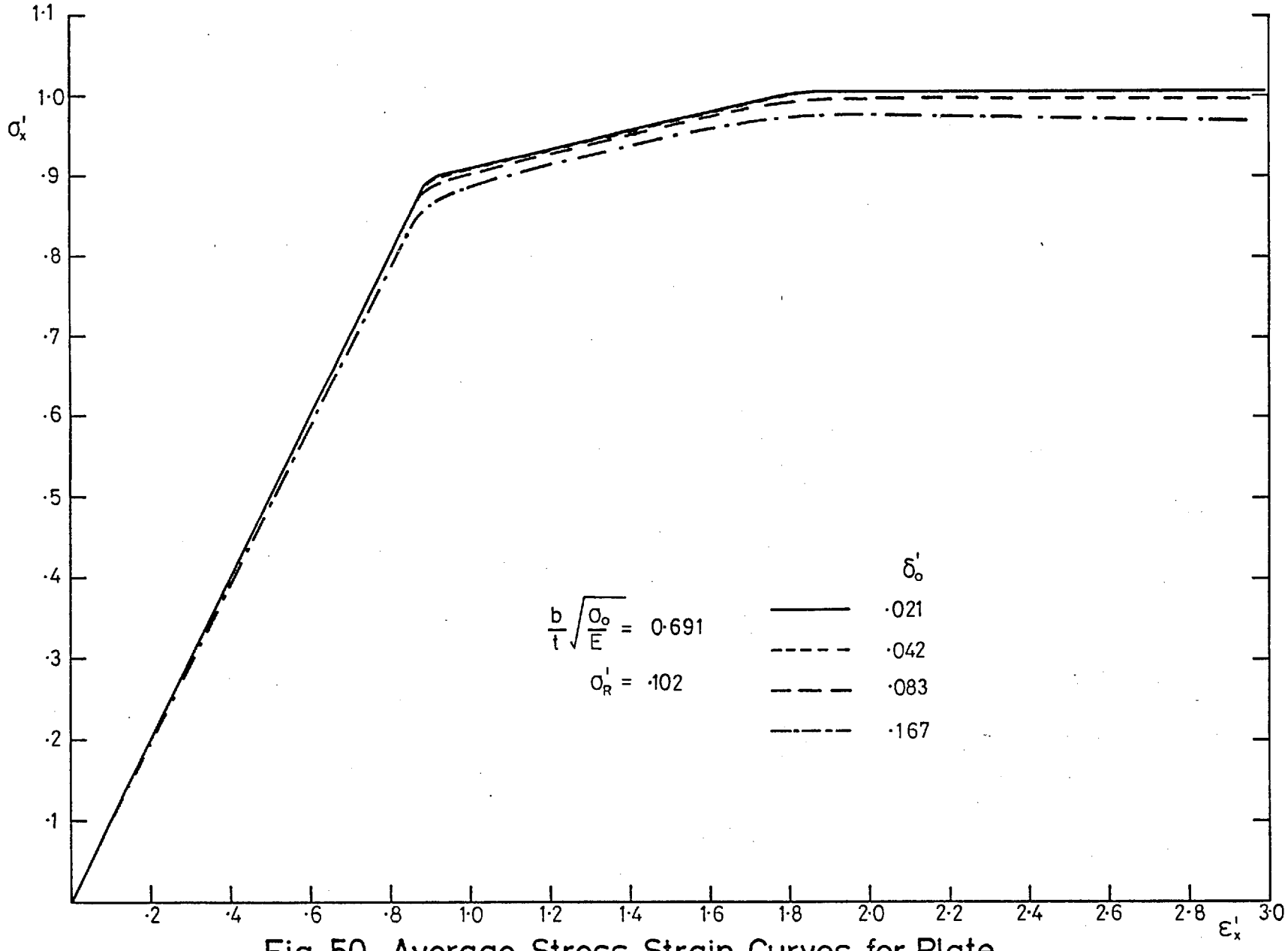

Fig. 50. Average Stress-Strain Curves for Plate in Compression with Constrained Edges

Effect of Varying Initial Deformation

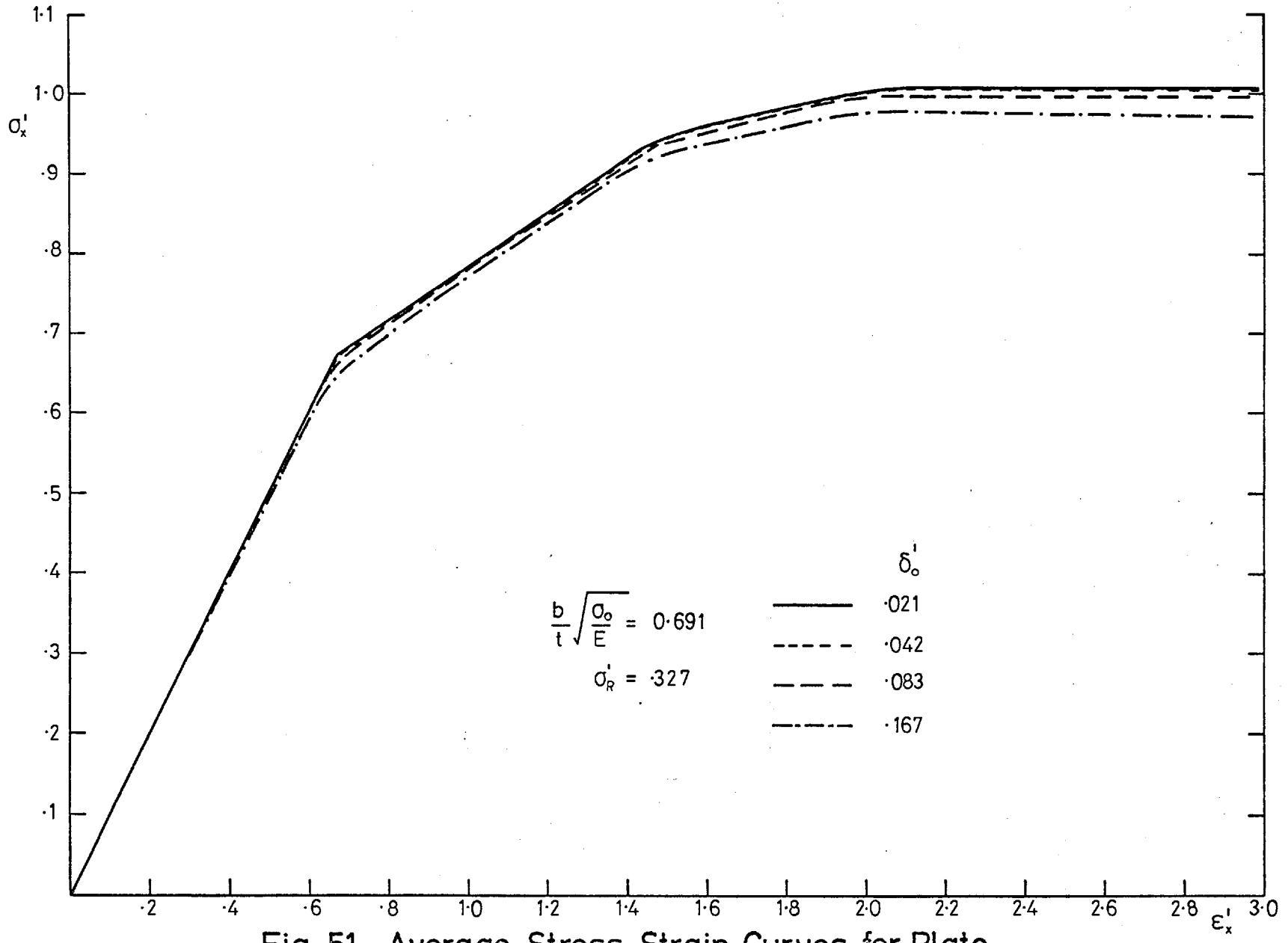

Fig. 51. Average Stress-Strain Curves for Plate in Compression with Constrained Edges

Effect of Varying Initial Deformation

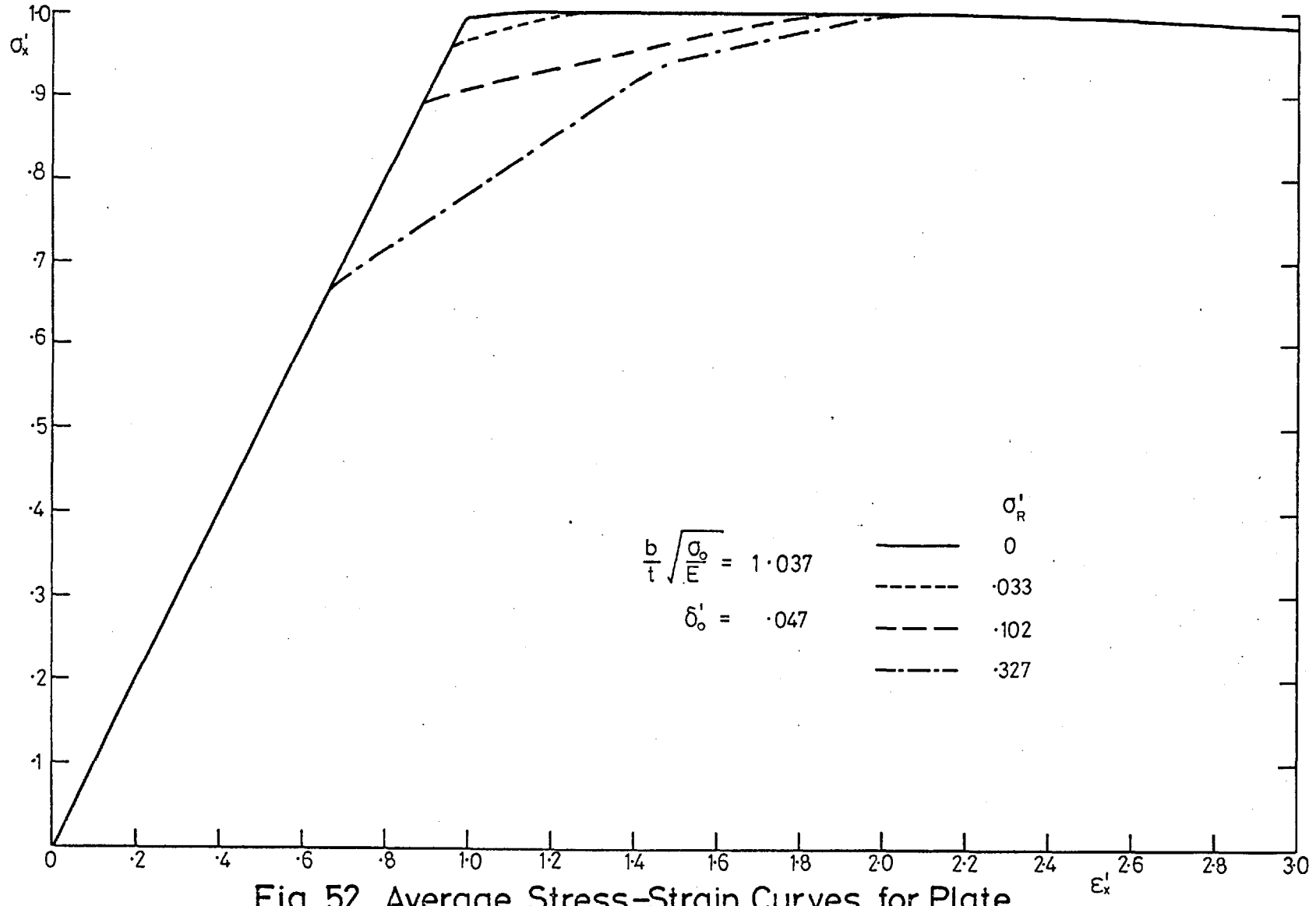

Fig. 52. Average Stress-Strain Curves for Plate in Compression with Constrained Edges

Effect of Varying Residual Stress

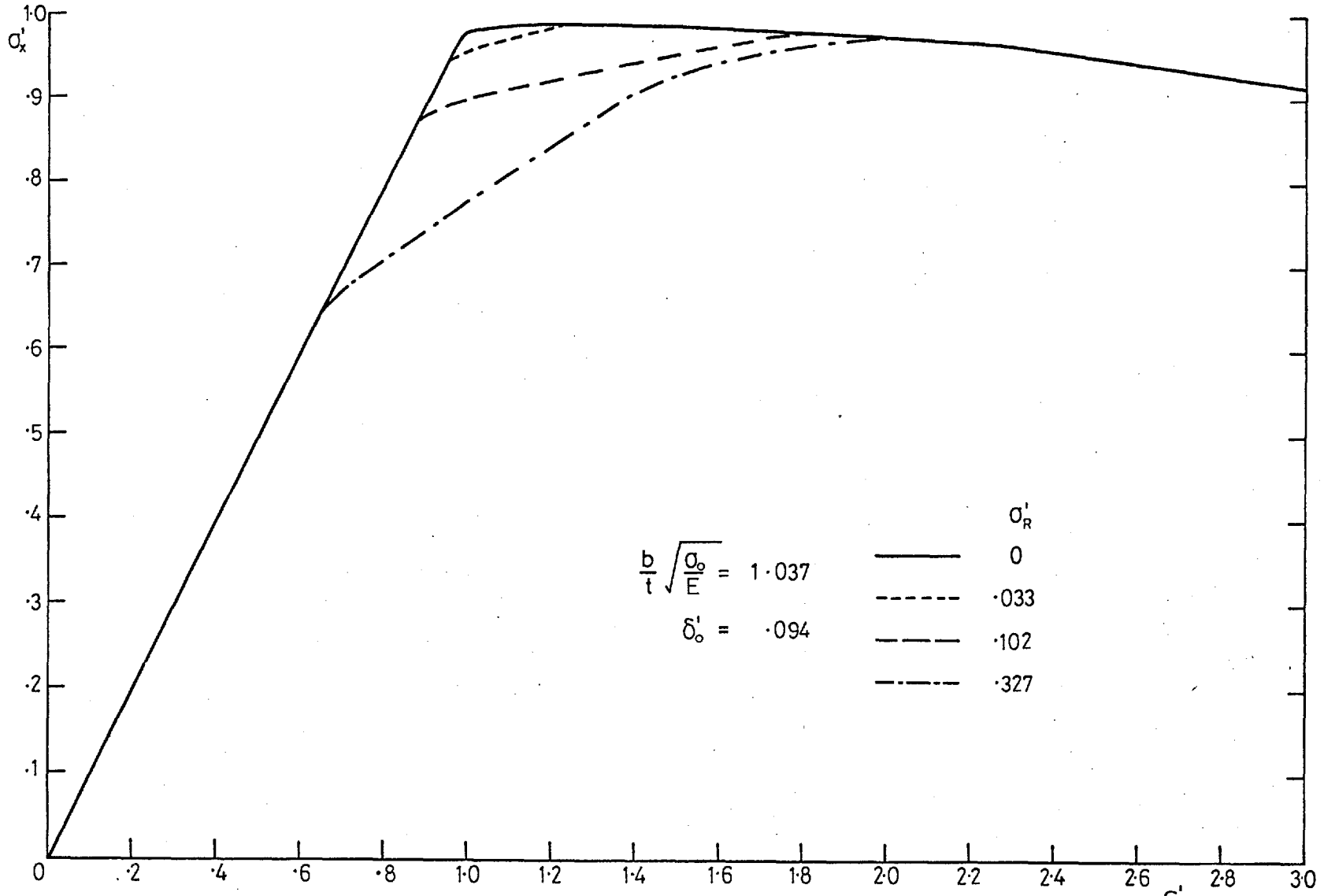

Fig. 53. Average Stress-Strain Curves for Plate in Compression with Constrained Edges

Effect of Varying Residual Stress

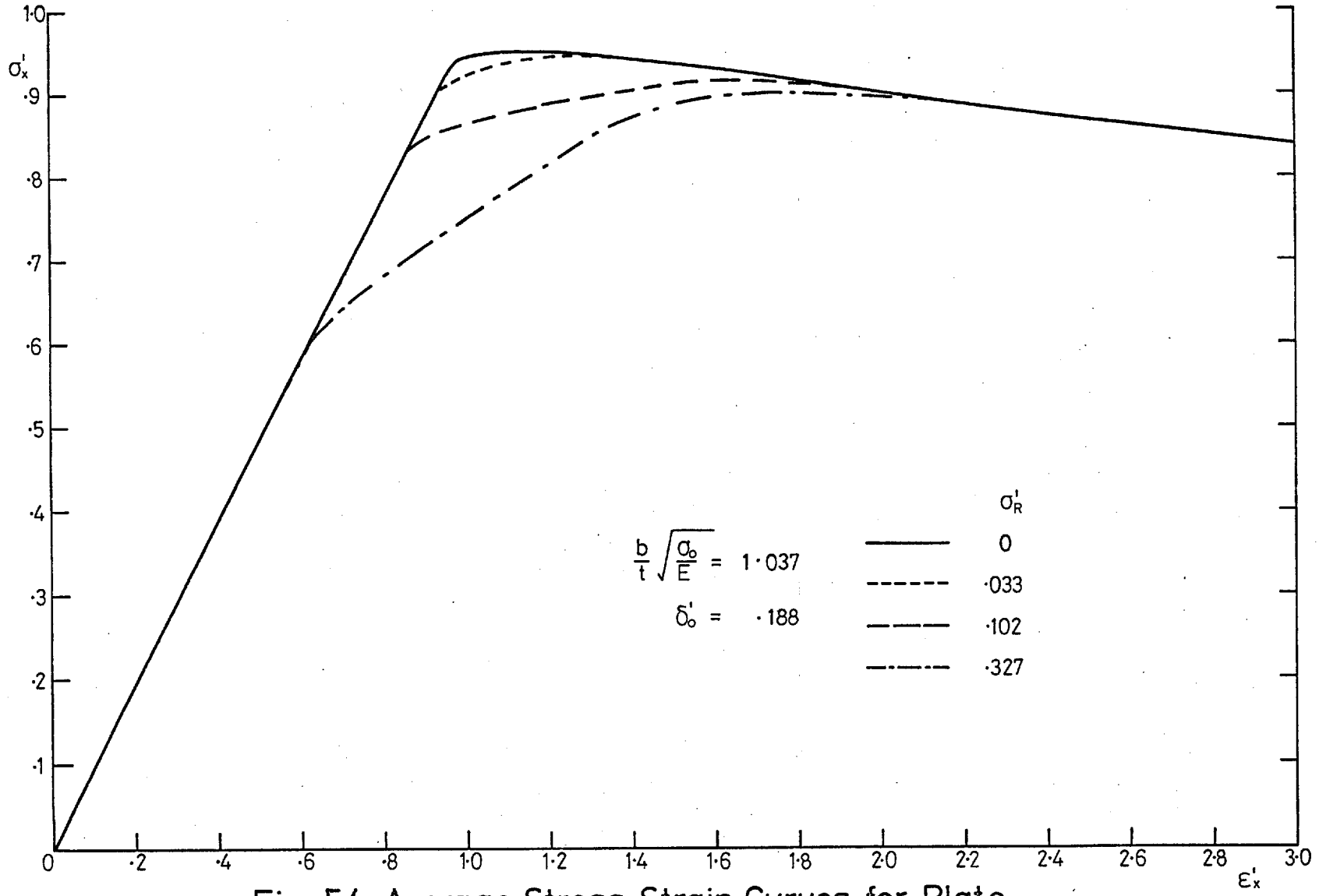

Fig. 54. Average Stress-Strain Curves for Plate in Compression with Constrained Edges

Effect of Var in Residual Stress

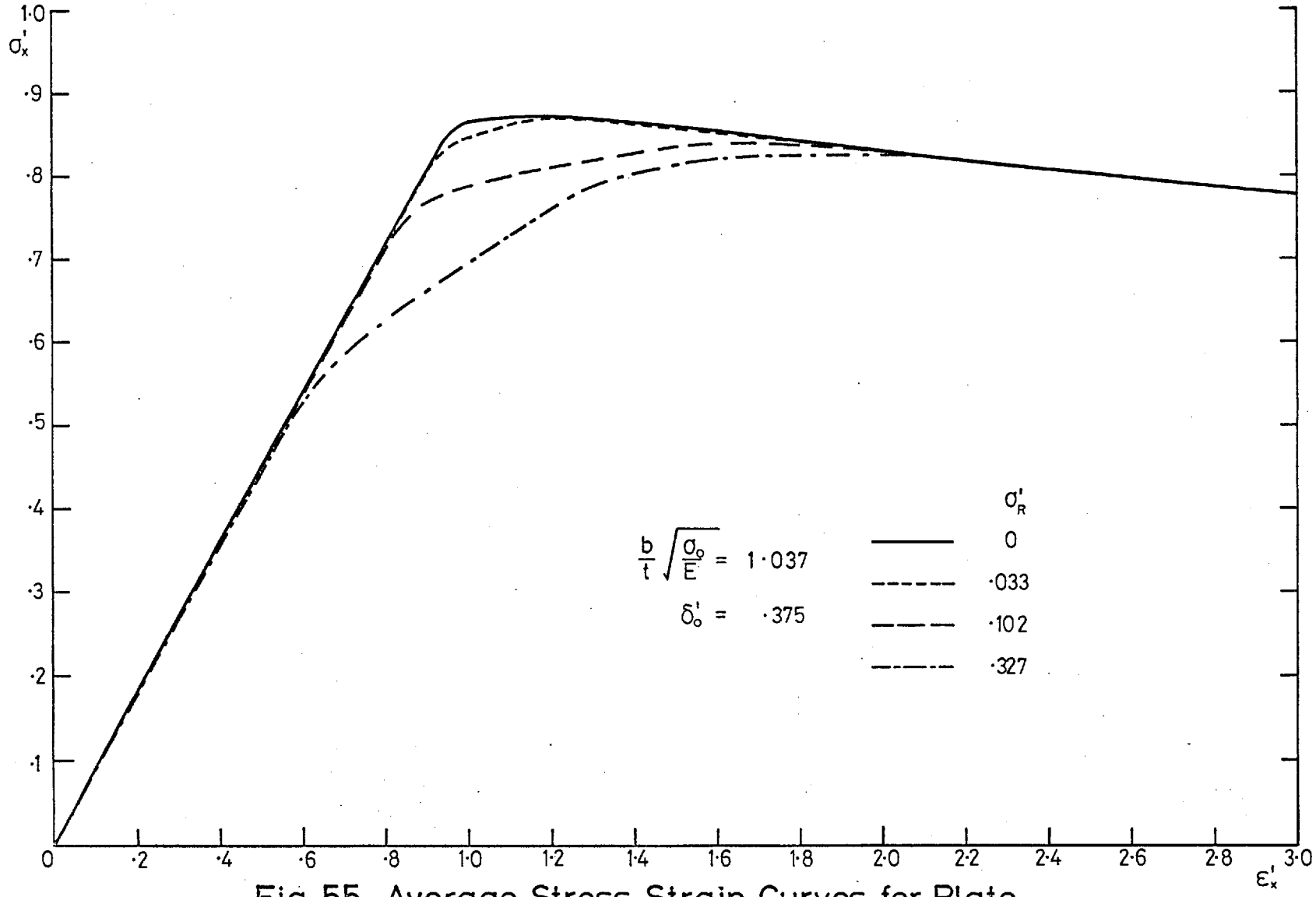

Fig. 55. Average Stress-Strain Curves for Plate in Compression with Constrained Edges

Effect of Varying Residual Stress

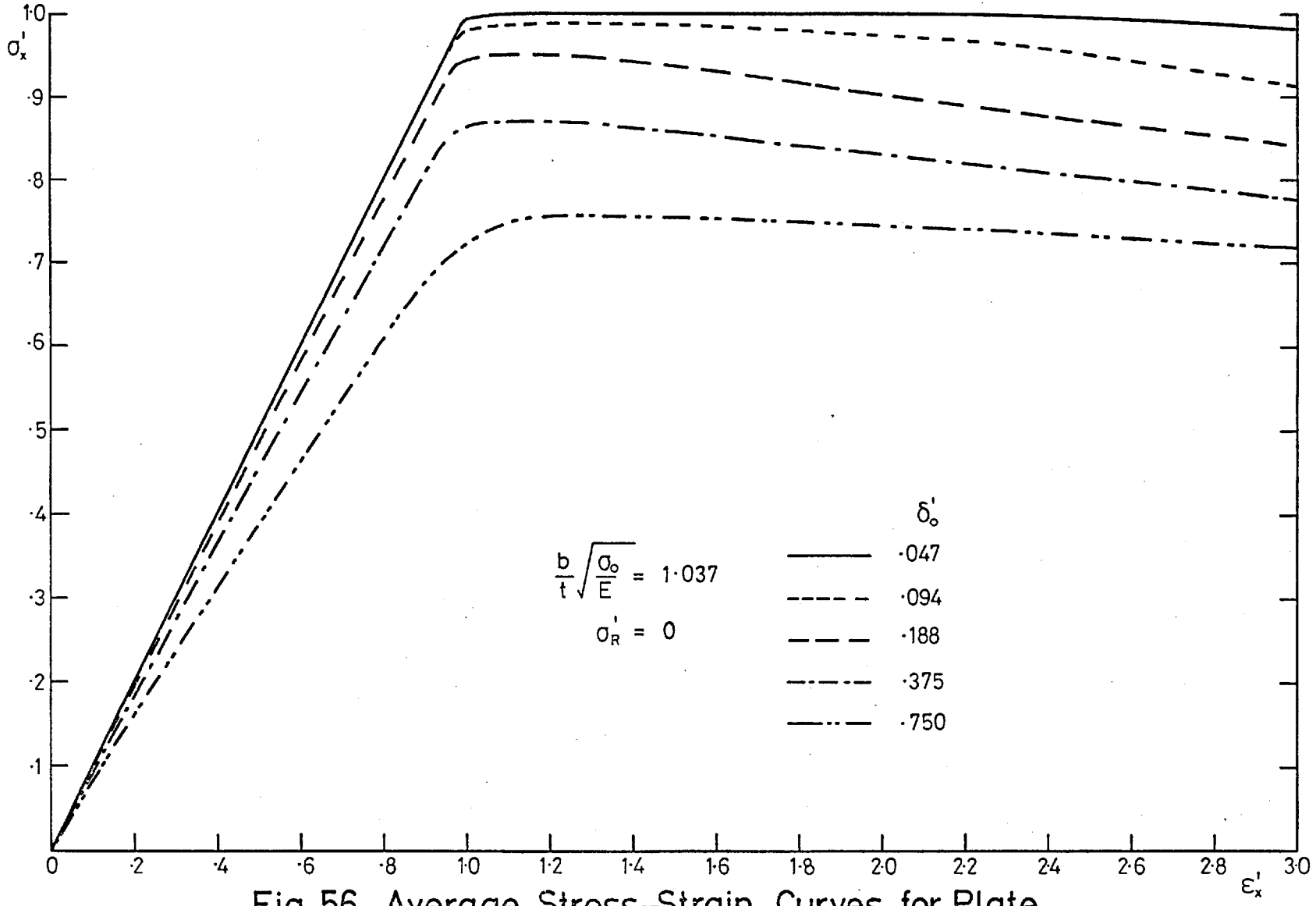

Fig. 56. Average Stress–Strain Curves for Plate in Compression with Constrained Edges

Effect of Varying Initial Deformation

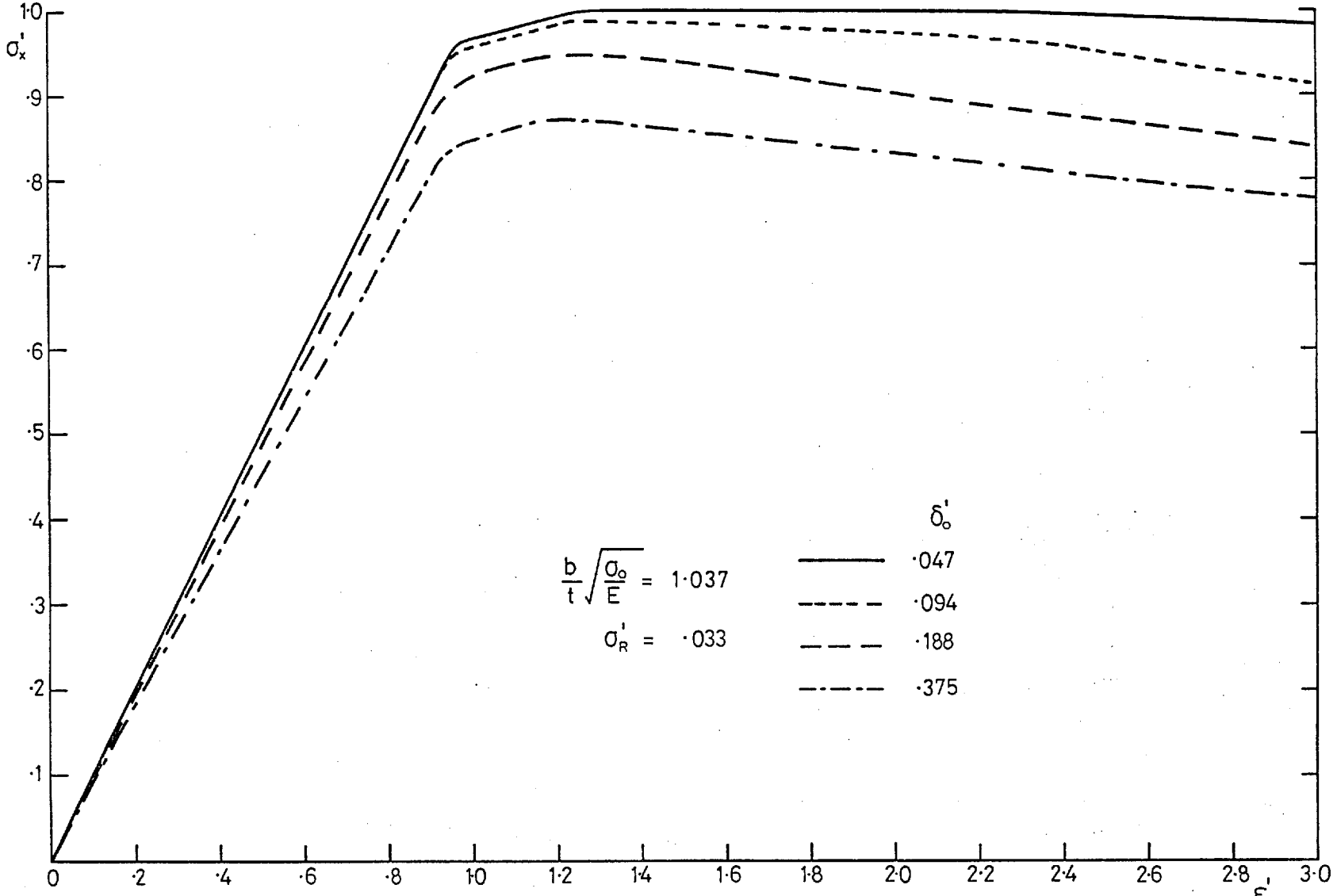

Fig. 57. Average Stress–Strain Curves for Plate in Compression with Constrained Edges

Effect of Varying Initial Deformation

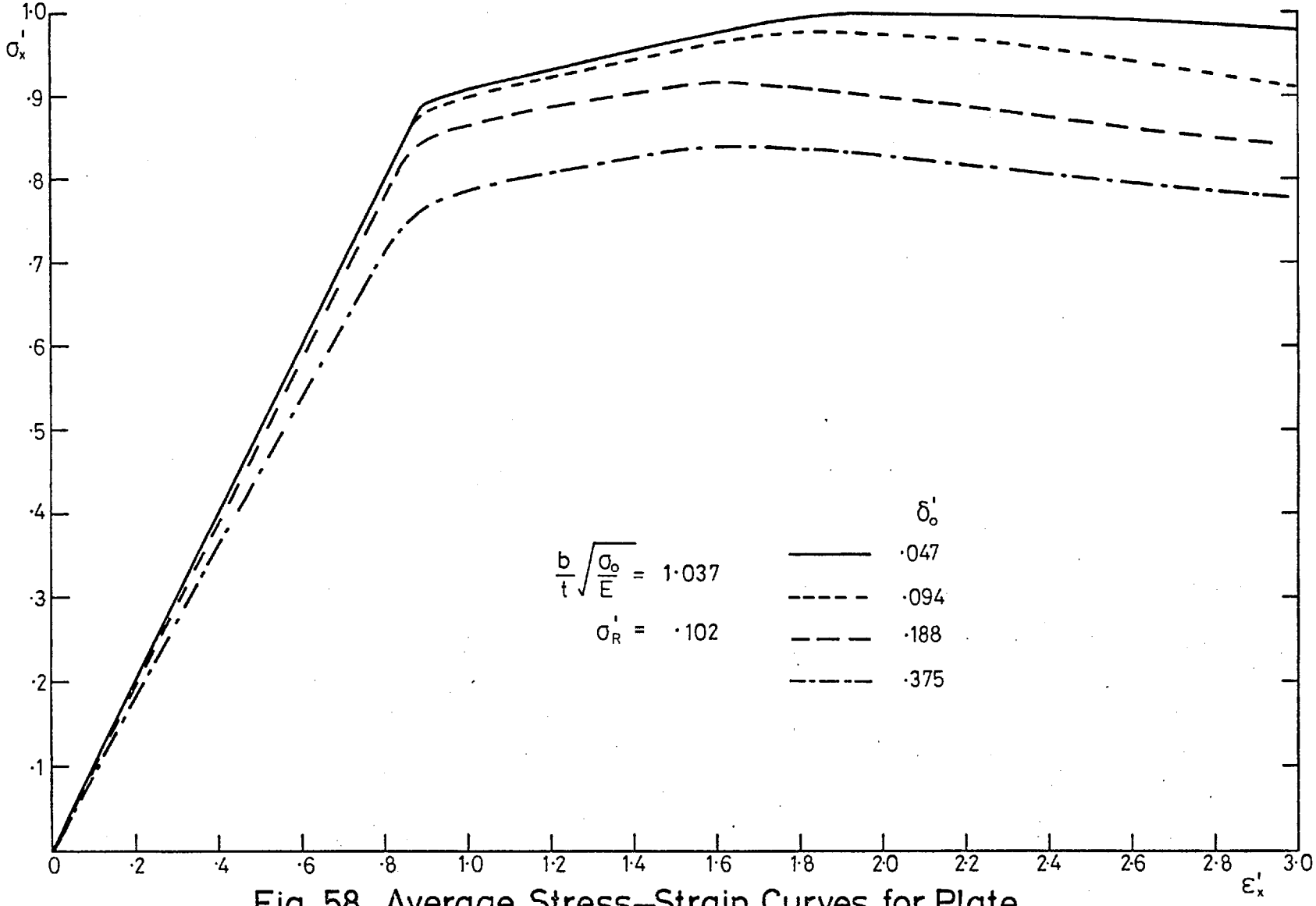

Fig. 58. Average Stress–Strain Curves for Plate in Compression with Constrained Edges

Effect of Varying Initial Deformation

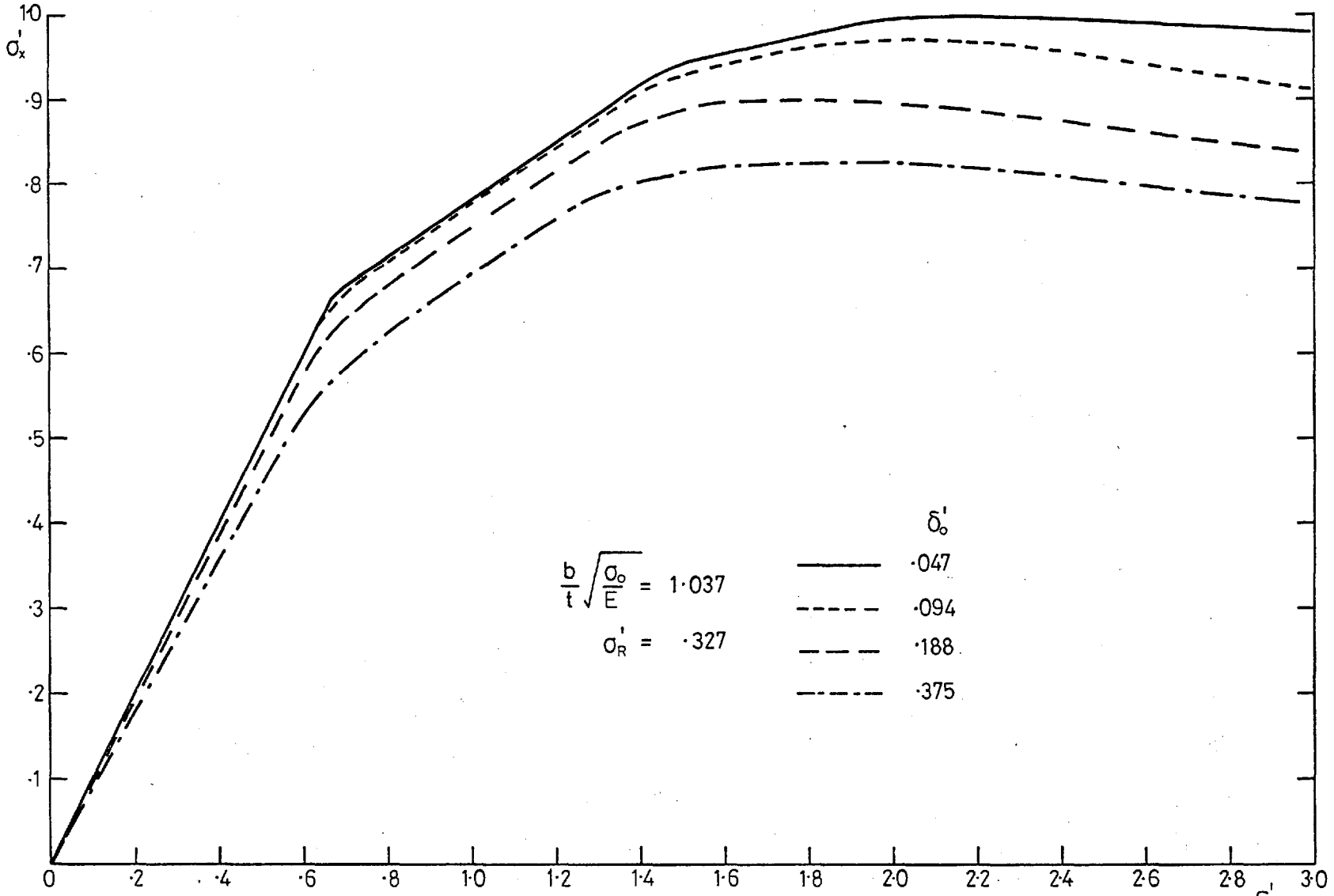

Fig. 59. Average Stress–Strain Curves for Plate in Compression with Constrained Edges

Effect of Varying Initial Deformation

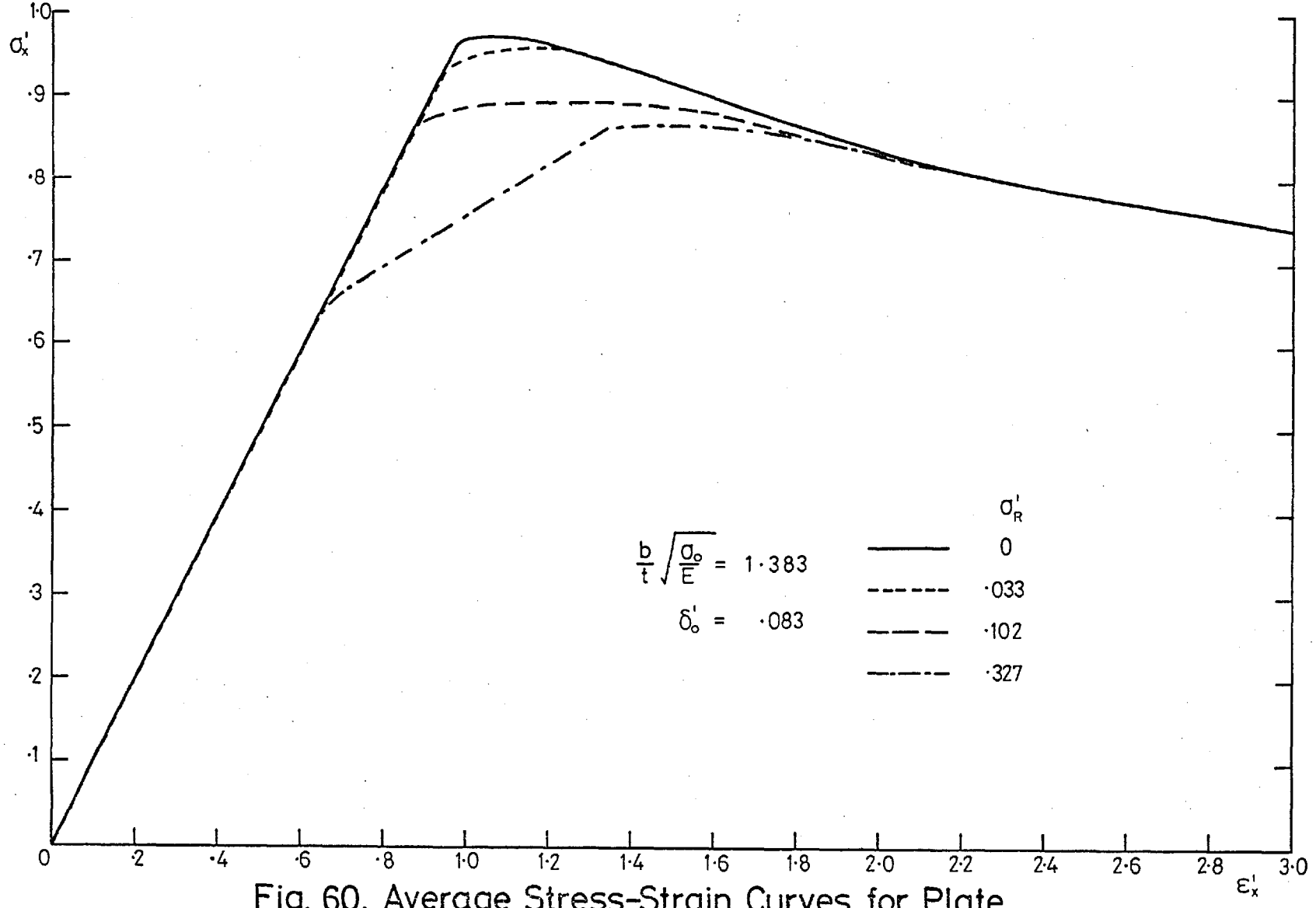

Fig. 60. Average Stress-Strain Curves for Plate in Compression with Constrained Edges

Effect of Varying Residual Stress

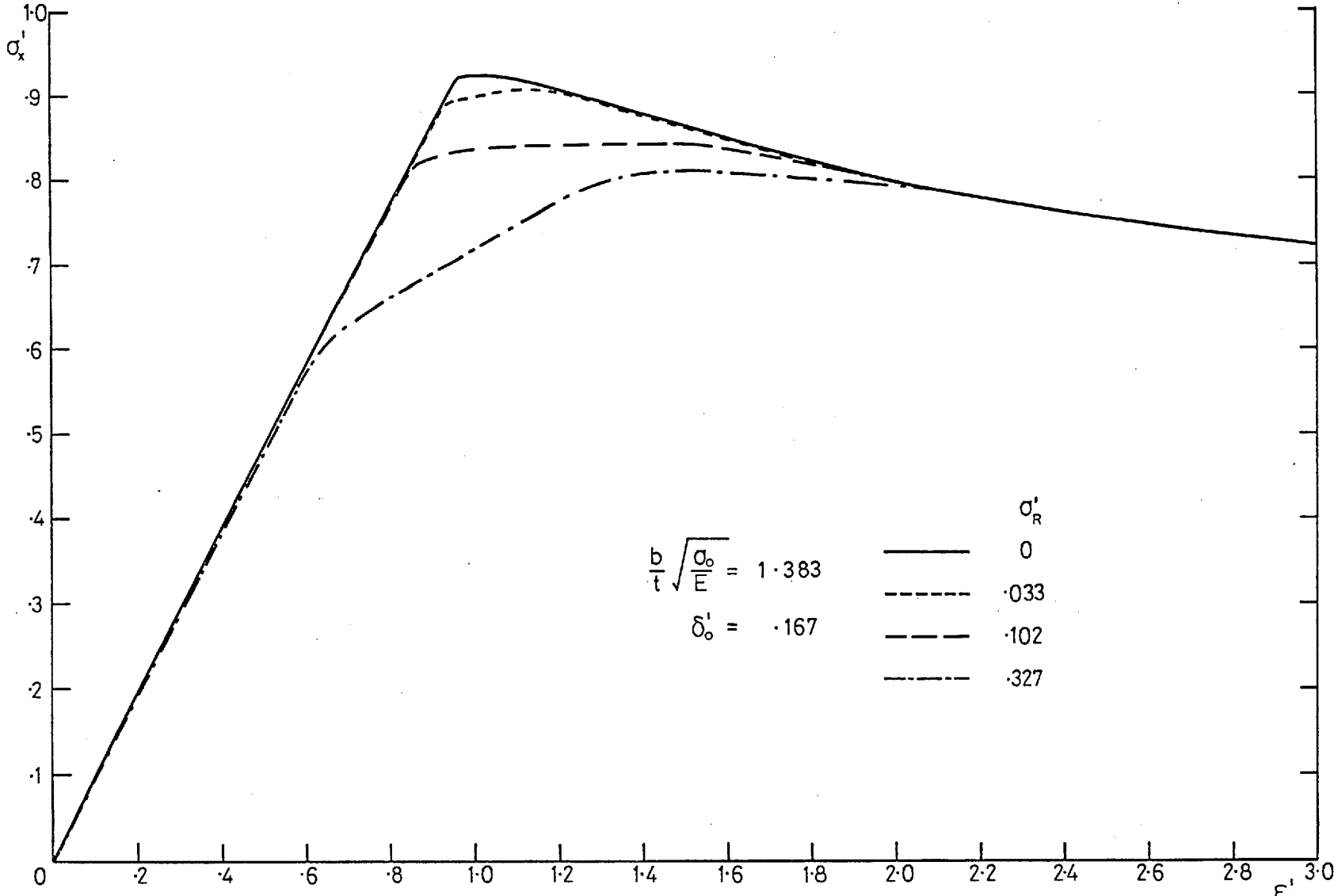

Fig. 61. Average Stress-Strain Curves for Plate in Compression with Constrained Edges

Effect of Varying Residual Stress

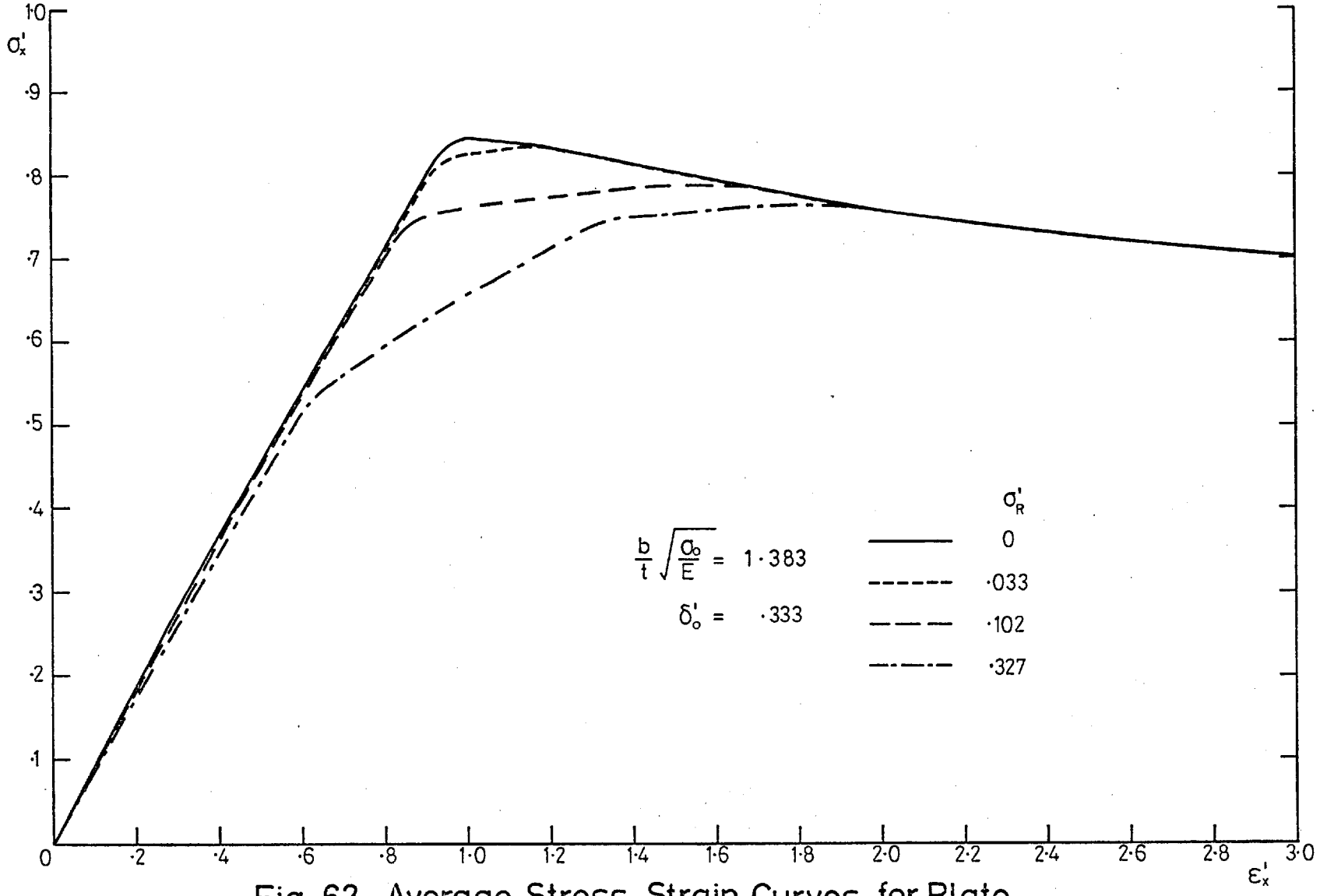

Fig. 62. Average Stress-Strain Curves for Plate in Compression with Constrained Edges

Effect of Varying Residual Stress

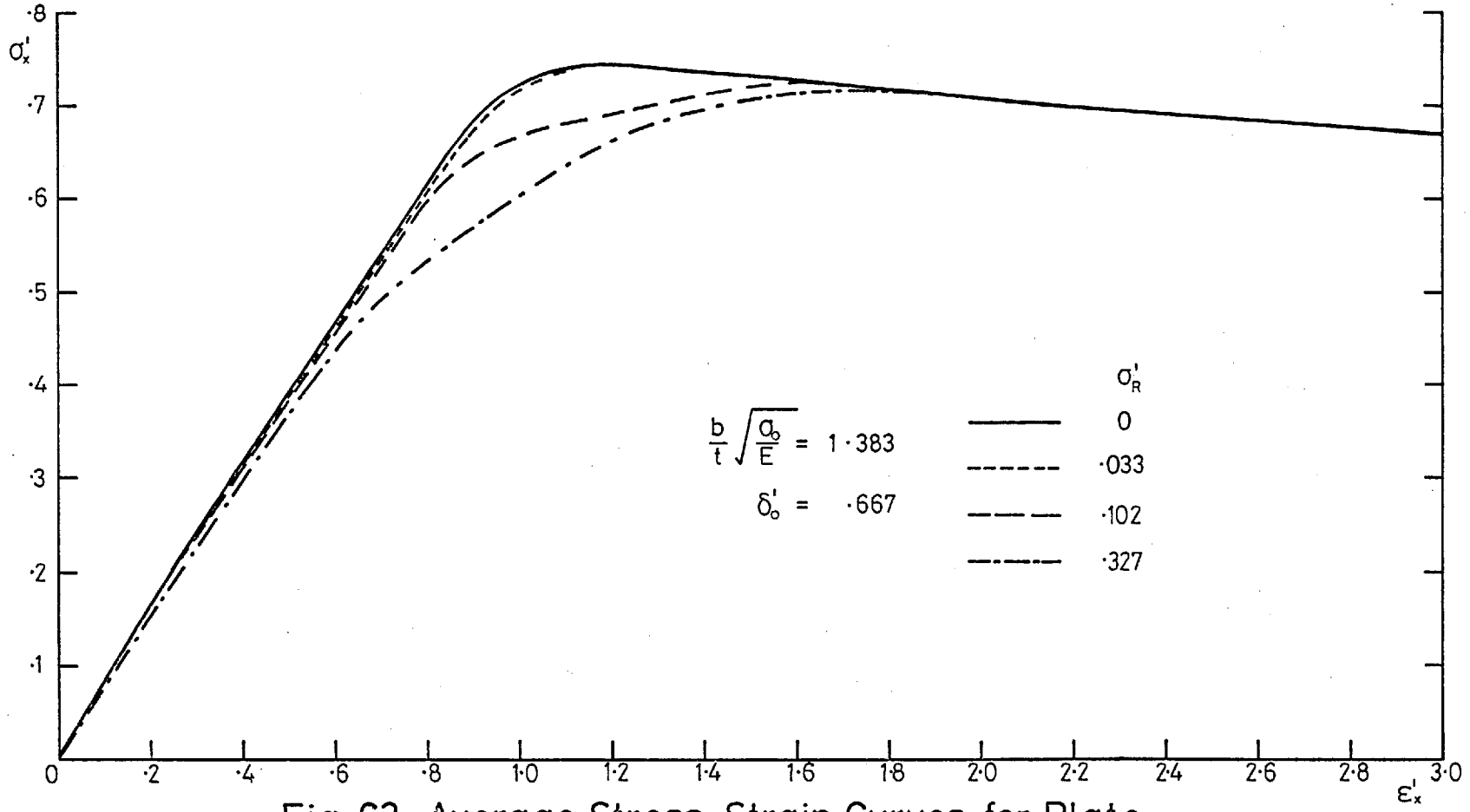

Fig. 63. Average Stress-Strain Curves for Plate in Compression with Constrained Edes

Effect of Varying Residual Stress

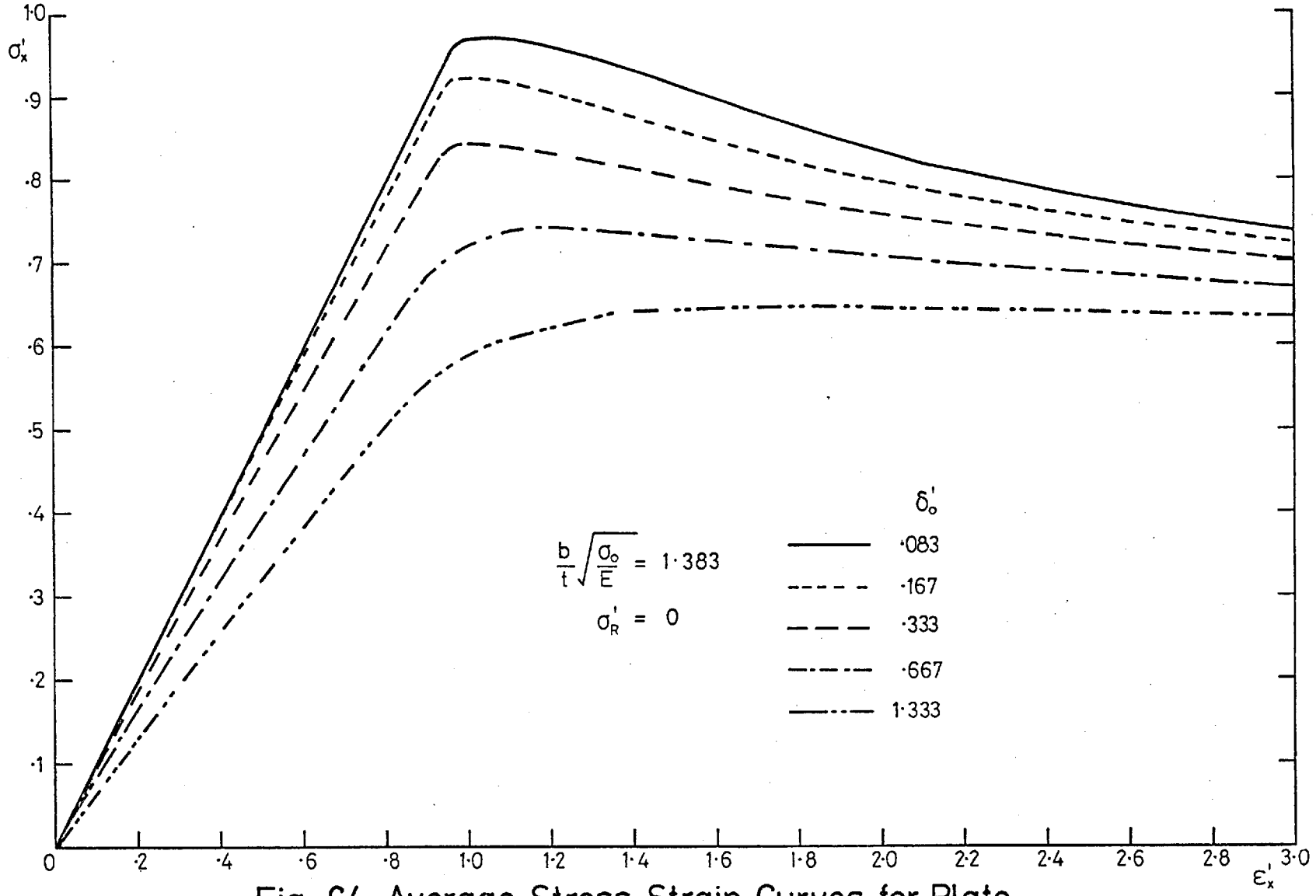

Fig. 64. Average Stress-Strain Curves for Plate in Compression with Constrained Edges

Effect of Var ing Initial Deformation

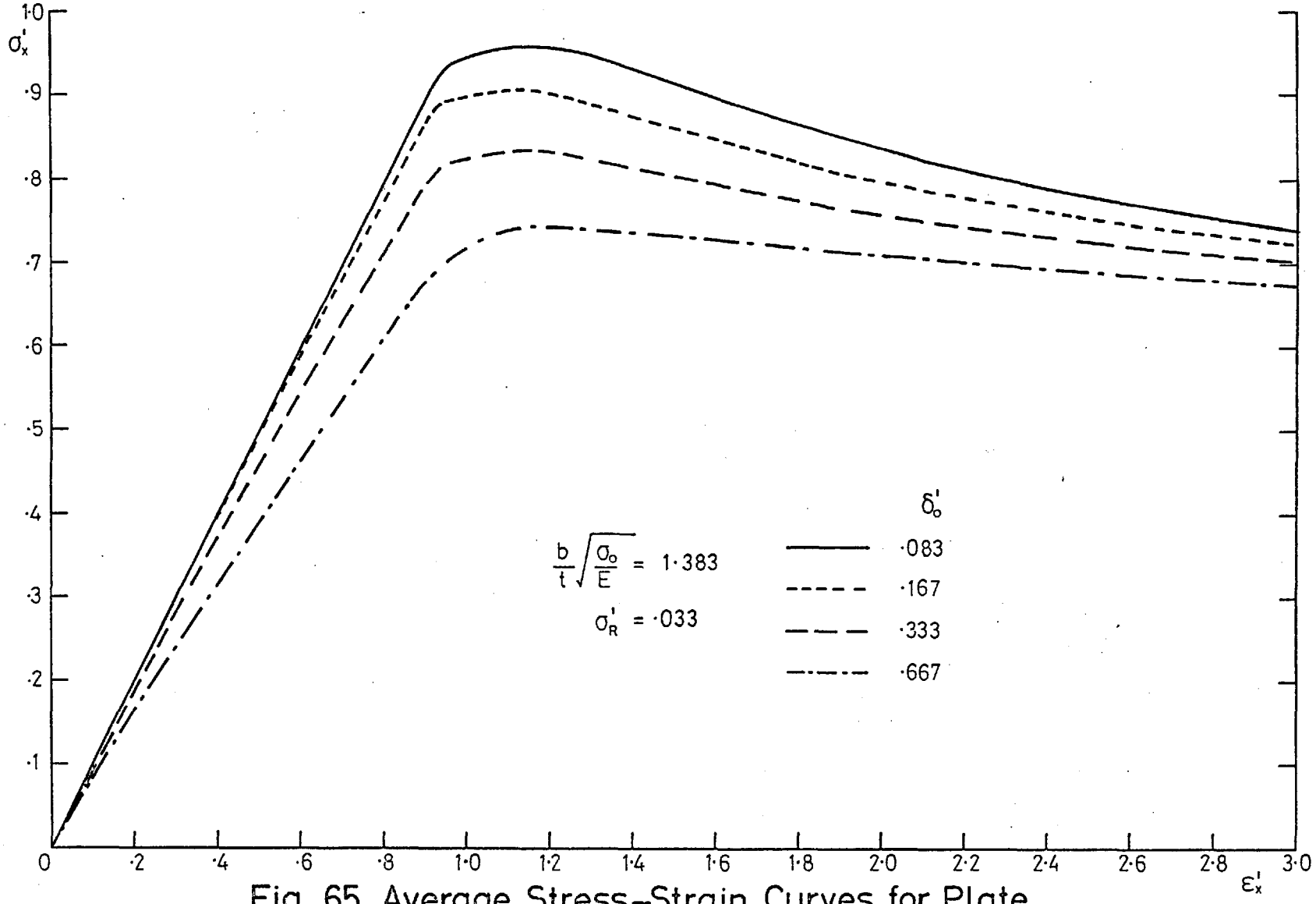

Fig. 65. Average Stress–Strain Curves for Plate in Compression with Constrained Edges

Effect of Varying Initial Deformation

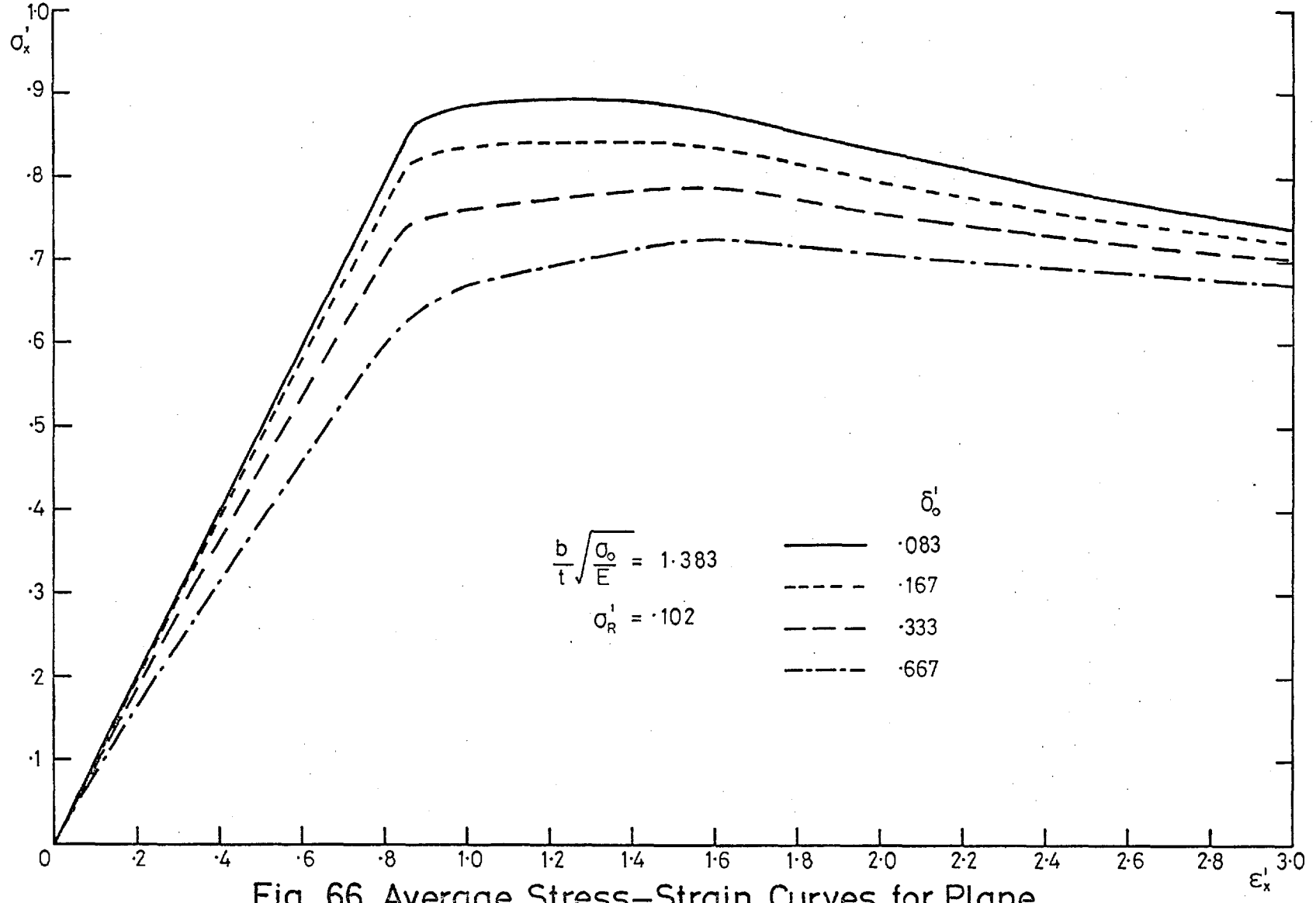

Fig. 66. Average Stress–Strain Curves for Plane in Compression with Constrained Edges

Effect of Varying Initial Deformation

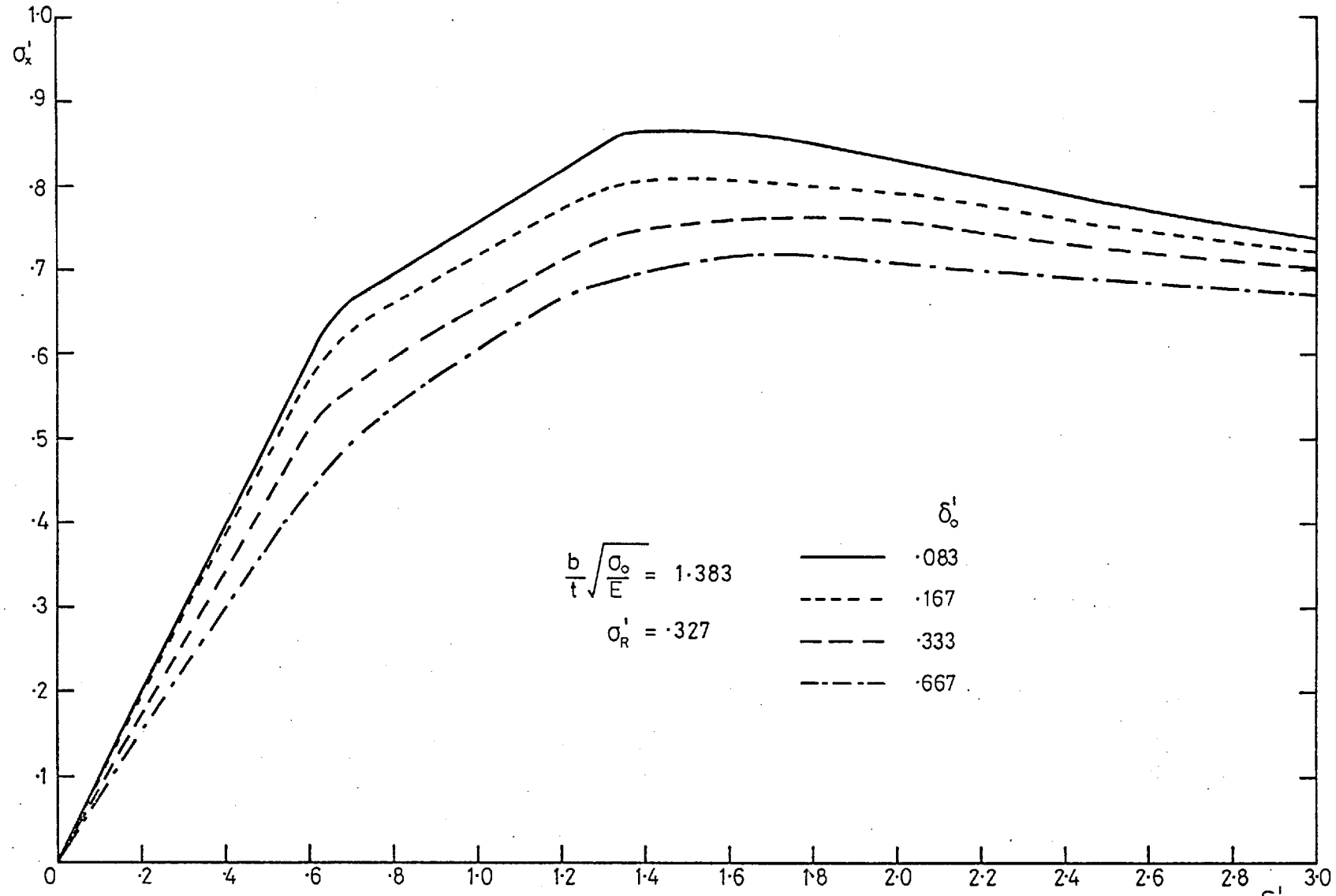

Fig. 67. Average Stress–Strain Curves for Plate in Compression with Constrained Edges
Effect of Varying Initial Deformation

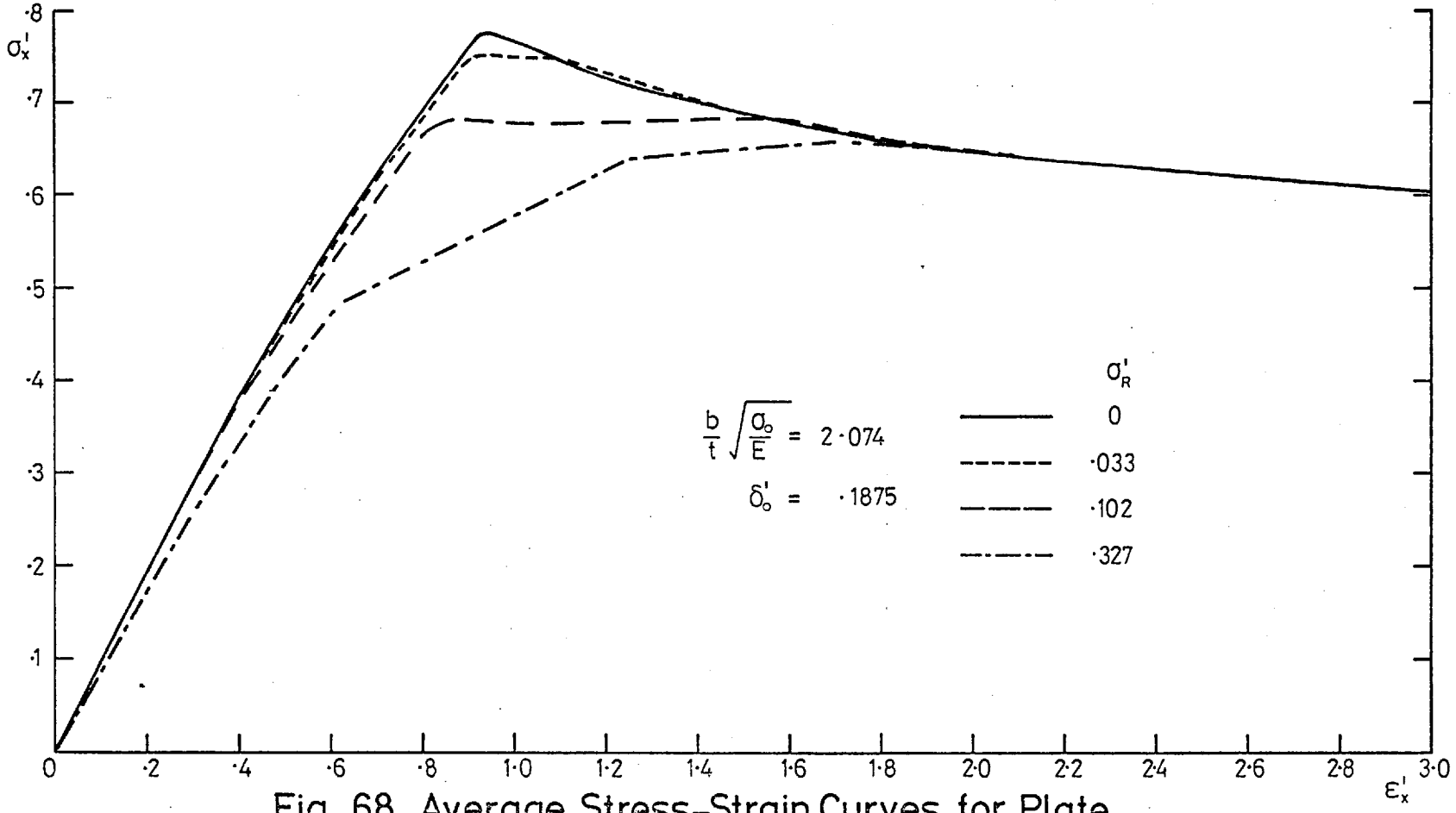

Fig. 68. Average Stress-Strain Curves for Plate in Compression with Constrained Edges

Effect of Varying Residual Stress.

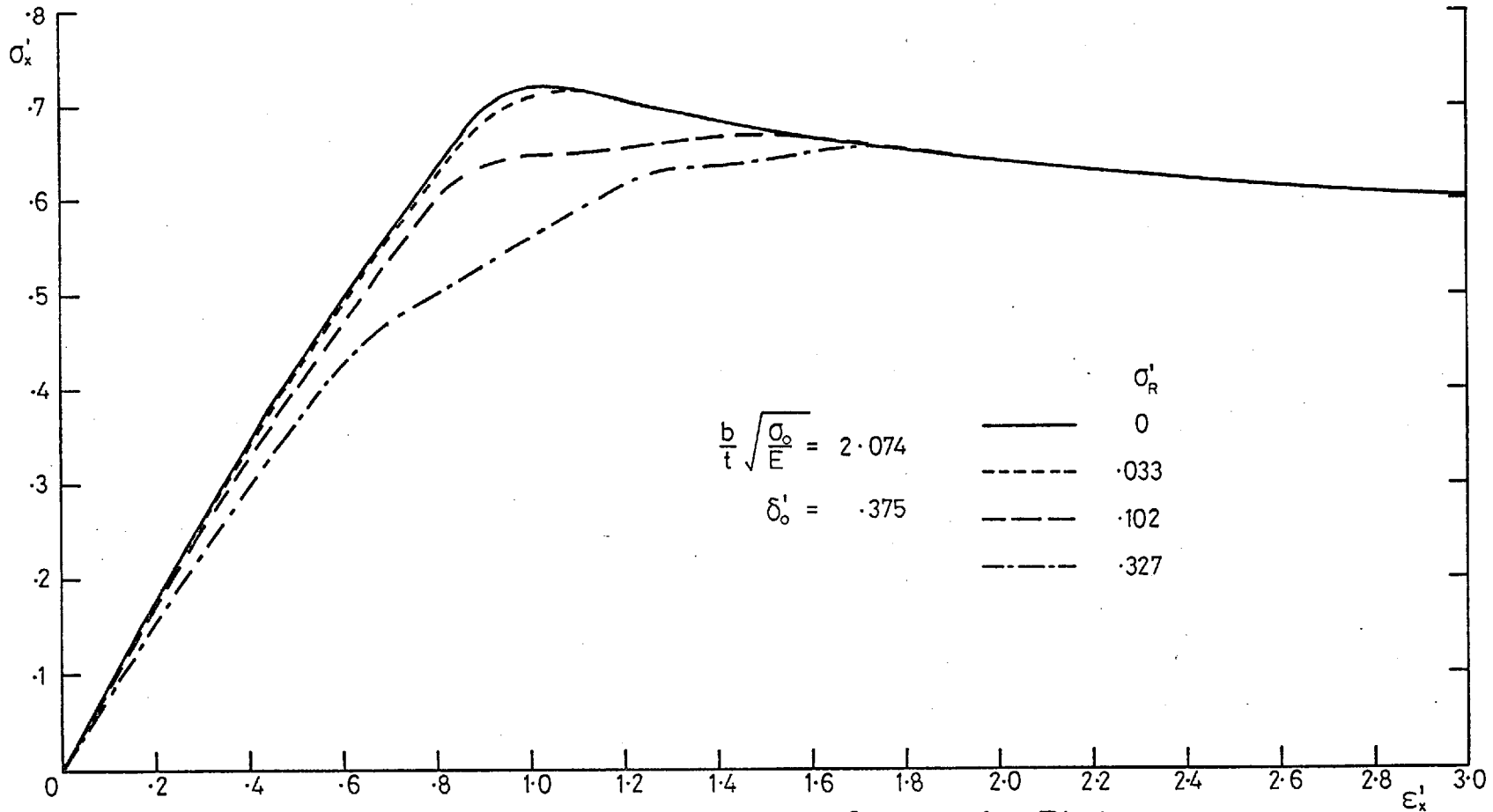

Fig. 69. Average Stress–Strain Curves for Plate in Compression with Constrained Edges

Effect of Varying Residual Stress

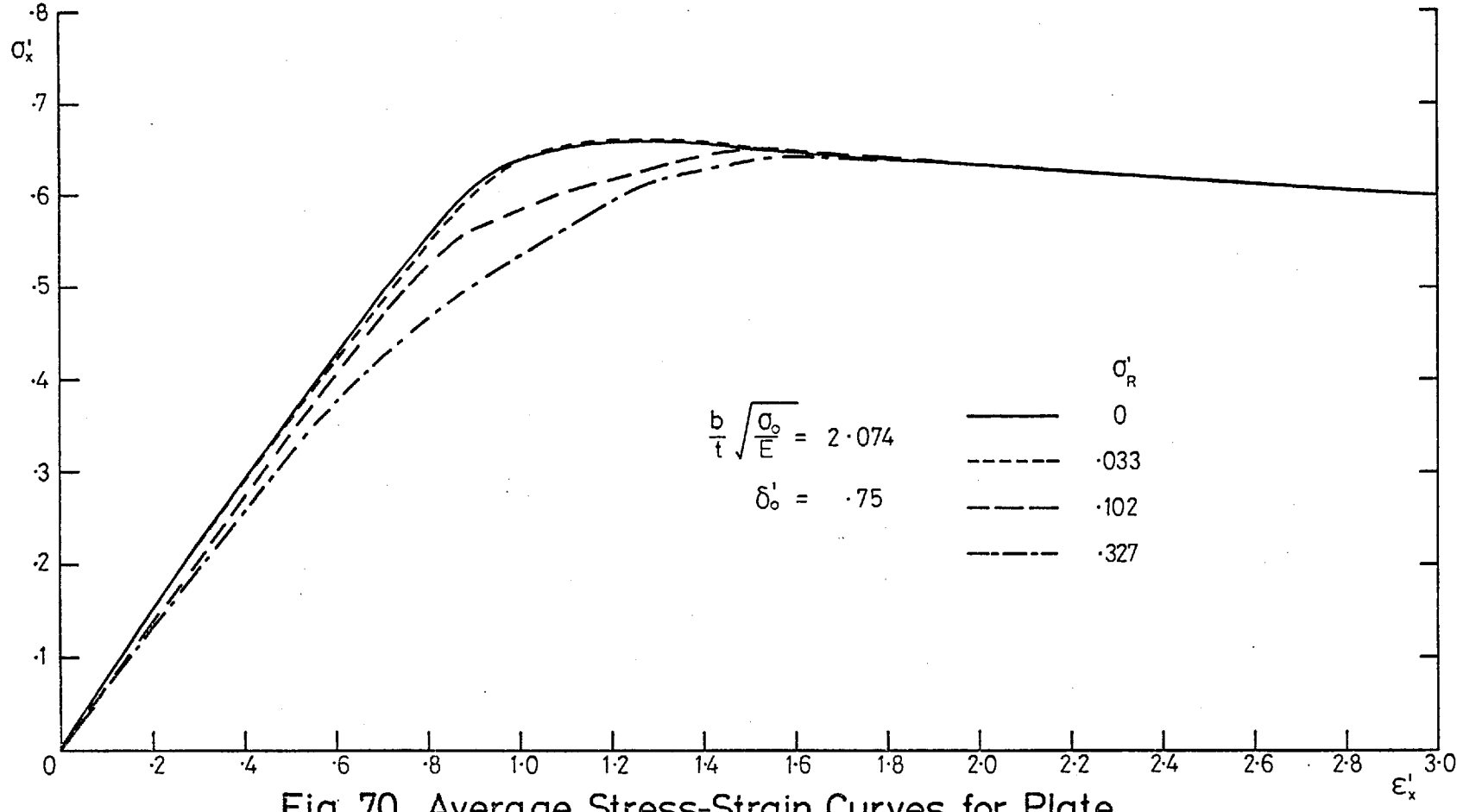

Fig. 70. Average Stress-Strain Curves for Plate in Compression with Constrained Edges

Effect of Varying Residual Stress.

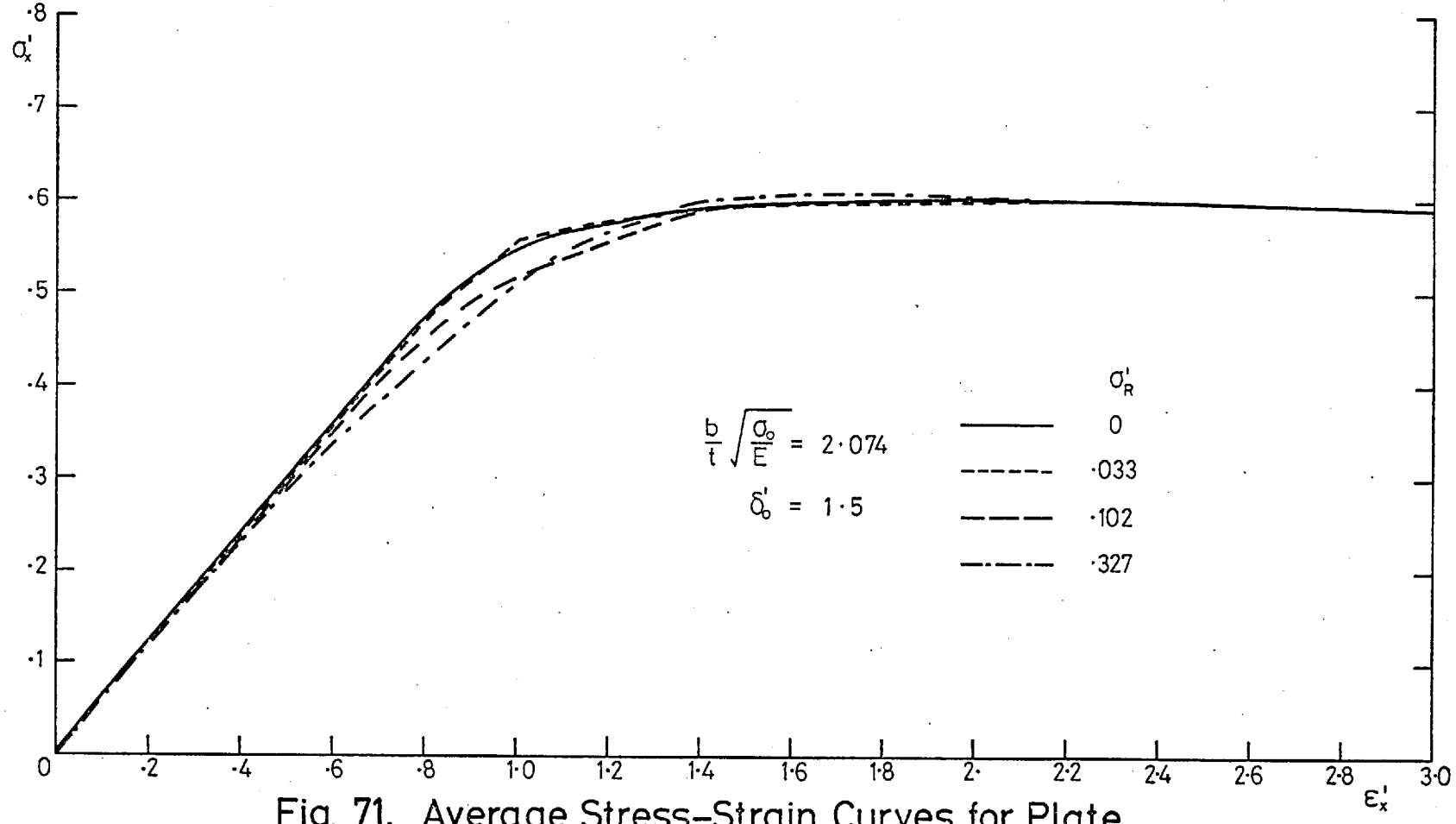

Fig. 71. Average Stress–Strain Curves for Plate in Compression with Constrained Edges

Effect of Varying Residual Stress

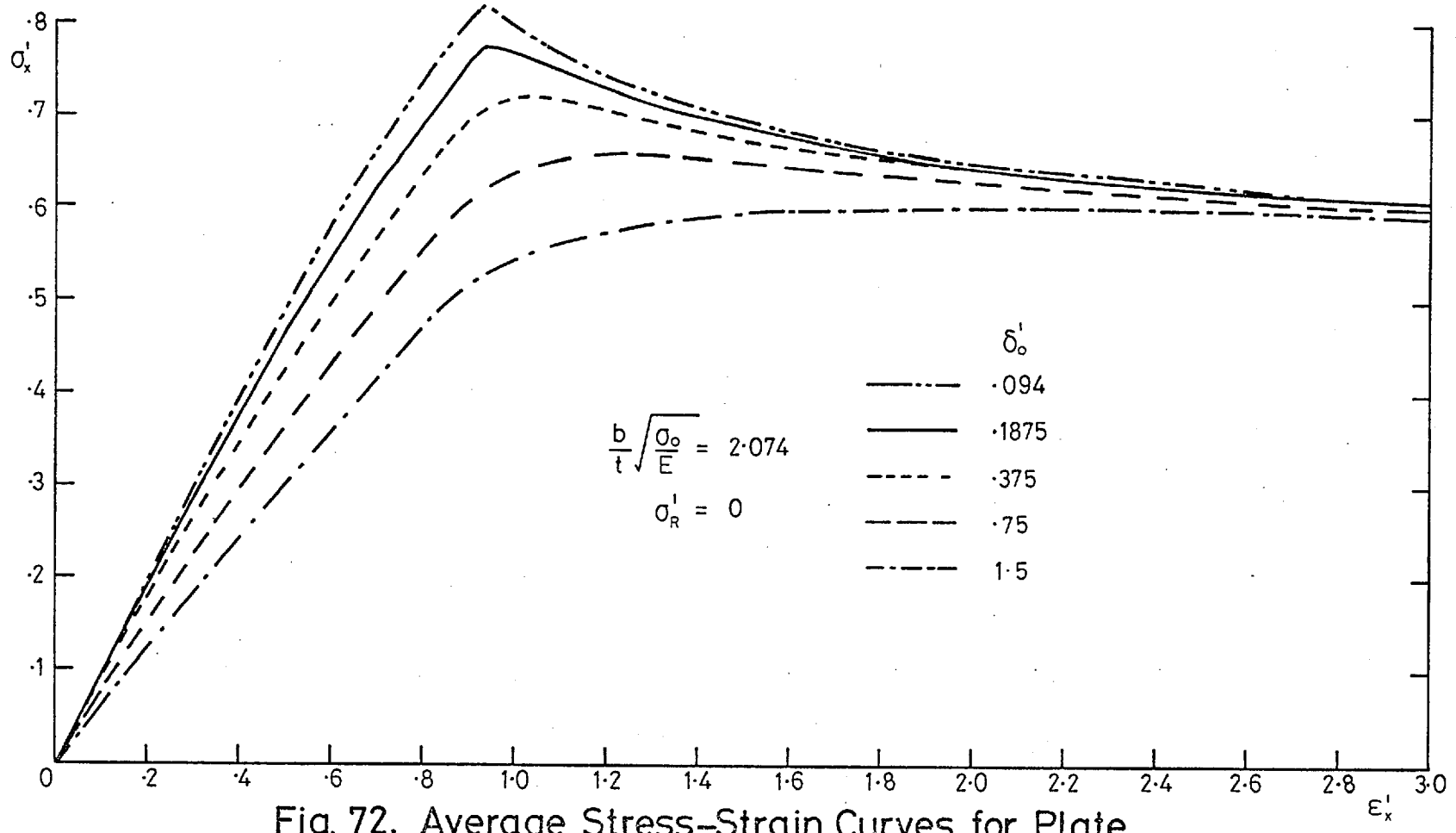

Fig. 72. Average Stress–Strain Curves for Plate in Compression with Constrained Edges

Effect of Varying Initial Deformation

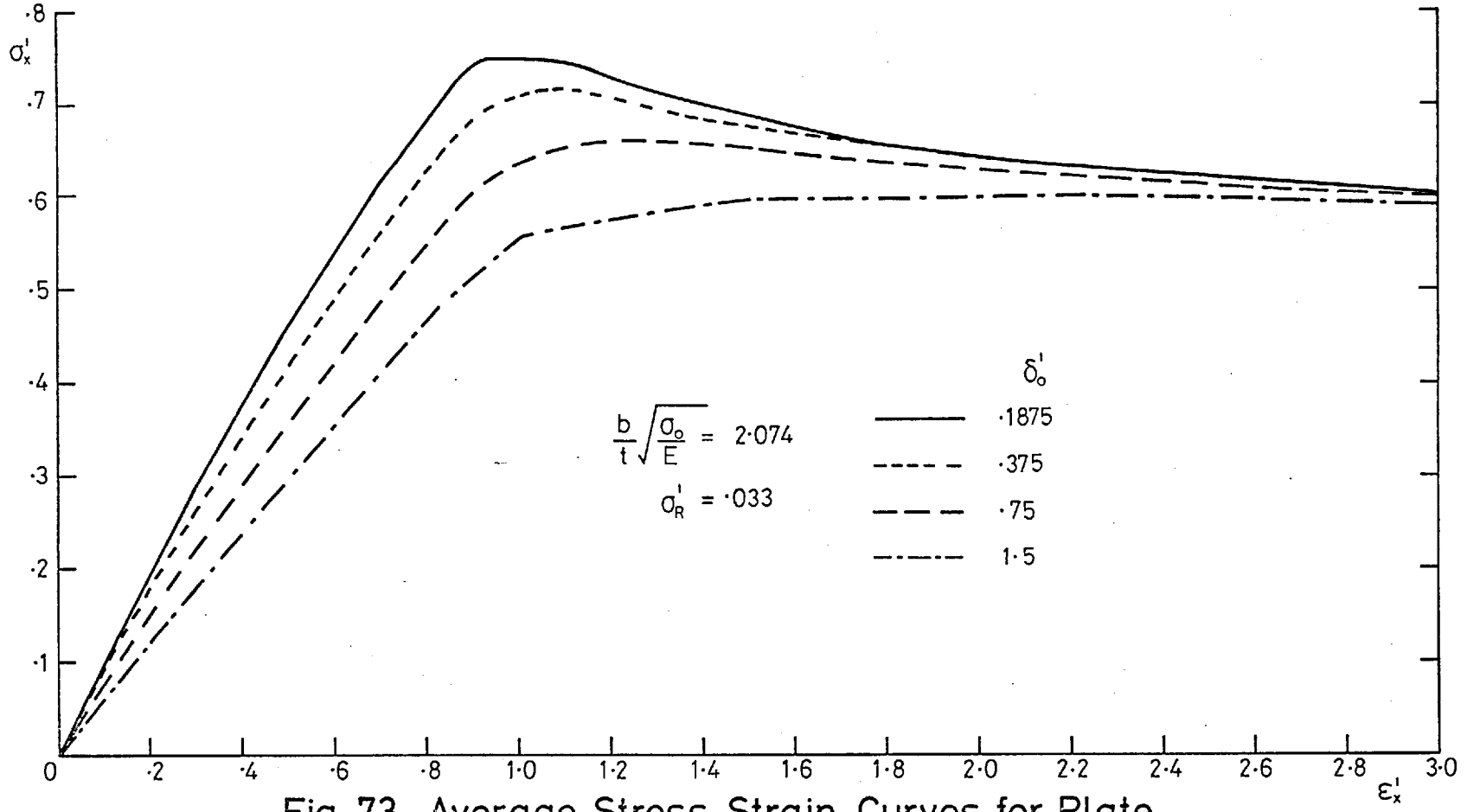

Fig. 73. Average Stress–Strain Curves for Plate in Compression with Constrained Edges

Effect of Varying Initial Deformation

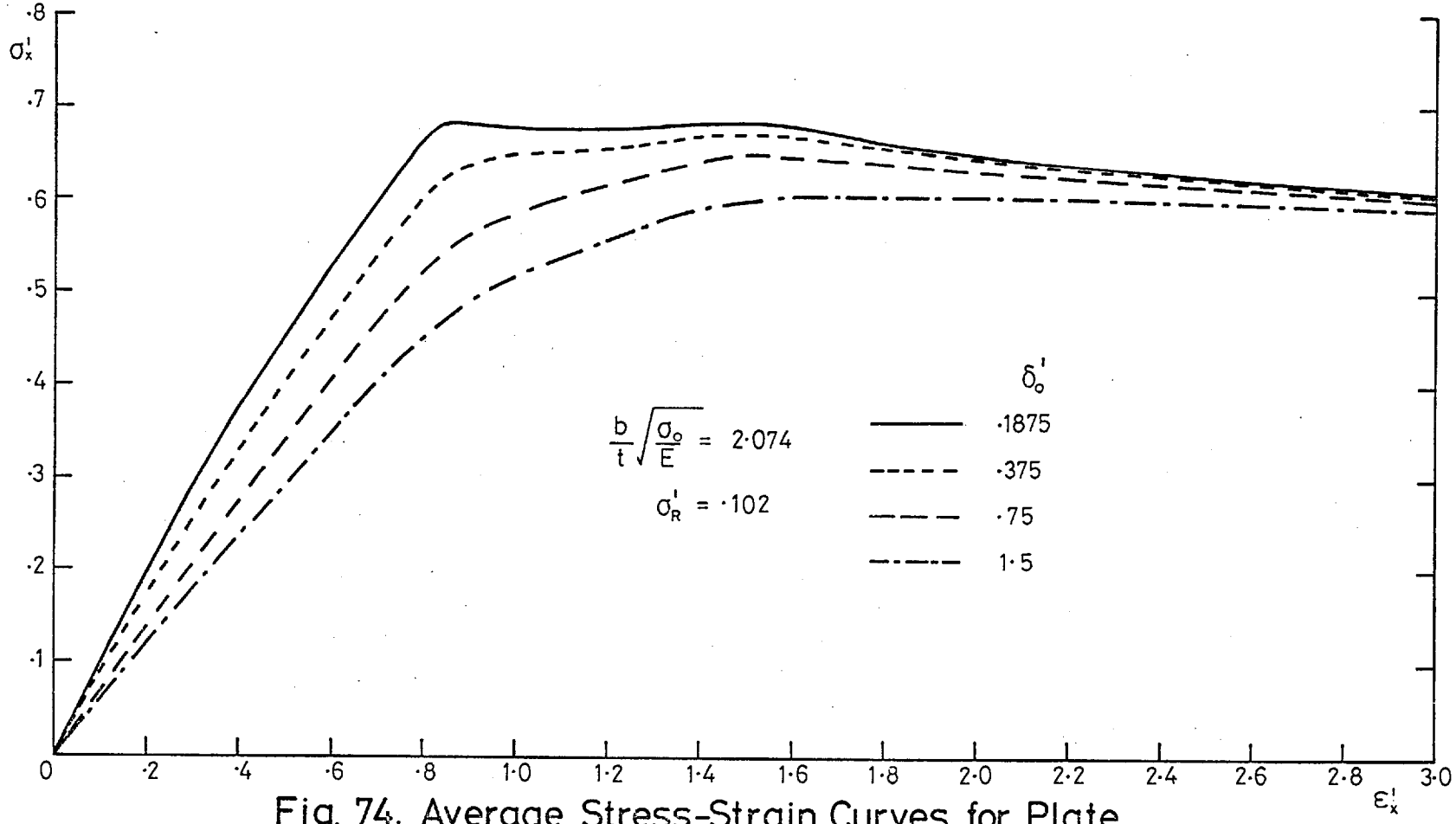

Fig. 74. Average Stress-Strain Curves for Plate in Compression with Constrained Edges

Effect of Varying Initial Deformation

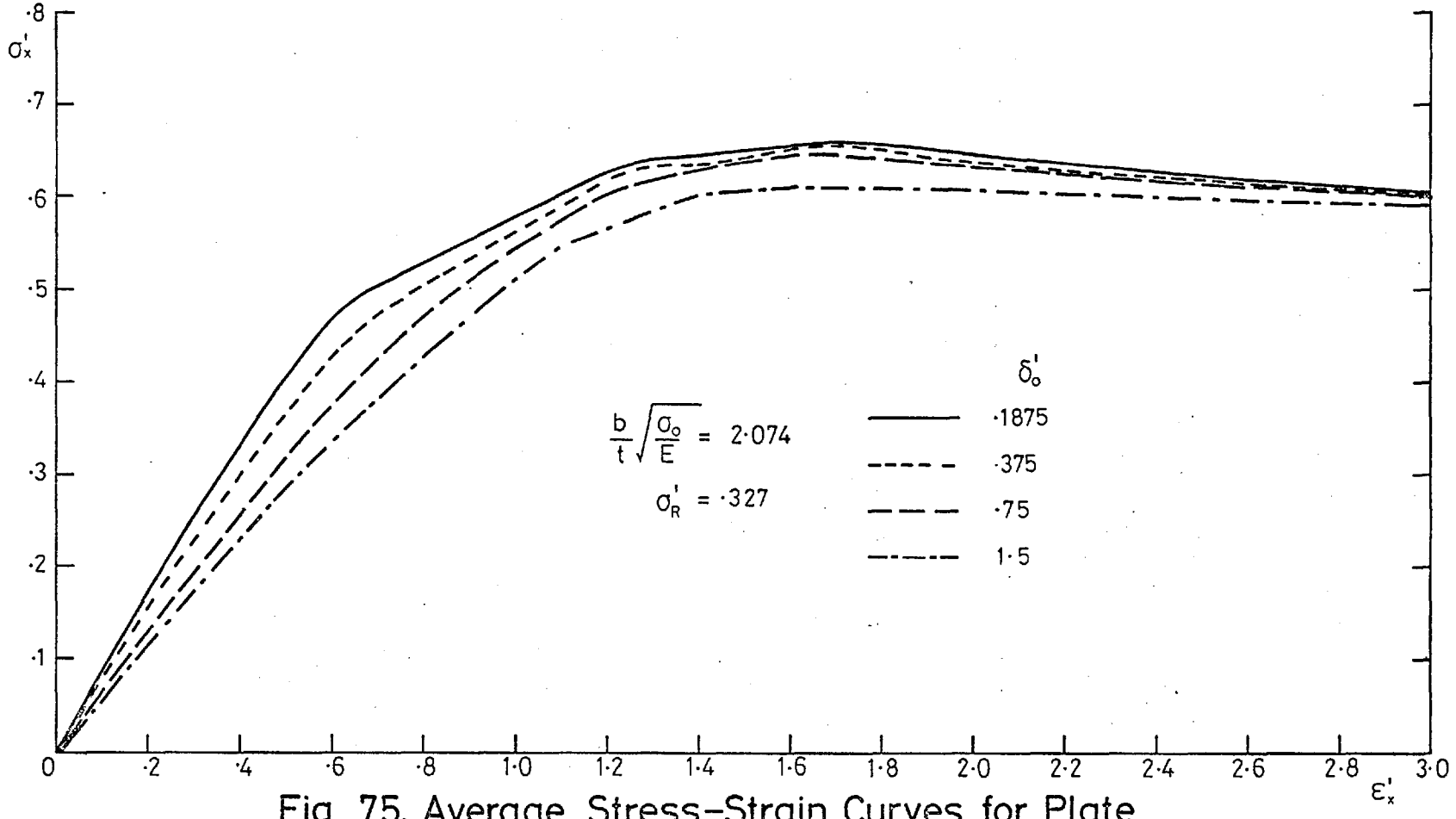

Fig. 75. Average Stress–Strain Curves for Plate in Compression with Constrained Edges

Effect of Varying Initial Deformation

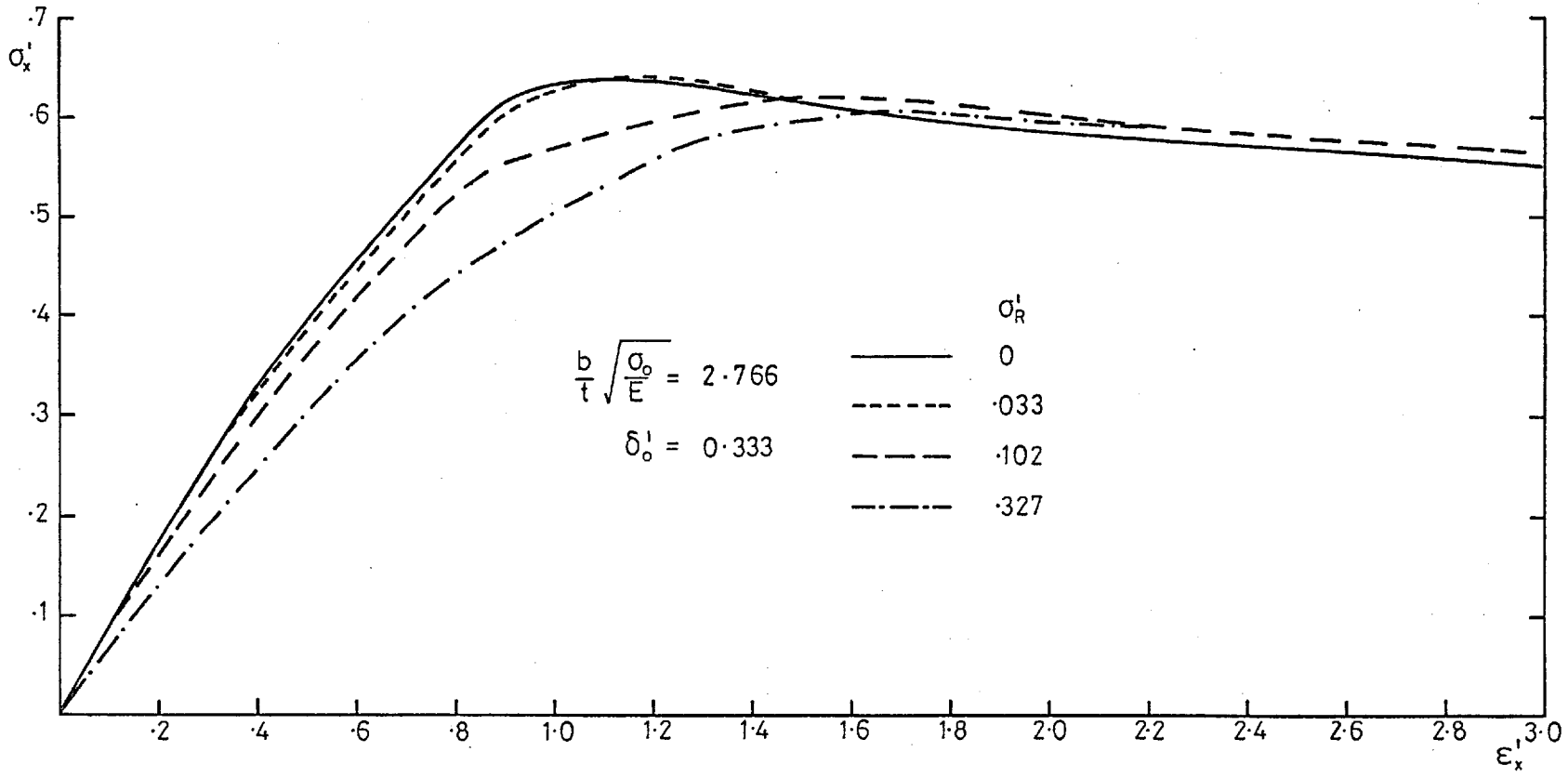

Fig. 76. Average Stress–Strain Curves for Plate in Compression with Constrained Edges.

Effect of Varying Residual Stress

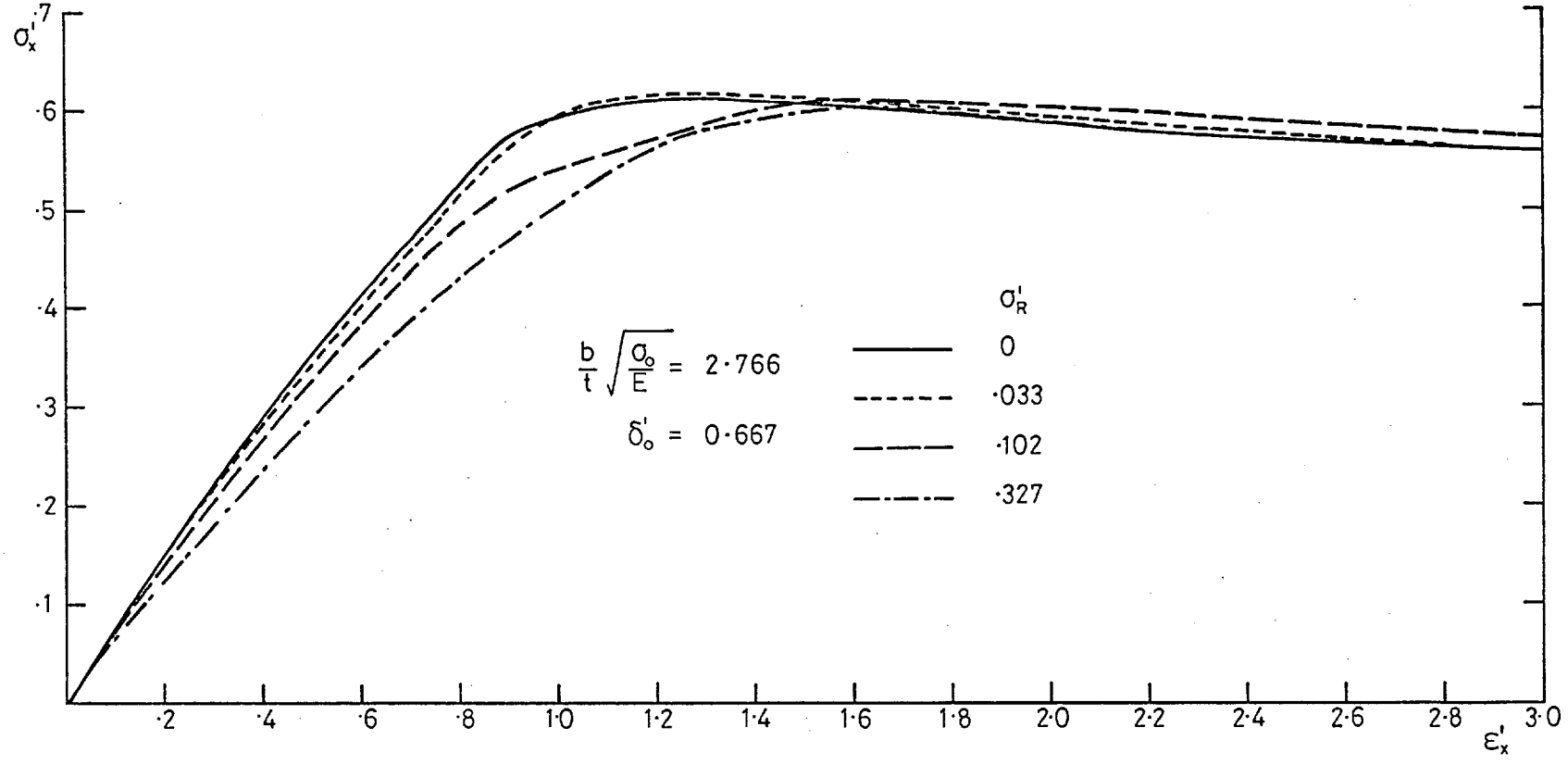

Fig. 77. Average Stress–Strain Curves for Plate in Compression with Constrained Edges.

Effect of Varying Residual Stress

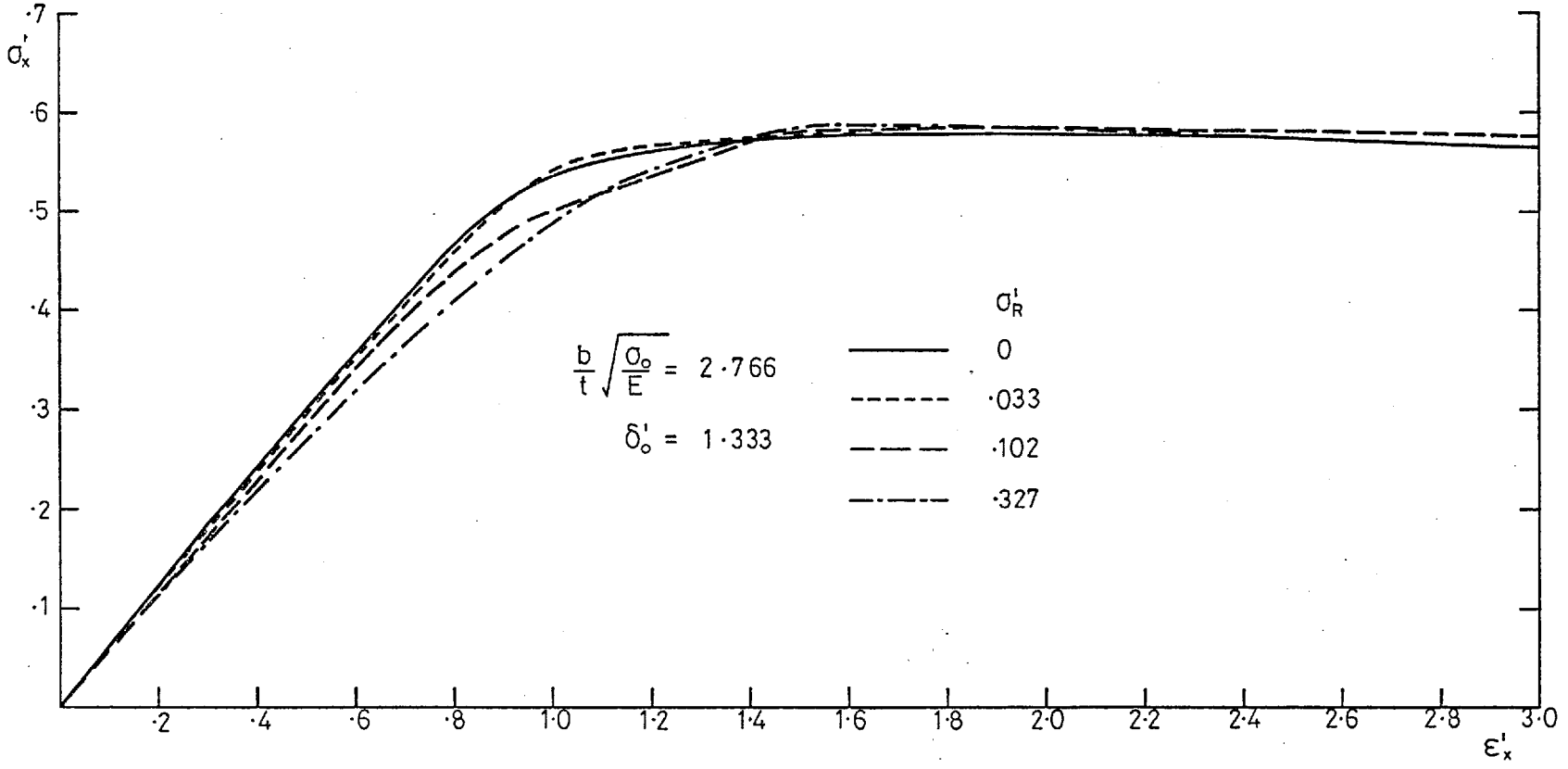

Fig. 78. Average Stress–Strain Curves for Plate in Compression with Constrained Edges.

Effect of Varying Residual Stress

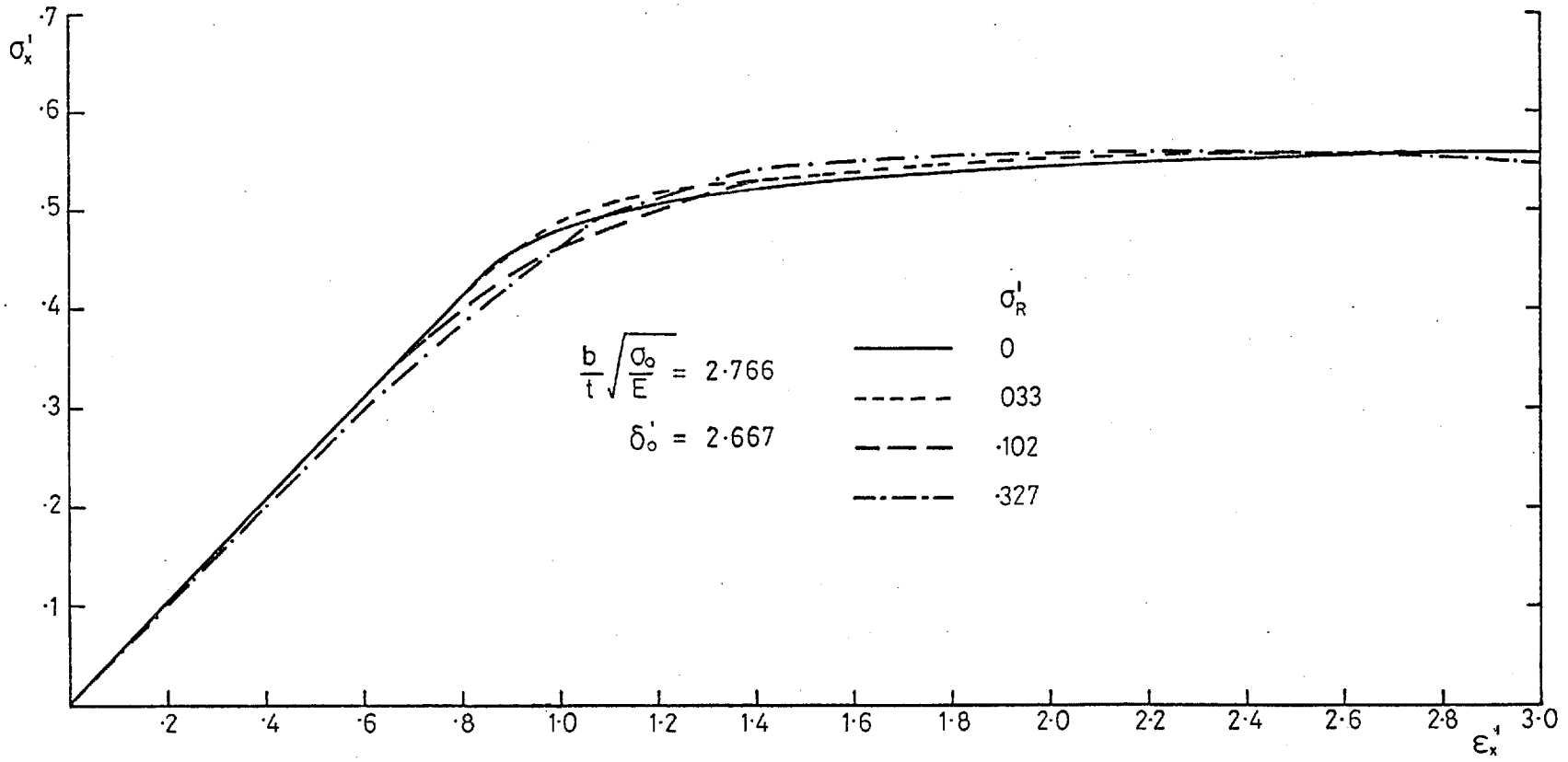

Fig. 79. Average Stress–Strain Curves for Plate in Compression with Constrained Edges

Effect of Varying Residual Stress.

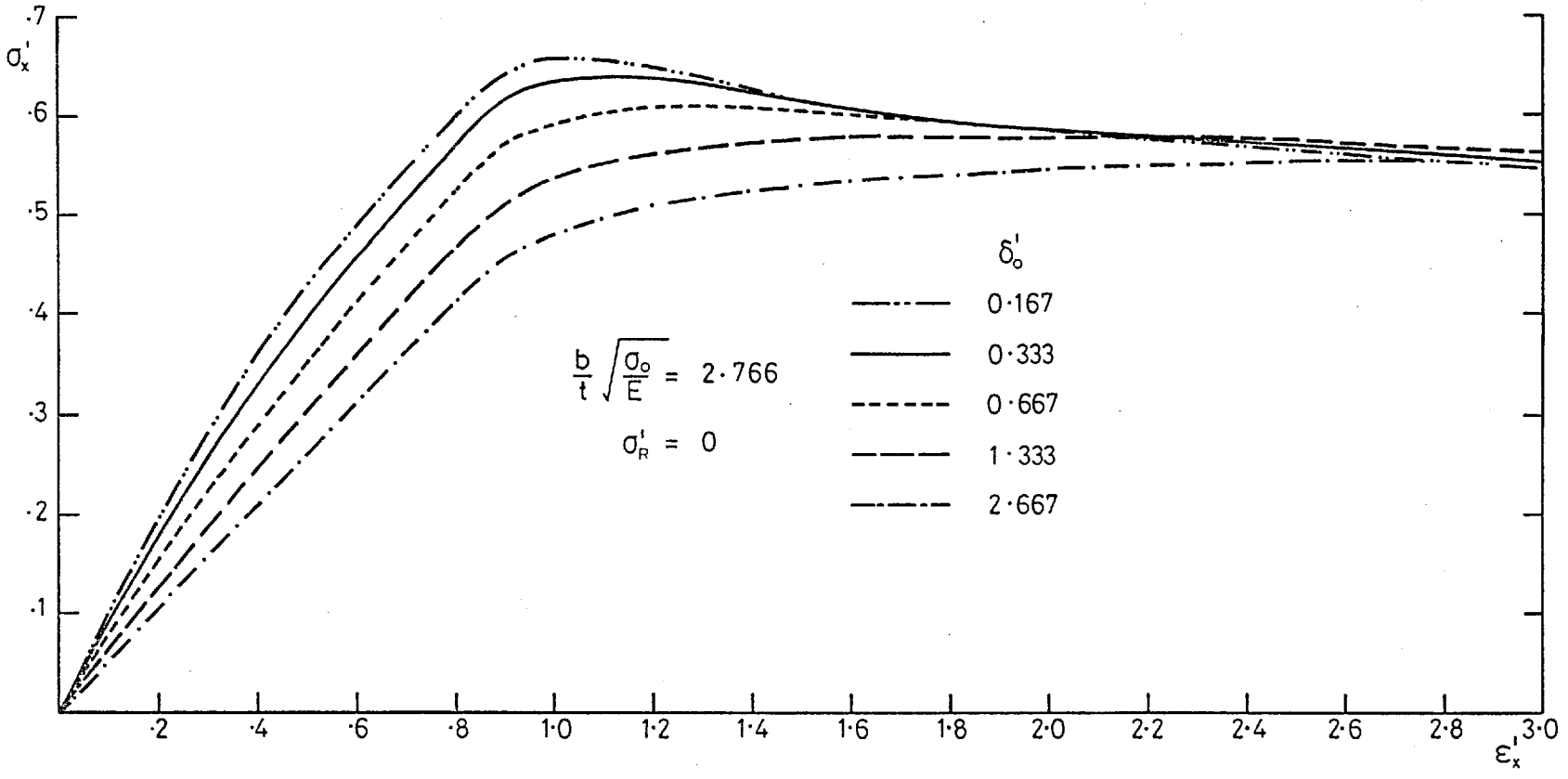

Fig. 80. Average Stress–Strain Curves for Plate in Compression with Constrained Edges.

Effect of Varying Residual Stress

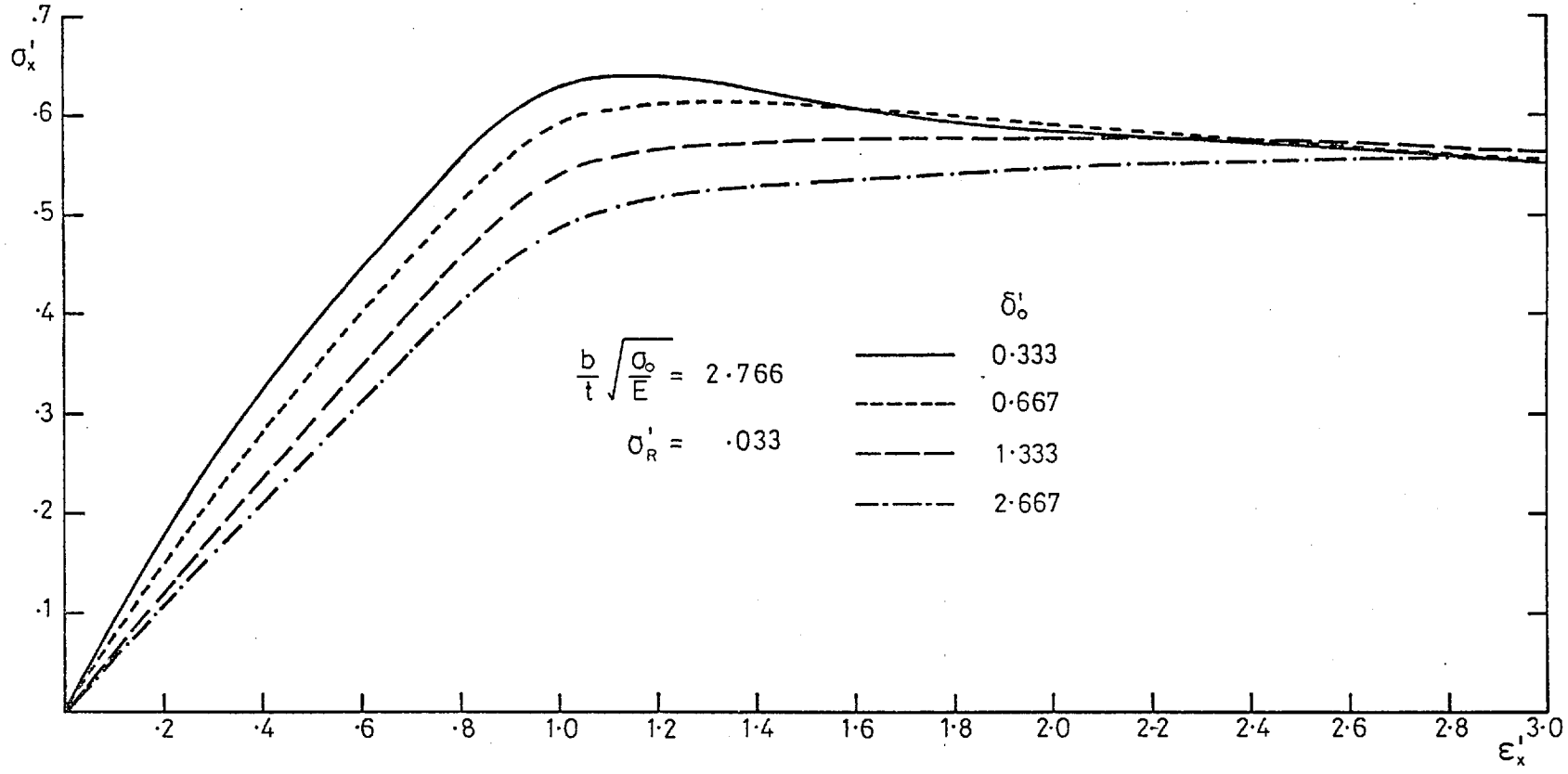

Fig. 81. Average Stress–Strain Curves for Plate in Compression with Constrained Edges.

Effect of Varying Residual Stress

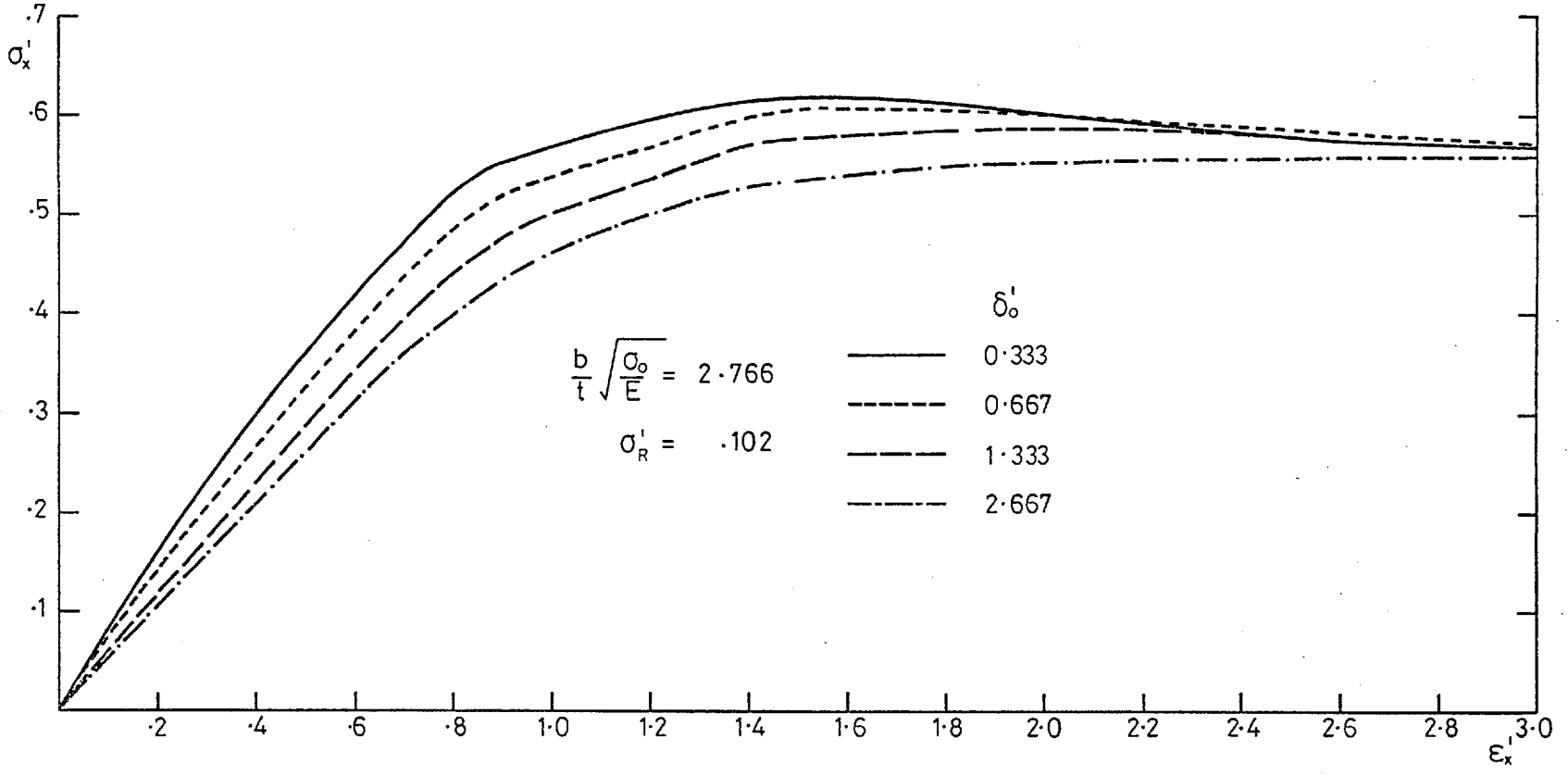

Fig. 82. Average Stress–Strain Curves for Plate in Compression with Constrained Edges.

Effect of Varying Residual Stress

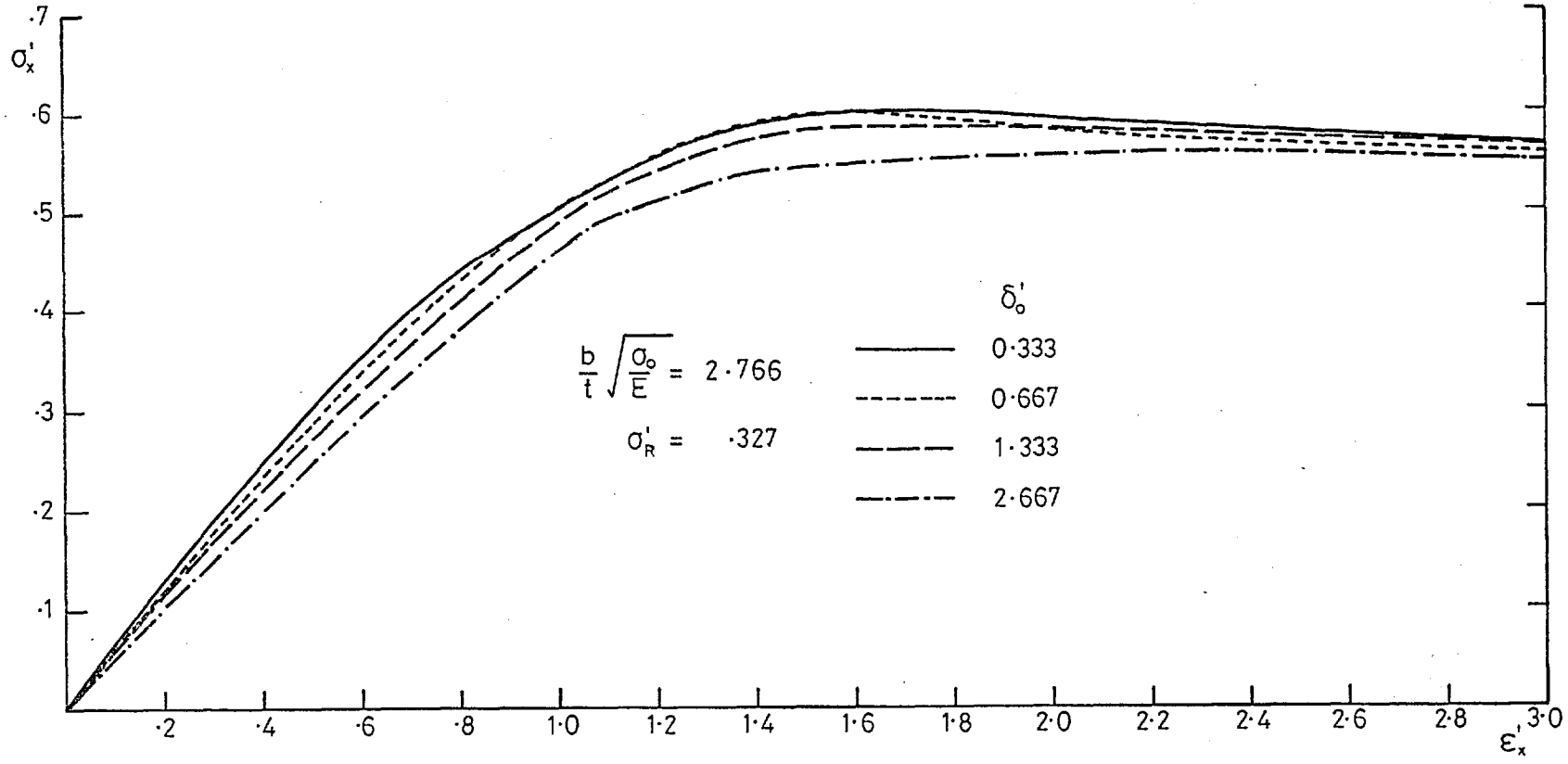

Fig. 83. Average Stress–Strain Curves for Plate in Compression with Constrained Edges.

Effect of Varying Residual Stress

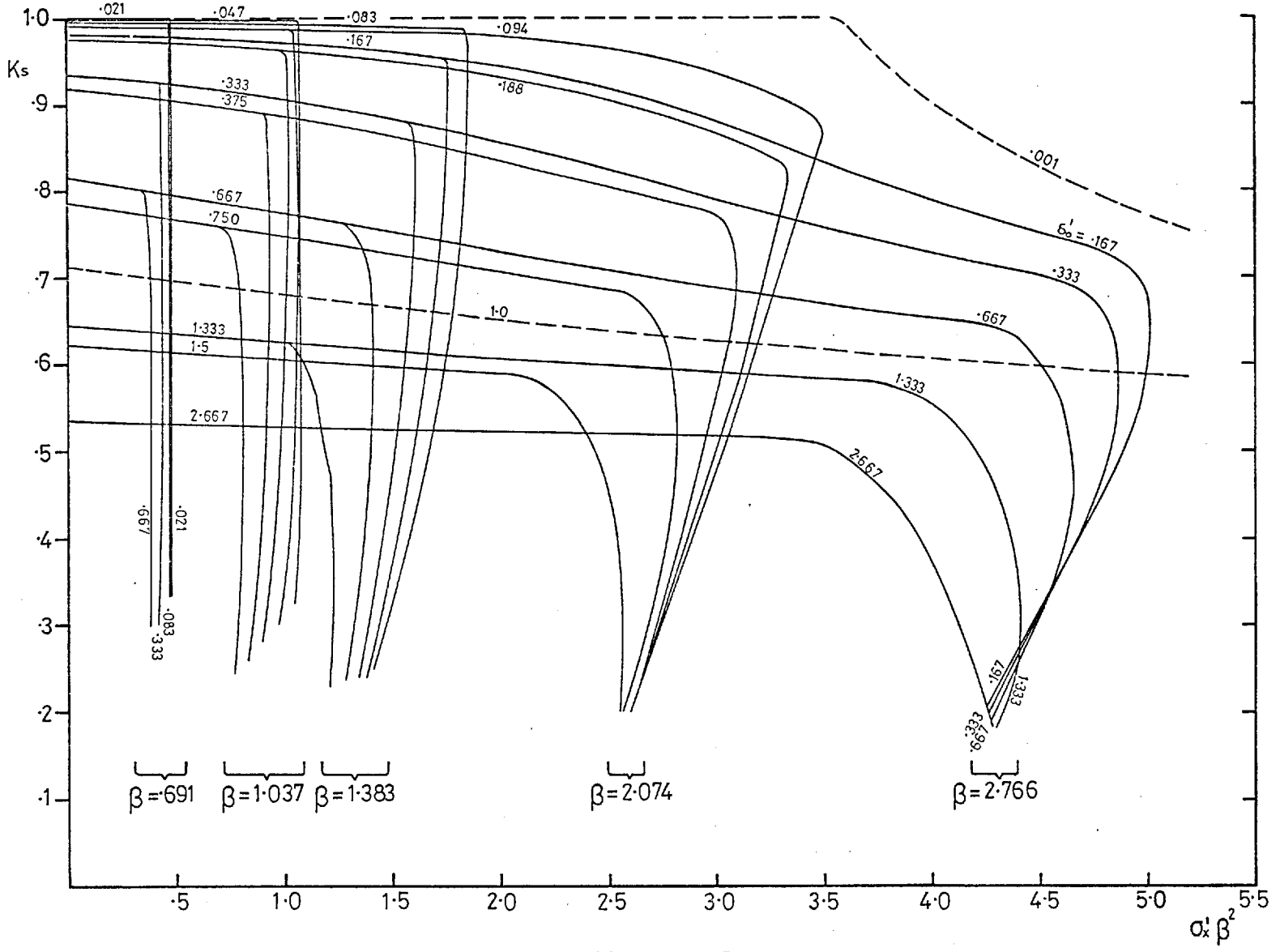

Fig. 84. Elasto-Plastic Secant Stiffness-Stress Curves for Plates with Constrained Edges

δ'_o is indicated on curve and $\sigma'_R = 0$ in all cases
Elastic stiffness curves for $\delta'_o = \cdot001$ & 1·0 are shown for comparison

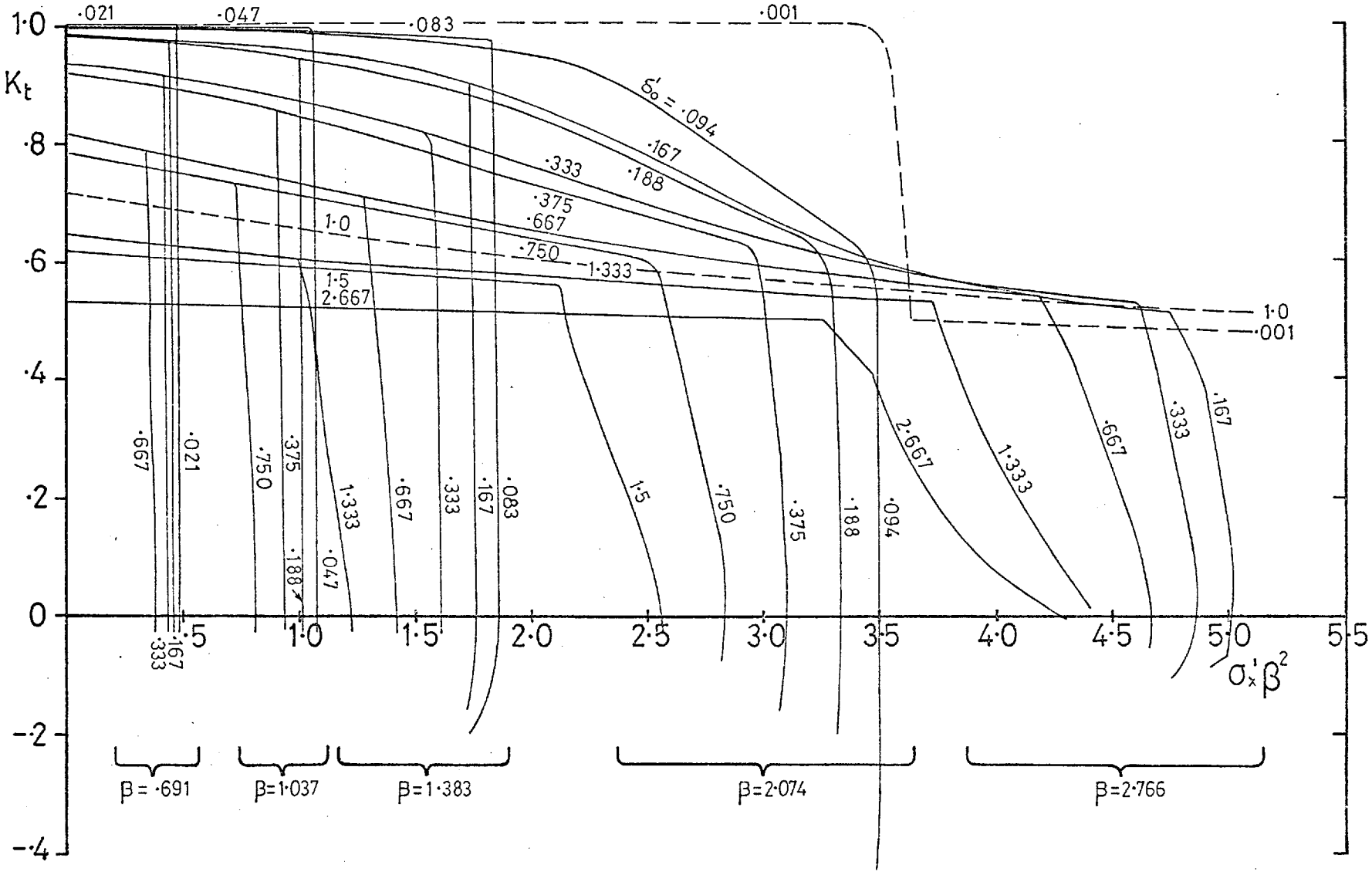

Fig. 85. Elasto–Plastic Tangent Stiffness–Stress Curves for Plates with Constrained Edges

δ'_o is indicated on each curve and $\sigma'_R = 0$ in all cases
Elastic stiffness curves for $\delta'_o = \cdot001$ & 1·0 are shown for comparison

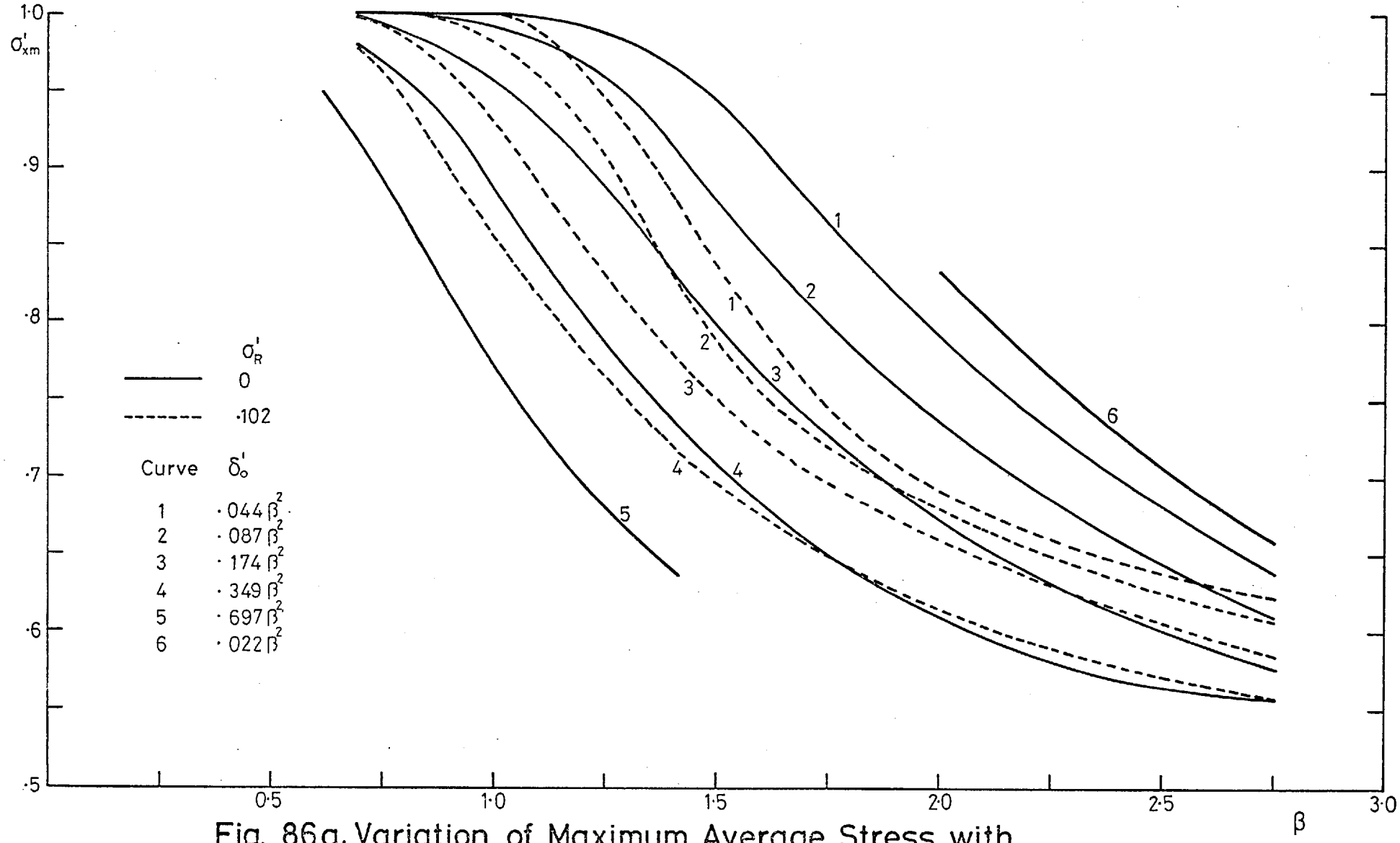

Fig. 86a. Variation of Maximum Average Stress with Slenderness Ratio for Constrained Plates.

Effect of Varying Initial Imperfections

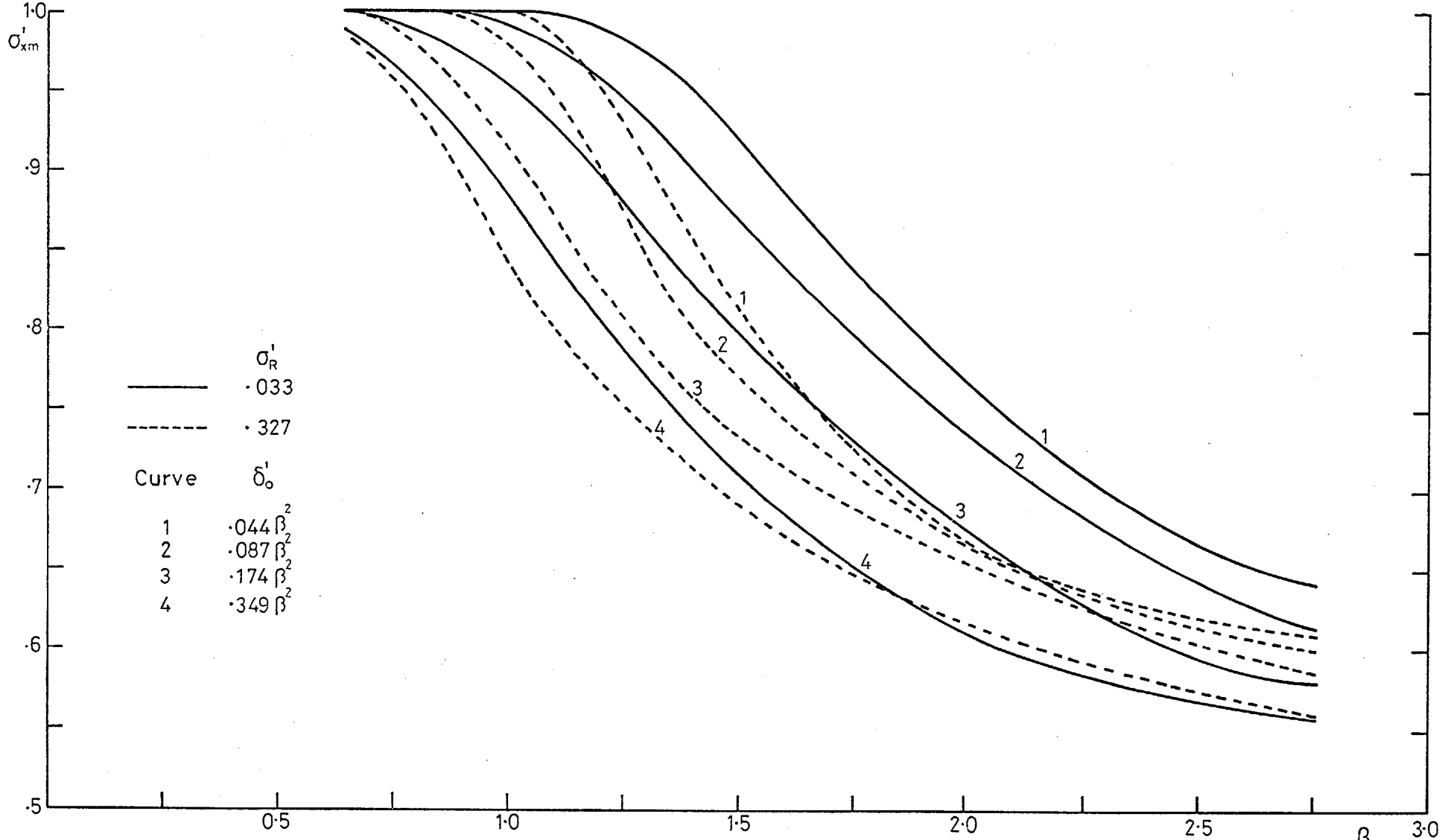

Fig. 86b. Variation of Maximum Average Stress with Slenderness Ratio for Constrained Plates.

Effect of Varying Initial Imperfections

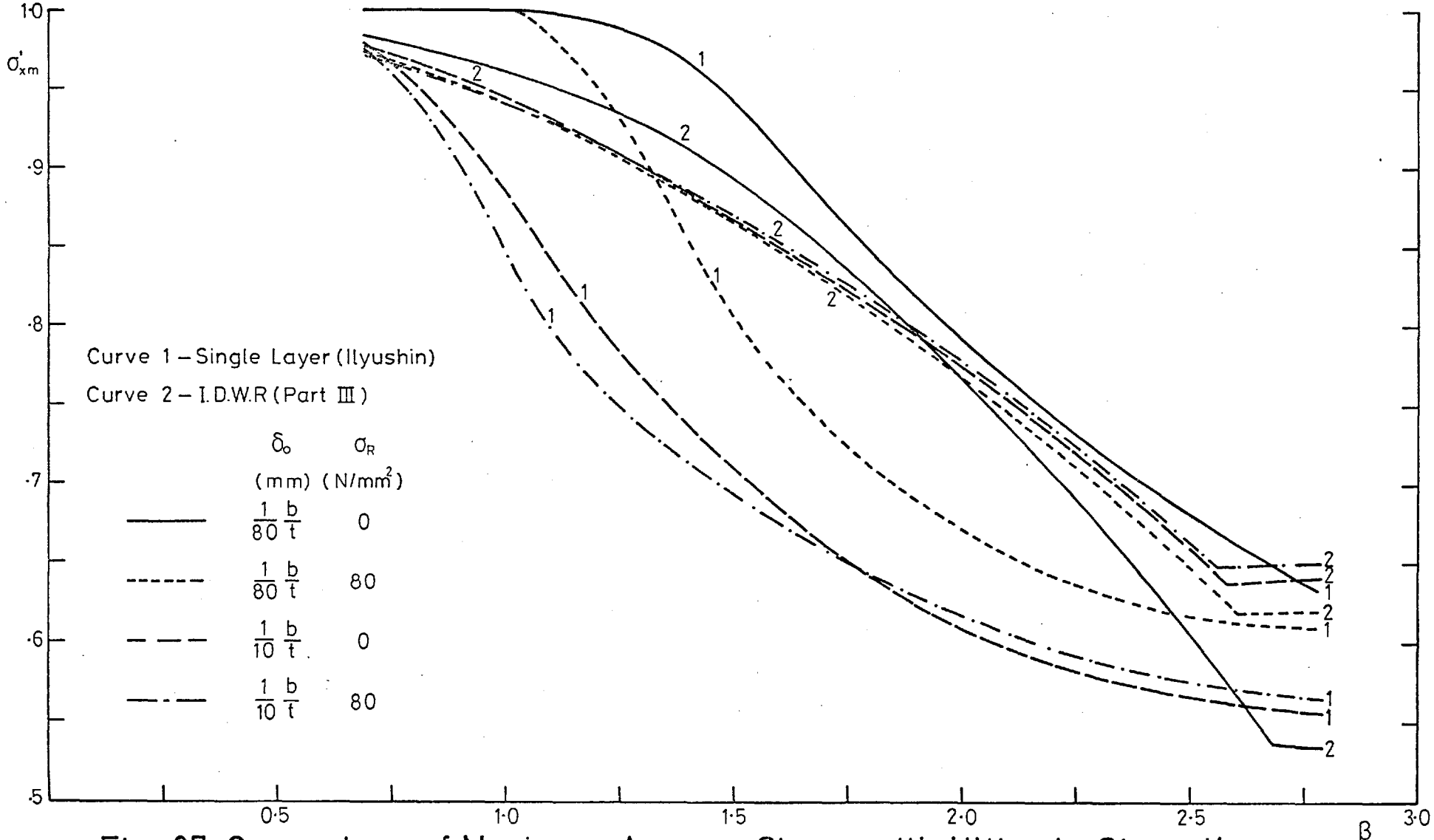

Fig. 87. Comparison of Maximum Average Stress with Ultimate Strength Predicted by Interim Design Rules for Constrained Plates.

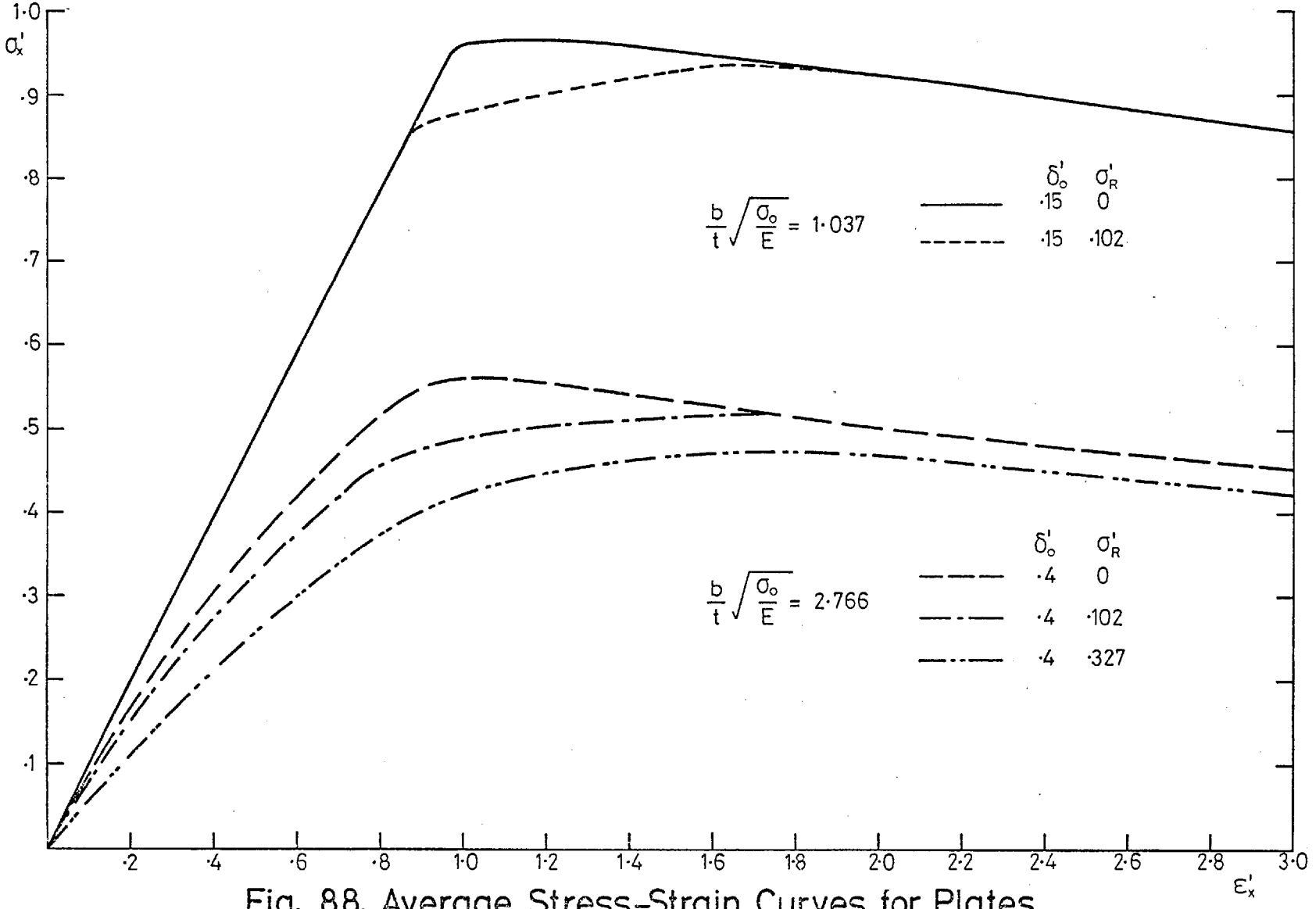

Fig. 88. Average Stress-Strain Curves for Plates in Compression with Unrestrained Edges.

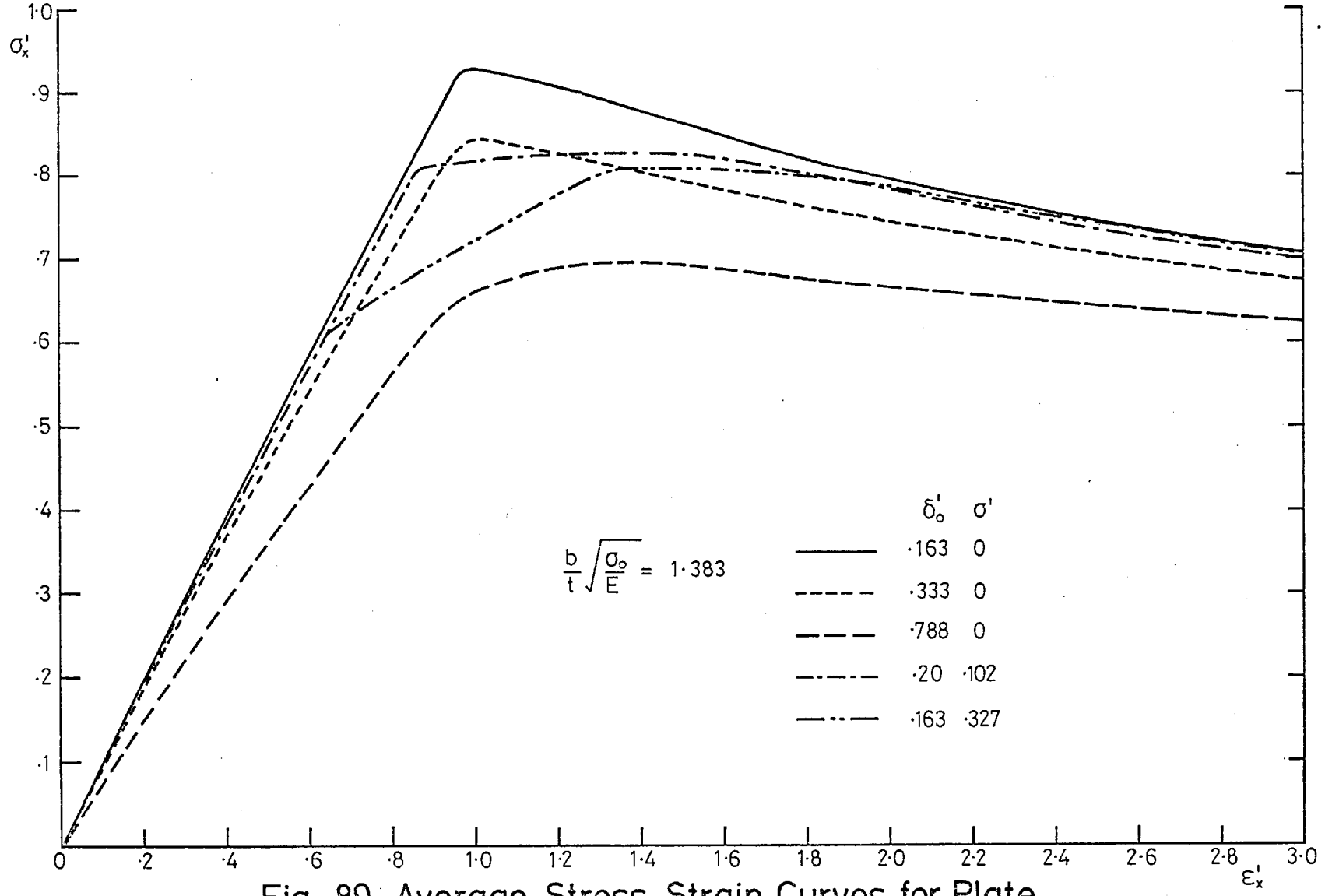

Fig. 89. Average Stress-Strain Curves for Plate in Compression with Unrestrained Edges

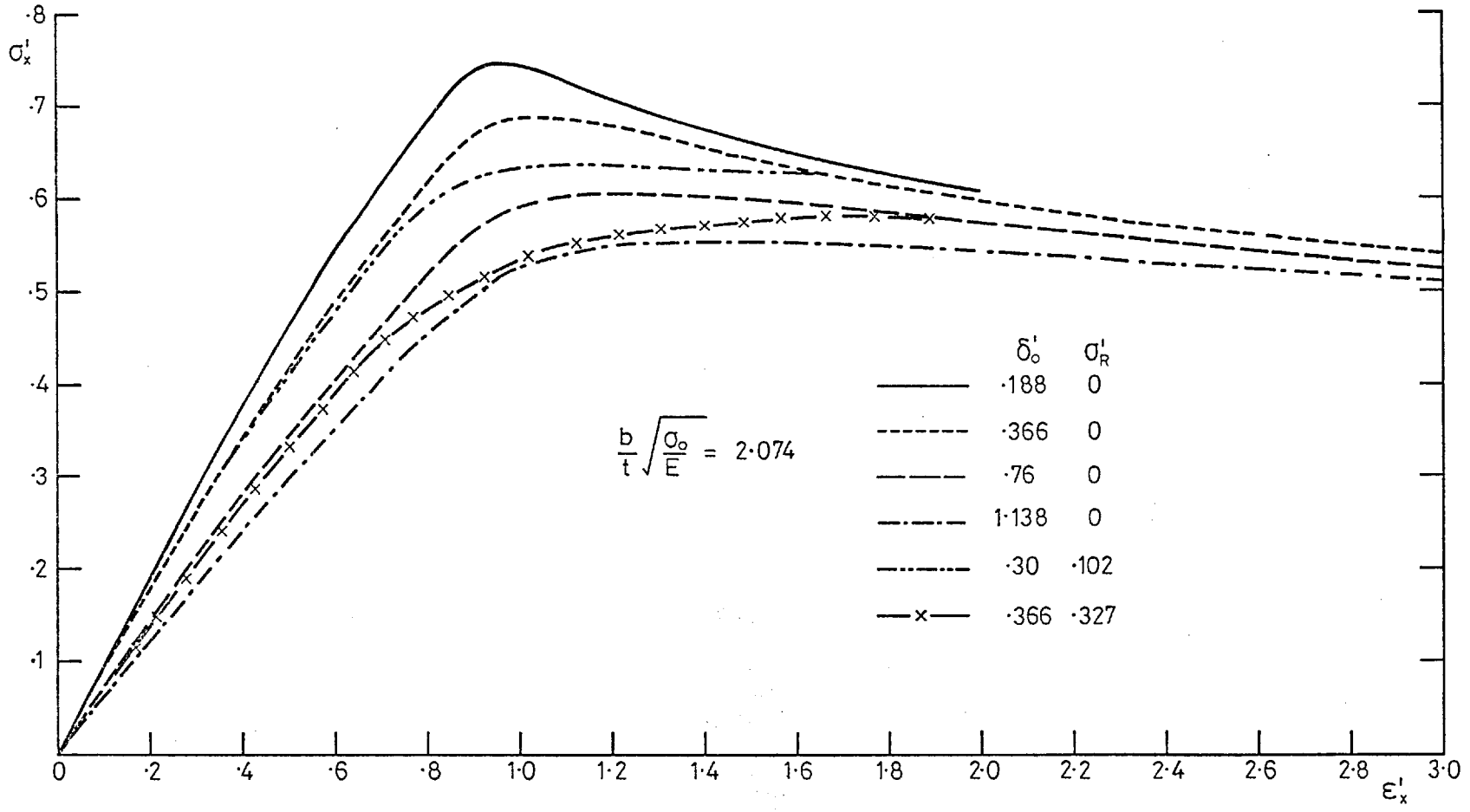

Fig. 90. Average Stress-Strain Curves for Plate in Compression with Unrestrained Edges

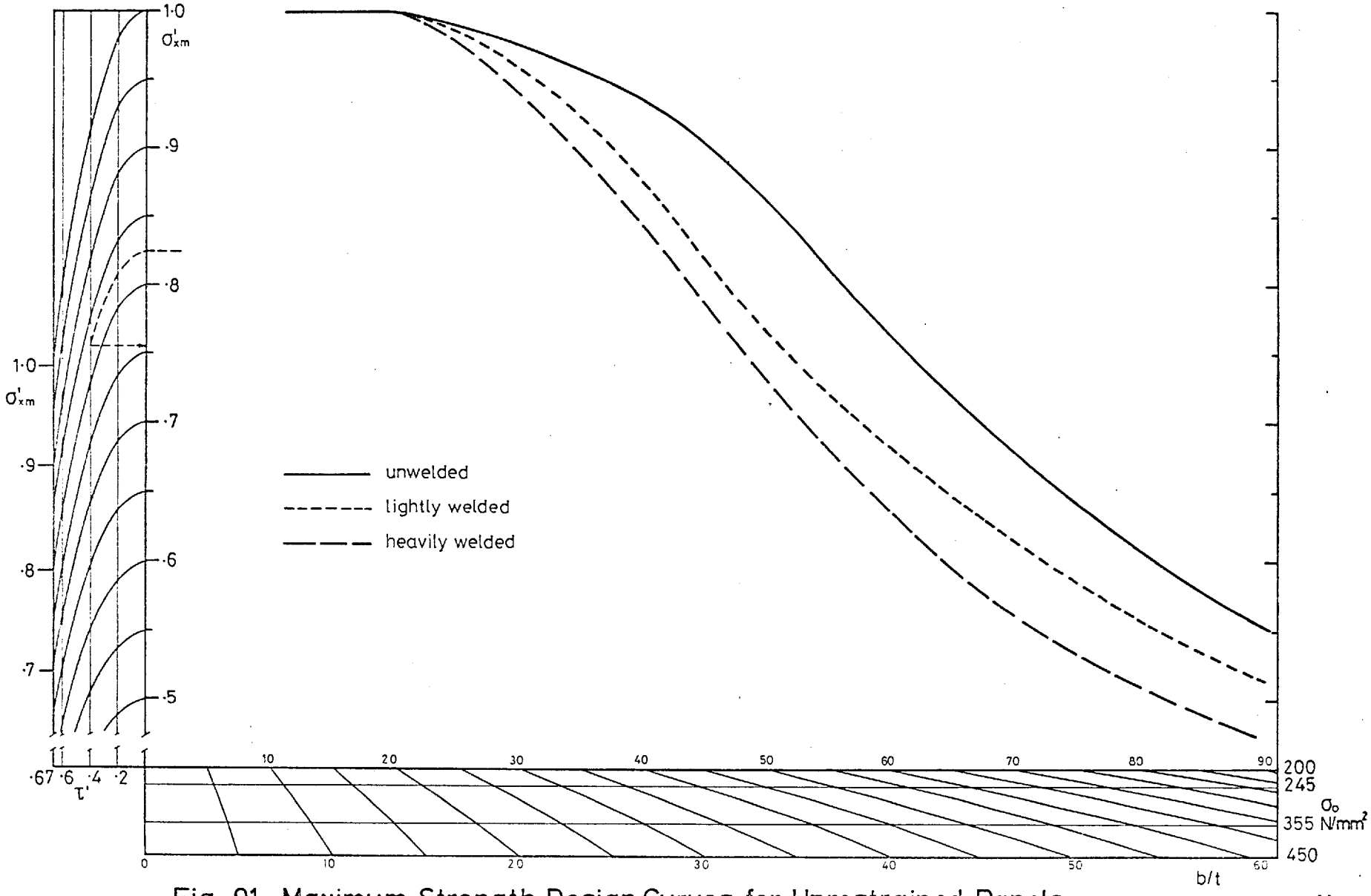

Fig. 91. Maximum Strength Design Curves for Unrestrained Panels

Note the curves which allow for coexistant shear

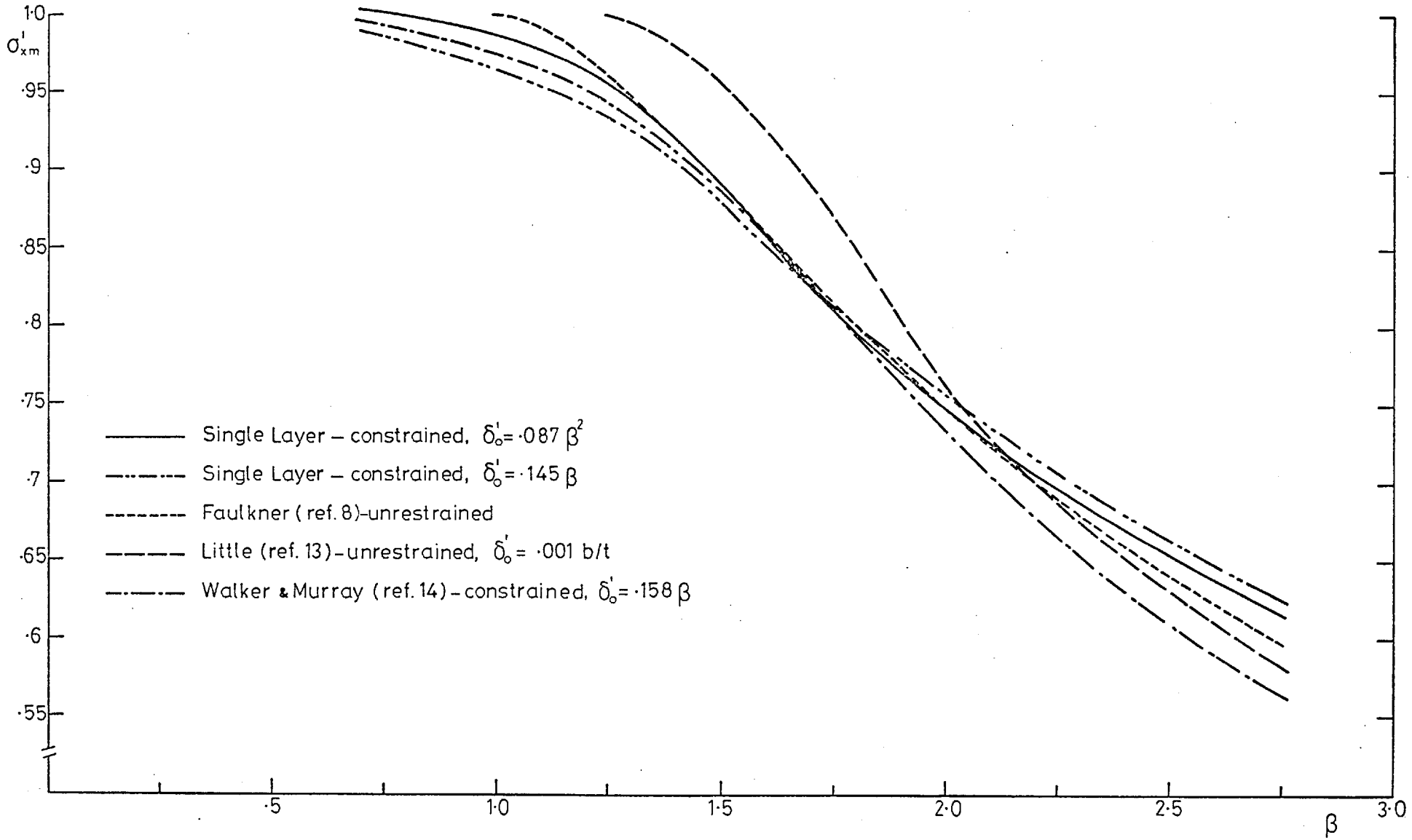

Fig. 92. Comparison of Maximum Plate Strength Curves

Unloaded edge condition and initial out-of-planeness are indicated where appropriate. Walker & Murray's solution includes allowance for residual stress

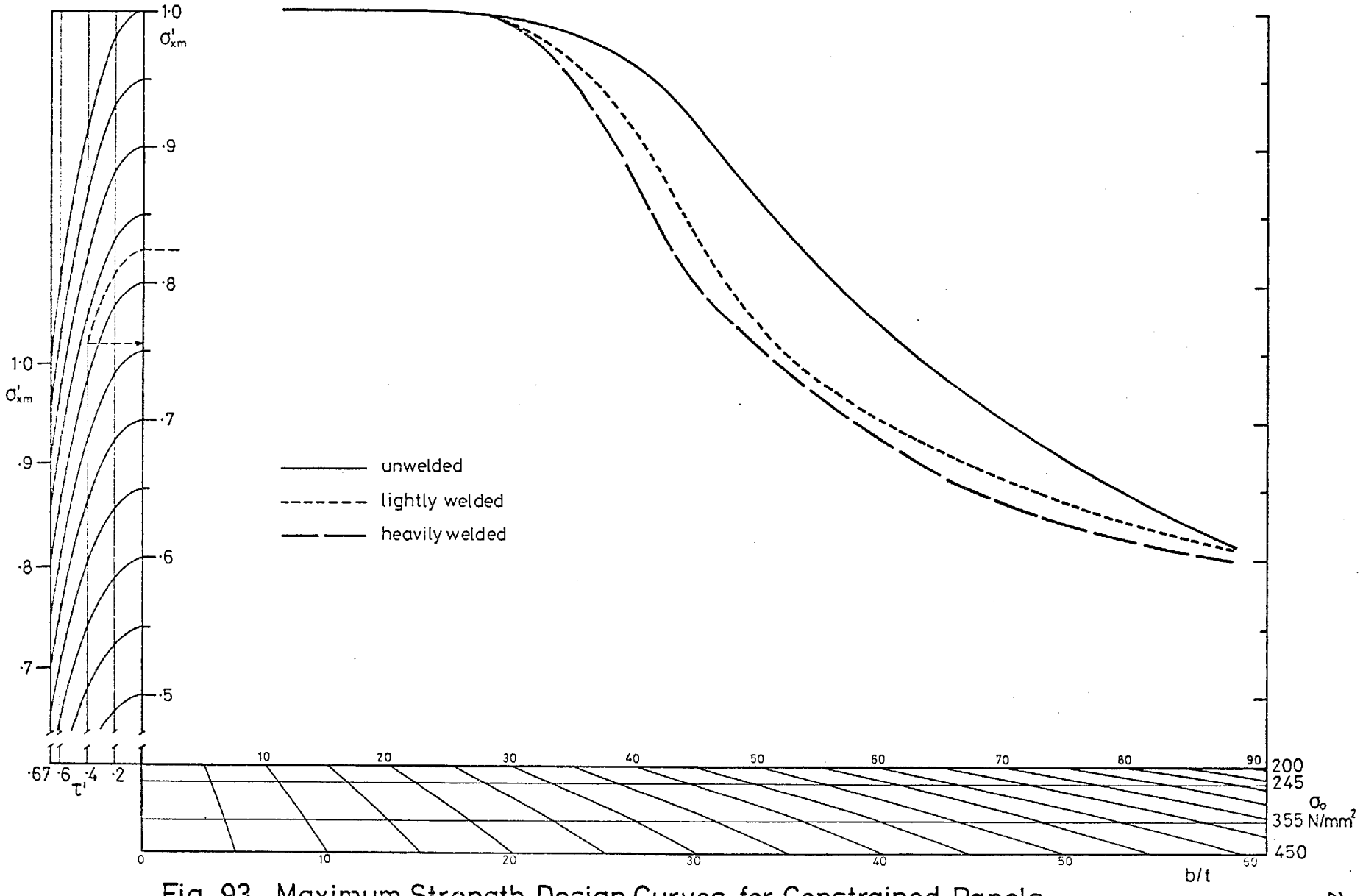

Fig. 93. Maximum Strength Design Curves for Constrained Panels

Note the curves which allow for coexistant shear